2012-05-03

Synthesis and Characterization of Transition Metal Complexes with Bulky Tin Ligands for Application in Small Molecule Activation

Veeranna Yempally
University of Miami, vyempally@gmail.com

UNIVERSITY OF MIAMI

SYNTHESIS AND CHARACTERIZATION OF TRANSITION METAL COMPLEXES WITH BULKY TIN LIGANDS FOR APPLICATION IN SMALL MOLECULE ACTIVATION

By

Veeranna Yempally

A DISSERTATION

Submitted to the Faculty
of the University of Miami
in partial fulfillment of the requirements for
the degree of Doctor of Philosophy

Coral Gables, Florida

May 2012

UNIVERSITY OF MIAMI

A dissertation submitted in partial fulfillment of
the requirements for the degree of
Doctor of Philosophy

SYNTHESIS AND CHARACTERIZATION OF TRANSITION METAL COMPLEXES WITH BULKY TIN LIGANDS FOR APPLICATION IN SMALL MOLECULE ACTIVATION

Veeranna Yempally

Approved:

_____ Burjor Captain, Ph.D. Professor of Chemistry	_____ Terri A. Scandura, Ph.D. Dean of the Graduate School
_____ Carl. D. Hoff, Ph.D. Professor of Chemistry	_____ Rajeev Prabhakar, Ph.D. Professor of Chemistry
_____ Priyamvada Rai, Ph.D. Professor of Medicine Miller School of Medicine	

YEMPALLY, VEERANNA (Ph.D., Chemistry)
Synthesis and Characterization of Transition Metal Complexes with Bulky Tin Ligands for Application in Small Molecule Activation (May 2012)

Abstract of a dissertation at the University of Miami.

Dissertation supervised by Professor Burjor Captain.
No. of pages in text. (191)

The role of bulky tin ligands in the stabilization of transition metal complexes with electronic unsaturation has been studied to understand the mode of binding of small molecules at an unsaturated metal center. We were able to isolate electronically unsaturated Pt-Sn bimetallic complexes effective in the reversible activation of small molecules including CO, H_2, C_2H_4, and NH_3 at room temperature. We have examined the effect of the modification of ligands in Pt-Sn bimetallic complexes for the activation of small molecules and have observed that the $Pt(SnBu^t_3)_2(CNBu^t)_2$ bimetallic complex reversibly activates hydrogen at room temperature both in the solid state and in solution. Similarly, we have also prepared bimetallic Pt-Sn complexes with an NHC carbine ligand which were also shown to activate hydrogen and alkenes reversibly. A bimetallic Fe-Sn cluster complex, Fe_2 $(\mu\text{-}SnBu^t_2)_2(CO)_8$, was synthesized from the reaction of Bu^t_3SnH with the $Fe_2(CO)_9$ and shown to be selective at activating the benzylic C-H bond of alkylaromatic solvent molecules. The new complexes containing tin have been characterized spectroscopically to gain an insight into the reaction mechanism involved in small molecule activation.

ACKNOWLEDGEMENTS

It is with great honor that I am able to dedicate this work to my father. Without the guidance of my father Veershetty, I would never have imagined myself as a chemist. Without the loving support of my mother Hymavathi, there is simply no way I would be the person I am today. Equally as important, I give tremendous thanks to my research mentor Dr. Burjor Captain. He had a strong influence over my way of thinking about science and constantly motivated me to do productive research work. I am infinitely fortunate to have been in his group and the research techniques he has taught me have broadened my experimental and analytical skills. I am thankful to him for his encouragement to think independently and for creating a friendly atmosphere in the lab.

I must thank postdoctoral research assistant Dr. Lei Zhu, who has shared his excellent research techniques with me and provided a helping hand in advancing my research in a fruitful direction. I am also thankful to the exceptional people I have shared the lab with during my time at UM: Dr. Derek Isrow, Sumit Saha, and Anjaneyulu Koppaka. It is because of these fine men that I am able to write this work. I appreciate the help received from Dr. George Fortman in the initial stages of our collaborative work. I would like to extend my sincere thanks to Elizabeth. K. Batchelor for her kind support.

Much appreciation goes to Dr. Carl. D. Hoff for his intuitive, thought provoking ideas and motivation. I am deeply grateful to my committee members Dr. Rajeev Prabhakar, Dr. Carl. D. Hoff, and Dr. Priyamvada Rai for their assistance and guidance throughout my time in the chemistry department.

Lastly, I would like to thank the Department of Chemistry for providing excellent research facilities and the University of Miami for many years of wonderful experiences as well as financial support.

TABLE OF CONTENTS

LIST OF FIGURES

CHAPTER 1

CHAPTER 2

CHAPTER 3

CHAPTER 4

CHAPTER 5

CHAPTER 6

APPENDIX A

APPENDIX B

APPENDIX C

APPENDIX D

LIST OF SCHEMES

CHAPTER 1

CHAPTER 2

CHAPTER 3

CHAPTER 4

CHAPTER 5

CHAPTER 6

LIST OF TABLES

APPENDIX A

APPENDIX B

APPENDIX C

APPENDIX D

APPENDIX E

Chapter 1: Electronically unsaturated transition metal complexes for small molecule activation

1.1. Introduction

Important biological functions in nature are accompanied by activation of thermodynamically stable small molecules like H_2, N_2, and O_2 which are store-houses of chemical energy. Most of these activation processes are catalyzed by metal ions in low oxidation states, providing low-barrier reaction pathways for the binding of small molecules at a metal center. The existence of more than one oxidation state of a transition metal has resulted in variations in coordination geometry upon binding a substrate and allowed transition metals to serve as the chief building blocks for synthesis of a- wide variety of homogeneous and heterogeneous catalysts.

The ever increasing gap between the consumption of fossil fuels and the availability of fuel resources has triggered the quest for alternate renewable sources of energy. Small molecules like H_2, CH_4 and CO_2 are potential reservoirs of chemical energy and are abundantly available in nature. The chemical energy stored in these molecules can be converted into electrical energy to meet the demands of growing energy needs. For example, hydrogen can be used as a fuel in fuel cells to generate sufficient electricity to power automobiles and house hold appliances.[1-3] Unsaturated transition metal complexes are found to be suitable candidates for promoting the activation of small molecules with low-energy barriers.[4] This potential has led to the tremendous growth of research interests in the 21st century aimed at synthesis of transition metal complexes with a wide variety of ligands and at understanding the mode of binding of these small molecules at the metal center.

1.2. Activation of small molecules at an unsaturated transition metal centers

Recent developments in probing techniques such as time resolved spectroscopy and neutron diffraction techniques have shed light on the binding of H_2 at a transition metal centers.[5, 6] For example, the crucial step in activation of molecular hydrogen is its coordination at the metal center (see Figure 1.1).

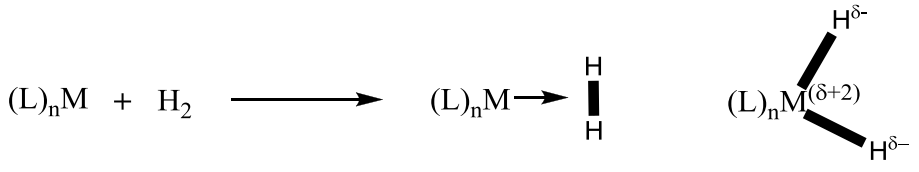

Figure 1.1 Coordination modes of hydrogen at a metal center.

Pioneering work by Kubas et al. on activation of di-hydrogen by the tungsten carbonyl complexes $W(CO)_3(PR_3)_2$ has revealed that back-donation of electrons is critical for the activation of hydrogen and stability of metal hydride complexes.[7, 8] The back-donation of the electrons from the filled metal orbitals to the anti-bonding σ* orbital of hydrogen initiates cleavage of H-H bond. It has been found that the ancillary ligands bonded to the metal center control the back-donation, and the nature of the formed metal-hydride complexes is dictated by the nature of the ligands.[7] Design of new ligands for application in the field of catalysis is another driving force for the advancement of organometallic chemistry.

For the activation of H_2 by transition metal complexes, the metal center should be either coordinately unsaturated or electronically unsaturated. The coordinative unsaturation can be attained by including either a bulky chelating ligand, weakly bound solvent molecules, or labile CO ligands in the metal system.[9, 10, 11] The coordination of

H_2 is facilitated by elimination of the solvent molecule or CO ligand. Recently, Crabtree et al. mimicked the intramolecular heterolytic cleavage of H_2 by the Ir complex with weakly bound water molecule (see Scheme 1.1).[12]

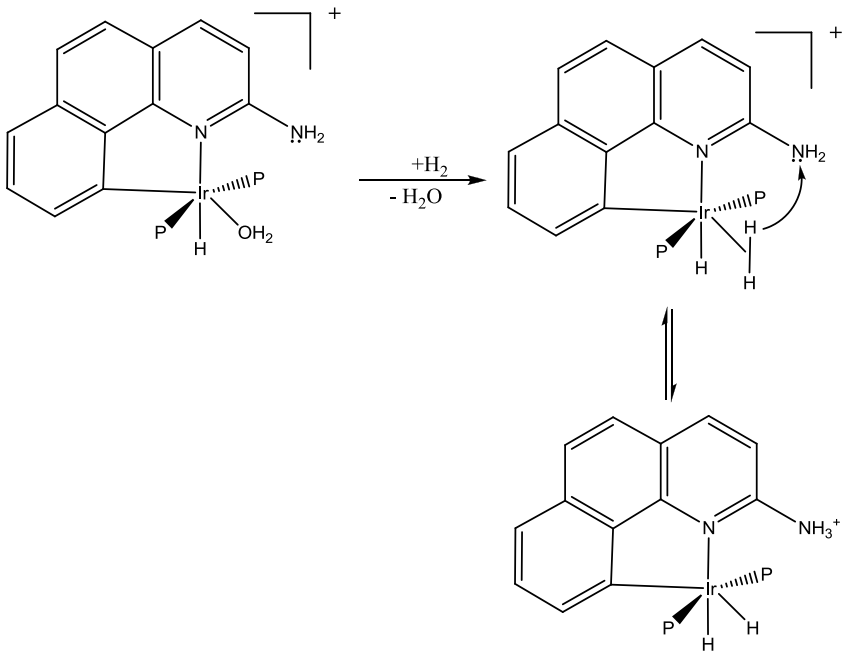

Scheme 1.1

Electronic unsaturation in transition metal complexes is induced by bulky ligands. As seen in Figure 1.2, the bulky ligands shield the metal center from approach of large molecules, leaving enough room for the selective approach of small molecules.[13] Bulky ligands such as phosphines,[14] and NHC carbenes[15-17] stabilize the reactive intermediates of transition metal complexes, where the metal is lacking the necessary number of electrons to attain an 18 electron configuration. Based on this approach, several unsaturated transition metal complexes have been synthesized and the reactivity of these complexes in small molecule activation is well known.[18-20]

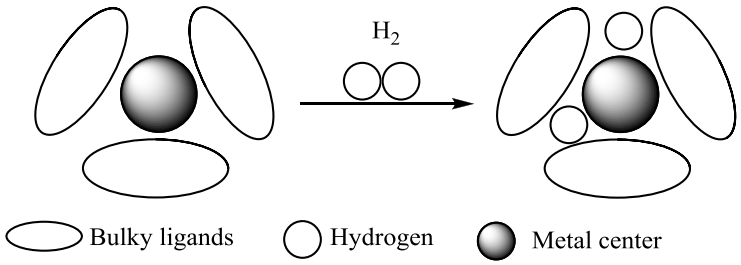

Figure 1.2 Activation of hydrogen at an unsaturated metal center.

1.3. Phosphine ligands as building blocks for the synthesis of unsaturated metal cluster complexes

Extensive research on the use of bulky phosphine ligands as building blocks for the preparation of transition metal complexes with low coordination numbers has revealed the capability of these metal clusters to act as catalytic precursors for organic transformations of industrial importance.[21-24] Transition metal complexes possessing PR_3 phosphine ligands (R = Bu^t, ^iPr, Cy, and Ph) have laid the foundation for the synthesis of transition metal hydride complexes for application in catalytic hydrogenation reactions[25-28] and also have provided insight into the role of steric effects in the stabilization of low-valent transition metal complexes. Some examples of unsaturated mononuclear transition metal complexes with phosphine ligands are shown in Figure 1.3.

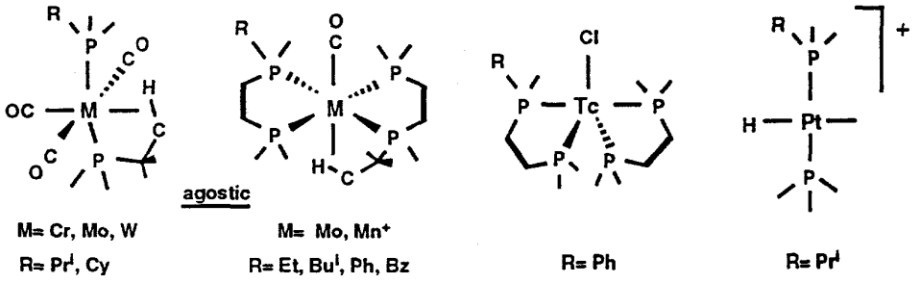

Figure 1.3 Unsaturated metal phosphine complexes.[29-31]

In polynuclear complexes, as well, Adams et al. demonstrated that the unsaturated heterometallic cluster $Pt_3Re_2(CO)_6(PBu^t_3)_3$ reacts with three equivalents of H_2 at room temperature to yield the hexahydrido complex $[Pt_3Re_2(CO)_6(PBu^t_3)_3(\mu\text{-}H)_6]$ in 90% yield[32]. The addition of hydrogen is sequential and the di- and tetra- hydrido intermediates have also been isolated and characterized. The authors state that the Pt-Re bimetallic complex $[Pt_3Re_2(CO)_6(PBu^t_3)_3(\mu\text{-}H)_6]$ eliminates hydrogen reversibly under the influence of UV-Vis irradiation (see Scheme 1.2).

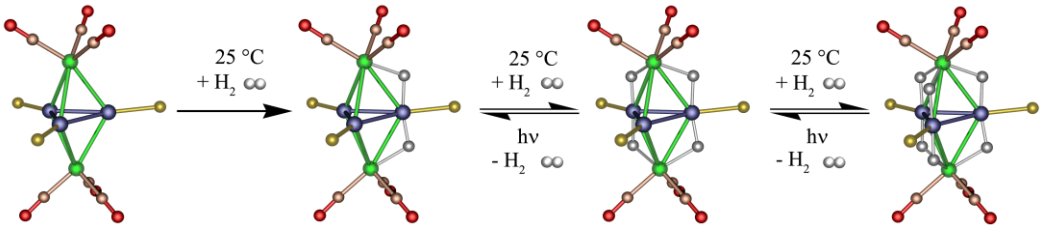

Pt (blue) Re (green) P (gold) C (pink) O (red)

Scheme 1.2

Recently, Hoff et al. examined the reactivity of two coordinate [Pd(L)(L')] (L = N-heterocyclic carbene (NHC) and L' = NHC or PR_3) complexes for the activation of O_2, and they observed that O_2 binds to [Pd(IPr)(P(*p*-tolyl)$_3$)] rapidly to form $[Pd(\eta^2\text{-}O_2)_2(IPr)(P(p\text{-tolyl})_3)]$.[33]

Koridze et al. also demonstrated activation of small molecules like CO, H_2, N_2 and O_2 by the Rh-pincer complex $RhH(Cl)[2,6\text{-}(Bu^t_2PO)_2C_6H_3]$, **1.1**.[34] The Rh hydrido chloride pincer complex **1.1** was shown to activate CO readily with the reductive elimination of HCl. Similarly, the 14 electron complex generated from the reaction of **1.1** with $NaOBu^t$ has been shown to activate H_2 and N_2 to afford rhodium dihydrogen and rhodium

dinitrogen complexes respectively. The authors also found that these Rh-pincer complexes with small molecules interconvert among themselves as shown in Scheme 1.3.

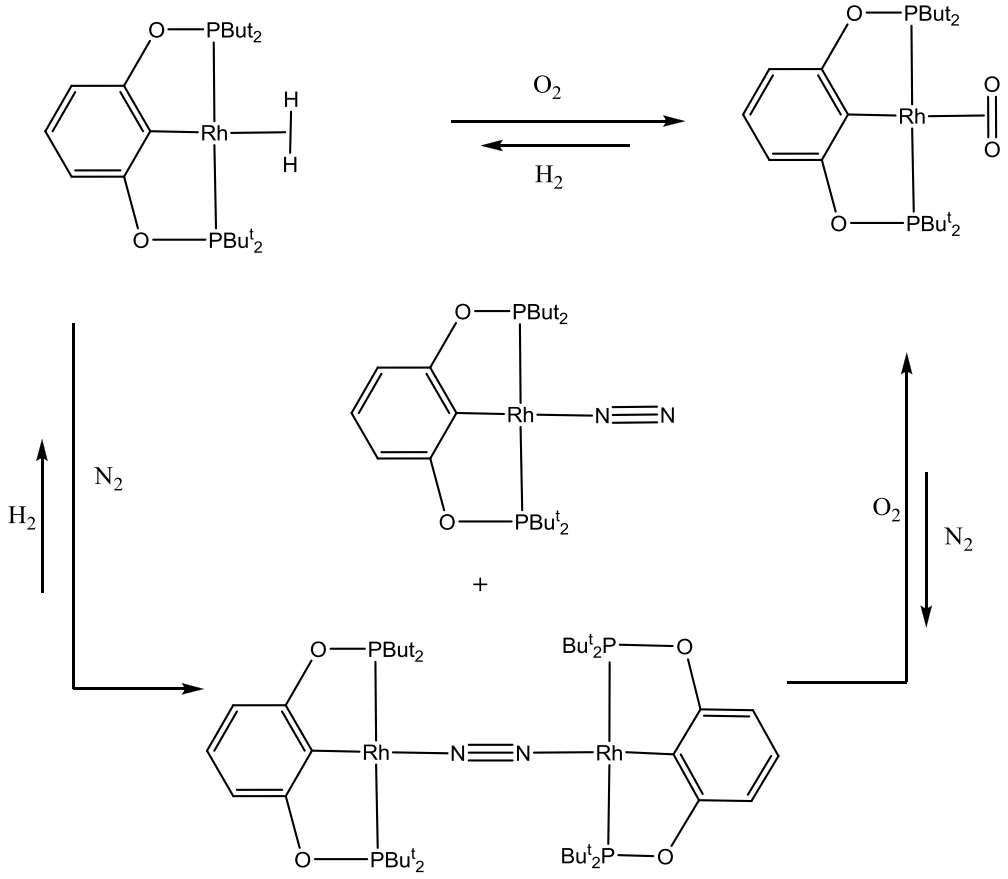

Scheme 1.3

The positive effects of phosphine ligands on enhancing selectivity and catalytic activity in traditional industrial processes have been exemplified in many reports.[35-38] However, the high toxicity and, the high cost involved in synthesizing tertiary phosphine ligands, and their degradative tendency to convert into phosphine oxides during the catalytic cycles necessitated a search for cheaper and bulky ligands such as NHC ligands. More recently, bulky ligands based on main group metals like Al,[39, 40] Sn[41, 42] have been slowly gaining momentum as alternatives for phosphine ligands. This field is still in its

early stages and more research has to be done to explore the reactivity of these ligands in small molecule activation.

1.4. Bimetallic complexes containing tin ligands

Organotin derivatives are widely used as catalysts for esterification and *trans*-esterification of mono- and polyesters.[43, 44] These products have applications in the manufacture of synthetic lubricants, coatings and also in polyurethane foam production.[45-48] Facile formation of Sn-C bond, ease of generation of tin radicals, and the acidic nature of Sn have stimulated the use of organotin reagents in organic synthesis.

The use of bulky substituents like $[CH(SiMe_3)_2]_2$ and $[N(SiMe_3)_2]$ on tin has facilitated isolation of stable and reactive divalent stannylene radicals ($:SnR_2$). The Lewis base behavior of these tin radicals has been explored in the synthesis of transition metal complexes with these tin ligands.[49] A brief summary of these reactions is highlighted in Scheme 1.4.

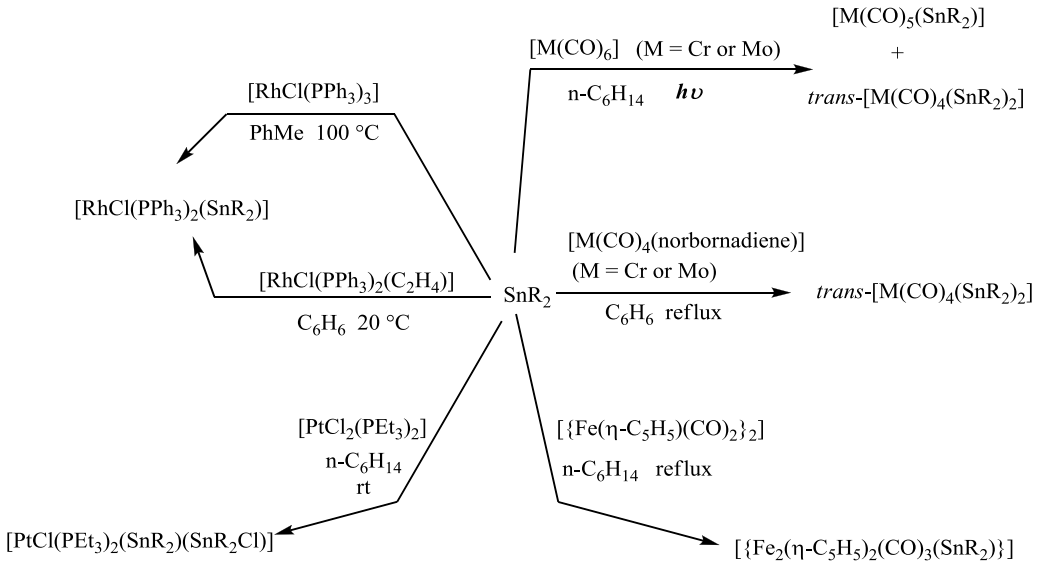

Scheme 1.4

It has been found that the bulky substituents increase the life time of stannylene radicals, thus allowing them to react with transition metal carbonyl compounds and leading to isolation of predominantly *trans*-substituted products. Insertion (or oxidative addition) of an SnR_2 groups into the M-X bond (X = Cl, H, Me) of transition metal complexes is also well known.[49]

Tetravalent tin compounds, such as tri-organotin hydrides and tri-organotin halides have also been shown to undergo oxidative addition reactions with transition metal complexes.[42] Oxidative addition is the major synthetic route for the preparation of transition metal complexes comprise of tin ligands. Recently, the Esturuela group prepared an osmium tetrahydride complex with a bis(stannyl) derivative, where Os metal is in a high oxidation state from the oxidative addition of four equivalents of Ph_3SnH to $OsH_2Cl_2(P^iPr_3)_2$,[50] (see Scheme 1.5).

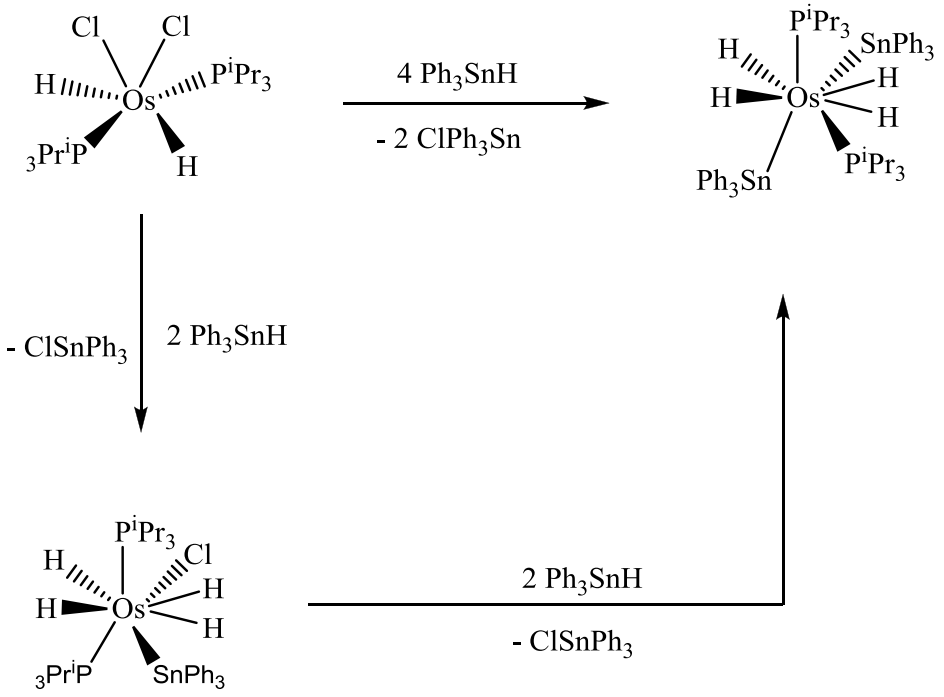

Scheme 1.5

Other synthetic methods, including salt elimination,[51] elimination of small molecules,[52, 53] and oxidative elimination,[54, 55] have previously been used for preparation of TM-Sn bimetallic complexes (TM = transition metal).

The effect of addition of tin on improving catalytic activity and selectivity of transition metal complex have been observed in a number of transition metal systems.[56-58] For instance, selectivity in the dehydrogenation of isobutane to isobutene (see Figure 1.4) over a Pt-Sn/SiO_2 bimetallic catalyst was increased to 100% from a 93% selectivity found when using only a Pt/SiO_2 system due to the formation of hydrogenolysis products with this catalyst.[59]

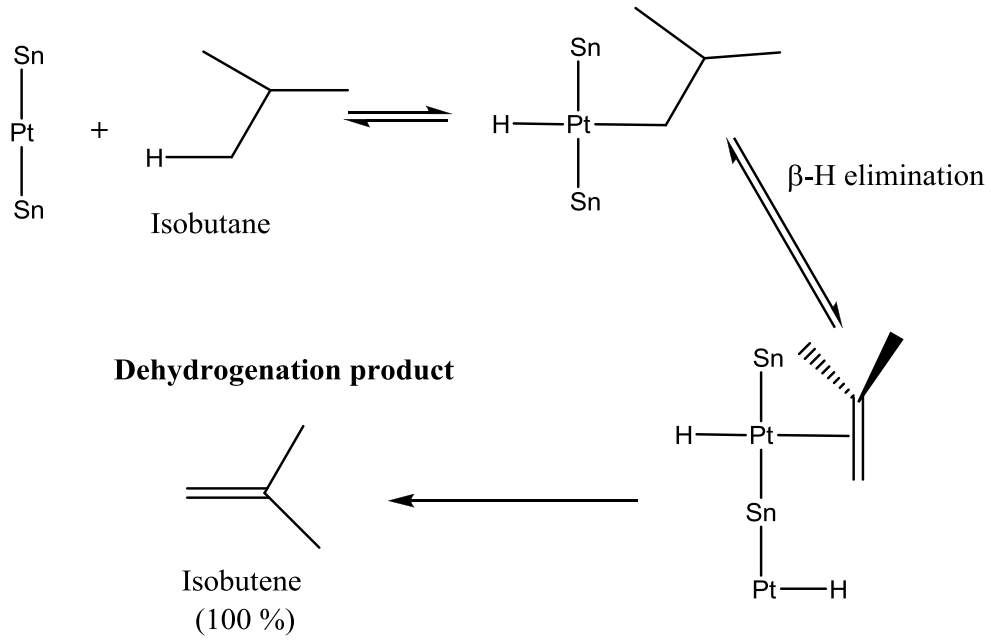

Figure 1.4 Selective dehydrogenation of isobutane to isobutene over a Pt-Sn catalyst.

Recent studies have shown that in comparison to mononuclear complexes, bimetallic cluster complexes supported on mesoporous silica exhibit superior product selectivity and catalytic activity in catalysis reactions.[60-62] These studies have revealed that the tin plays

a major role in anchoring the metal nanoparticles to the catalyst support surface, and selectively deactivates the catalytic active sites responsible for formation of side products, thus enhancing the selectivity and stability of the catalyst.[63, 64]

In the past ten years, numerous heterometallic cluster complexes comprised of tin ligands anchored on mesoporous silica have been prepared and their application in heterogeneous catalysis of hydrogenation and dehydrogenation of olefins have been thoroughly investigated.[58, 61] The research on the active catalytic intermediates involved in these reactions will shed light on the role of sterics in stabilization of these intermediates, and synthesis of model unsaturated TM-Sn bimetallic complexes will provide a platform for understanding the reaction mechanisms involved. The task of identifying a catalyst comprised of earth abundant cheaper metals that can work at ambient conditions (room temperature and 1 atm) is still a major challenge for the field of organometallic catalysis.

1.5. Statement of purpose

There are very few examples of unsaturated transition metal complexes containing bulky tin ligands. The quest to synthesize potential hydrogenation and dehydrogenation catalysts motivated us to investigate the activation of small molecules with unsaturated TM-Sn bimetallic complexes. We have examined the role of bulky groups in the stabilization of unsaturated metal clusters and the reactivity of these clusters toward small molecule activation at ambient conditions. The potential application of these bimetallic cluster complexes in homogenous catalysis of hydrogenation of olefins was also

explored. *The reason for using bulky tin groups is twofold—(i) tin adds to ligand properties in terms of sterics AND (ii) tin provides an extra metal for catalytic interest*.

A bulky tetravalent organotin ligand Bu^t_3SnH (tri-*tert*-butylstannane) was obtained in a decent yield by modification of existing literature synthesis methods. The versatility of this bulky organotin ligand in the stabilization of transition metal complexes in low oxidation states have been examined with known Pt(0) precursor complex $Pt(COD)_2$ (COD = 1,5-Cyclooctadiene) to afford Pt(II)-Sn and Pt(IV)-Sn mono- and dinuclear complexes. The Pt-Sn bimetallic cluster complexes were characterized with the help of ^1H NMR, single crystal X-ray crystallography, and IR spectroscopy. The effect of modification of ligands on Pt-Sn bimetallic complexes was also investigated with respect to the activation of H_2 and CO.

With the aim of synthesizing bimetallic complexes with cheaper metals we have investigated the selective benzylic C-H bond activation of alkyl aromatic compounds by the Fe-Sn bimetallic cluster complex Fe_2 $(\mu\text{-}SnBu^t_2)_2(CO)_8$, synthesized from $Fe_2(CO)_9$ and Bu^t_3SnH. The facile formation of a Sn radical by cleavage of a *tert*-butyl group from Sn ligand ($SnBu^t_2$) was a key step in the activation of the benzylic C-H bond of alkyl aromatic compounds. This reaction mechanism was investigated and a free radical mechanism is proposed based on supporting information.

Given the interest in synthesis of heterometallic carbide clusters for application in catalysis, the reaction of $Ni(Cp)_2$ (Cp = Cyclopentadiene) with $Fe_5(C)(CO)_{15}$ was also investigated and the products were characterized by a combination of IR spectroscopy and single crystal X-ray diffraction technique. The cleavage of a Cp fragment from

$Ni(Cp)_2$ in refluxing conditions facilitated isolation of a Fe_5Ni heterometallic cluster complex. Detailed description of synthesis methods, isolation of stable reaction intermediates and reaction mechanisms will be discussed in the next chapters.

Chapter 2: Synthesis, characterization and activation of small molecules by new bimetallic Pt-Sn complexes

2.1. Background

Platinum complexes modified by tin ligands are widely used in the petroleum refinery industry as potential heterogeneous catalysts for hydrogenation, dehydrogenation, and hydroformylation of alkenes.[65-69] Under homogeneous conditions Pt-Sn bimetallic complexes have also been shown to catalyze many important reactions such as hydrogenation and isomerization of olefins and the water gas shift reaction.[70, 71, 65] Pt-Sn complexes supported on silica/alumina are also used in catalytic coupling reactions of CO_2 with ethylene in the presence of water to produce lactic acid.[72, 73] Recently, tin modified Pt complexes supported on carbon or carbon nanotubes has received substantial attention as catalysts in CO and ethanol oxidation in direct alcohol fuel cells.[74, 75]

The oxophilic nature of tin and its alloy forming capability with transition metals aid in the enhancement of catalytic activity and product selectivity by modifying the electronic environment around the metal center.[76] The common feature observed in most of the Pt-Sn bimetallic heterogeneous catalysts used for hydroformylation and hydrogenation is the formation of a labile $SnCl_3$ ligand, which facilitates addition of alkenes and small molecules (H_2, CO) to the Pt metal center through the *trans*-effect.[77, 78] Stability of the catalytically active low valent Pt[Pt(0)/Pt(II)] intermediates is accomplished by synthesis of Pt complexes containing chelating phosphine ligands or N-donating ligands.[79-82]

Oxidative addition of organotin ligands (R_3E-X, E = Sn, X = halogens or hydrogen, R = Ph, alkyl groups) to Pt(0) complexes is a well-established synthetic route for the synthesis of Pt-Sn organometallic complexes.[83-85] For instance, the Pt(IV) compounds containing tin ligands have been isolated as insoluble precipitates from the reaction of tri-organotin hydrides, R_3SnH (R = Ph, $PhCH_2$) with carbanatobis(phosphine)platinum(II) complexes, $[Pt(CO)_3L_2]$ (L = $PMePh_2$ or PEt_3), in ethanol solution.[86] The reactions were accompanied by oxidative addition of an Sn-H bond to the Pt metal and evolution of CO_2 gas. Pt(IV) complexes tend to decompose easily to Pt(II) complex with the reductive elimination of H_2 and R_3SnH or R_3SnCl. For example, complexes of $Pt(chelate)(SnMe_3)_2$ type have been prepared by the addition of tri-organotin hydride to $Pt(chelate)_2$ compounds in benzene solution, followed by reductive elimination of hydrogen (see Scheme 2.1).[85]

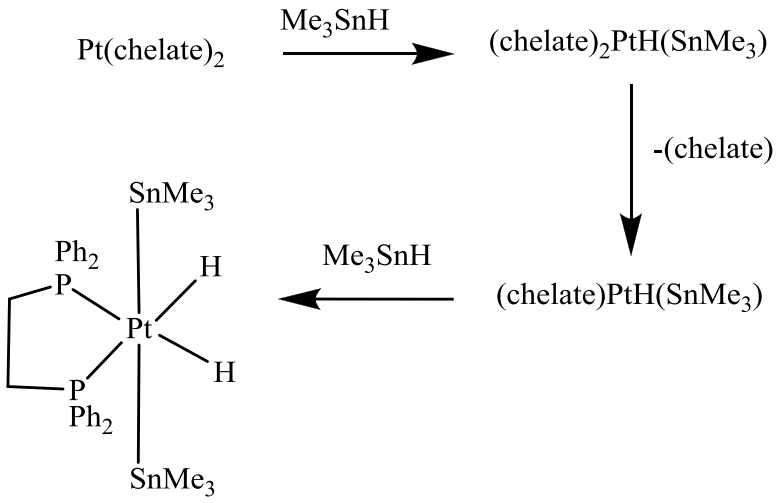

Scheme 2.1

Al-Allaf, reported the reactions of organotin (IV) compounds, SnR_xCl_{4-x} (R = Me, Ph; x = 4-0) with the Pt(0) complex $Pt(COD)_2$ to yield platinum(II) complexes containing a Pt-Sn bond. It has been found that in these complexes Pt has been inserted into either Sn-

Cl or Sn-R bonds, displacing one COD ligand.[87] Structures of Pt-Sn compounds were postulated based on ^{1}H NMR and IR spectroscopy; no crystal structures were reported.

Braddock-Wilking et al. prepared mono- and dinuclear Pt-Sn and Pt-Ge bimetallic complexes by the addition of $PhEH_2$ (E = Ge, Sn) to the Pt(0) precursor $Pt(C_2H_4)(PPh_3)_2$ through the oxidative addition of an E-H bond to the Pt(0) center.[88] It has been found that the germanium dinuclear complex is symmetrical, and the tin dinuclear complex is unsymmetrical (see Figure 2.1).

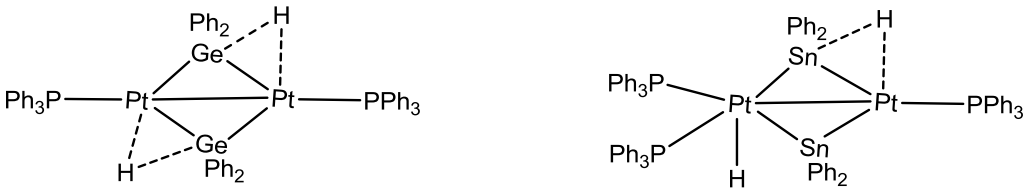

Figure 2.1 Line drawings for $[(PPh_3)Pt(\mu\text{-}\eta^2\text{-H-}GePh_2)]_2$ and $[(PPh_3)_2Pt(H)(\mu\text{-}SnPh_2)(PPh_3)Pt(\mu\text{-}\eta^2\text{-H-}SnPh_2)])]$.

Pt-Sn complexes possessing carbonyl ligands, formula $[(M\{\mu_2\text{-}\ M'(NR_2)_2(CO)_3]$ (M = Pt, Pd, M′ = Ge, Sn and R = $SiMe_3$ or $CH(SiCH_3)_2$), are prepared in high yield from $[M\ M'\{(NR_2)_2\}_3]$ and CO.[89] The carbene analogue **:**SnR_2 ligands have been used to synthesize homoleptic Pt(0) complexes $[Pt\{Sn(NR_2)_2\}_3]$ from the reaction between $Pt(COD)_2$ and **:**SnR_2 ligand in toluene solution (see Eq. 1).[90] The molecular structure of the Pt(0) complex $[Pt\{Sn(NR_2)_2\}_3]$ was also reported for this complex based on crystallographic analysis.

$$Pt(COD)_2 \quad + \quad \underset{\text{(excess)}}{:Sn(NR_2)_2} \quad \xrightarrow[\text{rt}]{\text{toluene}} \quad \underset{R = SiMe_3}{[Pt\{Sn(NR_2)_2\}_3]} \qquad (1)$$

Recently, a trigonal bipyramidal Pt-carbonyl cluster containing an $SnCl_2$ ligand, $[Pt_5(CO)_5\{Cl_2Sn(\mu\text{-}OR)SnCl_2\}_3]^{3-}$ was isolated from the reaction of Pt-carbonyl anion $[Pt_{15}(CO)_{30}]^{2-}$ with $SnCl_2$.[91] A suitable synthesis method and the use of bulky ligands or chelating ligands are the key factors governing the isolation of reactive unsaturated Pt-Sn bimetallic complexes for application in small molecule activation or catalysis.

More recently, bis(stannylene) and bis(germylene) ligands have garnered much attention as prospective ligands for the stabilization of transition metal complexes in low oxidation states.[42, 92] Transition metal oxidation states can be tuned by varying steric demand of stannylene ligands. A chelating benzannulated bisstannylene ligand have been used by the Zabula group to prepare Pt(0) hetero-and homoleptic complexes (see Scheme 2.2).[79]

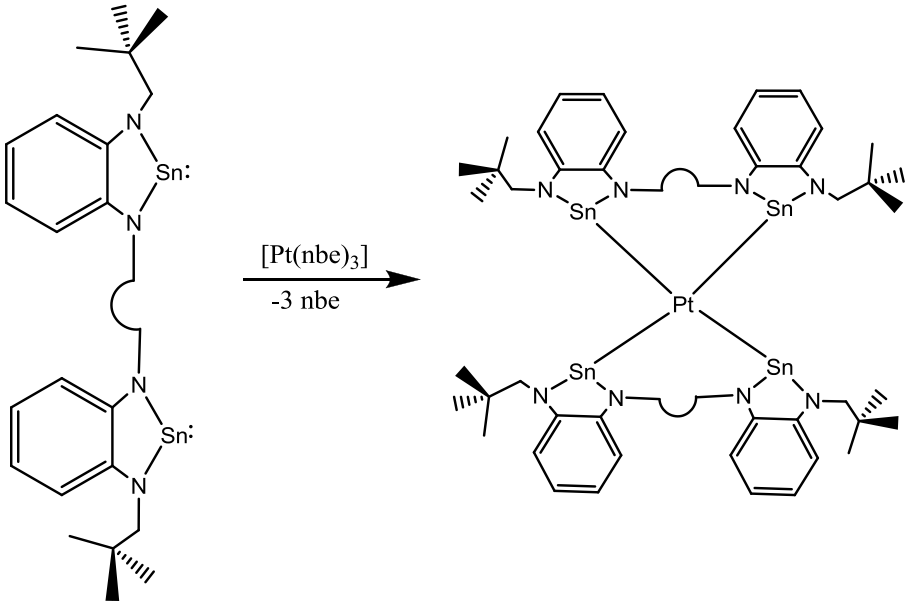

Scheme 2.2

The majority of the Pt-Sn complexes reported thus far uses either phosphine ligands or chloride ligands. Very few neutral Pt-Sn complexes comprised of only bulky tin

ligands are characterized crystallographically and reported in literature.[79, 90] Adams et al. synthesized several bimetallic complexes with a Ph_3SnH ligand addition to transition metal carbonyl clusters:- some of them are shown in Figure 2.2.[41, 93-95] Ru-Sn and, $PtRu_5Sn$ complexes are shown to be effective hydrogenation catalysts.[58, 41] We have also reported the selective hydrogenation of nitrobenzene to aniline using $Pt_2Ru_2Sn_2$ nanoparticles supported on mesoporous silica.[96]

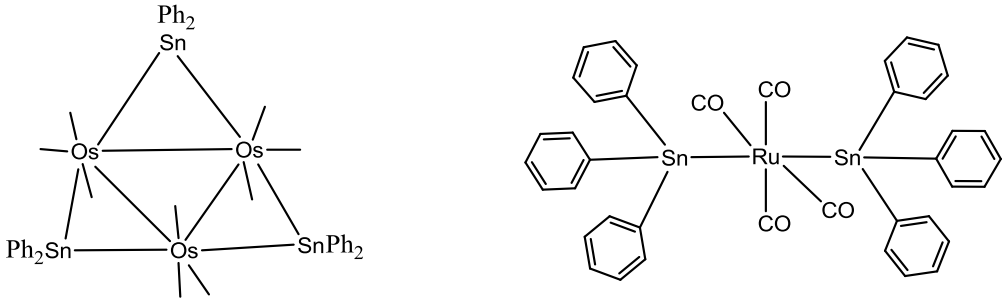

a) $Os(CO)_9(\mu\text{-}SnPh_2)_3$ b) $Ru(CO)_4(SnPh_3)_2$

Figure 2.2 Line diagrams for Os and Ru bimetallic carbonyl cluster complexes with tin ligands.

There are very few reports on the use of *tert*-butyltin ligands in the synthesis of Pt-Sn cluster complexes.[97] There are ample opportunities to exploit the reactivity of *tert*-butyl tin ligand in the synthesis of unsaturated bimetallic Pt-Sn cluster complexes. Here our focus is to use bulky tri-*tert*-butyltin ligand to synthesize electronically unsaturated Pt-Sn complexes for small molecule activation. As expected, the Sn-H bond of the Bu^t_3SnH ligand was activated readily by Pt(0) precursor complex $Pt(COD)_2$ at room temperature to yield Pt(II) and Pt(IV) mononuclear and dinuclear unsaturated Pt-Sn complexes. The bulky *tert*-butyl groups on Sn favored formation of *trans*-compounds. The effect of bulky tin ligands on activation of small molecules such as H_2, CO, and *tert*-butyl isocyanide at Pt metal center was investigated.

2.2. Results and discussion

The Pt(0) precursor complex $Pt(COD)_2$ is very reactive and effective in activation of the Sn-H bond. The steric effects of bulky stannane ligand (Bu^t_3SnH) in stabilization of mononuclear and dinuclear Pt(II) and Pt(IV) complexes were investigated with the combination of ^1H NMR spectroscopy, single crystal X-ray diffraction technique, and Infrared spectroscopy (IR). The results are discussed in this section with supporting reaction mechanisms for activation of small molecules.

Reaction of $Pt(COD)_2$ with one equivalent of Bu^t_3SnH: The step wise addition of Bu^t_3SnH to the $Pt(COD)_2$ complex allowed us to understand the reaction pathway for the formation of new unsaturated Pt-Sn bimetallic complexes. Addition of one equivalents of Bu^t_3SnH to $Pt(COD)_2$ at room temperature in hexane solvent affords a mononuclear 16 electron Pt(II) complex [$HPt(COD)(SnBu^t_3)$], **2.1**, with the elimination of one COD ligand, followed by oxidative addition of an Sn-H bond across the Pt metal center (see Eq. 2).

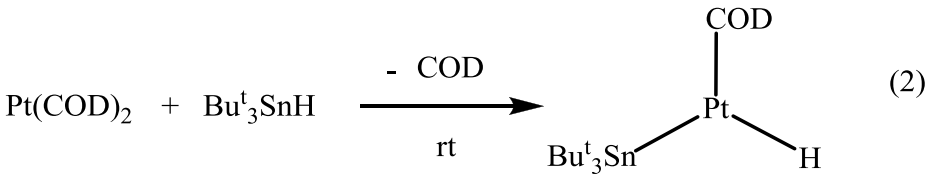

(2)

The complex **2.1** is very reactive, decomposes slowly when exposed to air, and has to be handled under nitrogen atmosphere. The Pt(II) complex [$HPt(COD)(SnBu^t_3)$] was characterized by combination of ^1H NMR and single crystal X-ray crystallography. The molecular structure of complex **2.1** is shown in Figure 2.3. In the molecular structure one

can clearly see the bending of the COD ligand slightly away from the Pt center to accommodate the terminal hydride ligand.

The Pt-Sn bond length in compound **2.1** is 2.598(18) Å, and Pt-H bond length is 1.45(3) Å, consistent with reported Pt-Sn single bond length in Pt(II) complexes.

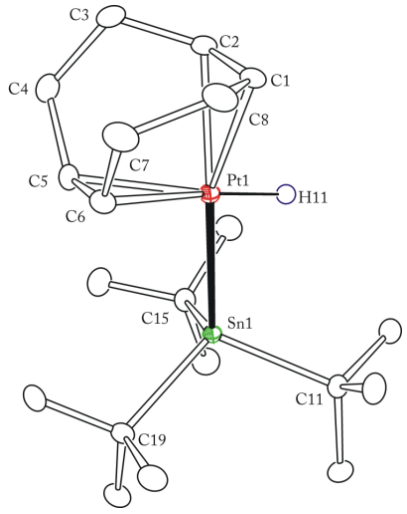

Figure 2.3 The molecular structure of [HPt(COD)($SnBu^t_3$)], **2.1**.

The hydride ligand is located and refined during crystallographic analysis performed at 100 K. The presence of the hydride ligand was also confirmed by ^1H NMR spectroscopy. The hydride peak appears at -5.45 ppm in C_6D_6 solvent with appropriate one- bond coupling to Pt and two-bond coupling to Sn. Compound **2.1** is a 16 electron unsaturated bimetallic Pt-Sn complex that is very reactive and can be used as a precursor to synthesize Pt(IV) and Pt(II) complexes either by substitution of COD ligand with another Bu^t_3SnH group or by other bulky ligands such as NHC (NHC = N-Heterocyclic Carbene), or $CNBu^t$ (*tert*-butyl isocyanide). The synthesis of Pt-Sn complexes with the substitution of the NHC ligand will be discussed in chapter 3.

Addition of one more equivalent of Bu^t_3SnH to compound 2.1: Our aim here was to isolate an unsaturated 14 electron Pt(IV) complex with two terminal Bu^t_3Sn ligands and two hydride ligands, $H_2Pt(SnBu^t_3)_2$, **2.3** (see Scheme 2.3). Very few 14 electron neutral Pt complexes are characterized and reported in literature.[98-100] Addition of one more equivalent of Bu^t_3SnH to compound **2.1** in C_6D_6 solvent was investigated by ^1H NMR spectroscopy.

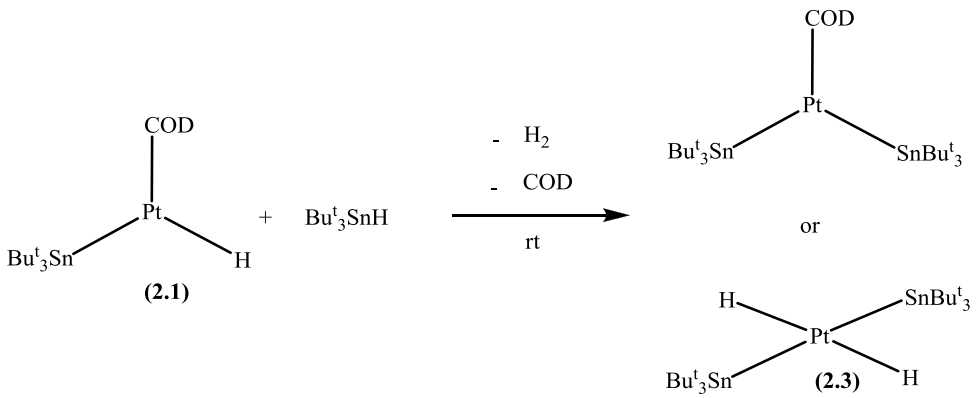

Scheme 2.3

After three hours we observed the appearance of new peaks in the hydride region at -7.8 ppm; however we have not been able to correctly assign the nature of these complexes. One possible structure is shown in compound **2.3**. The reaction mixture was dissolved in dichloromethane and plated on TLC to collect a yellow band, which on crystallization in hexane solvent at -20 °C gave an unexpected new Pt-Sn cluster complex $[H_2Pt(\mu\text{-}SnBu^t_2)(SnBu^t_3)]_2$, **2.4**. The yield was low due to decomposition on the TLC plate.

Braddock-Wilking et al. prepared a similar dinuclear Pt-Sn complex $[(PPh_3)_2Pt(H)(\mu\text{-}SnPh_2)(PPh_3)Pt(\mu\text{-}\eta^2\text{-}H\text{-}SnPh_2)])]$ through the intermediate mononuclear complex $(Ph_3P)_2Pt(H)(SnPh_2H)$,[88] (see Scheme 2.4).

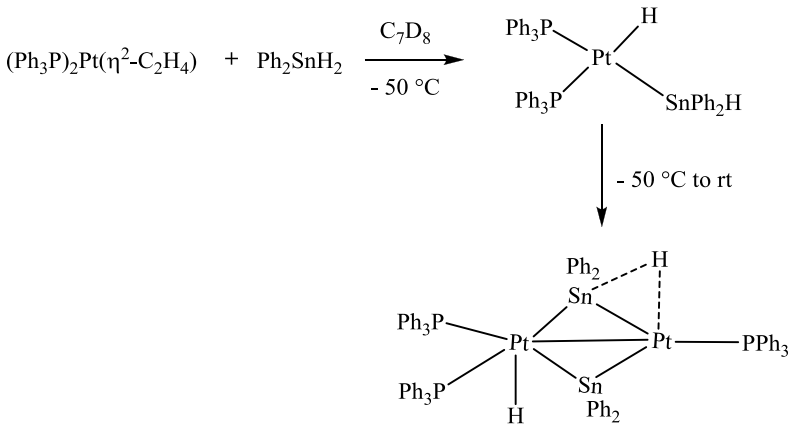

Scheme 2.4

The compound **2.4** was characterized by a combination of ^{1}H NMR and single crystal X-ray crystallography and mass spectrometry. The molecular structure of complex **2.4** is shown in Figure 2.4.

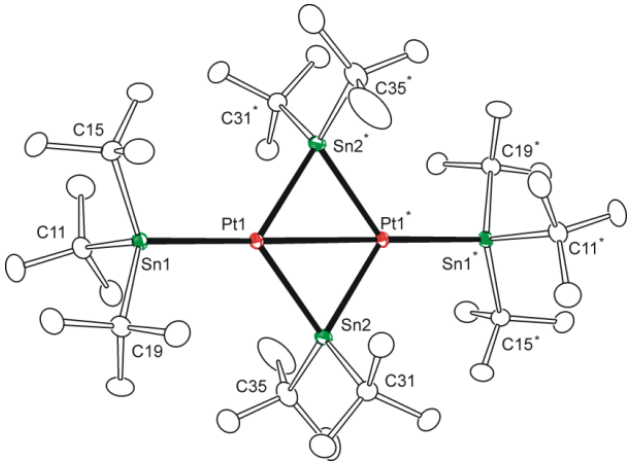

Figure 2.4 The molecular structure of $[H_2Pt(\mu\text{-}SnBu^t_2)(SnBu^t_3)]_2$, **2.4**.

Activation of CO by Pt-Sn complex: The reaction between two equivalents of Bu^t_3SnH dissolved in hexane and $Pt(COD)_2$ was repeated in the presence of CO gas at room temperature. The progress of the reaction was monitored by IR spectroscopy. We observed new peaks corresponding to the CO stretching region in hexane solution after

10 minutes during the course of reaction. The reaction mixture was filtered through silica plug to yield a green compound $Pt(CO)_2(SnBu^t_3)_2$, **2.5**, in 91% yield. This compound is analogous to compound **2.3**, and we assume that the hydride ligands in $(H)_2Pt(SnBu^t_3)_2$, were substituted by two CO ligands to afford the green-colored 16 electron Pt(II) mononuclear complex **2.5** (see Scheme 2.5). Adams et al. recently reported a similar Pt(II) carbonyl complex with $GePh_3$ ligands, $Pt(CO)_2(GePh_3)_2$,[101] and Braunschweig group prepared an analogous Pt(0) carbonyl complex with phosphine ligands $[(Cy_3P)_2Pt(CO)_2]$.[102]

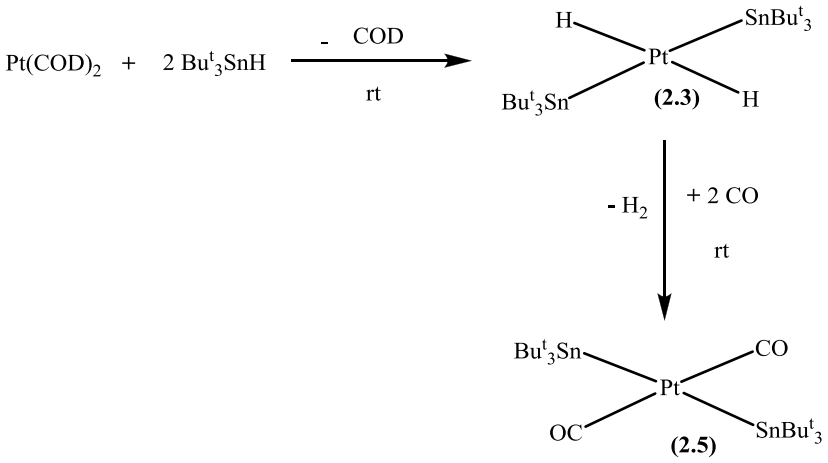

Scheme 2.5

Compound **2.5** has also been isolated as a bi-product in the reaction of $Pt_2Ru_4(CO)_{18}$ with Bu^t_3SnH in refluxing hexane solvent. The Pt(II) carbonyl complex **2.5** in solid state is stable in air for several hours, but decomposes slowly after 24 hours at room temperature. The compound **2.5** was characterized by a combination of ^1H NMR, single crystal X-ray crystallography, and IR spectroscopy. The molecular structure of complex **2.5** is shown in Figure 2.5. The complex has a square planar geometry common for Pt(II) 16 electron complexes, and CO ligands are bonded to the Pt in a *trans* position with

respect to each other. This arrangement can be attributed to the presence of bulky tin ligands favoring *trans* addition to relieve the Pt from steric repulsions. The Pt-Sn bond length for compound **2.5** is 2.7317 Å, slightly longer than that observed in compound **2.1**. The Pt1-C1 bond length (1.894 Å) is in the same range as reported for similar Pt-carbonyl complexes.[101]

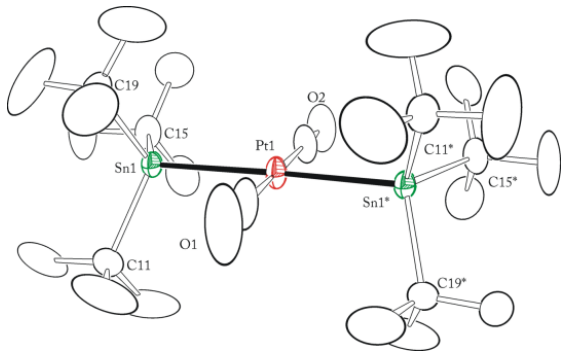

Figure 2.5 The molecular structure of $Pt(CO)_2(SnBu^t_3)_2$, **2.5**.

The IR spectrum of **2.5** in hexane solution shows a single strong absorption peak corresponding to a υ_{CO} stretching frequency at 2007 cm^{-1} in agreement with a *trans*-conformation. The CO ligands on $Pt(CO)_2(SnBu^t_3)_2$ are labile and they can be substituted with other ligands. Based on this approach, we have synthesized new Pt-Sn bimetallic complexes with isocyanide and NHC ligands. The details about synthesis and properties of these complexes can be found in chapters 3 and 4.

Reaction of $Pt(COD)_2$ with excess of Bu^t_3SnH: We have further explored the reaction of $Pt(COD)_2$ with an excess of Bu^t_3SnH in benzene solution. Drop-wise addition of Bu^t_3SnH dissolved in benzene to $Pt(COD)_2$ at room temperature in a glove box, followed by slow evaporation of solvent afforded light yellow crystals covered with brown oily residue. Crystals were washed with dichloromethane several times to yield

pure crystals of compound **2.4** in decent yields, in comparison to the addition of only two equivalents of Bu^t_3SnH.

Compound **2.4**, with four hydride ligands, is a 30 electron unsaturated symmetrical dinuclear Pt-Sn cluster complex. Each platinum has two terminal hydride ligands: one bridging $SnBu^t_2$ group and one terminal $SnBu^t_3$ group (see Figure 2.6).

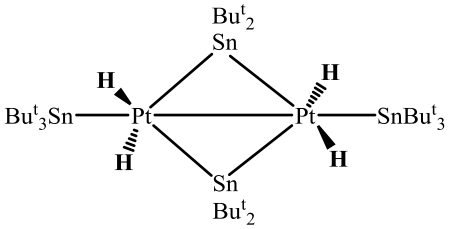

Figure 2.6 The line drawing for Pt(IV) complex $[H_2Pt(\mu\text{-}SnBu^t_2)(SnBu^t_3)]_2$, **2.4**.

The ^1H NMR spectrum of compound **2.4** in toluene-d_8 solvent confirms the presence of four hydride ligands. The hydride peaks appear at -3.45 ppm with appropriate one-bond coupling to Pt and two-bond coupling to Sn. The Pt-Pt bond length in compound **2.4** is 3.0877 Å, longer than the average Pt-Pt single bond distance {(2.70 Å)[101, 103, 104]}. In the analogous Pt-Ge dinuclear complex $[(GePh_3)(CO)Pt(\mu\text{-}GePh_2)]_2$, a Pt-Pt bond distance of 2.8394 (3) Å was reported.[101] We suspect that the longer bond length in **2.4** is due to sterics induced by bulky tin ligands.

The Pt(IV) tetrahydride complex **2.4** is resistant to moisture and air in the solid state, and poorly soluble in most organic solvents. Solubility can be increased by heating the solution. Compound **2.4** is stable in solution up to 100 °C for four hours but on prolonged heating the *tert*-butyl groups cleave off from the tin, producing isobutane gas and un-identified tin bi-products. A similar phenomenon was observed with $Fe_2(CO)_8(\mu$-

$SnBu^t_2$) cluster complex[105] in refluxing toluene solution. The details of this process are discussed in chapter 5.

Proposed reaction mechanism for the formation of 2.4: The following reaction mechanism is proposed based on experimental observations. The first step is the oxidative addition of two equivalents of Bu^t_3SnH to the Pt center followed by reductive elimination of the COD ligand to yield the unstable, highly reactive intermediate compound **2.3**. The second step is the cleavage of one *tert*-butyl group from the Bu^t_3Sn group to yield the proposed intermediate compound **2.6** accompanied by the abstraction of a hydride by the cleaved *tert*-butyl group to produce isobutane gas (see Scheme 2.6).

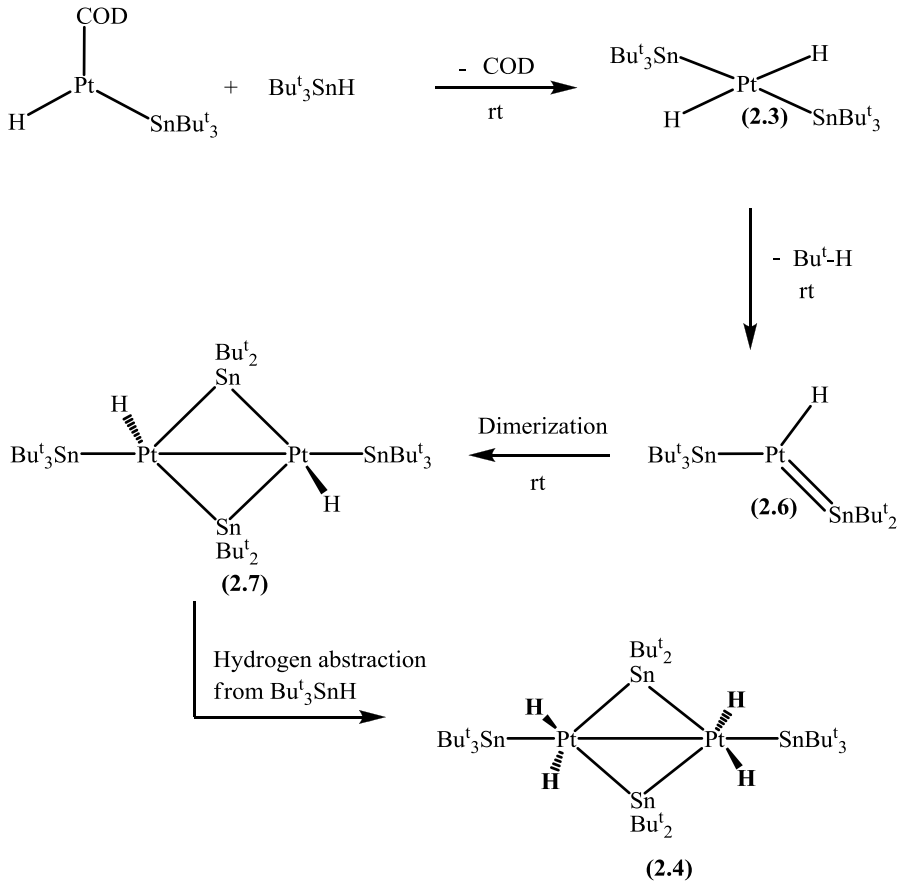

Scheme 2.6

We do observe peaks corresponding to free isobutane in the ^{1}H NMR spectrum when the reaction is performed in toluene-d_8 solution in the NMR tube. Cleavage of an alkyl group from organotin ligands bonded to transition metals has been previously observed.[106,107] Compound **2.6** dimerizes at room temperature to afford a 28 electron unsaturated dinuclear Pt-Sn bimetallic complex $[HPt(\mu\text{-}SnBu^t_2)(SnBu^t_3)]_2$, **2.7**. The unusual electronic unsaturation at platinum initiates the abstraction of hydride from excess Bu^t_3SnH to yield compound **2.4** (see Scheme 2.6). The activation of Si-H and C-H bonds is a common feature of unsaturated Pt complexes. The Bercaw group recently demonstrated the activation of cycloalkanes at a cationic Pt complex.[108, 109] An increase in the product yield in the presence of excess Bu^t_3SnH supports this reaction mechanism and we have not been able to isolate the 28 electron species **2.8**.

Another possible intermediate in the oxidative addition of two equivalents of Bu^t_3SnH to the $Pt(COD)_2$ is $Pt(COD)(SnBu^t_3)_2$, see Scheme 2.3 on page 20. A similar intermediate was observed by Adams et al.[110] in the reaction of $Pt(COD)_2$ with Ph_3SnH (see Eq. 3), and also by the Glocking group in the oxidative addition of Me_3SnH to the $[Pt(Ph_2PCH_2)_2)_2]$ complex.[85]

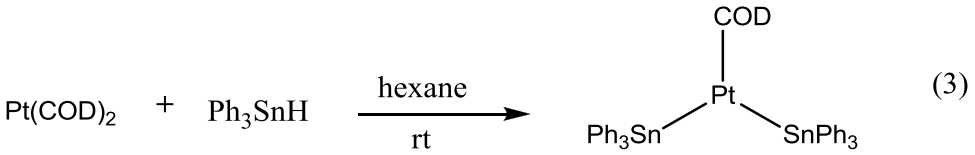

(3)

Low yields (5%) for the formation of **2.4** in the course of the reaction of $Pt(COD)_2$ with excess of Bu^t_3SnH can be attributed to the formation of unidentified oily tin bi-products. Computational modeling of this compound and theoretical calculations on

intermediate complexes will be more helpful to gain further insight into the reaction mechanism.

Reaction of 2.4 with D_2 gas: Addition of D_2 gas to compound **2.4** at room temperature affords $[D_2Pt(\mu\text{-}SnBu^t_2)(SnBu^t_3)]_2$, **2.8**, in quantitative yield. Compound **2.8** was characterized by ^1H NMR and mass spectrometry. The proton NMR shows only one single peak for the *tert*-butyl groups on Sn ligand; no splitting of the peaks due to H-D coupling was observed in the hydride region. The structure of **2.8** is similar to that of compound **2.4**, where hydride ligands are substituted by deuterium atoms.

Activation of CO by $[H_2Pt(\mu\text{-}SnBu^t_2)(SnBu^t_3)]_2$, 2.4: The dinuclear Pt-Sn complex **2.4** activates CO gas reversibly at room temperature both in solid state and in solution. When a hexane solution of **2.4** is exposed to CO gas at room temperature, the solution color turns dark yellow instantaneously to afford $[H_2(CO)Pt(\mu\text{-}SnBu^t_2)(SnBu^t_3)]_2$, **2.9**. Compound **2.9** is moderately stable. Removal of the CO atmosphere by applying vacuum or introducing argon gas results in regeneration of the starting material in quantitative yield (see Eq. 4).

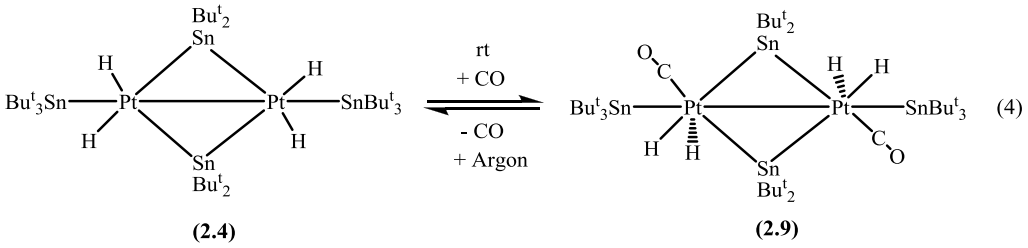

(2.4) **(2.9)** (4)

The solubility of dinuclear Pt-Sn carbonyl complex **2.9** is better than that of compound **2.4**, but it decomposes readily when exposed to air while in solution. The

compound **2.9** was also characterized by a combination of ^{1}H NMR, single crystal X-ray crystallography, and IR spectroscopy.

The molecular structure of **2.9** is shown in Figure 2.7. Compound **2.9** is a 34 electron dinuclear Pt-Sn cluster complex. Its structure is similar to compound **2.4** except that the CO ligands are added in *trans*-positions to each other. The Pt-Pt bond distance (3.1894 (6) Å) in compound **2.9** is slightly longer than that observed in compound **2.4** (3.0149 A). The Pt1-C11(1.929 Å) bond distance is consistent with the known Pt-C distance in Pt-carbonyl complexes (1.888 Å).[101] The CO groups lie perpendicular to the plane of Pt_2Sn_2 square to avoid steric repulsion from tin ligands.

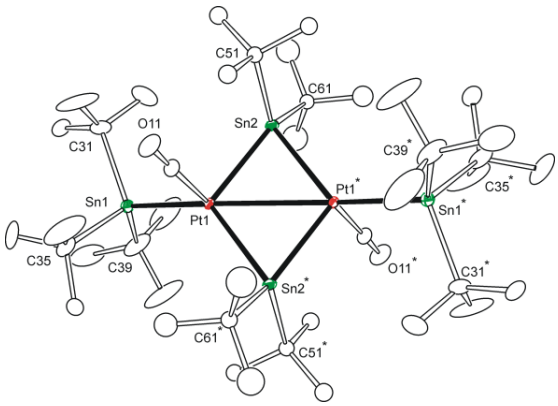

Figure 2.7 The molecular structure for $[H_2(CO)Pt(\mu\text{-}SnBu^t_2)(SnBu^t_3)]_2$, **2.9**.

With the addition of CO, there is a dramatic shift in the hydride resonance of hydride ligands on Pt. In toluene-d_8 solution, hydride peak resonance appears at - 12.78 ppm for compound **2.9** and for compound **2.4** it appears at - 3.445 ppm (see Figure 2.8). This might be due to the increased electron density around platinum by the back donation of electrons from the CO ligands. The coupling constant for one bond coupling to Pt in

compound **2.9** is $^{1}J_{Pt\text{-}H}$ = 702 Hz, slightly lower than the $^{1}J_{Pt\text{-}H}$ = 905 Hz observed for precursor compound **2.4**.

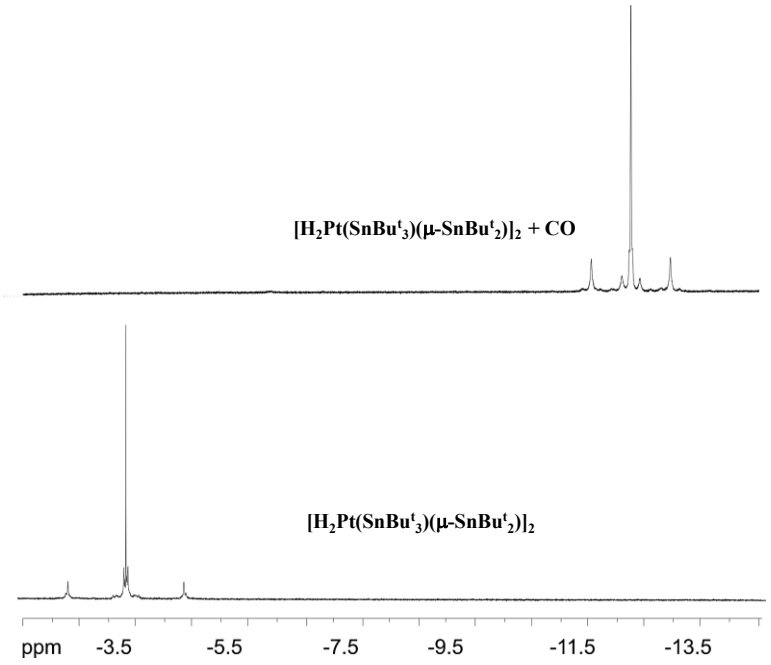

Figure 2.8 ^{1}H NMR spectrum in hydride region for compound **2.4** and compound **2.9**.

The ratio of integration of *tert*-butyl groups on Sn to that of hydride peak was 22.5:1, corresponding to the presence of four hydride ligands. This confirms that the addition of CO takes places without the elimination of hydride ligands. Appropriately, when the reaction was performed in toluene-d_8 solution in an NMR tube filled with CO gas, no free hydrogen peaks were observed in the ^{1}H NMR spectrum.

Activation of *tert*-butyl isocyanide(CNBu^{t}) by [H$_2$Pt(μ-SnBu$^{t}_2$)(SnBu$^{t}_3$)]$_2$, 2.4: Similar to CO addition, compound **2.4** readily adds CNBu^{t} at room temperature. When two equivalents of isocyanide were added to compound **2.4** in hexane solution, solution turns dark yellow indicating the formation of the Pt_2Sn_4 isocyanide complex [H$_2$Pt(CNBu^{t})(μ-SnBu$^{t}_2$)(SnBu$^{t}_3$)]$_2$, **2.10** (see Eq. 5).

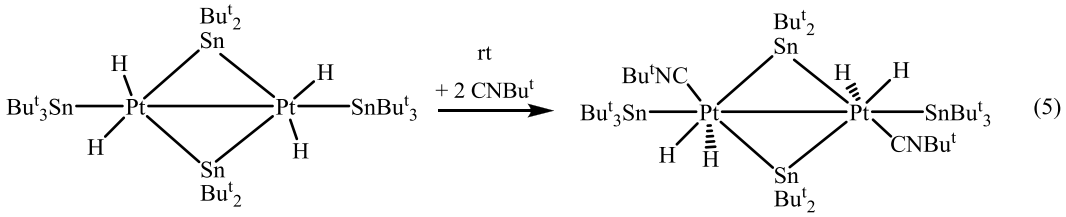

(2.4) **(2.10)** (5)

The compound **2.10** was characterized by a combination of ^{1}H NMR and single crystal X-ray crystallography. The molecular structure of compound **2.10** is shown in Figure A.1 in Appendix A. It has a similar structure to that of compound **2.9**. The two isocyanide ligands were added in a *trans* manner. A similar dinuclear Pt isocyanide complex, $[(Et_3P)Pt(CNBu^t)(\mu\text{-}SiPh_2)]_2$, with two terminal isocyanide ligands was reported recently by Yamada et al.[111] The Pt-Pt distance in this complex (3.9058 Å) is higher than the Pt-Pt distance observed in compound **2.10**.

The hydride resonance in the ^{1}H NMR spectrum appears at - 13.55 ppm for compound **2.10**. The ^{1}H NMR spectrum of **2.10** in C_7D_8 (toluene-d_8) solvent at room temperature shows broad peaks for *tert*-butyl isocyanide and Sn satellites overlapping; this made it difficult to acquire information about the number of hydride ligands in complex **2.10**.

Addition of $CNBu^t$ to the dinuclear Pt-Sn complex **2.4** is not reversible, in contrast to the addition of CO. It has been observed that compound **2.10** loses hydride ligands upon storage for several days, even at - 25 °C in the solid state. We assume that due to steric repulsion between *tert*-butyl groups of isocyanide and *tert*-butyl groups of Sn ligands, hydride ligands may be eliminated as free hydrogen (see Eq. 6).

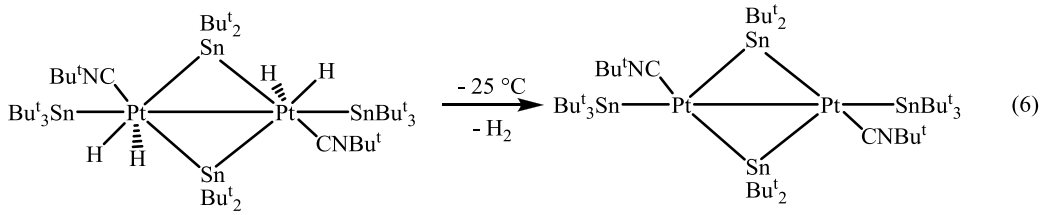

(2.10) (6)

When only one equivalent of isocyanide is added to compound **2.4**, a new Pt-Sn bimetallic complex with one isocyanide ligand $[H_4(CNBu^t)Pt_2(\mu\text{-}SnBu^t_2)_2(SnBu^t_3)_2]$, **2.11** was isolated. The compound **2.11** was characterized by a combination of ^{1}H NMR and single crystal X-ray crystallography. The molecular structure of compound **2.11** is shown in Figure A.2 in Appendix A. In the ^{1}H NMR, the hydride resonance for compound **2.11** also appears in the same region, as of **2.10**, at -13.55 ppm. We observed only one hydride resonance in the hydride region. We believe that the hydride ligand may be dynamically exchanging on both platinum atoms; this is the only possible explanation for the single hydride resonance.

While crystallizing the compound **2.10** in hexane solution in a glove box freezer at -25 °C, we observed that **2.10** slowly decomposes over a period of 3-5 days to yield compound **2.11** (see Eq. 7).

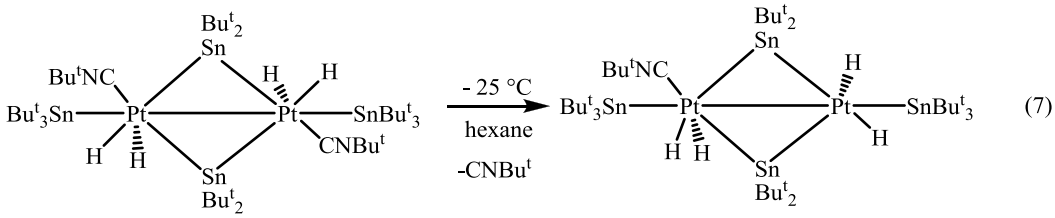

(2.10) **(2.11)** (7)

In order to gain more insight into the number and nature of hydride ligands in the dinuclear Pt-isocyanide complex $[H_4(CNBu^t)Pt_2(\mu\text{-}SnBu^t_2)_2(SnBu^t_3)_2]$, variable

temperature NMR (VT NMR) was performed over a range of -90 °C to 90 °C in toluene-d_8 solution in a sealed NMR tube. The changes in the resonance of hydride peaks in hydride region were monitored with the change in temperature. The stack of ^{1}H NMR s at different temperatures is shown in Figure 2.9.

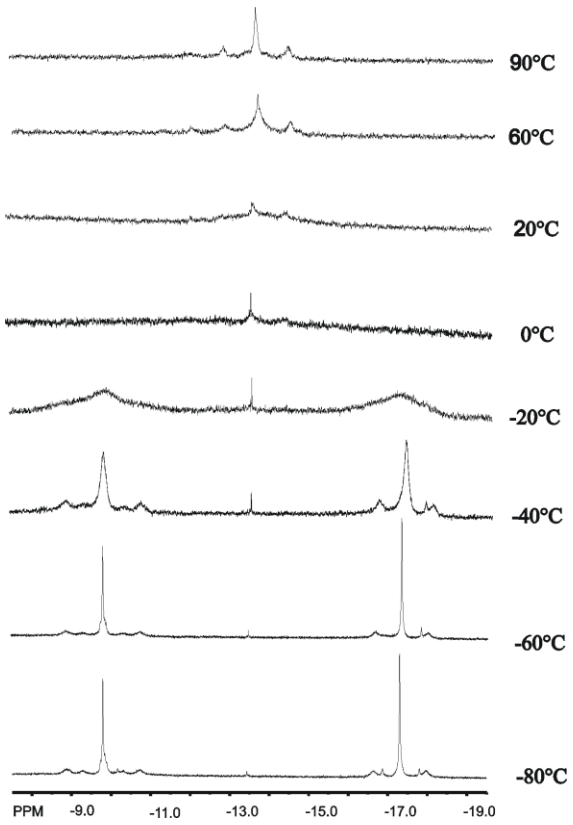

Figure 2.9 The ^{1}H NMR spectra at 400 MHz of compound **2.11** at various temperatures in toluene-d_8 solvent.

Based on the VT NMR spectrum, we deduced that the hydride ligands are exchanging dynamically from the terminal to the bridging position. As the temperature lowered down to -25 °C, we observed two well resolved peaks separated in the hydride region of the ^{1}H NMR spectrum with appropriate coupling to Pt and Sn, which apparently converges to a single broad peak as the temperature is raised to room temperature. One possible mechanism is intramolecular exchange of the hydride ligands. Based on the

information gathered from the VT-NMR spectrum, we believe that the hydride ligand is bridging the Pt and $SnBu^t_2$ group, and changing to the terminal position dynamically. The $CNBu^t$ group is also dynamically migrating from the terminal position to the equivalent bridging position, giving a single broad and average resonance peak at room temperature (see Scheme 2.7). Bridge-terminal coordination rearrangement of $CNBu^t$ ligands has been observed previously by Grundy et al..[112, 113]

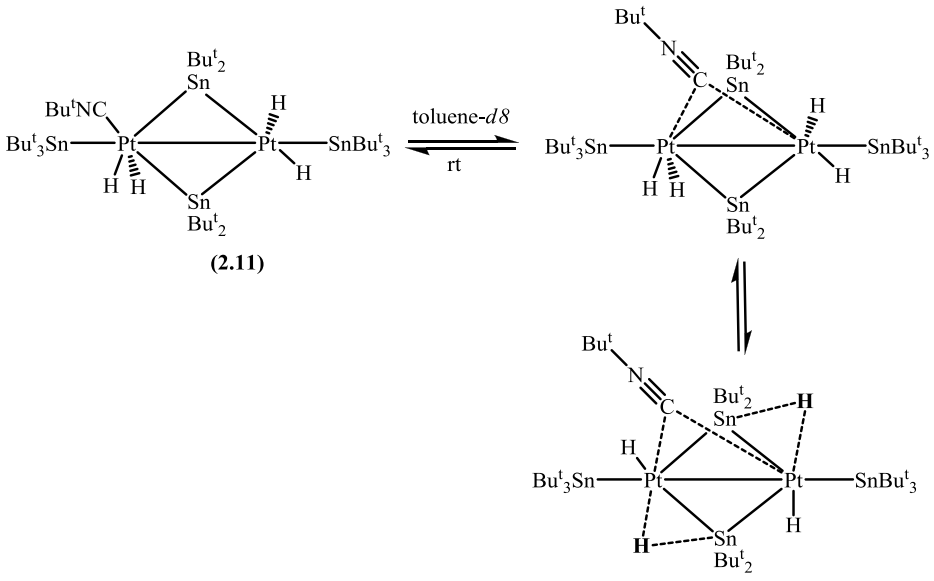

(2.11)

Scheme 2.7

The compound **2.11** is very reactive and decomposes at room temperature. We were unable to characterize this compound through other spectroscopic techniques. The neutron diffraction technique is the best method to identify the number and nature of hydride ligands in multinuclear cluster complexes.[114] Characterization of the dinuclear Pt-Sn isocyanide cluster complexes **2.10** and **2.11** with the help of neutron diffraction technique will aid in complete understanding of the structure and reactivity of these complexes. We have also synthesized mononuclear Pt-Sn isocyanide complexes by

ligand substitution on compound **2.5**. The details of the synthetic method and their reactivity in small molecule activation will be discussed in chapter 4.

Synthesis of dinuclear Pd-Sn complex $[H_2Pd(\mu\text{-}SnBu^t_2)(SnBu^t_3)]_2$, 2.12: Given the interest in synthesizing mononuclear Pd-Sn complex [HPd(allyl)($SnBu^t_3$)] analogous to compound **2.1** [HPt(COD)($SnBu^t_3$)], we have investigated the oxidative addition reaction of Bu^t_3SnH with Pd(allyl)(Cp) at room temperature. To orange crystals of Pd(allyl)(Cp) complex dissolved in hexane solution was added 1.5 equivalents of Bu^t_3SnH and stirred at room temperature for 15 minutes to afford yellow-colored crystals of the dinuclear Pd-Sn complex $[H_2Pd(\mu\text{-}SnBu^t_2)(SnBu^t_3)]_2$, **2.12** in 42% yield.

The reaction proceeds in a similar manner as that observed in the case of formation of compound **2.4**, through the reactive intermediate complex $Pd(H)_2(SnBu^t)_3$ which dimerizes at room temperature to afford compound **2.12** (see Scheme 2.8).

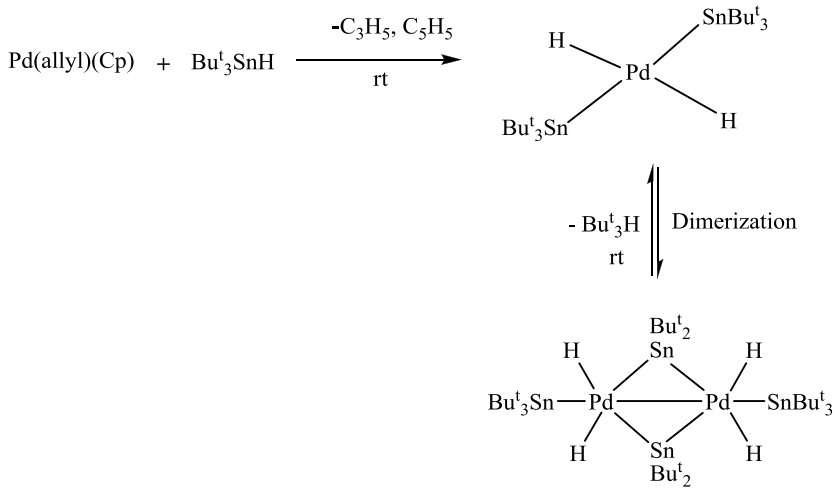

(2.12)

Scheme 2.8

The dinuclear Pd-Sn complex **2.12** is also obtained in 47% yield from the reaction of two equivalents of Bu^t_3SnH dissolved in distilled toluene and Pd(0) precursor complex $Pd(dba)_2$ stirred at room temperature for four hours (see Eq. 8). The dinuclear Pd-Sn complex **2.12** is readily soluble in all organic solvents and stable in air in the solid state. Prolonged exposure to air while in the solution yields unidentified black Pd metallic particles.

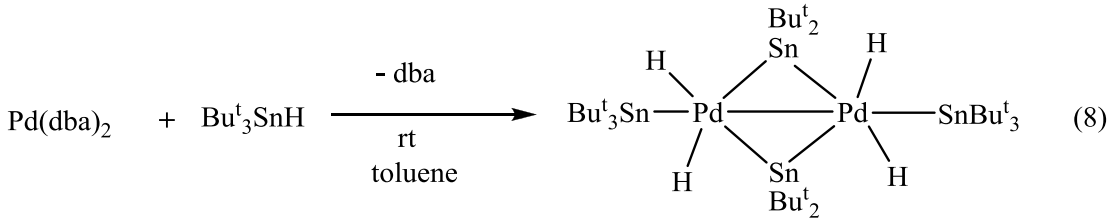

(8)

The compound **2.12** was characterized by a combination of ^1H NMR, X-ray crystallography and mass spectrometry. The molecular structure of **2.12** is shown in Figure 2.10.

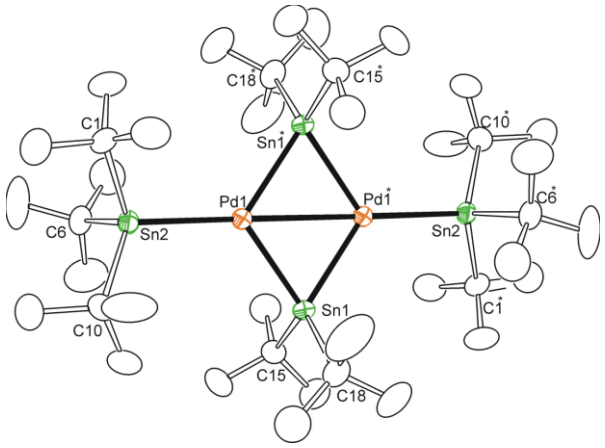

Figure 2.10 The molecular structure for $[H_2Pd(\mu\text{-}SnBu^t_2)(SnBu^t_3)]_2$, **2.12**.

Compound **2.12** has a similar structure to **2.4** and reacts with CO in a similar manner as that observed with the dinuclear Pt-Sn complex **2.4**. The reactivity of **2.12** with other

small molecules is still under investigation. We have also synthesized a few mononuclear Pd-Sn complexes with isocyanide ligands and their synthesis and characterization will be discussed in chapter 4.

2.3. Conclusions

We have investigated the oxidative addition reactions of Bu^t_3SnH with the Pt(0) complex $Pt(COD)_2$ at room temperature. We have isolated both mono- and dinuclear Pt-Sn bimetallic complexes. Bulky *tert*-butyl groups on tin increased the stability of compounds **2.1** and **2.4**, facilitating the isolation of unsaturated mononuclear Pt(II) and dinuclear Pt(IV) complexes.

The bulky *tert*-butyl tin ligands favored the addition of CO ligands in *trans* positions to relieve the steric repulsion around the Pt metal center in $Pt(CO)_2(SnBu^t_3)_2$. Stability and reactivity of these complexes were examined to understand the effect of bulky organotin ligands, in promotion of small molecule activation by unsaturated Pt-Sn complexes.

The CO adds to the compound **2.4** reversibly at room temperature, and the hydride ligands were kept intact during the addition of two CO ligands to the electronically unsaturated dinuclear Pt-Sn complex **2.4**. Variable temperature NMR experiments on compound **2.11** confirmed the dynamic exchange of hydride ligands shifting from bridging mode to terminal mode at lower temperatures. It was observed that the addition of $CNBu^t$ to compound **2.4** was not reversible.

Even though we were able to synthesize and characterize unsaturated 16 electron mononuclear, and 30 electron dinuclear Pt-Sn complexes, no 14 electron unsaturated

mononuclear Pt-Sn complexes were isolated during the oxidative addition of Bu^t_3SnH to the Pt(0) precursor complex. Addition of more bulky organic groups on Sn might favor the synthesis and isolation of 14 electron Pt-Sn complexes. We continued further research of our mononuclear Pt(II) complexes **2.1** and **2.5** by substituting COD and CO ligands by NHC ligands, respectively with the aim of isolating 14 electron Pt-Sn complexes. These results will be discussed in next chapter.

2.4. Experimental section

General Data

Unless indicated otherwise, all reactions were performed under an atmosphere of Argon. Reagent grade solvents were dried by the standard procedures and were freshly distilled prior to use. Infrared spectra were recorded on a Nicolet 380 FT-IR spectrophotometer. ^1H NMR were recorded on a Bruker 300 and 400 spectrometer operating at 300.13 MHz and 399.99 MHz respectively. Elemental analyses were performed by Columbia Analytical Services (Tuscon, AZ). Mass spectrometric measurements performed by a direct–exposure probe using electron impact ionization (EI) were made on a VG 70S instrument at the University of South Carolina, Columbia, SC. Tertiary butylisocyanide, $CNBu^t$, and $Pd(dba)_2$ were purchased from Strem chemicals and used without further purification. Bis(1,5-cyclooctadiene)platinum, $Pt(COD)_2$,[115] and tri-*tert*-butylstannane, Bu^t_3SnH,[105] and Pd(allyl)(cp)[116] were prepared according to the published procedures. Silica gel (60-200 μm, 70-230 mesh) used for chromatographic seperations was purchased from Silicycle.

Synthesis of Pt($SnBu^t_3$)(COD)(H), 2.1.

In a glove box, under an atmosphere of argon, 25.0 mg of Bu^t_3SnH (0.087 mmol) dissolved in 3 mL of freshly distilled hexane were added to 30.0 mg of $Pt(COD)_2$ (0.073 mmol). The reaction mixture immediately turned dark brown. The reaction mixture was stirred at room temperature for an additional 10 minutes and filtered through a kimwipe and the solvent was evaporated under argon gas flow until the mixture was completely dry. The yellowish-brown solid residue was redissolved in diethylether and placed in a -20 °C freezer overnight, which gave crystalline Pt($SnBu^t_3$)(COD)(H), **2.1**, covered with black oily residue. After washing the crystalline product with isopropyl alcohol (3 x 0.3 mL), 13.2 mg (30% yield) of **2.1** was obtained. Spectral data for **2.1**: ^{1}H NMR (C_6D_6, rt, in ppm): δ = 5.80 (m, $^2J_{Pt-H}$ = 51.4 Hz, $^3J_{Sn-H}$ = 5.0 Hz, 2H; CH- cod), 5.45 (m, $^2J_{Pt-H}$ = 44.7 Hz, $^3J_{Sn-H}$ = 6.5 Hz, 2H; CH- cod), 1.82-1.51 (broad m, 8H; CH_2-cod); 1.53 (s, $^3J_{Sn-H}$ = 52.5 Hz, 27H, $SnBu^t_3$); -3.74 (s, $^1J_{Pt-H}$ =1223.2 Hz, $^2J_{Sn-H}$ = 48.2 Hz, 1H, hydride).

Synthesis of [H_2Pt($SnBu^t_3$)(μ-$SnBu^t_2$)]$_2$, 2.4.

In a glove box, under an atmosphere of argon, 583 mg of Bu^t_3SnH {2.00 mmol (excess)} was dissolved in 1 mL of freshly distilled toluene was added slowly dropwise to 103 mg of $Pt(COD)_2$ (0.250 mmol) over a period of 20 minutes at room temperature with continuous stirring. The solvent was allowed to evaporate in a drybox overnight. The black-colored oily residue was washed with dichloromethane solvent several times until the solution was colorless, yielding 34 mg of **2.4** (5% yield). Yield is low because of unidentified side products. Spectral data for **2.4**: ^{1}H NMR (C_7D_8, rt, in ppm): δ = 1.58 (s, 36 H, $SnBu^t_2$, $^2J_{Sn-H}$ = 64 Hz), 1.50 (s, 54H, $SnBu_3^t$, $^3J_{Sn-H}$ = 60 Hz); -3.71 (s, 4H,

hydride, $^{1}J_{Pt\text{-}H}$ = 905 Hz, $^{2}J_{Sn\text{-}H}$ = 32 Hz). (Note: The compound is moderately soluble in any solvent and solubility increases with temperature). Mass Spec. EI/MS *m*/*z*. 1440 (M^{+}), 1383 (M^{+}-Bu^{t}), 1326(M^{+}-2Bu^{t}). The isotope pattern is consistent with the presence of two platinum and four tin atoms.

Synthesis of $Pt(SnBu^{t}_{3})_{2}(CO)_{2}$, 2.5.

A 53.0 mg (0.128 mmol) amount of $Pt(COD)_2$ was transferred into a 10 mL schlenk tube and the flask was evacuated and refilled with argon several times. 80.0 mg of $Bu^{t}_{3}SnH$ (0.274 mmol) dissolved in 8 mL of distilled hexane solvent was added to $Pt(COD)_2$ under argon. The brown-colored reaction mixture was stirred at room temperature for 5 minutes after which time CO gas was bubbled through the solution for an additional 30 minutes. The solution was filtered through a silica plug to give a green color solution. The solvent was removed in *vacuo* to obtain 98.0 mg (91% yield) of green solid. Spectral data for **2.5**: ^{1}H NMR ($CDCl_3$, rt, in ppm): δ = 1.38 (s, 54 H, $SnBu^{t}_{3}$, $^{3}J_{Sn\text{-}H}$ = 59 Hz. ^{1}H NMR (C_6D_6, rt, in ppm): δ = 1.44 (s, 54 H, $SnBu^{t}_{3}$, $^{3}J_{Sn\text{-}H}$ = 59 Hz); IR ν_{CO} (cm^{-1} in hexane): 2007(vs). Elemental Anal, calc.: C, 37.56; H, 6.54 % Found: C, 37.77; H, 6.42 %.

Synthesis of $[D_2Pt(SnBu^{t}_{3})(\mu\text{-}SnBu^{t}_{2})]_2$, 2.8 from 2.4.

7.0 mg (0.005 mmol) amount of crystalline **2.4** was charged into NMR tube containing 0.6 mL of C_6D_6 solvent. The NMR tube was sealed under argon, and heated in a water bath for 20 minutes to dissolve crystalline **2.4**. D_2 gas was purged through solution for 5 minutes and ^{1}H NMR indicated complete consumption of starting **2.4** in quantitative yield to **2.8**. The solvent was evaporated the solvent in a glove box

overnight to obtain 6.9 mg of crystalline **2.8** (98%). Spectral data for **2.8**: ^{1}H NMR (C_6D_6, rt, in ppm): δ = 1.55 (s, 36 H, $SnBu^{t}_2$, $^{2}J_{Sn-H}$ = 64 Hz), 1.48 (s, 54H, $SnBu_3^{t}$, $^{3}J_{Sn-H}$ = 60 Hz). Mass Spec. EI/MS *m*/*z*. 1444 (M^+), 1386 (M^+-Bu^t), 1327 (M^+-2Bu^t). The isotope pattern is consistent with the presence of two platinum and four tin atoms.

Synthesis of $[H_2(CO)Pt(SnBu^{t}_3)(\mu\text{-}SnBu^{t}_2)]_2$, 2.9.

In a 10 mL schlenk tube, under atmosphere of argon, 25.0 mg of **2.4** dissolved in 3 mL of hexane was transferred. The reaction mixture was colorless and turbid. With the purging of CO gas through solution at room temperature for 10 min, the solution color turned to dark yellow and the solution became clear. The reaction mixture was filtered through a kimwipe and crystallized in an ice bath (0 °C) under a CO gas stream to obtain 20.0 mg (75% yield) of yellow crystals (after washing two times with small portions of hexane). Spectral data for **2.9**: ^{1}H NMR (C_7D_8, rt, in ppm): δ = 1.69 (s, 36 H, $SnBu^{t}_2$, $^{2}J_{Sn-H}$ = 72 Hz), 1.45 (s, 54 H, $SnBu^{t}_3$, $^{3}J_{Sn-H}$ = 61 Hz); - 12.77 (s, 4H, hydride, $^{1}J_{Pt-H}$ = 702 Hz, $^{2}J_{Sn-H}$ = 28 Hz); IR ν_{CO} (cm^{-1} in hexane): 2163(w), 2027(vs), 2008 (m). Elemental Anal, calc.: C, 33.76; H, 6.20 % Found: C, 33.73; H, 6.16 %.

Conversion of 2.9 to 2.4 in solution.

In a 10 mL schlenk tube, 10.0 mg of **2.9** (0.006 mmol) was dissolved in 2 mL of hexane. The solvent was removed overnight in a glove box, during which time the color of the solution changed from yellow to colorless. This yielded 9.0 mg (93% yield) of crystalline **2.4**. The ^{1}H NMR spectrum shows complete conversion of starting material into **2.4**.

Synthesis of $[H_2(CNBu^t)Pt(SnBu^t_3)(\mu\text{-}SnBu^t_2)]_2$, 2.10.

In a 10 mL schlenk tube, under atmosphere of argon, 17.0 mg (0.011 mmol) of **2.4** dissolved in 3 mL of hexane was transferred. The reaction mixture was colorless and turbid. 2.0 mg of $CNBu^t$ was added to the solution at room temperature and stirred for 10 min, after which the solution color turned to dark yellow and the solution became clear. The reaction mixture was filtered in a glove box through a kimwipe and the filtrate was placed in a -20 °C freezer overnight which gave 13.5 mg (77% yield) of crystalline $[H_2(CNBu^t)Pt(SnBu^t_3)(\mu\text{-}SnBu^t_2)]_2$, **2.10**. Spectral data for **2.10**: ^{1}H NMR (C_7D_8, rt, in ppm): δ = 1.63 (s, 36 H, $SnBu^t_2$, $^2J_{Sn\text{-}H}$ = 72 Hz), 1.52 (s, 54 H, $SnBu^t_3$, $^3J_{Sn\text{-}H}$ = 61 Hz), 1.01 (s, 18 H, Bu^t on isocyanide); - 13.58 (s, 4H, hydride, $^1J_{Pt\text{-}H}$ = 697 Hz, $^2J_{Sn\text{-}H}$ = 34 Hz).

Synthesis of $[H_4(CNBu^t)Pt_2(SnBu^t_3)_2(\mu\text{-}SnBu^t_2)_2]$, 2.11.

In a 10 mL schlenk tube, under atmosphere of argon, 17.0 mg (0.011 mmol) of **2.4** dissolved in 3 mL of hexane was transferred. The reaction mixture was colorless and turbid. 1.0 mg of $CNBu^t$ (only one equivalent) was added to the solution at room temperature and stirred for 10 minutes, after which the solution color turned to dark yellow and solution became clear with some insoluble precipitate of **2.4**. The reaction mixture was filtered in a glove box through a kimwipe and the filtrate was placed in a -20 °C freezer overnight which gave 8.5 mg (51% yield) of crystalline $[H_4(CNBu^t)Pt_2(SnBu^t_3)_2(\mu\text{-}SnBu^t_2)_2]$, **2.11**. Spectral data for **2.11**: ^{1}H NMR (C_7D_8, rt, in ppm): δ = 1.63 (s, 36 H, $SnBu^t_2$, $^2J_{Sn\text{-}H}$ = 72 Hz), 1.52 (s, 54 H, $SnBu^t_3$, $^3J_{Sn\text{-}H}$ = 61 Hz);

1.01 (s, 18 H, Bu^t on isocyanide); - 13.58 (s, 4H, hydride, $^1J_{Pt-H}$ = 697 Hz, $^2J_{Sn-H}$ = 34 Hz).

Synthesis of $[H_2Pd(SnBu^t_3)(\mu\text{-}SnBu^t_2)]_2$, 2.12 from Pd(Allyl)(Cp).

In a glove box, under an atmosphere of argon, 42.0 mg of Bu^t_3SnH (0.141 mmol) dissolved in 1mL of freshly distilled hexane was added to 20.0 mg of Pd(allyl)(Cp) dissolved in hexane (0.094 mmol) at room temperature with continuous stirring for 20 min. The dark red-colored solution immediately turned black on addition of Bu^t_3SnH. The solvent was allowed to evaporate in drybox overnight to yield light yellow crystals of $[H_2Pd(SnBu^t_3)(\mu\text{-}SnBu^t_2)]_2$, **2.12** covered with black residue. The crystals were washed with hexane 2 times to yield 25.0 mg (42 % yield) of pure crystalline **2.12**. Spectral data for **2.12**: ^{1}H NMR (C_6D_6, rt, in ppm): δ = 1.56 (s, 36 H, $SnBu^t_2$, $^2J_{Sn-H}$ = 68 Hz), 1.50 (s, 54 H, $SnBu^t_3$, $^3J_{Sn-H}$ = 60 Hz); - 1.50 (s, 4H, hydride).

Synthesis of 2.12 from Pd(0) complex $Pd(dba)_2$.

In a glove box, under an atmosphere of argon, 21.0 mg of Bu^t_3SnH (0.069 mmol) dissolved in 1mL of freshly distilled toluene was added to 20.0 mg of $Pd(dba)_2$ dissolved in toluene (0.034 mmol) at room temperature with continuous stirring for four hours. After four hours the violet-colored solution turned black. The solvent was allowed to evaporate in a drybox under stream of argon flow to obtain black residue. The black residue was redissolved in dichloromethane and filtered through a small silica plug to obtain yellow filtrate. The filtrate was left overnight in -25 °C freezer to yield light yellow crystals of 10 mg (47% yield) of **2.12**.

2.5. Crystallographic analyses

Colorless crystals of **2.1** suitable for diffraction analysis were grown by slow evaporation of a solution of **2.1** in hexane solvent under a slow stream of argon gas at 0 °C (ice-water bath). Green-colored crystals of **2.5** suitable for diffraction analysis were grown by slow evaporation of solvent from a hexane solution in a -80 °C freezer. Light yellow crystals of **2.4** suitable for diffraction analysis were grown by slow evaporation of solvent from a benzene solution at room temperature in a glove box.

Dark yellow crystals of **2.9** suitable for diffraction analysis were grown by slow evaporation of a solution of **2.4** in hexane solvent under a slow stream of CO gas at 0 °C (ice-water bath). Red crystals of **2.10** were grown at room temperature from the evaporation of benzene solution under argon flow. Orange crystals of **2.11** and yellow crystals of **2.12** suitable for diffraction analysis were grown by slow evaporation of solvent from a hexane solution at -20 °C in a glove box.

Each data crystal was mounted onto the end of a thin glass fiber using Paratone-N. X-ray intensity data were measured by using a Bruker SMART APEX2 CCD-based diffractometer using Mo Kα radiation (λ = 0.71073 Å).[117] The raw data frames were integrated with the SAINT+ program by using a narrow-frame integration algorithm. Corrections for Lorentz and polarization effects were also applied with SAINT+. An empirical absorption correction based on the multiple measurement of equivalent reflections was applied using the program SADABS. Both structures were solved by a combination of direct methods and difference Fourier syntheses, and refined by full-matrix least-squares on F^2, by using the SHELXTL software package.[118] Crystal data,

data collection parameters, and results of the analyses are listed in Tables A.1- A.4 in Appendix A.

Compound **2.1** crystallized in the monoclinic crystal system. The systematic absences in the intensity data identified the unique space group $P2_1/n$. The hydride ligand was located from the difference map but refined on its positional parameters with a fixed isotropic thermal parameter.

Compound **2.4** crystallized in the monoclinic crystal system. The systematic absences in the intensity data identified the unique space group $P2_1/n$. With Z = 4, there is half a formula equivalent of the molecule present in the asymmetric unit that has crystallographic center of inversion symmetry.

Compound **2.5** crystallized in the monoclinic crystal system. The systematic absences in the intensity data identified the unique space group $C2/c$. With Z = 4, there is half a formula equivalent of the molecule present in the asymmetric unit that has crystallographic center of inversion symmetry.

Compound **2.9** crystallized in the triclinic crystal system. The space group $P\ \bar{1}$ was assumed and confirmed by the successful refinement and solution of the structure. The CO-Pt-Pt-CO core in the molecule is disordered over two orientations which were refined with fixed site-occupancy factors in the ratio 50/50. The two orientations are mirror images of each other and the CO-Pt-Pt-CO core as seen in Figure 2.11 are offset by an angle of 12.07°.

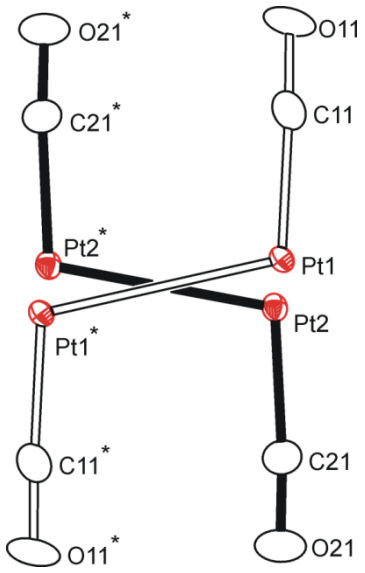

Figure 2.11 An ORTEP of the disordered CO-Pt-Pt-CO core in **2.9**.

Atoms Pt1 and Pt1* lie above and below the Sn1-Sn2-Sn1*-Sn2*plane at a distance of 0.4411(4) Å, while atoms Pt2 and Pt2* lie above and below the Sn1-Sn2-Sn1*-Sn2* plane at a distance of 1.0020(4) Å. The carbon atoms of the two Bu^t groups attached to atom Sn2 are also disordered. The disorder components in the Bu^t groups were located from the difference map and refined with fixed site-occupancy factors in the ratio 50/50. The hydride ligand was not located and included in the refinement. There is still minor disorder present in the structure which was not accounted for due to satisfactory low R values (R1 = 3.91%) during the final stages of the refinement cycles.

Compound **2.10** crystallized in the triclinic crystal system. The space group $P\ \bar{1}$ was assumed and confirmed by the successful refinement and solution of the structure. With Z = 4, there are two half a formula equivalent of the molecules present in the asymmetric unit that has crystallographic center of inversion symmetry. Half a molecule of benzene from the crystallization solvent, co-crystallized with the complex.

Compound **2.11** crystallized in the monoclinic crystal system. The systematic absences in the intensity data identified the unique space group $P2_1/c$. There was a slight disorder in the solvent molecule, which was not accounted for due to satisfactory low R values (R1 = 3.81%) during the final stages of the refinement cycles. Compound **2.12** crystallized in the monoclinic crystal system. The systematic absences in the intensity data identified the unique space group $P2_1/c$. With Z = 4, there is half a formula equivalent of the molecule present in the asymmetric unit that has crystallographic center of inversion symmetry.

Chapter 3: Synthesis and characterization of Pt-Sn complexes containing NHC ligand

3.1. Background

Synthesis and crystallographic characterization of stable NHC ligands by Arduengo et al.[119] triggered widespread use of TM-NHC complexes (TM = transition metal, NHC = N-heterocyclic carbene) in catalysis as a potential substitute for phosphine ligands.[120] Pioneering work by Hermann further fuelled extensive research on use of NHC ligands for synthesis of low coordinate transitional metal complexes.[121-123] Strong donor capability and the stable M-C(NHC) bond facilitate formation of coordinately-unsaturated transition metal systems with enhanced catalytic activity. A wide range of donor capability and access to varying bulkiness on heteroatom (N) substituents offers a valuable tool to tailor the geometry and coordination around the metal center for a chosen application. Grubbs[124-126] and Nolan[127-130] developed the field of olefin metathesis using NHC substituted metal complexes, and Organ[131-133] extended the application of NHC ligands in cross coupling reactions too. Recently, more emphasis has been placed on activation of small molecules, and also C-H bond activation, at electronically unsaturated TM-NHC complexes (TM = Ir, Rh, Pd, Ni).[33, 134, 135]

Nolan et.al. reported a 14 electron mononuclear Pd complex [Pd(IPr)(PCy_3)], with a terminal NHC ligand. It was found that H_2 has been activated by a Pd(0) complex containing the NHC ligand to yield a monomeric palladium(II)dihydride complex, [$Pd(H)_2$(IPr)(PCy_3) (see Scheme 3.1).[136] The Hazari group also demonstrated activation of CO_2 at Ni in a Ni-NHC complex.[137] The Pt(0) carbene complexes have been also used in catalytic hydrosilylation of olefins with high selectivity and efficiency.[138]

Pd-, Rh-, Ir-, and Au-NHC complexes are well studied and their catalytic activity is known to be superior to corresponding phosphine complexes,[139, 140] but there is less understanding on the effect of addition of another metal on the reactivity of TM-NHC complexes. Synthesis of bimetallic NHC carbene clusters will aid in understanding the role of electronic and steric effects an additional metal exerts on the transition metal.

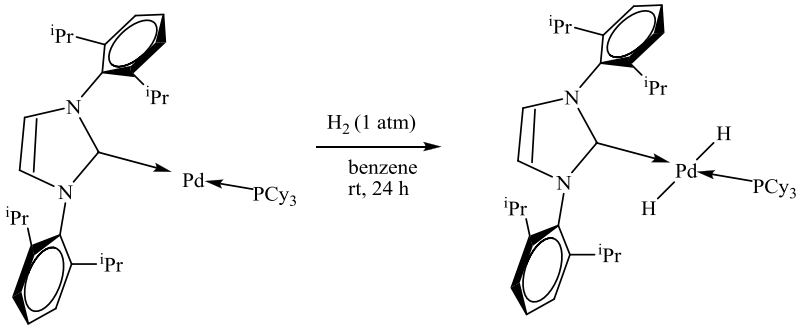

Scheme 3.1

There are several examples for Pt-NHC carbene complexes with a wide range of substituents on hetero atom N or on Pt, but very few Pt-NHC carbene complexes containing Pt-group(IV) metal bond are known in the literature. A Pt-stannaborane complex with an IPr {(1,3-bis(2,6-diisopropylphenyl)imidazole-2-ylidene)} NHC ligand has been prepared by the Marx group and its molecular structure was also determined.[141] A 14 electron Y-shaped tri-coordinate Bis(silyl)platinum(II)-NHC complex was isolated and characterized by the Marko group as an intermediate in hydrosilylation reaction (see Eq. 1).[142]

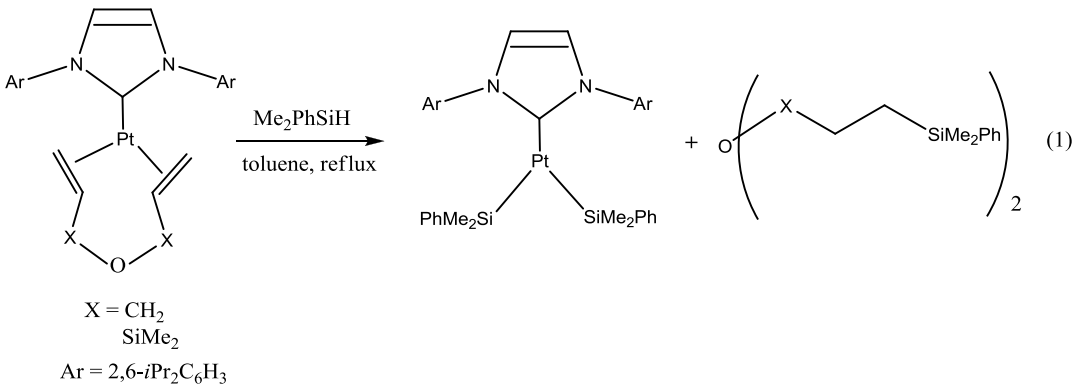

Wang et al. examined the reactivity of R_3Sn-BAM ligands, {R = Me or Ph, BAM = bis(7-azaindol-1-yl)}, with $[PtR_2(\mu\text{-}SMe_2)]_n$ to prepare unexpected novel Pt(IV) complexes, Pt(*N*,*C*,*N*-BAM)($SnMe_3$)R_2 (R = Me or Ph), via oxidative cleavage of the C_{BAM}-Sn bond[143] (see Scheme 3.2).

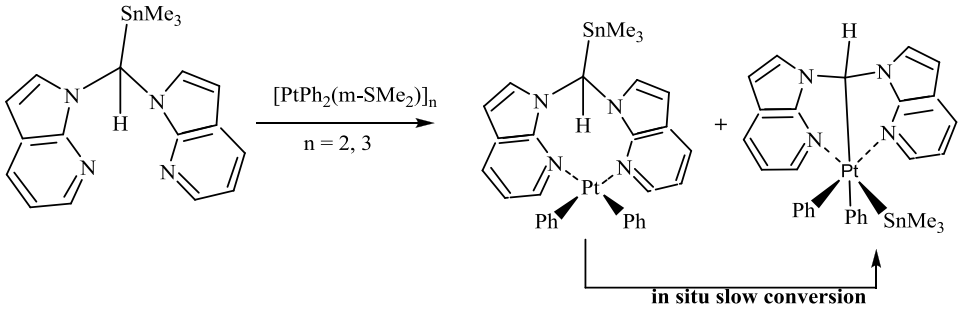

Scheme 3.2

Only one or two Pt-Sn complexes possessing ylidene NHC ligands have been reported in the literature so far.[141] It is interesting to examine the effect of NHC ligands on the reactivity of Pt-Sn complexes in homogeneous catalysis. The bimetallic synergetic effect in Pt-Sn NHC complexes has to be explored further to identify efficient homogeneous catalysts for hydroformylation and small molecule activation.

Rh-NHC complexes are considered potential catalysts for hydroformylation of olefins.[139, 144, 145] The stability of Rh(I)-NHC bond and the presence of NHC ligand in the

coordination sphere of rhodium during hydroformyaltion aids in the activation of hydrogen to generate a hydrido complex, which is the active form of hydroformylation catalyst (see Figure 3.1).[146]

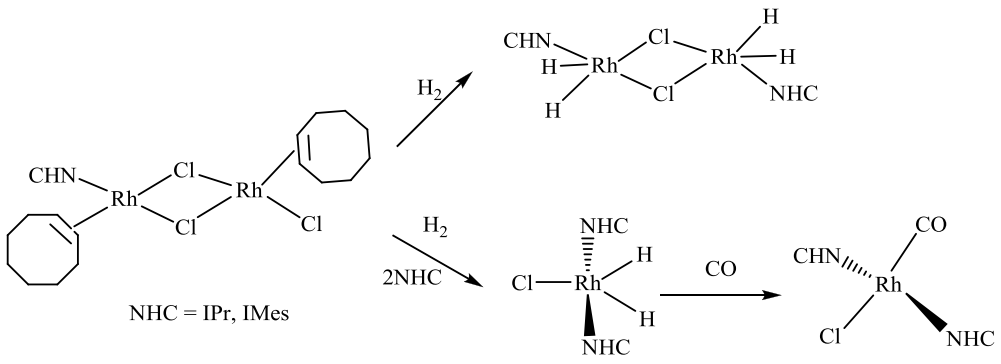

Figure 3.1 Formation of hydrido dimeric and monomeric Rh-NHC complexes.

Recently, C-4 bound carbenes are gaining much attention owing to unusual reactivity compared to C-2 bound carbenes.[147, 148] The C-4 bound abnormal carbenes have high donor capability and are exceptionally basic ligands than their C-2 bound analogues (see Figure 3.2 for C-2 bound and C-4 bound metal carbene complex).[148]

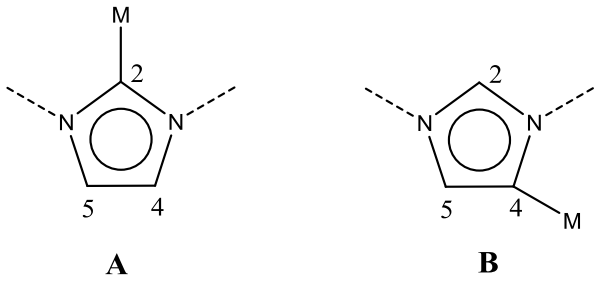

Figure 3.2 Formation of M-NHC complexes A) normal C-2 bound NHC complex B) abnormal C-4 bound NHC complex.

In rhodium (III)-NHC complexes it was observed that with the C-4 bound NHC coordination mode; the catalytic activity of the rhodium center increases and allows for

efficient transfer in the hydrogenation of ketones in ^{i}PrOH/KOH.[148] Similar evidence has been provided for enhanced catalytic activity of palladium bis(carbene) complexes with C-4 NHC coordination in olefin hydrogenation.[149]

The activation of a C-H bond of ylidene NHC carbene (IBu^{t}) in the reaction between Pt(COD)Me$_2$ and IBu^{t} (N,N′-di-*tert*-butylimidazol-2-ylidene) NHC ligand has been reported by the Nolan group.[150] The authors explained the role of sterics in isolation of the abnormal C-4 bound Pt-NHC complex (see Eq. 2). The C-4 bound ruthenium and osmium complexes are also isolated in good yields from the room temperature addition of one equivalent of IBu^{t} to a THF solution of $Ru_3(CO)_{12}$ and $Os_3(CO)_{12}$ with the elimination of CO.[151, 152]

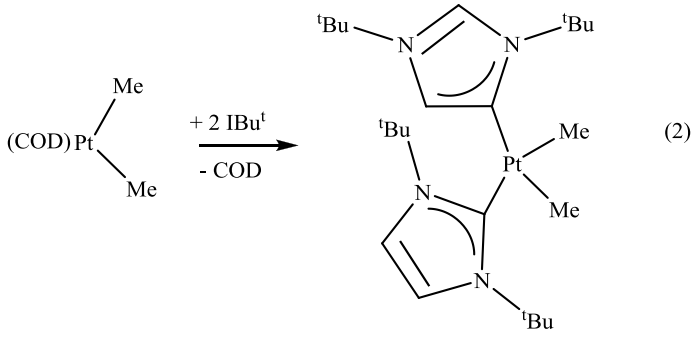

(2)

Very few complexes of Pt with C-4 bound NHC ligands have been reported thus far.[153] We have adopted an easier synthesis method: substitution of labile CO ligands on [Pt(SnBu$^{t}_3$)(CO)$_2$] with the bulky IBu^{t} NHC ligand to synthesize stable abnormal C-4 bound carbene complexes of Pt-Sn. We have examined the reactivity of the C-4 bound Pt-Sn NHC complex with transition metal clusters and small molecules. The results of these studies are presented in this chapter.

Promising results in small molecule activation by our Pt-Sn bimetallic complexes prompted us to synthesize stable Pt-Sn NHC complexes for application in hydroformylation of olefins. A bulky two-electron donating N,N′-di-*tert*-butylimidazol-2-ylidene (IBu^t) ligand has been used to replace the four electron donating COD ligand in Pt(II) complex [$HPt(COD)(SnBu^t_3)$] to yield the electronically unsaturated dinuclear Pt complex $[HPt(IBu^t_2)(SnBu^t_3)]_2$ with the bridging hydride ligands. Effects of substitution of bulky ylidene-NHC carbene (IBu^t) on Pt-Sn complexes in activation of small molecules like H_2, CO, and alkenes were studied to gain an insight into factors responsible for the reactivity of these Pt-Sn complexes. The viability of using these complexes as potential hydroformylation and hydrogenation catalysts was also investigated.

3.2. Results and discussion

A toluene solution of bulky NHC carbene ligand, N, N′-di-*tert*-butylimidazol-2-ylidene (IBu^t) was added at room temperature in a drybox to a toluene solution of [$HPt(COD)(SnBu^t_3)$], **2.1**, to yield a red solid Pt-Sn carbene complex, $[Pt(SnBu^t_3)(IBu^t)(H)]_2$, **3.1**, in 75% yield. The COD ligand in compound **2.1** is replaced by IBu^t carbene to yield perhaps an unstable intermediate 14 electron Pt(II)-NHC complex [$Pt(SnBu^t_3)(IBu^t)(H)$], **3.2**. We were unable to isolate and characterize compound **3.2**. Compound **3.2** dimerizes at room temperature to afford a dinuclear unsaturated Pt-Sn complex with C-2 bound NHC ligand (see Scheme 3.3). This work has been done in collaboration with Prof. Carl. D. Hoff at the University of Miami.

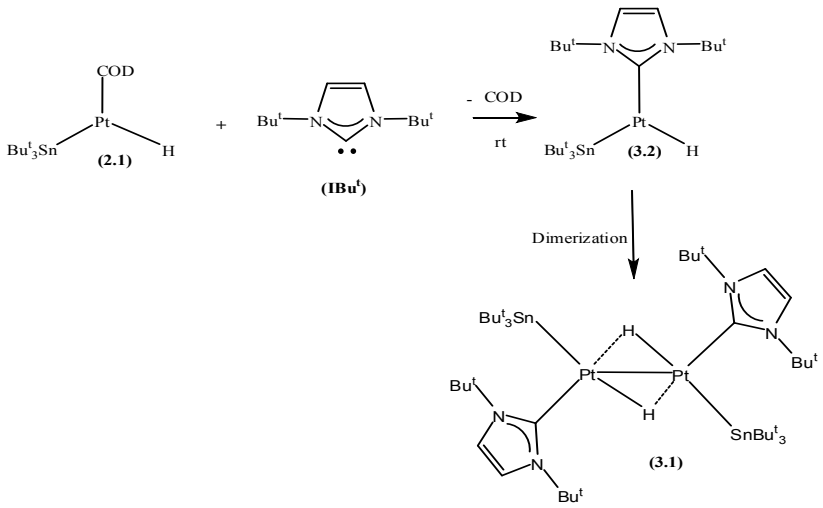

Scheme 3.3

Pt(II)carbene complex $[Pt(SnBu^t_3)(IBu^t)(H)]_2$, **3.1**, is stable in air in the solid state, but decomposes slowly in solution at room temperature on exposure to air. The molecular structure of **3.1** is shown in Figure 3.3.

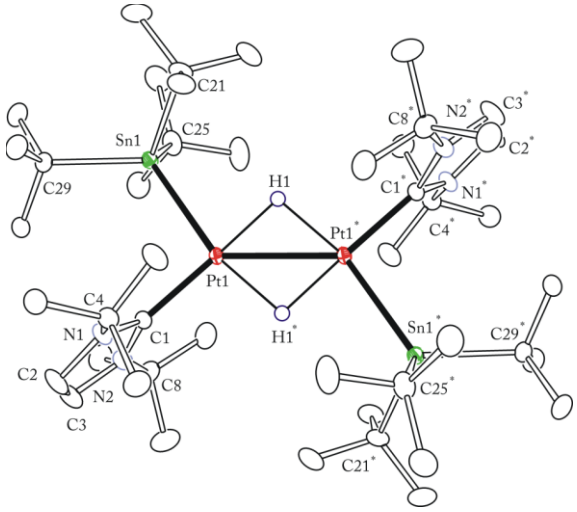

Figure 3.3 The molecular structure of $[HPt(SnBu^t_3)(IBu^t)]_2$, **3.1**.

Compound **3.1** has two terminal $SnBu^t_3$ groups and two IBu^t groups positioned *trans* to each other. The Pt-Pt metal bond is bridged by two hydrides and the presence of two

hydride ligands was confirmed by ^{1}H NMR. The Pt-Pt bond length in compound **3.1** is 2.681 Å and is consistent with Pt-Pt single bonds. Stone has reported a similar complex $[Pt(\mu\text{-}H)(SiR_3)PR_3]_2$,[154] with a Pt-Pt distance of 2.692 Å. The hydride resonance was observed at -5.35 ppm with appropriate one-bond coupling to Pt and two-bond coupling to Sn. Compound **3.1** is also an unsaturated 28 electron Pt dinuclear complex with bulkytin and C-2 bound IBu^t ligands.

We performed Fenske-Hall molecular orbital calculations on compound **3.1** to obtain a clear picture of its unsaturation.[155-157] These calculations revealed the presence of a low lying unoccupied molecular orbital, LUMO, which could accommodate two valence bonding electrons to bring the electron count to 30, making the cluster saturated. The LUMO, which is shown in Figure 3.4, shows that the contours of the orbital are based predominantly on the platinum atoms. Based on these observations, we believe that the addition or activation of small molecules will be occurring at the Pt metal center.

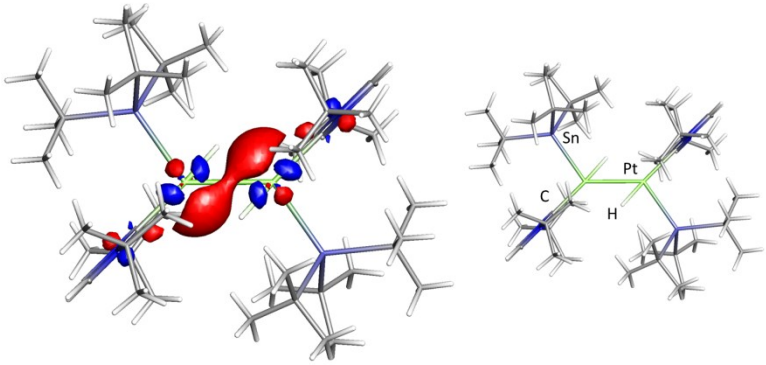

Figure 3.4 The LUMO orbital for $[HPt(SnBu^t_3)(IBu^t)]_2$, **3.1**.

Activation of a CO molecule by Pt-Sn NHC complex 3.1: To investigate the reactivity of the unsaturated dinuclear platinum complex **3.1**, we exposed this complex to

a CO atmosphere at room temperature. The orange-red colored solution of **3.1** in toluene solvent turned to light yellow instantaneously upon addition of 1 atm of CO gas to yield [Pt($SnBu^t_3$)($IBut_2$)(CO)(H)], **3.3**, in a quantitative yield (90%). We observed that the Pt-Pt bond breaks with the addition of CO to afford the mononuclear Pt(II)-carbonyl compound [Pt($SnBu^t_3$)($IBut_2$)(CO)(H)], **3.3**, (see Eq. 3).

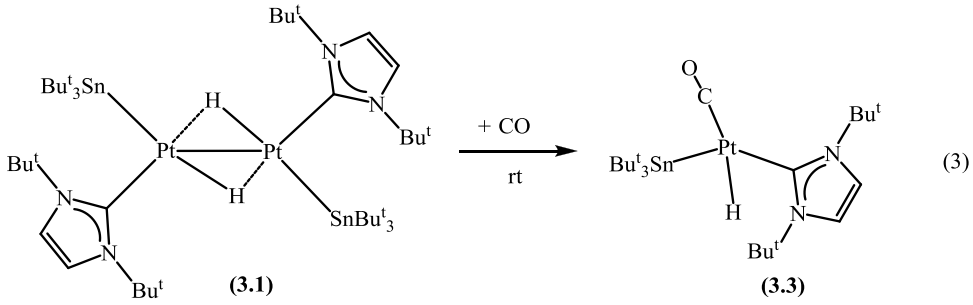

(3)

The compound **3.3** was characterized by a combination of ^{1}H NMR spectroscopy, single crystal X-ray diffraction technique, and IR spectroscopy. The molecular structure of compound **3.3** is shown in Figure 3.5. Compound **3.3** is a 16 electron mononuclear complex with the CO and hydride ligand positioned *trans* to each other. The position of the hydride ligand was determined and refined crystallographically.

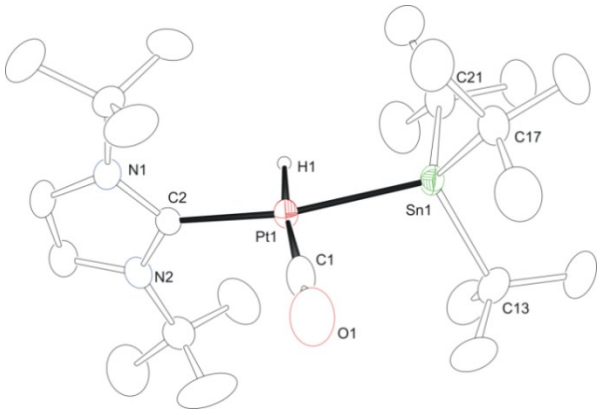

Figure 3.5 The molecular structure of [Pt($SnBu^t_3$)($IBut_2$)(CO)(H)], **3.3**.

The C(1)-Pt(1)-Sn(1) bond angle in compound **3.3** is 94.79^{o} and the C(1)-Pt(1)-C(2) bond angle has a value of 105.06^{o}. As seen from these bond angles, compound **3.3** seems to have distorted square planar geometry. The distortion from square planar is believed to be due to the small sterics of the hydride.

Compound **3.3** is stable at room temperature in the solid state, and can be handled in air. Addition of CO to compound **3.1** is irreversible. The ^{1}H NMR spectrum shows a single hydride resonance peak at -2.46 ppm with appropriate coupling to Pt and Sn. The IR spectrum of **3.3** in hexane solution shows a medium intensity peak at 2104 cm^{-1} for υ_{Pt-H} stretching frequency and a very strong peak for the Pt-bound carbonyl group at 1979 cm^{-1}. Pt complexes with terminal hydride ligands are known to have a υ_{Pt-H} stretching frequency in the range of 2050-2120 cm^{-1}.[158, 159]

Activation of H_2 molecule by Pt-Sn NHC complex 3.1: We further investigated the addition of H_2 with complex **3.1** at room temperature. The H_2 gas was purged through the C_6D_6 solution of complex **3.1** in a sealed NMR tube. After vigorous shaking for 5 minutes the ^{1}H NMR spectra of the reaction mixture indicated the disappearance of the hydride resonance peaks corresponding to complex **3.1**, and appearance of a new hydride resonance showing one-bond coupling to Pt and two-bond coupling to Sn (see Figure 3.6).

Similar to addition of CO to compound **3.1**, H_2 addition also proceeds through the breaking of Pt-Pt bond in dinuclear Pt(II)-NHC complex **3.1** to afford the mononuclear complex [Pt(SnBu$^{t}_3$)(IBut$_2$)(H)$_3$], **3.4**. We propose this pathway based on the presence of only one set of tin satellites in the ^{1}H NMR spectra of the reaction mixture after addition

of H_2 (see Figure 3.6). The number and nature of the hydride ligands in complex **3.4** have to be further investigated using neutron diffraction technique, and DFT calculations to know exact number of hydrides and mode of binding to the Pt center.

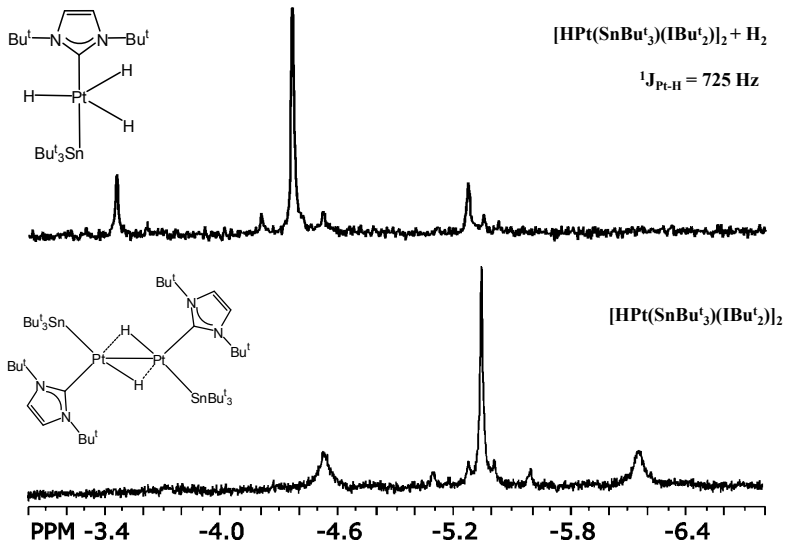

Figure 3.6 ^{1}H NMR spectrum of compound **3.1**and **3.3** in the hydride region.

The addition of H_2 to **3.1** is reversible at room temperature; replacing the H_2 atmosphere with argon gas results in formation of compound **3.1** (see Eq. 4).

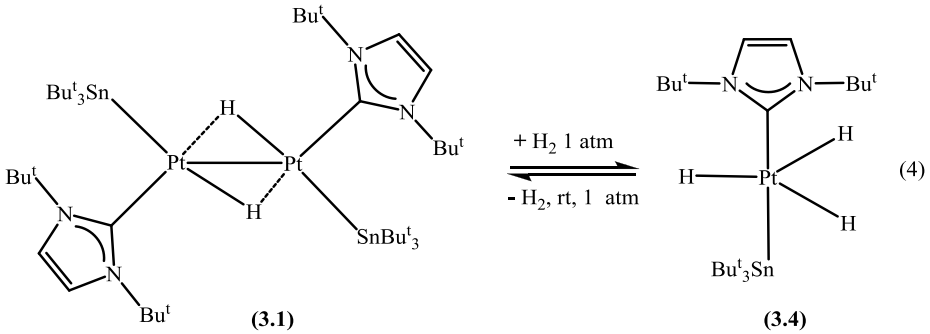

(4)

Recently, Nolan et al. prepared an analogous 14 electron Pd(0)dihydride complex [Pd(Ipr)$(H)_2(PCy_3)$] with IPr NHC ligand.[136] To our knowledge, Pt-carbene complexes with three hydrides are unknown; no precedent examples exist for comparison. A similar

dihydride Ir-NHC carbene complex has been also reported by Crabtree et al.[160] We were unable to isolate and characterize the compound **3.4** crystallographically.

Addition of D_2 to 3.1: Compound **3.1** also activates D_2 reversibly at room temperature in a similar manner to the activation of hydrogen. A ^1H NMR spectrum of the reaction mixture shows a splitting of the hydride peak into a triplet due to H-D coupling as shown in Figure 3.7. Replacing the D_2 atmosphere with argon gas results in the formation of compound **3.1**. There is a possibility of formation of three isotopomers in this reaction, and we believe that there is a dynamic exchange between these isotopomers.

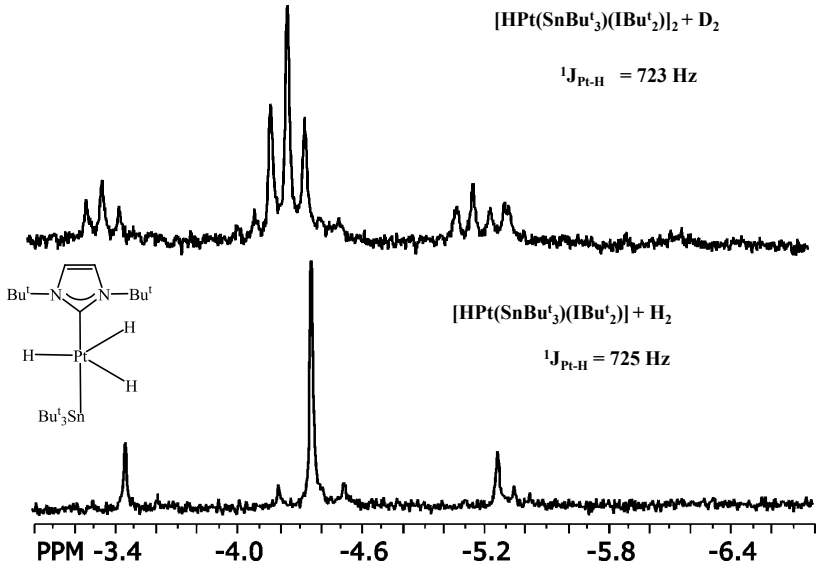

Figure 3.7 ^1H NMR spectrum in the hydride region for D_2 addition to compound **3.1**.

Advanced computational studies and variable temperature NMR experiments are required to fully characterize these isotopomers and to propose a feasible reaction mechanism for their formation.

Activation of ethylene by Pt-Sn NHC complex 3.1: With the aim of using compound **3.1** as potential hydroformylation catalyst, we have examined the reaction of ethylene with compound **3.1**. As observed in the case of the addition of CO to compound **3.1**, ethylene addition also yields a mononuclear Pt-carbene complex. The ethylene is bound in η^2 mode through π-bond to the Pt-metal to yield a 16 electron Pt-ethylene complex, $[Pt(SnBu^t_3)(IBu^t)(C_2H_4)]$ (**3.5**).

The addition of ethylene to **3.1** is also reversible both in the solid state and in solution at room temperature. Replacing the ethylene atmosphere with argon gas or by applying vacuum results in the formation of compound **3.1**. The crystals for X-ray diffraction were also grown under an ethylene atmosphere. Compound **3.5** was characterized by a combination of ^{1}H NMR spectroscopy and single crystal X-ray diffraction technique. The molecular structure of compound **3.5** is shown in Figure 3.8.

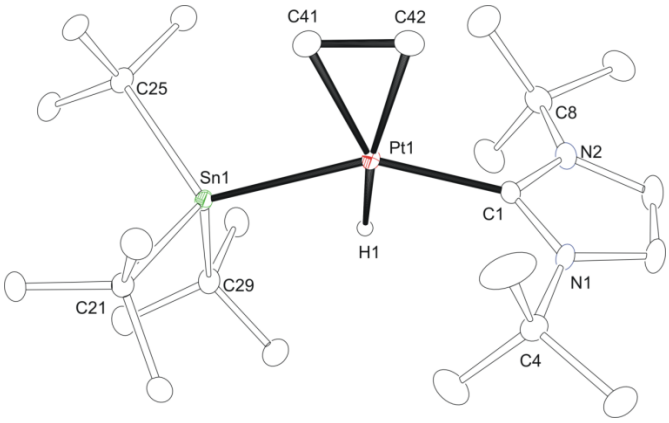

Figure 3.8 The molecular structure of $[Pt(SnBu^t_3)(IBu^t)(C_2H_4)]$, **3.5**.

Compound **3.5** has a structure similar to compound **3.3**; ethylene is added in the *trans* position to the hydride ligand and the position of the hydride ligand was determined and refined crystallographically at 100 K.

The presence of the hydride ligand was also confirmed by ^{1}H NMR spectroscopy. The proton resonance of the hydride ligand appears at -3.57 ppm with appropriate one-bond coupling to Pt and two-bond coupling to Sn. The C41-C42 (ethylene) bond distance in compound **3.5** is 1.410 Å, which is also seen in a similar ethylene-bound mononuclear Pt-complex $Pt(PPh_3)_2(C_2H_4)$, where the C=C bond length is 1.434 Å.[161]

Attempted catalytic hydroformylation reaction of ethylene with compound 3.1: The hydroformylation of ethylene with compound **3.1** was investigated in a small parr-reactor sealed with an equimolar mixture of H_2 and CO gas (1:1 ratio) at room temperature. The reactor was pressurized with an excess of ethylene gas to yield compound **3.5**. The progress of the reaction was monitored by ^{1}H NMR spectroscopy. After 24 hours we did observe the disappearance of peaks corresponding to ethylene complex **3.5** and complete conversion of compound **3.5** into Pt-carbonyl compound **3.3** (see Scheme 3.4).

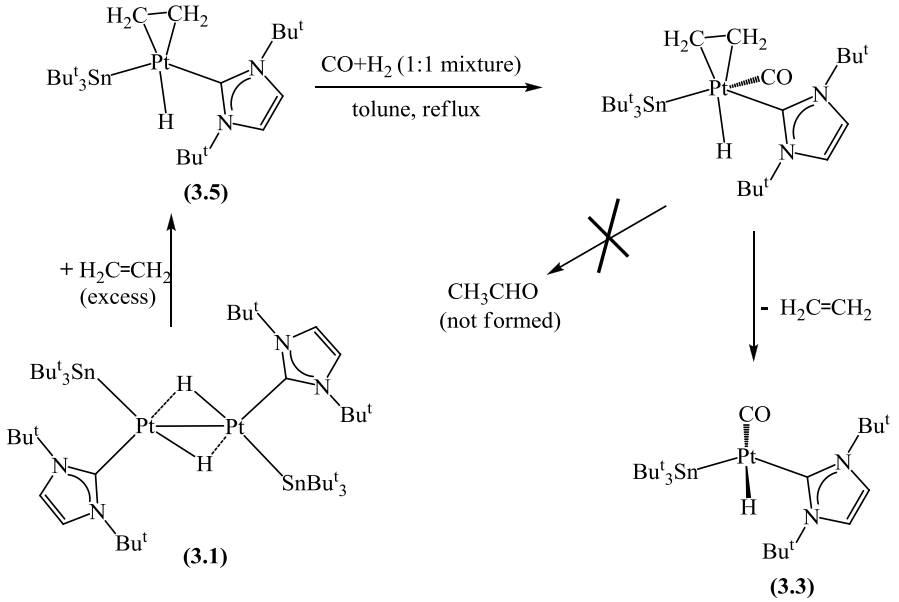

Scheme 3.4

Unfortunately, we were unable to identify any peaks corresponding to acetaldehyde in the ^{1}H NMR spectra of the reaction mixture. We have also repeated the reaction in refluxing toluene solution, but no products corresponding to the hydroformylation of ethylene were detected. Varying reaction conditions or modification of substituents on the nitrogen atom of the NHC ligand may promote hydroformylation of olefins. Further studies must be carried out to test the catalytic hydroformylation reaction of other alkenes in the presence of compound **3.1**.

Reaction of CO_2 with ethylene complex 3.5: The Hazari group demonstrated that Ni-NHC complexes possessing an allyl ligand are effective in the activation of CO_2.[137] A catalytic coupling reaction of ethylene with CO_2 to form lactones is considered one of the options to reduce global warming.[162, 163] We have also tested the reactivity of compound **3.5** in the activation of CO_2 at room temperature. We did see, however, that ethylene is displaced by CO_2 gas and converted back into the starting material **3.1** (see Eq. 5).

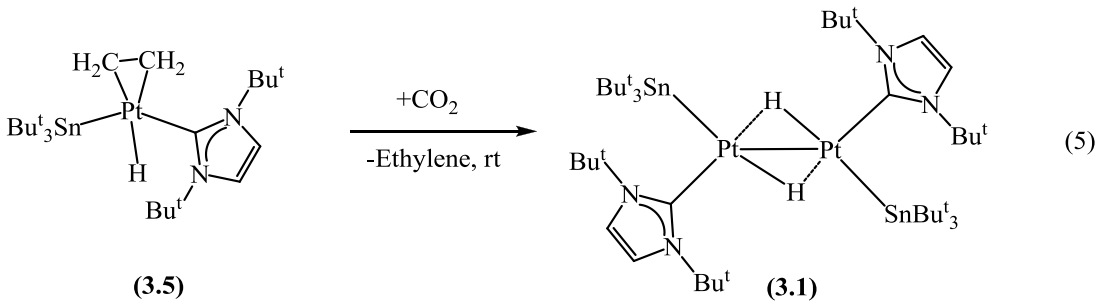

(3.5) **(3.1)** (5)

Activation of NH_3 by compound 3.1: We have further investigated the reactivity of compound **3.1** with NH_3 gas at room temperature. With the addition of NH_3 gas the solution color changes instantaneously from red to light yellow. The ^{1}H NMR spectrum of the reaction mixture indicates the formation of a new product

[Pt(NH_3)(H)($SnBu^t_3$)(IBu^t)], **3.6**, and the disappearance of peaks corresponding to compound **3.1**.

Addition of NH_3 to compound **3.1** is also reversible; by removing NH_3 atmosphere compound **3.6** loses the NH_3 ligand and dimerizes to yield compound **3.1** at room temperature (see Eq. 6).

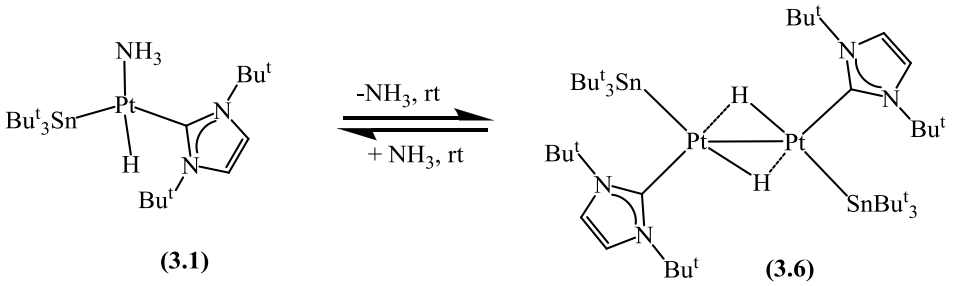

(6)

Several attempts were made to characterize compound **3.6** crystallographically, but no suitable X-ray quality crystals have been obtained thus far. Compound **3.6** slowly decomposes in the air to yield a Pt(IBu^t)$_2$ complex by the reductive elimination of Bu^t_3SnH and NH_3 (see Eq. 7). A similar phenomenon was previously reported for Pt-carbene complexes by the Nolan group .[150]

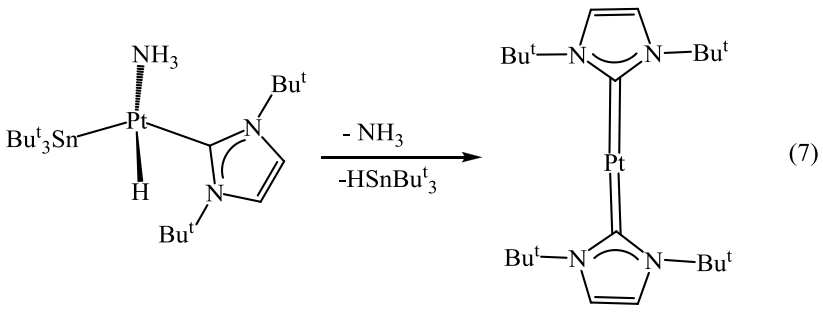

(7)

Synthesis of abnormal C-4 bound Pt-Sn NHC complex: In an attempt to study the lability of CO ligands on one of our Pt-Sn complexes Pt($SnBu^t_3$)$_2$(CO)$_2$ (**2.5)**, we observed the C-H bond activation of IBu^t NHC ligand by compound **2.5**. When the

green-colored hexane solution of compound **2.5** was treated with one equivalent of IBu^t NHC carbene at room temperature in a drybox, the color of the solution slowly turned to orange after 30 minutes of stirring. Evaporation of solvent yielded an orange-colored, air stable abnormal Pt-Sn carbene complex Pt(CO)(IBu^t)(SnBu$^t_3$)$_2$, **3.7**, accompanied by elimination of the CO ligand (see Scheme 3.5).

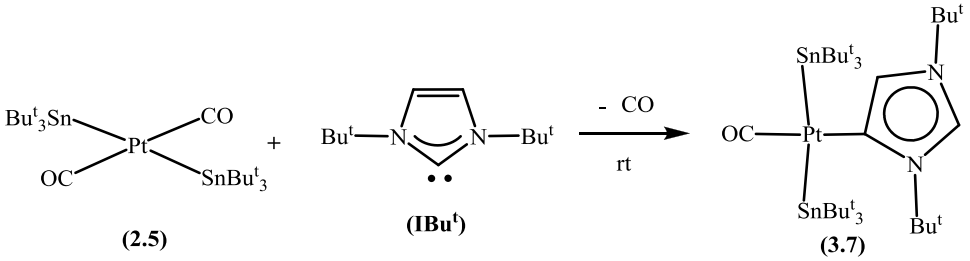

(2.5) **(IBu^t)** **(3.7)**

Scheme 3.5

The Pt-Sn complex with the C-4 bound NHC ligand Pt(CO)(IBu^t)(SnBu$^t_3$)$_2$, **3.7**, was characterized by a combination of ^{1}H NMR spectroscopy, IR spectroscopy, and single crystal X-ray diffraction technique. The molecular structure of compound **3.7** is shown in Figure 3.9.

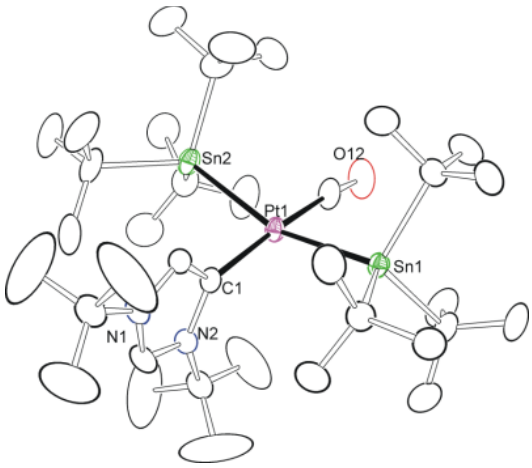

Figure 3.9 The molecular structure of Pt(CO)(IBu^t)(SnBu$^t_3$)$_2$, **3.7**.

Compound **3.7** has CO and NHC ligands located *trans* to each other and two terminal $SnBu^t_3$ groups attached to Pt in *trans* manner, as well. Compound **3.7** is also a 16 electron mononuclear Pt complex with a square planar geometry. Selective C-H bond activation of the IBu^t NHC carbene ligand can be attributed to steric repulsion between the bulky *tert*-butyl groups on Sn and the nitrogen atoms of IBu^t ligand in C-2 bound Pt-NHC complex (see Figure 3.10). C-4 bound NHC will experience minimum repulsions from the *tert*-butyl groups of the terminal Sn ligand. Similar C-H activation was also observed by Nolan et al. in the reaction of IBu^t ligand with $Pt(Me)_2(COD)$.[150] The role of steric repulsion in the favorable formation of C-4 bound M-NHC carbene complexes is well known in the literature.[150, 147]

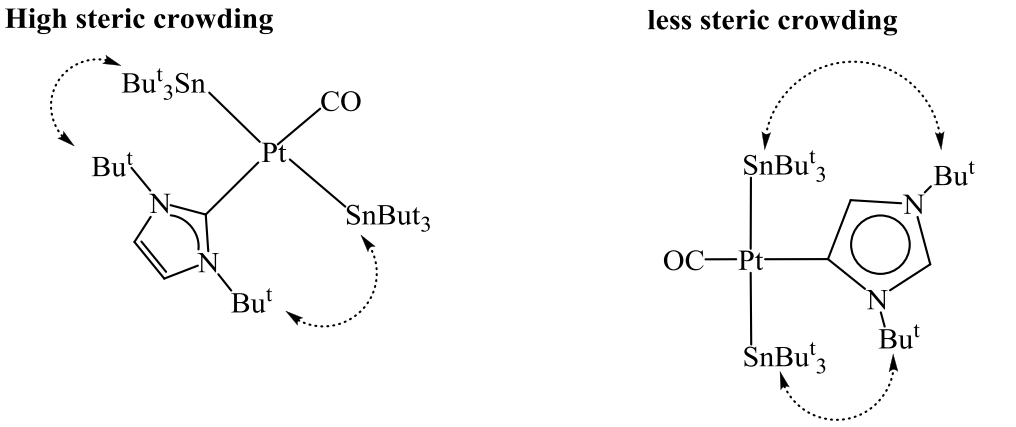

Figure 3.10 Comparison of steric crowding in C-2 bound carbene complex and C-4 bound carbene complex of compound **3.7**.

We were interested in comparing the reactivity of C-2 bound complex **3.3** with that of complex **3.7**. Compound **3.3** has hydride and CO ligands positioned *trans* to each other, while in compound **3.7** IBu^t is in the *trans* position to CO ligand (see Figure 3.11). Selective intramolecular bond distances and bond angles in compounds **3.3** and **3.7** are

listed in Table B.1 in Appendix B. Elongation of the Pd-Cl bond *trans* to the NHC ligand was previously reported for square planar Pd(II)-NHC complexes.[164]

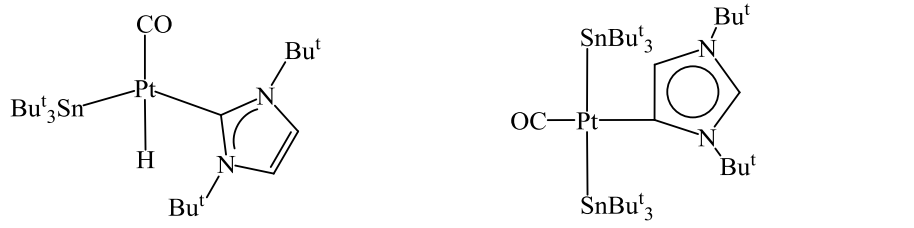

(3.3) a) C-2 bound Pt-NHC carbonyl complex

(3.7) b) C-4 bound Pt-NHC carbonyl complex

Figure 3.11 Line drawings for compound [HPt(CO)(SnBu$^t_3$)(IBu^t)], **3.3** and [Pt(CO)(SnBu$^t_3$)$_2$], **3.7**.

The donor strength of C-2 bound and C-4 bound IBu^t ligands can be compared based on the shift in CO stretching frequencies. The ν_{CO} stretching frequency for parent square planar Pt(II)-carbonyl complex Pt(CO)$_2$(SnBu$^t_3$)$_2$ is observed at 2007 cm^{-1}. The IR spectrum of the C-4 bound Pt-NHC carbene complex **3.7** in hexane solution shows a single strong absorption peak at 2011 cm^{-1} (ν_{CO} stretching frequency). This is in the expected range observed for other TM-NHC (TM = Ir) carbonyl complexes containing C-4 bound carbene ligand.[165] The C-2 bound Pt-Sn carbonyl complex **3.3** shows ν_{CO} stretching frequency around 1979 cm^{-1}, lower than expected CO stretch frequency for C-2 bound TM-NHC complexes (the average range of υ_{CO} is 2017-2020 cm^{-1}).[166, 121] The shifting of ν_{CO} stretching frequency to lower values in compound **3.3** can be explained based on the presence of trans hydride ligand, causing a strong σ-π back donation to the CO ligand.

Reactivity of abnormal C-4 bound Pt-Sn NHC complex, 3.7: Compound **3.7** appears to be more stable than the analogous compound **3.3**. In contrast to other mononuclear transition metal carbonyl complexes with NHC ligands, the CO ligand in complex **3.7** is not labile; there was no reaction with hydrogen and alkenes. While many attempts were made to remove the CO group from **3.7** to afford an unsaturated 14 electron mononuclear Pt-Sn carbene complex $Pt(IBu^t)(SnBu^t_3)_2$ (see Eq. 8), we had no success thus far. We assume that the bulky *tert*-butyl groups on the two terminal Sn ligands are imparting unusual stability to complex **3.7**.

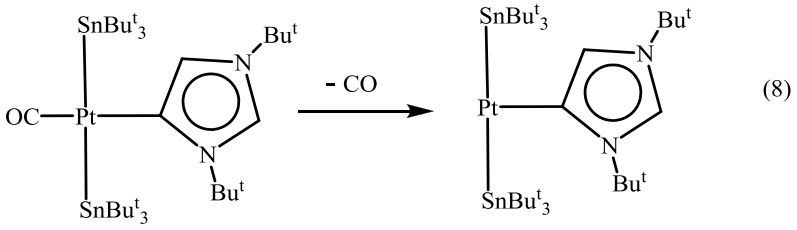

(8)

We further investigated the stability of the C-4 bound Pt-Sn carbene complex with the strong sigma donating ligand *tert*-butyl isocyanide ($CNBu^t$). We were interested in replacing the CO ligand with isocyanide ligand, but to our surprise we have observed the formation of known Pt-Sn complex $Pt(Bu^tNC)_2(SnBu^t_3)_2$.[167] Both CO and IBu^t ligands in $Pt(CO)(IBu^t)(SnBu^t_3)_2$ were cleaved and replaced by $CNBu^t$ ligand to yield $Pt(Bu^tNC)_2(SnBu^t_3)_2$, (see Scheme 3.6). The synthesis and characterization of this complex is described in the next chapter. The strong *trans* influence of $CNBu^t$ may be the reason for elimination of the NHC ligand after addition of one Bu^tNC ligand.

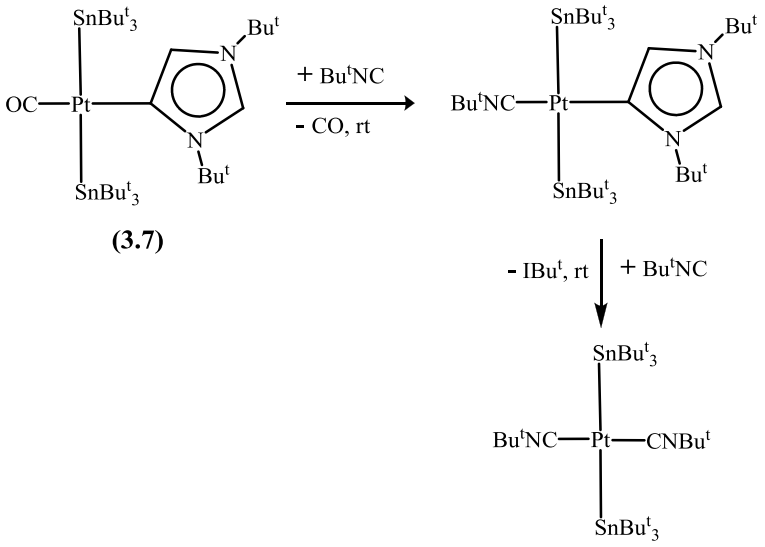

Scheme 3.6

Reaction of $Ru_5(C)(CO)_{15}$ with compound 3.7: With the aim of synthesizing multi-metallic complexes, we studied the reaction of complex **3.7** with various transition metal carbonyl compounds and we observed that complex **3.7** is stable and no new products were isolated. But when compound **3.7** was reacted with the pentaruthenium carbide cluster complex $Ru_5(C)(CO)_{15}$ in refluxing toluene solution, a new product $Ru_5Pt(IBu^t)(CO)_{15}$, **3.8**, was isolated in good yields. The Ru_5-Pt cluster complex is formed by reductive elimination of $SnBu^t_3$ groups to form hexa-*tert*-butyl distannane and yielding an unstable intermediate Pt-carbonyl complex with IBu^t ligand $Pt(CO)(IBu^t)$, which attacks the Ru_5 cluster to yield a Pt-capped Ru_5 carbide cluster (see Scheme 3.7).

In complex **3.8** the IBu^t ligand is also bonded to Pt through the C-4 carbon. The molecular structure of compound **3.8** is shown in Figure B.1 in Appendix B. To our knowledge this is the first example of carbide cluster with a C-4 bound NHC carbene ligand. The reactivity of the abnormal C-4 bound Pt(II)-NHC carbonyl complex **3.8** has

to be studied further for applications in homogeneous catalysis of hydroformylation reaction.

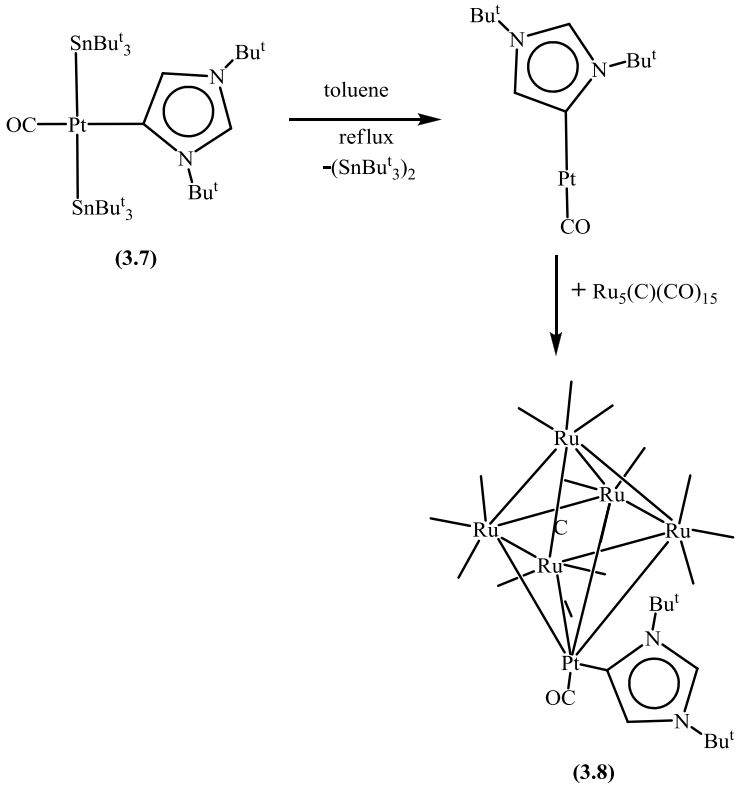

(3.7) **(3.8)**

Scheme 3.7

We are further investigating the substitution of CO ligand in $Pt(CO)_2(SnBu^t_3)_2$, with other bulky NHC ligands to prepare an unsaturated 14 electron Pt-Sn complexes comprising of NHC ligands.

3.3. Conclusions

Simple substitution of the (COD) ligand in [HPt(COD)($SnBu^t_3$)], **2.1** by IBu^t ligand yielded the unsaturated 28 electron dinuclear Pt-Sn complex $[Pt(SnBu^t_3)(IBu^t)(H)]_2$, **3.1**. The reactivity of compound **3.1** in small molecule activation was investigated and it was found that compound **3.1** activates hydrogen reversibly at room temperature. Compound

3.1 also activates CO at room temperature, but the reaction is not reversible, as seen in the activation of H_2. It was observed that the Pt-Pt bond in the dinuclear Pt-Sn NHC complex **3.1** breaks down during the addition of CO, H_2, and C_2H_4 to afford the mononuclear Pt-Sn NHC complexes **3.3**, **3.4**, and **3.5**, respectively. Compound **3.1** activates C_2H_4 and NH_3 reversibly at room temperature.

We have also demonstrated the role of bulky *tert*-butyl ligands in stabilization of the abnormal C-4 bound Pt-Sn carbene complex **3.7**. The $Pt(CO)_2(SnBu^t_3)_2$ complex selectively activates the C-H bond of the IBu^t ligand to yield the air stable C-4 bound Pt-Sn carbene complex **3.7**. The heteronuclear cluster complex Ru_5Pt with C-4 bound NHC ligand was synthesized from $[Pt(CO)(IBu^t)(SnBu^t_3)]$, complex **3.7**, and it was observed that formation of this complex was accompanied by reductive elimination of $SnBu^t_3$ ligands from compound **3.7**.

The stability of compound **3.7** was studied with various ligands. The $CNBu^t$ ligand was shown to be effective in elimination of the NHC ligand from C-4 bound Pt-Sn carbene complex **3.7** to afford the $Pt(Bu^tNC)_2(SnBu^t_3)_2$ complex. The Pt-Sn isocyanide complex can also be directly synthesized from substitution of CO ligands in $Pt(CO)_2(SnBu^t_3)_2$ by $CNBu^t$. These reactions are discussed in chapter 4. The influence of Sn ligands in improving the catalytic activity of Pt-NHC carbene complexes has to be fully explored to identify potential hydroformylation and hydrogenation catalysts.

3.4. Experimental section

General Data

Unless otherwise indicated, all reactions were performed under an atmosphere of Argon. Reagent grade solvents were dried by standard procedures and were freshly distilled prior to use. Infrared spectra were recorded on a Nicolet 380 FT-IR spectrophotometer. ^{1}H NMR were recorded on Bruker 300 and 400 spectrometer operating at 300.13 MHz and 399.99 MHz respectively. Elemental analyses were performed by Columbia Analytical Services (Tuscon, AZ). Mass spectrometric measurements performed by a direct–exposure probe using electron impact ionization (EI) were made on a VG 70S instrument at the University of South Carolina, Columbia, SC. The NHC carbenes IBu^{t} and IPr were purchased from Strem chemicals and used without further purification. Ethylene, CO, and CO_2, H_2 gases of 99.9% purity were purchased from Air gas south and used without further purification. Tertiary butylisocyanide, $CNBu^{t}$, was purchased from Sigma-Aldrich and used without further purification. Bis(1,5-cyclooctadiene)platinum, $Pt(COD)_2$,[115] tri-*tert*-butylstannane, Bu^{t}_3SnH,[105] and $Ru_5(C)(CO)_{15}$,[168] were prepared according to the published procedures. Silica gel (60-200 μm, 70-230 mesh) used for chromatographic separations was purchased from Silicycle.

Synthesis of $[Pt(SnBu^{t}_3)(IBu^{t})(H)]_2$, 3.1.

In a glove box, under an atmosphere of argon, 30.0 mg of Bu^{t}_3SnH (0.103 mmol) dissolved in 3mL of freshly distilled hexane was added to 40.0 mg of $Pt(COD)_2$ (0.097 mmol). The reaction mixture immediately turned dark brown. The reaction mixture

stirred at room temperature for an additional 10 minutes and 17.0 mg of IBu^t dissolved in 0.5 ml of toluene solution was added to dark brown reaction mixture. The reaction mixture immediately turned red. The reaction was stirred for 30 minutes after which solvent was reduced to *c.a*. 1 mL. The solid was filtered and washed with 3x 3.0 mL of pentane to yield 48 mg (yield 75%) of cherry red powder. Spectral data for **3.1**: ^{1}H NMR (THF-*d8*, rt, in ppm): δ = 7.33 (s, 4H; imid), 2.03 (s, 36H; $C(CH_3)_3$), 1.09 (s, 54H; $^2J_{Sn-H}$ = 49.3 Hz, $C(CH_3)_3$); -5.61 (s, $^1J_{Pt-H}$ = 652 Hz, $^2J_{Pt-H}$ = 203 Hz, $^2J_{Sn-H}$ = 56.0 Hz, 2H, hydride). ^{1}H NMR (C_6D_6, rt, in ppm): δ = 6.60 (s, 4H; imid), 1.94 (s, 36H; $C(CH_3)_3$), 1.42 (s, 54H; $^2J_{Sn-H}$ = 49.3 Hz, $C(CH_3)_3$); -5.61 (s, $^1J_{Pt-H}$ = 652 Hz, $^2J_{Pt-H}$ = 203 Hz, $^2J_{Sn-H}$ = 56.0 Hz, 2H, hydride). Elemental analysis, Calc: C, 41.45; H, 7.26; N, 4.20 %, Found: C, 41.47; H, 7.41; N, 4.09 %.

Synthesis of [Pt($SnBu^t_3$)(IBu^t)(CO)(H)], 3.3.

A 25 mL schlenk tube was charged with 30 mg of **3.1** (0.023 mmol) which was subsequently dissolved in 4.0 mL of toluene. The red solution was under an atmosphere of *c.a.* 10 psi CO and shaken vigorously. The resultant solution turned light orange immediately. The solvent was removed under reduced pressure. The solid was then washed with 3x 0.25 mL heptane and yielded 28.6 mg (90% yield) of a khaki-colored powder. Spectral data for **3.3**: ^{1}H NMR (C_6D_6, rt, in ppm): δ = 6.60 (s, $^4J_{Pt-H}$ = 8.8 Hz, 2H; imid), 1.67 (s, 27 H, $SnBu^t_3$, $^3J_{Sn-H}$ = 51.8 Hz), 1.37 (s, 18 H, $C(CH_3)_3$); -2.48 (s, $^1J_{Pt-H}$ = 891.8 Hz, $^2J_{Sn-H}$ = 18.4 Hz, 1H, hydride). IR ν_{CO} (cm^{-1} in hexane): 1979(vs), 2104(m).

Reaction of 3.1 with H_2 gas.

A 5 mL NMR tube was charged with 10.0 mg of **3.1** which was subsequently dissolved in 0.5 mL of toluene-d_8. The NMR tube was sealed under argon, and the red solution was exposed to an atmosphere of *c.a.* 1 atm H_2 and shaken vigorously. The resultant solution turned light orange immediately to yield mononuclear Pt-Sn carbene complex with the three hydride ligands. Spectral data for **3.4**: ^{1}H NMR (C_6D_6, rt, in ppm): δ = 6.60 (s, $^4J_{Pt-H}$ = 8.8 Hz, 2H; imid), 1.56 (s, 27 H, $SnBu^t_3$, $^3J_{Sn-H}$ = 62.1 Hz), 1.41 (s, 18 H, $C(CH_3)_3$); -4.36 (s, $^1J_{Pt-H}$ = 726.5 Hz, $^2J_{Sn-H}$ = 127.5 Hz, 3H, hydride).

Reaction of 3.1 with D_2 gas.

A 5 mL NMR tube was charged with 10 mg of **3.1** which was subsequently dissolved in 0.5 mL of toluene-*d8*. The NMR tube was sealed under argon, and the red solution was exposed to an atmosphere of *c.a.* 1 atm D_2 and shaken vigorously. The resultant solution turned light orange immediately to yield mononuclear Pt-Sn carbene complex with the deuterium ligands. Spectral data for the deuteriated Pt-Sn NHC complex: ^{1}H NMR (C_6D_6, rt, in ppm): δ = 6.60 (s, $^4J_{Pt-H}$ = 8.8 Hz, 2H; imid), 1.56 (s, 27 H, $SnBu^t_3$, $^3J_{Sn-H}$ = 62.1 Hz), 1.41 (s, 18 H, $C(CH_3)_3$), -4.26 (t, $^1J_{Pt-H}$ = 726.5 Hz, $^1J_{D-H}$ = 34.0 Hz).

Synthesis of [Pt($SnBu^t_3$)(IBu^t)(C_2H_4)(H)], 3.5.

A 25 mL schlenk tube was charged with 30.0 mg (0.023 mmol) of **3.1** which was subsequently dissolved in 4.0 mL of toluene. The red solution was under an atmosphere of *c.a.* 10 psi ethylene and shaken vigorously. The resultant solution turned light yellow immediately. The solvent was removed under slow flow of ethylene gas to yield 26.6 mg (85% yield) of a light yellow-colored powder. Spectral data for **3.5**: ^{1}H NMR (toluene-

d_8, rt, in ppm): δ = 6.60 (s, $^4J_{Pt-H}$ = 8.8 Hz, 2H; imid), 2.45 (s, 4H, ethylene), 1.88 (s, 27 H, $SnBu^t_3$, $^3J_{Sn-H}$ = 51.8 Hz), 1.63 (s, 18 H, $C(CH_3)_3$); -3.57 (s, $^1J_{Pt-H}$ = 891.8 Hz, $^2J_{Sn-H}$ = 18.4 Hz, 1H, hydride).

Reaction of 3.1 with NH_3

A 25 mL schlenk tube was charged with 30 mg of **3.1** (0.023 mmol) which was subsequently dissolved in 4.0 mL of toluene. The red solution was under an atmosphere of *c.a.* 1 atm NH_3 gas and shaken vigorously. The resultant solution turned light yellow-colored immediately. The solvent was removed under the flow of NH_3 gas to yield 12.6 mg (80% yield) of a light yellow colored powder.

Reaction of 3.1 with a mixture of H_2 and CO (1:1 mole ratio).

In a typical reaction, a 10.0 mg of compound **3.1**, 1 mL of anhydrous toluene or toluene-d_8 and a magnetic stir bar were sealed in a Parr reactor under ethylene atmosphere. The Parr reactor was pressurized with 100 bar H_2 and 100 bar CO gas at room temperature. The reaction was monitored by ^{1}H NMR at different time intervals. After 24 hours the ^{1}H NMR of reaction mixture showed peaks corresponding to compound **3.3** and free ethylene. No peaks were observed corresponding to acetaldehyde. The Parr reactor was then placed in an oil bath with a stir that was pre-heated to 120 ºC. The reaction was monitored by ^{1}H NMR at different time intervals. After two days the ^{1}H NMR of reaction mixture showed peaks corresponding to compound **3.3** and free ethylene. There was no product observed resulting from hydroformylation of ethylene.

Reaction of 3.5 with CO_2.

A 25 mL schlenk tube was charged with 30.0 mg of **3.5** (0.043 mmol) which was subsequently dissolved in 4.0 mL of toluene. The red solution was under an atmosphere of *c.a.* 10 psi ethylene and shaken vigorously at room temperature. The resultant solution turned light yellow immediately. CO_2 gas was bubbled through the above reaction mixture through a needle. After 30 minutes the reaction mixture slowly started to turn back to a red color. The solvent was removed under reduced pressure to yield red-colored powder. The ^{1}H NMR of product matched the spectrum of compound **3.1**.

Synthesis of [Pt(SnBu$^t_3$)$_2$(IBu^t)(CO)], 3.7.

In a glove box, under an atmosphere of argon, 30.0 mg of [Pt(SnBu$^t_3$)$_2$(CO)$_2$] (0.0360 mmol) dissolved in 3mL of freshly distilled hexane was added to a 20 mL scintillation vial. To the above green-colored solution 14.0 mg of IBu^t was added at room temperature and stirred vigorously for one hour. The reaction mixture turned orange and, the solvent was evaporated in a drybox at room temperature overnight to obtain orange crystals of compound **3.7**. The orange crystals were washed with 3x 1 mL of hexane solution to yield 30.0 mg of pure **3.7** (86% yield). Spectral data for **3.7**: ^{1}H NMR (C_6D_6, rt, in ppm): δ = 7.45 (d, $^3J_{Pt\text{-}H}$ = 16.0 Hz, 1H; imid), 6.31 (d, $^4J_{Pt\text{-}H}$ = 29.9 Hz, 1H), 1.52 (s, 54 H, SnBu$^t_3$, $^3J_{Sn\text{-}H}$ = 51.8 Hz), 1.49 (s, 18 H, C(CH$_3$)$_3$). IR ν_{CO} (cm^{-1} in hexane): 2011(vs). Elemental Anal, calc.: C, 43.96; H, 7.58; N, 2.84 %; Found: C, 44.20; H, 7.46; N, 2.84 %.

Reaction of compound 3.7 with $CNBu^t$.

In a glove box, under an atmosphere of argon, 20.0 mg of **3.7** (0.020 mmol) dissolved in 3 mL of freshly distilled hexane was added to a 20 mL scintillation vial. To the above orange color solution 14.0 mg of $CNBu^t$ was added at room temperature and stirred vigorously for one hour. The reaction mixture turned purple and the solvent was evaporated in a drybox at room temperature overnight to obtain purple crystals of **3.7**. The purple crystals were washed with 3x 1 mL of acetonitrile solution to yield 15.0 mg of pure $Pt(SnBu^t_3)_2(CNBu^t)_2$. (Note: The spectral data for $Pt(SnBu^t_3)_2(CNBu^t)_2$ can be found in chapter 4 experimental section 4.4).

Reaction of 3.7 with $Ru_5(C)(CO)_{15}$.

A 20.0 mg amount of **3.7** (0.020 mmol) was dissolved in 20 mL of toluene in a 100 mL 3-neck flask. A 20.0 mg (0.020 mmol) of $Ru_5(C)(CO)_{15}$ was also charged into the flask. The reaction mixture was refluxed at 110 °C for 35 minutes to obtain a brownish-red solution. The solvent was removed in *vacuo* to obtain a brown solid. The product was separated by TLC by using hexane solvent to yield 10.2 mg (38% yield) of red-orange powder, $Ru_5Pt(C)(CO)_{15}(IBu^t)$, **3.8**. Spectral data for **3.8**: IR ν_{CO} (cm^{-1} in dichloromethane): 2076 (w), 2044 (m), 2025 (vs).

3.5. Crystallographic analyses

Red-colored crystals of **3.1** suitable for diffraction were grown by slow evaporation of toluene solution at room temperature in a glove box. Yellow crystals of **3.3** were grown by evaporation of hexane solution of **3.1** at 0 °C under the slow stream of the CO gas. Light yellow crystals of **3.5** of suitable quality for diffraction were grown by slow

evaporation of hexane solution under a stream of ethylene gas in an ice bath (0 °C). Orange-colored crystals of **3.7** were grown by evaporation of hexane solution in glove box at room temperature.

Red-colored crystals of **3.8** suitable for x-ray diffraction were grown by evaporation of dichloromethane solution in a -20 °C freezer. Each data crystal was mounted onto the end of a thin glass fiber using Paratone-N. X-ray intensity data were measured by using a Bruker SMART APEX2 CCD-based diffractometer using Mo Kα radiation (λ = 0.71073 Å).[117] The raw data frames were integrated with the SAINT+ program by using a narrow-frame integration algorithm.[117] Corrections for Lorentz and polarization effects were also applied with SAINT+. An empirical absorption correction based on the multiple measurement of equivalent reflections was applied using the program SADABS. Both structures were solved by a combination of direct methods and difference Fourier syntheses, and refined by full-matrix least-squares on F^2, by using the SHELXTL software package.[118] Crystal data, data collection parameters, and results of the analyses are listed in Tables B.2- B.4 in Appendix B.

The compound **3.1** crystallized in triclinic system. The space group $P\ \bar{1}$ was assumed and confirmed by the successful refinement and solution of the structure. The hydride ligand was located from the difference map but refined on its positional parameters with a fixed isotropic thermal parameter. Compound **3.3** crystallized in monoclinic system. The space group *P21/c* was confirmed on the basis of the systematic absences in the data. With Z= 8, there were two molecules in the structure and the hydride ligand was located from the difference map but refined on its positional parameters with a fixed isotropic thermal parameter.

Compound **3.5** crystallized in triclinic system. The space group $P\ \bar{1}$ was confirmed on the basis of the systematic absences in the data. The ether solvent molecule co-crystallized with the compound **3.5**. The hydride ligand was located from the difference map but refined on its positional parameters with a fixed isotropic thermal parameter.

Compound **3.7** crystallized in the orthorhombic crystal system. The space group $P2_12_12_1$ was confirmed on the basis of the systematic absences in the data. Compound **3.8** crystallized in monoclinic system. The space group *P21/n* was confirmed on the basis of the systematic absences in the data. There was a disorder in the solvent molecule and *tert*-butyl groups of IBu^t, giving a high R1 value for the compound **3.8**.

Chapter 4: Synthesis and characterization of Pt-Sn and Pd-Sn complexes comprising of isocyanide ligands.

4.1. Background

Insertion of isonitriles into various types of M-C bonds is a well-known phenomenon, yielding iminoacyl derivatives of great interest in organometallic transformations.[169] Organometallic complexes with isocyanide ligands immobilized on organic polymers have been used as catalysts in olefin isomerization,[170] hydroformylation[171] and also in hydrogenation.[172] The isolobal relationship between CO and organoisocyanides[173-175] (CNR) catalyzed the rapid growth of research interest in the synthesis of unsaturated metal isocyanide complexes over the past two decades. Organoisonitrile ligands are better σ donors and poorer π-accepting ligands than CO[176, 177] and offer the added advantage of steric variability facilitating stabilization of low-coordinate reactive metal centers for application in the small molecule activation and C-H bond activation.

Jones et al. recently showed that a photochemically generated reactive fragment [Tp′Rh(CNR)] (Tp = hydrotris (3,5-dimethylpyrazolyl) borate; R = CH_2CMe_3) selectively activates C-H bond of chloroalkanes such as chloromethane and dichloromethane.[178] The Figourea group also reported isolation of low coordinate unsaturated Ni and Pd isocyanide complexes effective in activation of small molecules such as I_2, O_2, and chloroalkanes (see Figure 4.1).[179, 180] In these derivatives it has been found that the bulky isocyanide groups enhanced the stability of these complexes and aided in the separation of reactive low coordinate transition metal isocyanide complexes of types ML_2 and ML_3 (M = Pd, Ni and L = CNR). There are several examples of Pt and

Pd isocyanide complexes containing phosphine ligands reported in literature.[181-185] Different synthetic methods are adopted to isolate these complexes:, for example, ligand substitution[186] and salt elimination[187] and their reactivity has been examined for various applications.

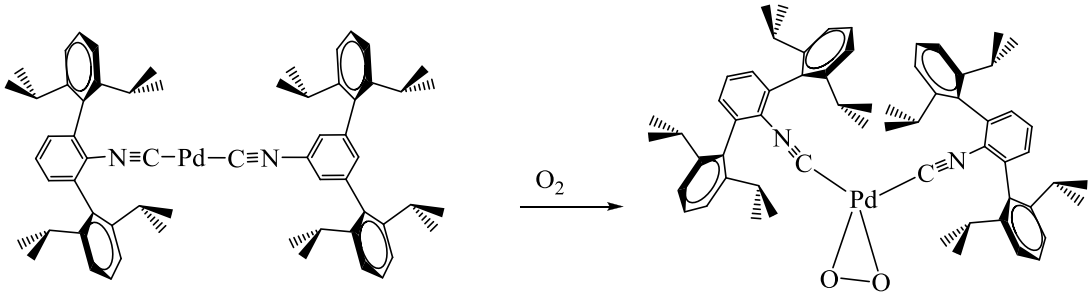

Figure 4.1 Activation of O_2 by $Pd(CNAr^{Dipp2})_2$ complex.

Some examples are also known for Pt and Pd isocyanide complexes bonded to Sn metal ligands.[187-190] The Pt(II) complex $Pt(CNAd)_2(Me_3Si)_2$ was synthesized from the reaction of $Pt_3(CNAd)_6$ (Ad = 1-adamantyl) with an excess of hexamethyldisilane (see Eq. 1).[191]

$$Pt_3(CNAd)_6 \xrightarrow[\text{benzene 80 °C}]{\text{30 eq } Me_3Si\text{-}SiMe_3} (Me_3Si)_2Pt(CNAd)_2 \quad (93\%) \qquad (1)$$

Pd isocyanide complexes with trichlorostannate, $SnCl_3$ ligand like $[Pd(SnCl_3)_2(CNR)_2]$ (R = Ph, Cy)[190, 192] are also known, but there are no crystal structures reported for these complexes. They were characterized by IR spectroscopy and elemental analysis. Pd-stannaborate complexes possessing isocyanide ligands (see Figure 4.2) have been synthesized to investigate the substitution equilibrium between isocyanides and stanna-*closo*-dodecaborate. These complexes were characterized by X-ray

crystallography, elemental analysis, and NMR spectroscopy.[189] Recently, Wesemann et al. reported isolation of a zwitterionic Pt(IV) complex comprising a cationic transition metal center and an anionic heteroborate cluster {stanna-closo-dodecaborate ($SnB_{11}H_{11}$)}, (see Scheme 4.1).[187]

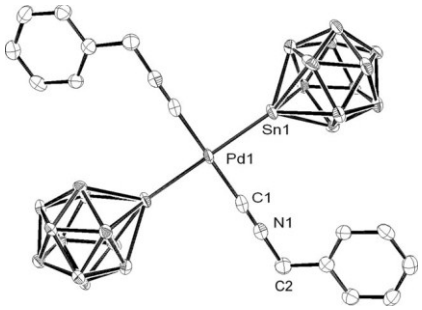

Figure 4.2 The molecular structure of the anion of $[Et_3NH]_2$[*trans*-$(C_6H_5CH_2NC)_2Pd(SnB_{11}H_{11})_2$].

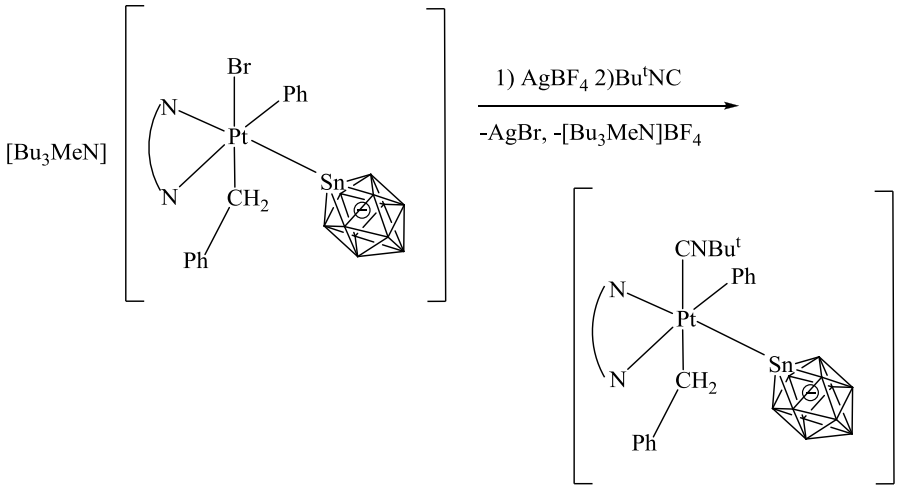

Scheme 4.1

Although there is a knowledge of synthesis and separation methods for isolation of reactive Pt and Pd-isocyanide complexes with group(IV) metals, the reactivity of these complexes toward small molecule activation and catalytic hydrogenation reactions is still unexplored.

Hydrogenation and dehydrogenation reactions are large set of reactions used in the petroleum refinery industry.[7, 193-195] Transition metal complexes catalyze these hydrogenation and dehydrogenation reactions. There is a huge demand for materials and molecules that can activate hydrogen reversibly at ambient conditions.[9, 13] It was with the discovery of Vaska's square planar Ir(I)complex $Ir(PPh_3)_2(CO)Cl$ and its ability to reversibly activate molecular hydrogen[196] and undergo a range of oxidative-addition reactions[197] that stimulated the growing field of homogeneous catalysis in the 1960s.[198]

Over the years, a number of unsaturated transition metal complexes have been prepared and were shown to undergo H_2 activation reactions.[199] As discussed in the chapter 1, the most common feature of these metal complexes that activate hydrogen is that they contain bulky phosphine ligands.[200-203, 13] A number of years ago, Eaborn and co-workers provided evidence based on *in situ* spectroscopic data for the reversible elimination of H_2 from the Pt-Sn phosphine complexes of the type $Pt(SnR_3)_2(PMe_2Ph)_2(H)_2$ (R = Ph, $PhCH_2$, o-, m-, or p-MeC_6H_4). No crystal structures reported for these complexes, they were only characterized by ^1H NMR and IR spectroscopy.[86] Herein, we present a new example of a metal complex system that reversibly activates hydrogen, but containing only isocyanide ligands and no phosphine ligands or NHC carbene ligands.

We have synthesized the air stable Pt(II) isocyanide complex $Pt(SnBu^t_3)_2(CNBu^t)_2$, **4.2** from the reaction of $Pt(SnBu^t_3)_2(CO)_2$, **2.5**, with $CNBu^t$ through CO elimination as stated in the previous chapter. The reaction between $Pt(COD)_2$ and $HSnBu^t_3$ followed by *in situ* addition of *tert*-butyl isocyanide also yielded the Pt(IV) dihydride complex $[Pt(SnBu^t_3)_2(CNBu^t)_2H_2]$, **4.1**. The Pt(II)-isocyanide complex **4.2**

activates hydrogen and CO at room temperature reversibly both in solution and in the solid state. Similarly, we have also synthesized analogous Pd(II) and Pd(IV) isocyanide complexes comprised of organotin groups from the reaction of Pd(allyl)(Cp) and *tert*-butyl isocyanide. The synthesis methods and the reactivity studies are reported in this chapter.

4.2. Results and discussion

Synthesis of Pt(IV) dihydride complex $[H_2Pt(SnBu^t_3)_2(CNBu^t)_2]$, 4.1: A colorless 18 electron Pt(IV) isocyanide complex comprising tri-organotin ligands $[H_2Pt(SnBu^t_3)_2(CNBu^t)_2]$, **4.1**, was obtained in 32% yield from the reaction of $Pt(COD)_2$ with two equivalents of Bu^t_3SnH in hexane solution, followed by addition of two equivalents of *tert*-butyl isocyanide($CNBu^t$) at room temperature (see Scheme 4.2).

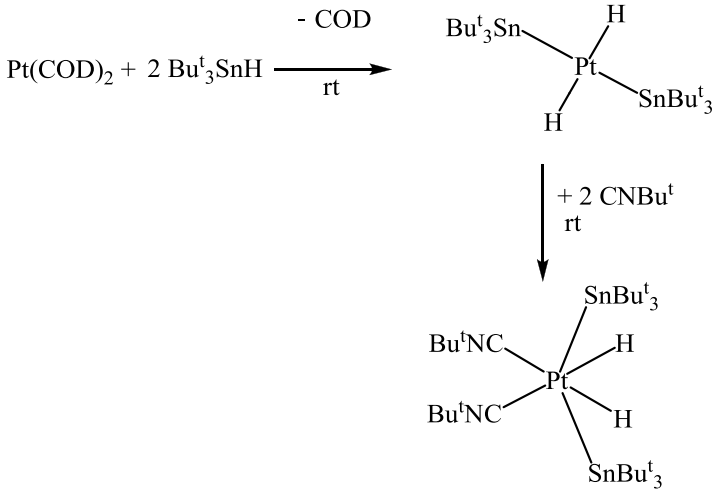

Scheme 4.2

The Pt(IV) complex **4.1** is a neutral mononuclear Pt-Sn complex with two terminal hydride ligands. Isolation of compound **4.1** was possible due to increased stability of the Pt(IV) complex imparted by the bulky Sn and isocyanide ligands. The compound **4.1**

was characterized by a combination of ^{1}H NMR, single crystal X-ray crystallography, and IR spectroscopy. The molecular structure of compound **4.1** is shown in Figure 4.3. The molecule has a slightly distorted octahedral geometry. The hydride ligands are located and refined in the structural analysis performed at 100 K.

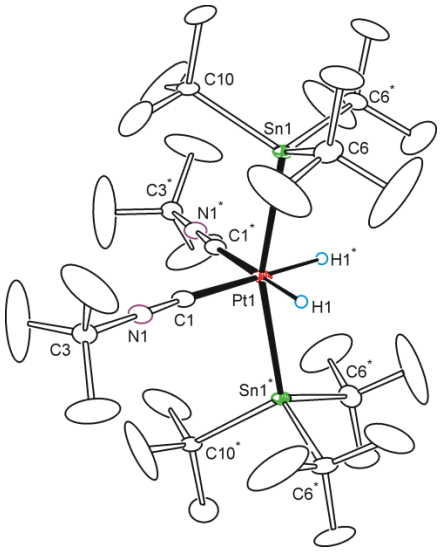

Figure 4.3 The molecular structure for $[H_2Pt(SnBu^t_3)_2(CNBu^t)_2]$, **4.1**.

As seen in Figure 4.3, the $SnBu^t_3$ groups are *trans* with respect to each other while the $CNBu^t$ groups and hydride ligands are in the *cis* position, such that the molecule has C_{2v} symmetry. Appropriately ^{1}H NMR shows one resonance for the two equivalent hydrides, - 13.52 ppm. The Pt-Sn bond distance in **4.1** is 2.6718(5) Å and the Pt-H bond distance is 1.65(9) Å. The Pt-Sn bond length is consistent with the range reported for mononuclear octahedral Pt(IV) complexes {2.554 Å for Pt-Stannaborate isocyanide complex[187]}.

Reversible activation of H_2 by Pt-Sn isocyanide complex $Pt(SnBu^t_3)_2(CNBu^t)_2$, 4.2: Interestingly, when solutions of compound **4.1** were purged with argon gas at room temperature for approximately 20 hours, H_2 gas was eliminated to afford the new

complex $Pt(SnBu^t_3)_2(CNBu^t)_2$, **4.2**, in 89% yield. Compound **4.2** was also characterized crystallographically. The molecular structure of **4.2** is shown in Figure 4.4.

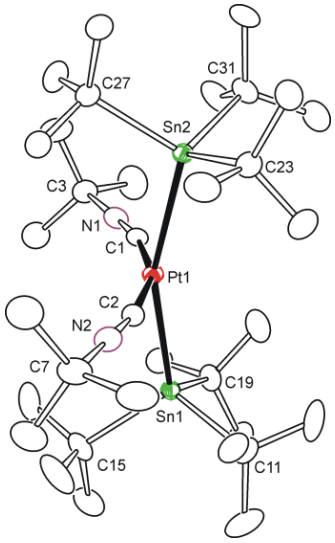

Figure 4.4 The molecular structure for $Pt(SnBu^t_3)_2(CNBu^t)_2$, **4.2**.

Compound **4.2** is formally a 16 electron Pt(II) species. As expected for platinum complexes in a d^8 configuration, the molecular geometry should be square planar. However, as seen in Figure 4.4 the structure of **4.2** is distorted from planarity due to steric crowding from the bulky $SnBu^t_3$ ligands, giving the complex approximate C_{2v} symmetry. Indeed, when hydrogen gas (1 atm) is passed through solutions of **4.2** at room temperature complex **4.1** is regenerated in 94% yield (see Eq. 3).

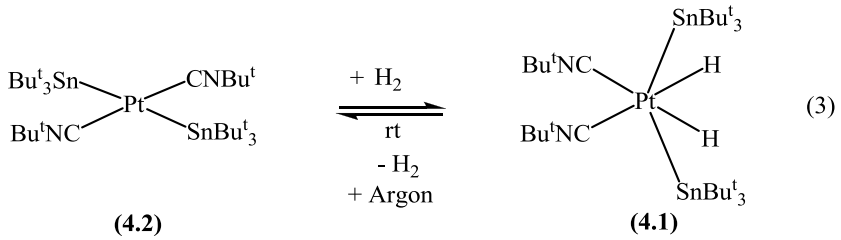

(4.2) **(4.1)** (3)

Analysis of the X-ray crystal structures reveals how the ligands in **4.2** rearrange to accommodate hydride ligands upon addition of hydrogen. The C2-Pt1-C1 bond angle in

compound **4.2** is 158.69(13)°, whereas the C1-Pt1-C1* bond angle in compound **4.1** is squeezed significantly to 102.5(4)° to accommodate the two hydride ligands (see Figure 4.5).[167] Such a rearrangement of coordination geometry of ligands is common in the addition of hydrogen or CO to the transition metal carbonyl clusters.[204-206] There is no considerable change in the Sn-Pt-Sn bond angle upon addition of H_2 to compound **4.2**. Similarly, the Pt-Sn bond lengths also remain essentially the same after addition of H_2.

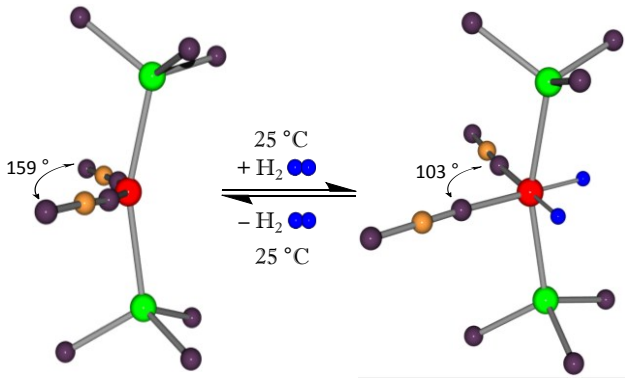

Figure 4.5 Change in coordination geometry of ligands after addition of H_2 to **4.2**.

Compound **4.2** was also characterized by IR spectroscopy. The ν_{CN} stretching frequency for Pt(II)-bound isocyanide complexes in general falls in the range of 2225-2170 cm^{-1}, as reported in literature.[186] The ν_{CN} stretching frequency for **4.2** in hexane solution shows a sharp peak around 2112 cm^{-1}, slightly lower than the expected range. The IR spectrum of compound **4.1** in hexane solution shows two peaks, one weak intensity peak at 2112 cm^{-1} corresponding to the two terminal hydrides (ν_{Pt-H} stretching frequency) and one sharp peak at 2139 cm^{-1} corresponding to ν_{CN} stretching of the $CNBu^t$ ligands. There is a slight shift in ν_{CN} stretching frequency (2112 cm^{-1} for **4.2**) upon addition of hydride ligands to Pt(II) isocyanide complex **4.2**, this might be due to increase

in electron density around the Pt-metal center in **4.1**. The absorption peak of ν_{Pt-H} for Pt(IV)hydride complex $[PtH_2(SnPh_3)_2(PMe_2Ph)_2]$ synthesized by Eaborn et al. several years ago also has ν_{Pt-H} values in the same range(2085, and 2115 cm^{-1}).[86]

Activation of H_2 by compound 4.2 in solid state: The compound **4.2** activates hydrogen at room temperature even in the solid state. Upon exposure of the purple-colored crystals of compound **4.2** to an H_2 atmosphere, the colorless crystals of compound **4.1** formed instantaneously in quantitative yield. Removing the hydrogen gas and placing the colorless crystals of compound **4.1** in vacuum for 12 hours regenerates purple crystals of compound **4.2**. Crystal to crystal transformations from the activation of small molecules (H_2, CO, and C_2H_4, NH_3) by [Ir]-N_2 pincer complex (see Figure 4.6) were recently reported by the Brookhart group.[207]

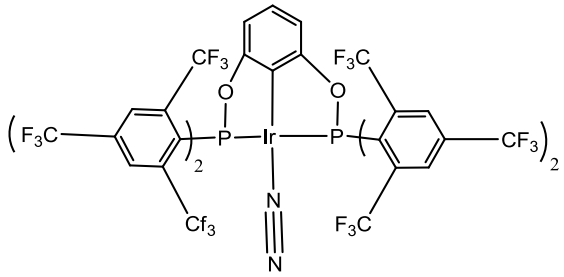

Figure 4.6 Line drawing for [Ir]-N_2 pincer complex.

Reaction of compound 4.2 with HD gas: The complex **4.1**-d_1 was prepared by the reaction of **4.2** with HD gas to test for the existence of direct H-H interactions in **4.1**. The ^{1}H NMR spectrum of **4.1**-d_1 did not show any H-D coupling, suggesting that there is no significant H-D interaction, which is consistent with the crystal structure analysis of **4.1**. In addition to the resonance of **4.1**-d_1, the hydride resonance for **4.1** was also present

in the ^{1}H NMR spectrum (see Figure 4.7). The small shift difference in the spectrum in Figure 4.8b is due to isotope shift effects.

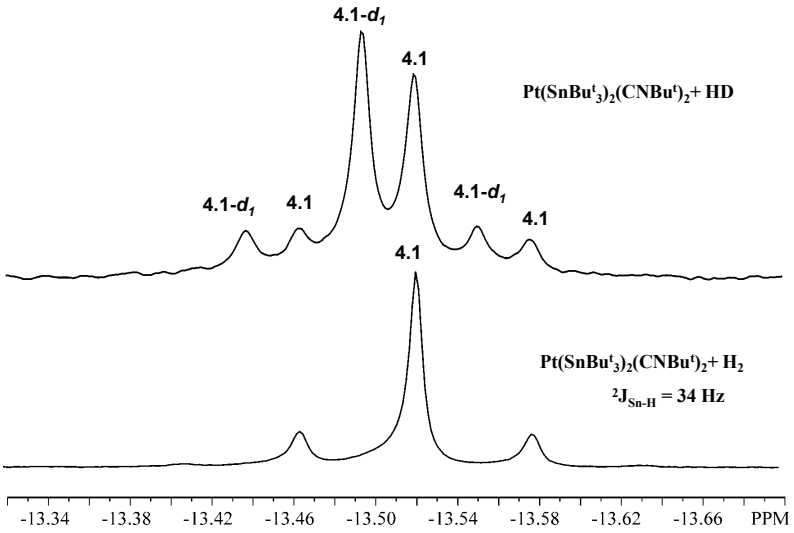

Figure 4.7 ^{1}H NMR spectra of the hydride region (a) for **4.1** from the addition of H_2 to **4.2** and (b) for the addition of HD to **4.2**. Pt-H one-bond coupling not shown.

H_2-D_2 scrambling studies on $Pt(SnBu^t_3)_2(CNBu^t)_2$, 4.2: In solution, complex **4.2** catalyzes the H_2-D_2 exchange to give HD at room temperature (see Eq. 4). The addition of an equimolar mixture of H_2 and D_2 to solutions of **4.2** resulted in the rapid formation of HD, which was detected by ^{1}H NMR. The solvent molecule is not participating in the isotopic exchange reactions. We observed isotopic H_2-D_2 scrambling even in the solid state at room temperature over a period of four hours. The effect of *tert*-butyl groups of Sn on the rate of the isotopic exchange reaction must be investigated further to understand the reaction mechanism.

$$H_2 + D_2 \underset{\text{rt, } C_6D_6}{\overset{Pt(SnBu^t_3)_2(CNBu^t)_2}{\rightleftharpoons}} 2HD \qquad (4)$$

Several years ago, HD gas was reported to be formed both from $[CpRu(PPh_3)(Bu^tNC)(H_2)]^+$ and D_2 in dichloromethane,[208] and in thermal H_2/D_2 exchange reactions of $Cr(CO)_4(H_2)_2$ in liquid xenon.[209] Kubas et al. also observed H_2/D_2 exchange over their $M(CO)_3(PR_3)_2(H)_2$ complex to produce HD gas both in solution and the solid state.[210]

We have monitored the catalytic H_2-D_2 exchange reaction with **4.2** in C_6D_6 solvent at room temperature by ^1H NMR. The ^1H NMR of a 1:1 molar ratio of H_2/D_2 mixture without catalyst **4.2** shows a single peak for free hydrogen (see Figure 4.8).

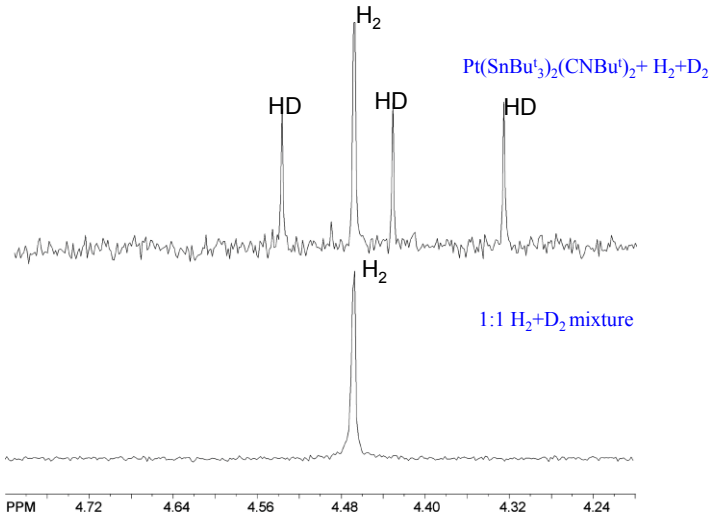

Figure 4.8 ^1H NMR spectra in C_6D_6 for catalytic H_2/D_2 scrambling by $Pt(SnBu^t_3)_2(CNBu^t)_2$, **4.2**.

After addition of a catalytic amount of **4.2** to the above solution, followed by vigorous shaking for 15 minutes, the ^1H NMR indicated the formation of HD gas. We continued monitoring the progress of reaction over a period of five days, but we observed contradictory results: the exchange process was rapid for four hours with the increase in

the percentage of HD gas (as indicated by increase in the intensity of peaks corresponding to HD in ^{1}H NMR). After a day we saw a small decrease in the percentage of HD gas, and a negligible increase again over a period of two days. After five days the rate of exchange appears to be same as that observed after two days.

A possible reason for this ambiguous rate of exchange could be decomposition of catalyst **4.2** slowly in solution by cleavage of the *tert*-butyl groups on Sn and subsequent competition in H_2/D_2 exchange reaction to give isobutane-d_1. We do observe cleavage of *tert*-butyl groups in the Fe_2Sn_2 cluster in refluxing toluene solution to give isobutane and isobutene gas.[105] Another reason for the conflicting exchange rates could be the stability of Pt(IV)dihydride complex **4.1**, we need either vacuum or argon gas to remove hydride ligands from **4.1**. The presence of labile H_2 ligand is necessary for rapid exchange of H_2/D_2 to give HD. More experiments need to be done in order to understand the isotopic H_2-D_2 exchange catalysis by compound **4.2**.

Isolation of Pt(II) isocyanide complex 4.2 from ligand substitution in $Pt(SnBu^t_3)_2(CO)_2$, 2.5: The Pt(II) isocyanide complex $Pt(SnBu^t_3)_2(CNBu^t)_2$, **4.2** is also obtained in quantitative yield (92%) from the labile CO ligand substitution in $Pt(SnBu^t_3)_2(CO)_2$, **2.5**, by $CNBu^t$ groups at room temperature in hexane solution. Addition of two equivalents of $CNBu^t$ to the green-colored solution of the Pt(II)-dicarbonyl complex **2.5** in hexane results in evolution of the CO gas from the reaction mixture and formation of a colorless precipitate of the intermediate Pt(II)-monocarbonyl complex $Pt(CO)(SnBu^t_3)_2(Bu^tNC)_2$, **4.3**, (see Scheme 4.3).

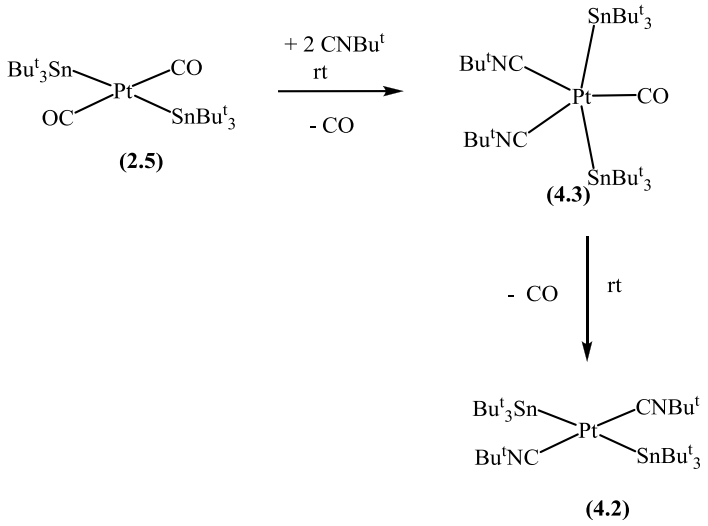

Scheme 4.3

In our lab Isrow also prepared two similar analogous isocyanide complexes $Ni(SnBu^t_3)_2(CO)(Bu^tNC)_2$ and trigonal bipyramidal $Ni(SnBu^t_3)_2(Bu^tNC)_3$. In our case, however, even addition of excess $CNBu^t$ to complex **2.5** yielded compound **4.2**: no $Pt(SnBu^t_3)_2(Bu^tNC)_3$ formation was observed in this reaction. We also did not observe any products resulting from isonitrile insertion into Pt-C bond.

Reversible activation of CO by compound 4.2: Compound **4.3** is stable in the solid state for considerable amount of time, *c.a.* 24 hours. In hexane solution **4.3** rearranges to **4.2** over a period of 12 hours at room temperature under argon atmosphere with the elimination of CO. Compound **4.2** in hexane solution activates the CO molecule at room temperature to afford $Pt(CO)(SnBu^t_3)_2(Bu^tNC)_2$, **4.3** in quantitative yield (see Eq. 5). Compound **4.3** was characterized by a combination of ^{1}H NMR, and single crystal X-ray crystallography and, IR spectroscopy.

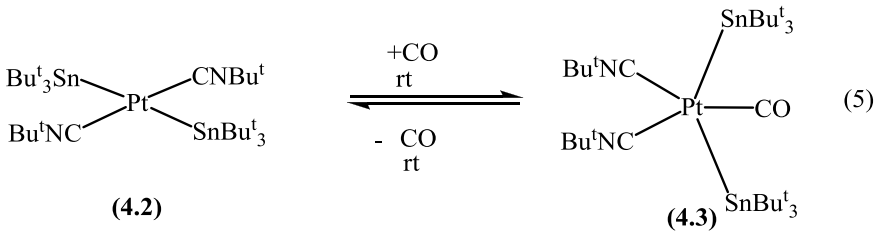

The molecular structure of compound **4.3** is shown in Figure.4.9. The geometry around the Pt(II) metal center in **4.3** is slightly distorted from trigonal bipyramidal (TBP) geometry due to sterics induced by $SnBu^t_3$ ligands. The Pt-Sn and Pt-CO bond lengths remain almost the same as observed in precursor complex **2.5**. The Pt-Sn bond length in complex **4.3** is 2.714 (8) Å, slightly longer than Pt-Sn bond length in complex **4.1**. The C1-Pt-C1* bond angle in **4.3** is the same as in compound **4.1**.

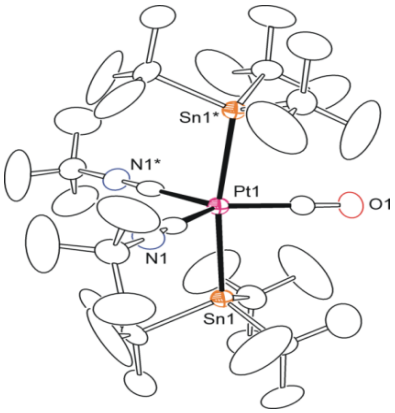

Figure 4.9 The molecular structure of $Pt(CO)(SnBu^t_3)_2(CNBu^t)_2$, **4.3**.

The addition of CO gas to compound **4.2** is reversible in the solid state too; as observed in the addition of H_2. The purple crystals of **4.2** turn colorless upon exposure to CO atmosphere in 15 minutes at room temperature to yield **4.3** quantitatively. Similarly, colorless crystals of **4.3** turn purple under argon flow after 24 hours, yielding quantitative amounts of **4.2**. The CO ligand in **4.3** is weakly bound to platinum and can be easily

exchanged with the hydride ligands. Addition of H_2 to compound **4.3** affords Pt(IV) isocyanide complex **4.1** at room temperature. The reversible activation of H_2 and CO molecules by the 16 electron Pt(II) isocyanide complex **4.2** are summarized in Scheme 4.4.

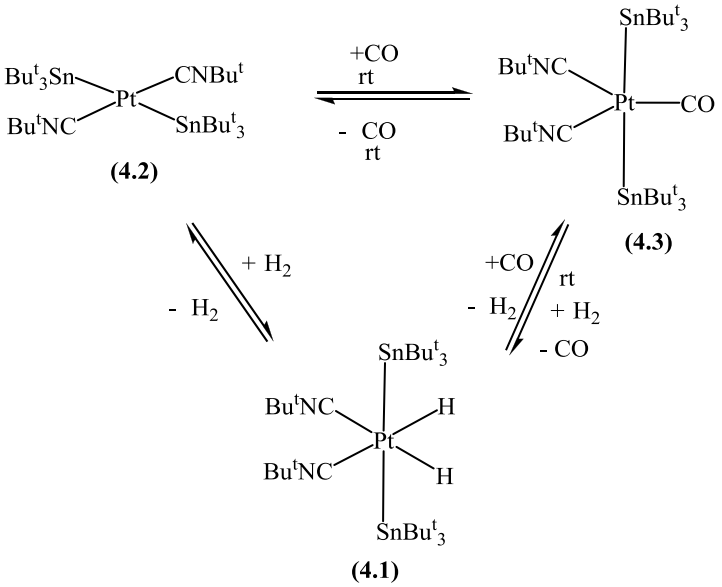

Scheme 4.4

Photolysis studies on Pt(SnBu$^t_3$)$_2$(CO)(CNBu^t)$_2$, 4.3: The yellow-colored Ni(II) isocyanide complex Ni(SnBu$^t_3$)$_2$(CO)(CNBu^t)$_2$, **4.4**, has been shown to be photoactive. Upon irradiation with a mercury lamp, compound **4.4** slowly turns purple, yielding [Ni(SnBu$^t_3$) (CO)(CNBu^t)$_2$], **4.5**. Anjaneyulu, a graduate student in our lab, observed that compound **4.5** acts as a radical initiator, catalyzing polymerization reactions. We have also investigated the photolysis of analogous Pt(II) isocyanide complex **4.3** with a mercury lamp, and monitored the reaction by IR spectroscopy. But surprisingly in our case no considerable reaction was observed at room temperature. We attribute this to the facile elimination of weakly bound CO from the Pt(II) center, resulting in the formation

of compound **4.2**. Further research on compound **4.2** is essential in the near future to understand the ability of **4.2** to catalyze hydrogenation and hydroformylation reactions of alkenes under ambient conditions.

In a separate experiment we monitored the conversion of compound **4.2** into compound **4.1**, under 1 atm of CO gas at room temperature under hood light, by IR spectroscopy at several intervals. The IR spectrum of compound **4.2** in hexane solution shows a sharp peak for ν_{CN} stretching frequency at 2112 cm^{-1}. After purging the solution for 15 minutes with 1 atm CO an additional peak corresponding to Pt bound carbonyl stretching frequency was observed in the IR spectrum at 1966 cm^{-1}. After four hours there was an appearance of peaks identical to that $[Ni(SnBu^t_3)(CO)(CNBu^t)_2]$, **4.5**, in hexane solution. Unfortunately, after evaporation of the solvent *in-vacuo*, we were unable to isolate the desired analogous Pt(II) complex $[Pt(SnBu^t_3)(CO)(BuNC)_2]_2$.

Reaction of $Pt(SnBu^t_3)_2(CO)_2$, 2.5 with benzyl isocyanide ($CNCH_2Ph$): We have further investigated the effect of varying bulkiness of organoisocyanide lignads on the reactivity of Pt(II) isocyanide complex **4.2**. A less bulky isonitrile ligand, benzyl isocyanide, was added to $Pt(SnBu^t_3)_2(CO)_2$, **2.5** instead of *tert*-butyl isocyanide to understand the role of steric bulkiness in stabilization of low coordinate transition metal isocyanide complexes. The addition of an excess of benzyl isocyanide to the hexane solution of **2.5** at room temperature affords the Pt(II) isocyanide complex $Pt(SnBu^t_3)_2(PhCH_2NC)_3$, **4.6**, analogous to $Ni(SnBu^t_3)_2(Bu^tNC)_3$ (see Eq. 6).

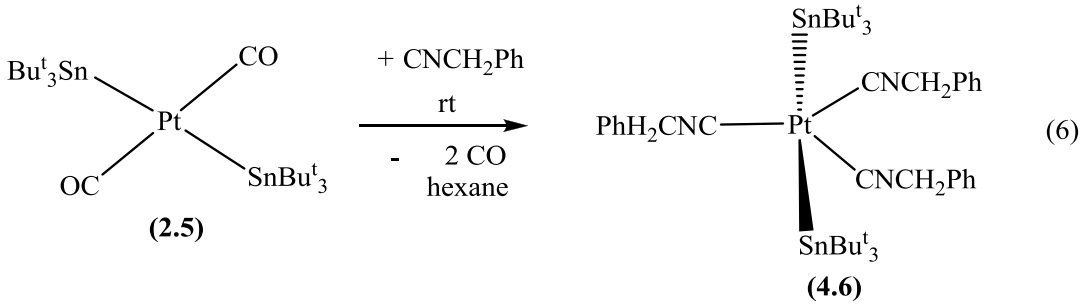

(6)

Compound **4.6** was characterized by a combination of ^{1}H NMR, single crystal X-ray crystallography, and IR spectroscopy. The molecular structure of compound **4.6** is shown in Figure C.1 in Appendix C. Compound **4.6** is a 18 electron mononuclear Pt(II) complex with trigonal bypiramidal geometry. The two axial SnBu$^t_3$ groups are bonded to Pt in the *trans* position and PhCH$_2$NC groups are in equatorial plane giving the molecule approximate D_{3h} symmetry. The Pt-Sn bond lengths are in the same range as that observed in compound **4.1**, but the Sn1-Pt1-Sn2 bond angle is 177.387(19)°, which is higher than Sn1-Pt-Sn1* bond angle of 103°.

Synthesis of Pt(SnBu$^t_3$)$_2$(CNPhCH$_2$)$_2$, 4.7: Compound **4.6** is slowly converted into Pt(II)-bis(isocyanide) complex Pt(SnBu$^t_3$)$_2$(CNCH$_2$Ph)$_2$, **4.7** under argon flow at room temperature in hexane solution with the elimination of one CNCH$_2$Ph ligand (see Scheme 4.5). We have characterized compound **4.7** by a combination of ^{1}H NMR, and IR spectroscopy. Based on the IR and ^{1}H NMR spectrum we assign a *trans* structure similar to compound **4.2**. We are still investigating the reactivity of this compound.

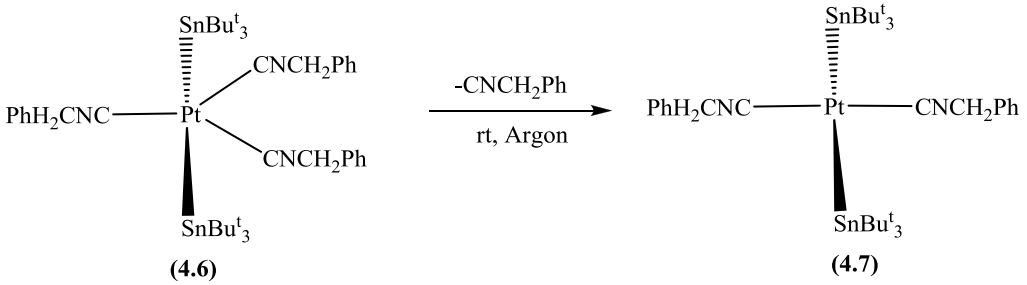

Scheme 4.5

Synthesis of Pd(II) isocyanide complexes: To understand the reactivity of *tert*-butyl isocyanide further, a palladium isocyanide complex has been synthesized from a Pd(allyl)(Cp) precursor complex by the addition of two equivalents of $CNBu^t$ in hexane solution, yielding a known Pd(0) isocyanide complex $Pd(CNBu^t)_2$, **4.8**. Compound **4.8** readily reacts with two equivalents of Bu^t_3SnH through oxidative addition of an Sn-H bond to a Pd(0) metal center, followed by the reductive elimination of the hydrogen affording the Pd(II) isocyanide complex $[Pd(SnBu^t_3)(CNBu^t)_2]$, **4.9**, in 30% yield (see Scheme 4.6).

Compound **4.9** was characterized by a combination of ^1H NMR and single crystal X-ray crystallography. Its structure is similar to $[Pt(SnBu^t_3)(CNBu^t)_2]$, **4.2**, having slightly distorted square planar geometry. We were unable to characterize the intermediate Pd(IV) isocyanide complex $[H_2Pd\ Pt(SnBu^t_3)(CNBu^t)_2]$; owing to high reactivity it loses hydride ligands readily, which made it difficult to obtain suitable crystals of X-ray quality. The molecular structure of compound **4.9** is shown in Figure C.3 in Appendix C. The Pd-Sn bond lengths are in the same range as that observed in the Pd-Sn closoborate isocyanide cluster.[189] The Pd(II) isocyanide complex $Pd(SnBu^t_3)_2(CNBu^t)_2$, **4.9**, also

shows similar reactivity as that of the analogous Pt complex **4.2** in the reversible activation of hydrogen at room temperature.

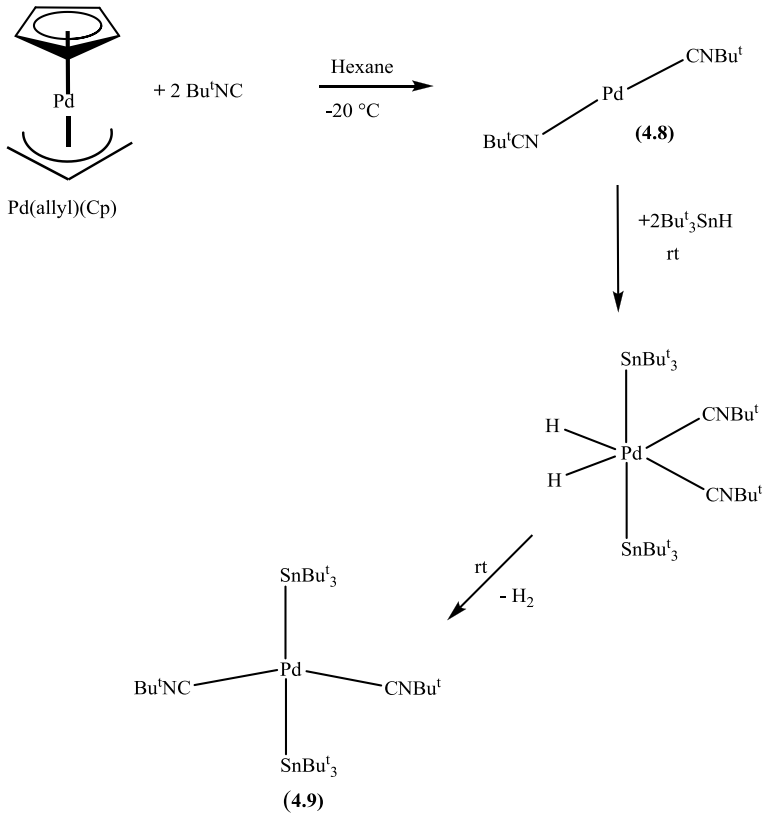

Scheme 4.6

The molecular structure of compound **4.9** is shown in Figure C.2 in Appendix C. The Pd-Sn bond lengths are in the same range as that observed in the Pd-Sn closoborate isocyanide cluster.[189] More experiments need to be conducted on this complex to test the ability to act as a homogeneous hydrogenation catalyst.

Synthesis of Pd(II) isocyanide complex Pd(SnBu$^t_3$)$_2$(CNBu^t)$_3$, 4.10 from Pd(dba)$_2$: With the addition of excess CNBu^t and two equivalents of Bu$^t_3$SnH to the Pd(0) precursor complex, Pd(dba)$_2$, in THF solution at room temperature we were able to isolate Pd(II) isocyanide complex Pd(SnBu$^t_3$)$_2$(CNBu^t)$_3$, **4.10**, (see Eq. 7).

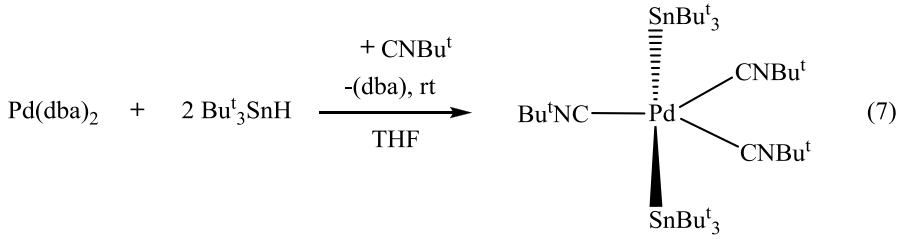

(4.10)

Compound **4.10** is also an 18 electron Pd(II) mononuclear complex with the three isocyanide ligands located in the equatorial plane and two $SnBu^t_3$ groups located *trans* to each other in the axial position. The compound **4.10** was characterized by a combination of ^1H NMR and single crystal X-ray crystallography. The molecular structure of compound **4.10** is shown in Figure 4.10.

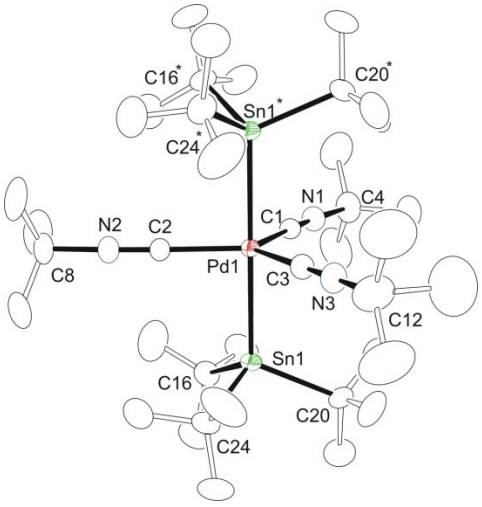

Figure 4.10 The molecular structure of $Pd(SnBu^t_3)_2(CNBu^t)_3$, **4.10**.

The Sn1-Pd-Sn1 bond angle is 179.76 9(3)°, giving the molecule trigonal bipyramidal geometry, and the Pd-Sn bond lengths are similar to that of Pt-Sn bond lengths in compound **4.6**. When kept under argon atmosphere for three hours at room temperature compound **4.10** slowly turns purple to yield $Pd(SnBu^t_3)_2(CNBu^t)_2$, **4.9** (see Eq. 8).

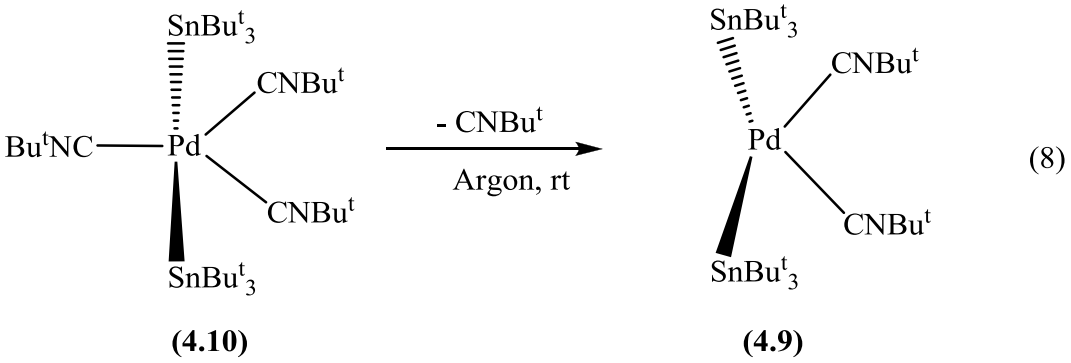

(4.10) **(4.9)** (8)

Pd isocyanide complex **4.9** tends to decompose more rapidly than analogous Pt isocyanide complex **4.2**. There are few examples for insertion of isocyanide into the Pd-C bond and also Pd-Sn bond.[174, 211, 212] Interestingly, in our case we have never observed products corresponding to insertion of isocyanides in the Pd-E bond (E=Sn) or Pd-C bond (of the dba ligand). Further studies on the reactivity of Pd(II) and Pd(IV) isocyanide complexes are currently in progress.

4.3. Conclusions

In the previous chapter we showed that the lability of CO ligands in complex **2.5** can be used in the synthesis of Pt-Sn NHC complexes by substitution of CO ligands. In this chapter we have demonstrated a simple synthesis method for the Pt(II) isocyanide complex $Pt(SnBu^t_3)_2(CNBu^t)_2$, **4.2**, from ligand substitution of the labile CO group in $Pt(SnBu^t_3)_2(CO)_2$, **2.5**, by $CNBu^t$ groups. The lability of the CO ligands in complex **2.5** can be used in the synthesis of a wide variety of Pt-Sn complexes by substitution of CO ligands.

Compound **4.2** was effective in the reversible activation of small molecules like H_2 and CO at ambient conditions both in solution and the solid state. The bulky $CNBu^t$ ligand facilitates the stabilization of the distorted square planer Pt(II) isocyanide complex

4.2 and rearranges appropriately on addition of H_2 to accommodate hydride ligands and give a nearly octahedral geometry Pt(IV) dihydride complex, **4.1**. Similarly, activation of CO by compound **4.2** yields the Pt(II) complex $Pt(SnBu^t_3)_2(CO)(CNBu^t)_2$, **4.3**, comprising both isocyanide and CO ligands and having a trigonal bipyramidal geometry.

The reversible activation of CO and H_2 at room temperature by **4.2** is attributed to the electronic unsaturation imparted by the bulky $SnBu^t_3$ groups and isocyanide ligands. Further research on compound **4.2** will aid in extending its application in catalytic hydrogenation and hydroformylation reactions. The H_2-D_2 scrambling reaction by **4.2** to produce HD gas is also another important aspect of its reactivity that need to be examined further to understand the reaction mechanism.

4.4. Experimental section

General Data

Unless otherwise indicated, all reactions were performed under an atmosphere of Argon. Reagent grade solvents were dried by standard procedures and were freshly distilled prior to use. Infrared spectra were recorded on a Nicolet 380 FT-IR spectrophotometer. ^{1}H NMR were recorded on a Bruker 300 and 400 spectrometers operating at 300.13 MHz and 399.99 MHz respectively. Elemental analyses were performed by Columbia Analytical Services (Tuscon, AZ). Mass spectrometric measurements performed by a direct-exposure probe using electron impact ionization (EI) were made on a VG 70S instrument at the University of South Carolina, Columbia, SC. CO and H_2 gases of 99.9% purity were purchased from air gas south and used without further purification. *tert*-butyl isocyanide, $CNBu^t$, and $Pd(dba)_2$ were purchased

from Strem chemicals and used without further purification. Bis(1,5-cyclooctadiene)platinum, $Pt(COD)_2$,[115] and tri-*tert*-butylstannane, Bu^t_3SnH,[105] Pd(allyl)(Cp)[116] were prepared according to the published procedures. Benzyl isocyanide was purchased from Acros organics and used without further purification.

Synthesis of $Pt(SnBu^t_3)_2(CNBu^t)_2(H)_2$, 4.1.

In a glove box under an atmosphere of argon, 49.5 mg of Bu^t_3SnH (0.170 mmol) dissolved in 5 mL of freshly distilled hexane was added to 35.0 mg of $Pt(COD)_2$ (0.085 mmol). The reaction mixture was stirred at room temperature for 5 minutes after which time 14.0 mg of $CNBu^t$ (0.170 mmol) was added and the reaction mixture stirred at room temperature for an additional 10 min. The solution was then filtered and the filtrate was placed in a -20 °C freezer overnight which gave crystalline $Pt(SnBu^t_3)_2(CNBu^t)_2(H)_2$, **4.1**. After washing the crystalline product with approximately 2 mL of acetonitrile, 26.0 mg (32% yield) of **4.1** was obtained. Spectral data for **4.1**: ^{1}H NMR (C_6D_6, rt, in ppm): δ = 1.57 (s, 54 H, $SnBu^t_3$, $^3J_{Sn-H}$ = 51 Hz), 0.96 (s, 18H, Bu^t); - 13.52 (s, 2H, hydride, $^1J_{Pt-H}$ = 697 Hz, $^2J_{Sn-H}$ = 34 Hz). Mass Spec. EI/MS *m*/*z*. 942 (M^+), 883 (M^+-H_2-Bu^t). The isotope pattern is consistent with the presence of one platinum and two tin atoms. IR ν_{CN} (cm^{-1} in hexane): 2139 (s), ν_{Pt-H} 2112 (m) cm^{-1}.

Conversion of 4.1 to $Pt(SnBu^t_3)_2(CNBu^t)_2$, 4.2 in solution.

A 15.0 mg amount of **4.1** (0.016 mmol) was dissolved in 50 mL of distilled hexane. With stirring, argon was then allowed to purge through the solution at 25 °C for approximately 20 h. Within minutes the colorless solution started to turn violet. ^{1}H NMR of the reaction mixture showed complete conversion of the starting **4.1** to **4.2**. The solvent was removed *in vacuo*, and the purple-colored residue was crystallized by

evaporation of a benzene/acetonitrile solvent mixture under a stream of argon at room temperature to yield 13.2 mg (89%) of crystalline **4.2**. Spectral data for **4.2**: ^{1}H NMR (C_6D_6, rt, in ppm): δ = 1.60 (s, 54 H, $SnBu^{t}_3$, $^{3}J_{Sn\text{-}H}$ = 49 Hz), 1.15 (s, 18H, Bu^{t}). Mass Spec. EI/MS *m*/*z*. 940 (M^{+}), 883 (M^{+}-Bu^{t}). The isotope pattern is consistent with the presence of one platinum and two tin atoms. IR ν_{CN} (cm^{-1} in hexane): 2112 (s).

Conversion of 4.2 to 4.1 in solution.

In a 10 mL schlenk tube, 28.0 mg of **4.2** (0.030 mmol) was dissolved in 5 mL of hexane. The solvent was removed under a slow stream of hydrogen gas (approximately 3 hours) during which time the color of the solution changed from violet to colorless. This yielded 26.2 mg (94% yield) of crystalline **4.1**.

Conversion of 4.1 to $Pt(SnBu^{t}_3)_2(CNBu^{t})_2$, 4.2 in the solid state.

In a 10 mL schlenk tube containing 10.0 mg of colorless crystalline **4.1** (0.011 mmol), argon gas was purged through the system for 24 hours in the dark at room temperature, at which time the color of the crystalline **4.1** turned to violet. ^{1}H NMR indicated complete consumption of starting **4.1** in quantitative yield to $Pt(SnBu^{t}_3)_2(CNBu^{t})_2$, **4.2**.

Solid state conversion of 4.2 to 4.1.

In a 10 mL schlenk tube containing 12.0 mg of violet crystalline **4.2** (0.013 mmol), hydrogen gas was purged through the system for 15 minutes in the dark at room temperature, at which time the color of the crystalline **4.2** turned to colorless. ^{1}H NMR indicated complete consumption of starting **4.2** in quantitative yield to **4.1**.

Synthesis of $Pt(CO)(SnBu^t_3)_2(CNBu^t)_2$, 4.3.

In a glove box, under an atmosphere of argon, a 40.0 mg(0.480 mmol) amount of $CNBu^t$ was added to 195 mg (0.230 mmol) of $Pt(CO)_2(SnBu^t_3)_2$, **2.5**, dissolved in 2 mL of freshly distilled hexane at room temperature. With the addition of $CNBu^t$ the CO gas evolves from the reaction mixture (gas bubbles can be seen), and the green-colored solution slowly turned colorless. Colorless crystals crashed out of the solution. The solution was placed in a -20 °C freezer overnight to obtain more crystals. The solvent is removed and colorless crystals were washed with 0.2 ml of hexane to afford 219 mg (96% yield). The crystals turned to a violet color on prolonged exposure to air. Spectral data for **4.3**: ^{1}H NMR (C_6D_6, rt, in ppm): δ = 1.57 (s, 54 H, $SnBu^t_3$, $^3J_{Sn-H}$ = 51 Hz), 0.96 (s, 18H, Bu^t); (Note: in CO atmosphere). IR ν_{CO} (cm^{-1} in hexane): 2144(w), 2112 (vs), 1966 (s).

H_2-D_2 scrambling reaction by 4.2

In an NMR tube 4.0 mg of **4.2** were dissolved in 0.6 mL of C_6D_6 solvent. The NMR tube was evacuated under a vacuum and an equimolar mixture of H_2 and D_2 gas was injected into the NMR tube using a syringe, at which time the violet-colored solution turned colorless. The ^{1}H NMR spectrum of the reaction mixture after approximately 15 minutes showed formation of HD gas (δ = 4.44, $^1J_{D-H}$ = 43 Hz) along with formation of the corresponding HD complex **4.1-*d*$_1$**. H_2 gas was also present (δ=4.47) as well as the H_2 complex **4.1**. Integration of the hydride region indicated that the HD complex **4.1-*d*$_1$** and the H_2 complex **4.1** were present in approximately a 4:1 ratio. There was no indication of any unreacted **4.2**.

Synthesis of $Pt(SnBu^t_3)_2(CNBu^t)_2$, 4.2 from 4.3.

A 219 mg (0.226 mmol) amount of crystalline **4.3** was washed with cold isopropyl alcohol (3x 0.1 mL) and the purple-colored powder was redissolved in benzene solvent. A few drops of acetonitrile was added to the purple-colored solution and evaporated the solvent under slow argon gas stream to obtain 184 mg (86% yield) of violet color crystalline $Pt(SnBu^t_3)_2(CNBu^t)_2$, **4.2**.

Conversion of 4.3 to 4.2 in solution

A 17.0 mg amount of **4.3** (0.0175 mmol) was dissolved in 10 mL of distilled hexane. With stirring, argon gas was then allowed to purge through the solution at 25 °C for approximately 10 minutes. Within minutes the colorless solution started to turn violet. An IR spectrum of the reaction mixture showed complete conversion of the starting **4.3** compound to **4.2**. The solvent was removed *in vacuo*, and the purple-colored residue was crystallized by evaporation of a benzene/acetonitrile solvent mixture under a stream of argon gas at room temperature to yield 15.0 mg (92 %) of crystalline **4.2**.

Conversion of 4.2 to 4.3 in solution

A 17.0 mg amount of **4.2** (0.0180 mmol) was dissolved in 25 mL of distilled hexane. With stirring, CO gas was then allowed to purge through the solution at 25 °C for approximately 10 minutes. Within minutes the purple solution started turning colorless. An IR spectrum of the reaction mixture showed complete conversion of the starting **4.2** to **4.3**. The solvent was removed *in vacuo*, and the purple-colored residue was crystallized by evaporation of a benzene/acetonitrile solvent mixture under a stream of CO gas at room temperature to yield 15.0 mg (86%) of crystalline **4.3**.

Conversion of 4.2 to 4.3 in solid state.

In a 10 mL schlenk tube containing 10.0 mg of purple crystalline **4.2** (0.010 mmol), CO gas was purged through the system for an hour in the dark at room temperature, at which time the color of the crystalline **4.2** turned to colorless. The ^{1}H NMR spectrum indicated complete consumption of starting **4.2** in quantitative yield to $Pt(CO)(SnBu^t_3)_2(CNBu^t)_2$, **4.3**.

Conversion of 4.3 to 4.2 in solid state.

In a 10 mL schlenk tube containing 10.0 mg of colorless crystalline **4.3** (0.010 mmol), argon gas was purged through the system for 16hoursin the dark at room temperature, at which time the color of the crystalline **4.3** turned to violet. The ^{1}H NMR spectrum indicated complete consumption of starting **4.3** in quantitative yield to $Pt(SnBu^t_3)_2(CNBu^t)_2$, **4.2**.

Synthesis of $Pt(SnBu^t_3)_2(CNCH_2Ph)_3$, 4.6.

In a glove box under an atmosphere of argon, an excess amount of $CNCH_2Ph$ was added to 80.0 mg (0.096 mmol) of $Pt(CO)_2(SnBu^t_3)_2$, **2.5**, dissolved in 2 mL of freshly distilled hexane at room temperature. With the addition of the $CNCH_2Ph$ the CO gas evolved from the reaction mixture (gas bubbles can be seen) and the green-colored solution slowly turned into colorless; the colorless crystals crashed out of the solution. The solution was placed in a -20 °C freezer overnight to obtain more crystals. The solvent was removed and the colorless crystals were washed with 0.2 mL of hexane to afford 90.0 mg of **4.6** (83% yield). The crystals turned to a pink color on prolonged exposure to air. Spectral data for **4.6**: ^{1}H NMR (C_6D_6, rt, in ppm): δ = 7.36-6.96 (m,

Phenyl group), δ = 4.36 (s, CH_2 on Phenyl group), δ = 1.56 (s, 54 H, $SnBu^t_3$, $^3J_{Sn-H}$ = 51 Hz). IR ν_{CN} (cm^{-1} in hexane): 2139(vs), 2104 (sh).

Synthesis of $Pt(SnBu^t_3)_2(CNCH_2Ph)_2$, 4.7 from 4.6.

A 60.0 mg (0.053 mmol) amount of crystalline **4.6** was washed with acetonitrile (3x 0.1 mL) and the pink color powder was redissolved in benzene solvent. A few drops of acetonitrile were added to the pink-colored solution and the solvent was then evaporated under a slow argon gas stream to obtain 50.0 mg (92% yield) of pink color crystalline $Pt(SnBu^t_3)_2(CNCH_2Ph)_2$, **4.7**. Spectral data for **4.7**: ^{1}H NMR (C_6D_6, rt, in ppm): δ = 7.36-6.96 (m, Phenyl group), δ = 4.36 (s, CH_2 on Phenyl group), 1.50 (s, 54 H, $SnBu^t_3$, $^3J_{Sn-H}$ = 49 Hz). IR ν_{CN} (cm^{-1} in hexane): 2139(vs).

Conversion of 4.6 to 4.7 in solution

A 17.0 mg amount of **4.6** (0.0150 mmol) was dissolved in 10 mL of distilled hexane. With stirring, argon gas was then allowed to purge through the solution at 25 °C for approximately 10 min. Within minutes the colorless solution started to turn pink. An IR spectrum of the reaction mixture showed complete conversion of the starting compound **4.6** to **4.7**. The solvent was removed *in vacuo* and the pink-colored residue was crystallized by evaporation of a benzene/acetonitrile solvent mixture under a stream of argon gas at room temperature to yield 15.0 mg (98%) of crystalline **4.7**.

Synthesis of $Pd(SnBu^t_3)_2(CNBu^t)_2$, 4.9.

In a glove box under an atmosphere of argon, 40.0 mg of $CNBu^t$ was added to 40.0 mg of Pd(allyl)(Cp) dissolved in 5 mL of distilled hexane at -20 °C in a medium scintillation vial. A yellow precipitate crashed out of the solution immediately. The

precipitate was washed with pentane (2x 0.1mL) to obtain 35 mg of yellow $Pd(CNBu^t)_2$ crystals. Then, 75.5 mg of Bu^t_3SnH (0.250 mmol) dissolved in 5 mL of freshly distilled hexane was added to 35.0 mg of $Pd(CNBu^t)_2$ (0.128 mmol). The reaction mixture was stirred at room temperature for five minutes, after which time the reaction mixture slowly turned to violet. The volume of the solution was reduced to 1mL and kept in a -25 °C freezer in glove box overnight to yield purple-colored crystals of **4.9** covered with oily residue. Crystals were washed with acetonitrile several times to yield 20 mg (60% yield) of pure **4.9**. Spectral data for **4.9**: ^{1}H NMR (C_6D_6, rt, in ppm): δ = 1.58 (s, 54 H, $SnBu^t_3$, $^3J_{Sn\text{-}H}$ = 46 Hz), 1.13 (s, 18H, Bu^t).

Synthesis of $Pd(SnBu^t_3)_2(CNBu^t)_3$, 4.10.

In a glove box under an atmosphere of argon, 45.5 mg of Bu^t_3SnH (0.156 mmol) dissolved in 5 mL of freshly distilled THF was added to 35.0 mg of $Pd(dba)_2$ (0.060 mmol). The reaction mixture was stirred at room temperature for 5 minutes after which time 14.0 mg of $CNBu^t$ (0.170 mmol) was added and the reaction mixture stirred at room temperature for an additional 10 min. The solution was then filtered and the filtrate was evaporated under argon flow to obtain a violet-colored solid residue. The solid residue was washed with pentane several times, and the washings were collected together and reducing the solvent volume to a small fraction afforded 20.0 mg (35% yield) of colorless crystals of **4.10**. Spectral data for **4.10**: ^{1}H NMR (C_6D_6, rt, in ppm): δ = 1.59 (s, 54 H, $SnBu^t_3$, $^3J_{Sn\text{-}H}$ = 46 Hz), 1.09 (s, 27H, Bu^t).

Conversion of 4.10 to $Pd(SnBu^t_3)_2(CNBu^t)_2$, 4.9 in solution.

A 17.0 mg amount of **4.10** (0.0181 mmol) was dissolved in 10 mL of distilled hexane. With stirring, argon gas was then allowed to purge through the solution at 25 °C for approximately 10 minutes. Within minutes the colorless solution started to turn pink. The ^{1}H NMR spectrum of the reaction mixture showed complete conversion of the starting compound **4.10** to **4.9**. The solvent was removed *in vacuo* and the pink-colored residue was crystallized by evaporation of a benzene/acetonitrile solvent mixture under a stream of argon gas at room temperature to yield 14.0 mg (90% yield) of crystalline **4.9**. Spectral data for **4.9**. ^{1}H NMR (C_6D_6, rt, in ppm): δ = 1.58 (s, 54 H, $SnBu^t_3$, $^3J_{Sn\text{-}H}$ = 46 Hz), 1.13 (s, 18H, Bu^t).

Conversion of 4.9 to $Pd(SnBu^t_3)_2(CNBu^t)_2$, 4.11 in solution.

A 15.0 mg amount of **4.9** (0.0176 mmol) was dissolved in 50 mL of distilled hexane. With stirring, argon was then allowed to purge through the solution at 25 °C for approximately 20 h. Within minutes the colorless solution starts to turn violet. ^{1}H NMR of the reaction mixture showed complete conversion of the starting **4.9** to **4.11**. The solvent was removed *in vacuuo*, and the purple color residue was crystallized by evaporation of a benzene/acetonitrile solvent mixture under a stream of argon at room temperature to yield 13.2 mg (85% yield) of crystalline **4.9**.

4.5. Crystallographic analyses

Colorless crystals of **4.1** suitable for diffraction analysis were grown by slow evaporation of a solution of **4.2** in diethyl ether solvent under a slow stream of hydrogen gas at 0 °C (ice-water bath). Crystals of **4.1** were also obtained as described above.

Violet-colored crystals of **4.2** suitable for diffraction analysis were grown by slow evaporation of solvent from a hexane solution at -20 °C in a glove box. Colorless crystals of **4.3** suitable for diffraction analysis were grown by slow evaporation of solvent from a hexane solution at -20 °C in a glove box.

Colorless crystals of **4.6**, **4.9** and **4.10** suitable for diffraction analysis were grown by slow evaporation of solvent from a hexane solution at -20 °C in a glove box. Pink-colored crystals of **4.7** were obtained from evaporation of benzene/acetonitrile solution under slow argon flow at room temperature. Violet color crystals of **4.10** were obtained from evaporation of diethyl ether solution under slow argon flow at room temperature.

Each data crystal was mounted onto the end of a thin glass fiber using Paratone-N. X-ray intensity data were measured by using a Bruker SMART APEX2 CCD-based diffractometer using Mo Kα radiation (λ = 0.71073 Å).[117] The raw data frames were integrated with the SAINT+ program by using a narrow-frame integration algorithm.[117] Corrections for Lorentz and polarization effects were also applied with SAINT+. An empirical absorption correction based on the multiple measurement of equivalent reflections was applied using the program SADABS. Both structures were solved by a combination of direct methods and difference Fourier syntheses, and refined by full-matrix least-squares on F^2, by using the SHELXTL software package.[118] Crystal data, data collection parameters, and results of the analyses are listed in Tables C.1- C.3 in Appendix C.

Compound **4.1** crystallized in the orthorhombic crystal system. The systematic absences in the intensity data were consistent with either of the space groups $Pmn2_1$ or *Pmmn*. The centrosymmetric space group *Pmmn* was assumed and confirmed by the

successful solution and refinement of the structure. With Z = 2 there is half a formula equivalent of the molecule in the asymmetric crystal unit about a site of *mm*2 symmetry. Half a molecule of diethyl ether from the crystallization solvent, co-crystallized with the complex on a crystallographic *mm*2 symmetry site. The hydride ligand was located and refined with an isotropic thermal parameter. All non-hydrogen atoms were refined with anisotropic displacement parameters. Hydrogen atoms were placed in geometrically idealized positions and included as standard riding atoms during the least-squares refinements.

Compounds **4.2** and **4.9** crystallized in the monoclinic crystal system. The space group $P2_1/n$ was confirmed on the basis of the systematic absences in the data. All non-hydrogen atoms were refined with anisotropic displacement parameters. Hydrogen atoms were placed in geometrically idealized positions and included as standard riding atoms during the least-squares refinements.

Compounds **4.3** and **4.10** crystallized in the orthorhombic crystal system. The space group *Pmmn* was confirmed on the basis of the systematic absences in the data for compound **4.3**. The centrosymmetric space group *Pmmn* was assumed and confirmed by the successful solution and refinement of the structure. With Z = 2 there is half a formula equivalent of the molecule in the asymmetric crystal unit about a site of *mm*2 symmetry. For compound **4**.**9** also *Pnnm* was assumed and confirmed by the successful solution and refinement of the structure. With Z = 2 there is half a formula equivalent of the molecule in the asymmetric crystal unit about a site of *nn*2 symmetry. There is a slight disorder for *tert*-butyl groups on Nitrogen.

Compound **4.6** crystallized in the monoclinic crystal system. The space group $P2_1/c$ was confirmed on the basis of the systematic absences in the data. All non-hydrogen atoms were refined with anisotropic displacement parameters. Hydrogen atoms were placed in geometrically idealized positions and included as standard riding atoms during the least-squares refinements

Chapter 5: Radical exchanges and structural transformations on the iron carbonyl-bulky tin cluster complex, $Fe_2(\mu\text{-}SnBu^t_2)_2(CO)_8$ by solvents toluene, xylenes and ethylbenzene.

5.1. Background

In the previous chapters we have seen that bulky tin ligands are bonded to platinum through oxidative addition of an Sn-H bond to afford unsaturated Pt-Sn bimetallic complexes. These Pt-Sn metal complexes are shown to be effective in the activation of small molecules and their reactivity is comparable to that of Pt complexes with phosphine ligands. With these positive results we were motivated to further investigate the reactivity of the bulky organotin ligand Bu^t_3SnH with the other cheaper transition metals such as nickel and iron. In this chapter we will present the synthesis of Fe-Sn bimetallic cluster complexes and the selective benzylic C-H bond activation of solvent molecules by these Fe-Sn cluster complexes.

Mixed-metal cluster complexes containing tin ligands present fascinating structural chemistry. In addition to the inherent beauty of some of these structures, they provide elegant chemistry in solution as well as valuable precursors to heterogeneous nano-catalysts. The pioneering work of Adams in cluster chemistry between transition metals and main group elements has been prominent in this area.[70, 95, 213, 214] We recently reported the benzylic additions of solvent toluene and *m*-xylene to a tin center by the bimetallic tin-containing complex $Fe_2(\mu\text{-}SnBu^t_2)_2(CO)_8$, **5.1**.[105] The activation of benzylic C-H bonds is of major importance industrially.[215-218] Efficient and catalytic functionalization of organic molecules from hydrocarbon feedstocks may lead to generation of renewable fuel sources, amongst other great benefits.

In recent years many transition metal complexes capable of quantitative benzylic sp^3 carbon C-H activation have been synthesized, but most will also affect sp^2 hybridized aryl C-H bonds and this may not always be desirable.[219-225] A good example of this is the tungsten phosphine hydride complex as shown in Scheme 5.1.[226]

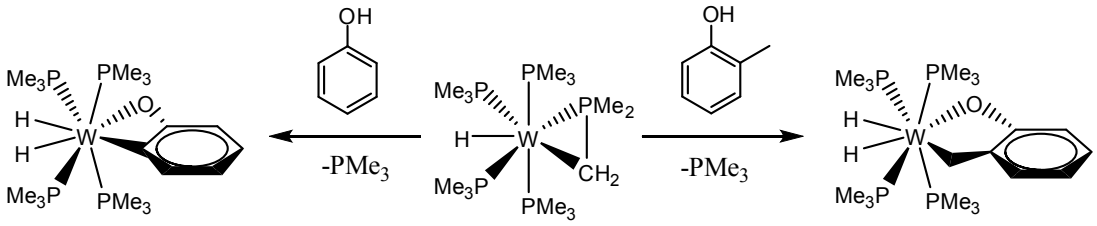

Scheme 5.1

Another tungsten compound, a remarkable cyclopentadiene-allyl-nitrosyl complex, was also shown to activate a wide variety of C-H bonds (see Scheme 5.2).[227] The vast majority of existing compounds for these C-H activation reactions are precious metals, Platinum and Rhodium predominantly.[219, 220] As supply shrinks and demand skyrockets, the need for cheaper and more abundant replacements for these precious metals grows exponentially.

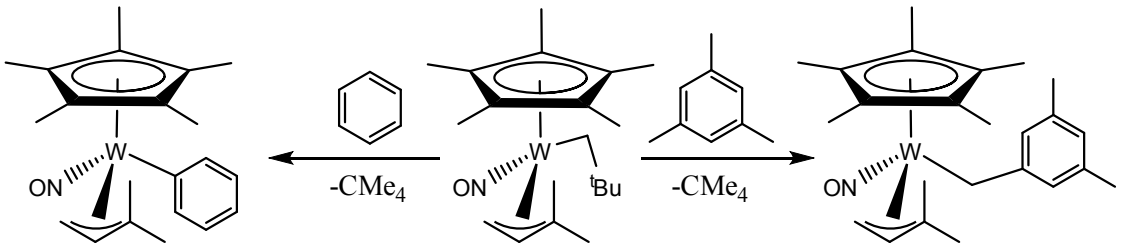

Scheme 5.2

A solution for this potential shortage problem may be in the field of bimetallics. The synergistic effects between heterometals have been shown to provide greater reactivity and catalytic ability than either counterpart metal alone.[228] Indeed, a recent iridium-tin

complex was shown to catalyze the alkylation of arenes, proceeding via aryl C-H activation of the arene substrate at the iridium center.[229, 230] Recent studies have shown that even some cyclopentadienyl complexes of Ytterium and Gadolinium can also activate C–H bonds (see Eq. 1).[231] Tin has also been shown to selectively activate the aryl C–H bonds in alkylaromatic compounds. For example, the complex ‘‘(CF3COO)4Sn”[232] activates the aryl C–H bond in benzene as well as in p-xylene.

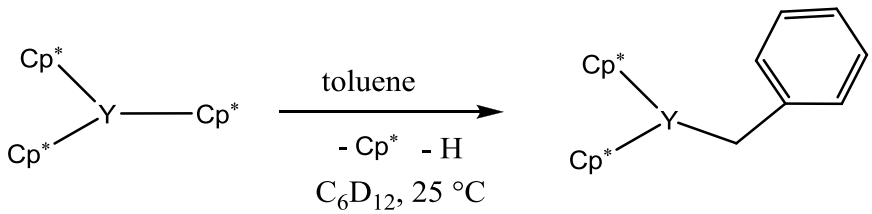

(1)

Iron has also been recently shown to activate the carbon-hydrogen bonds in heteroarenes,[233] and in fact, tin itself has also been proven to selectively activate the strong aromatic C-F bonds.[234] Herein we report the further study of compound **5.1** and its tin centered selective benzylic sp^3 C-H activation of appropriate substrates- toluene, xylenes, and ethylbenzene- and propose a radical mechanism for the reaction. This is the first example of selective benzylic C–H activation of alkylaromatic compounds at tin centers.

5.2. Results and discussion

Compound **5.1**, $Fe_2(\mu\text{-}SnBu^t_2)_2(CO)_8$, was prepared some years ago from the salt-elimination reaction of $Na_2Fe(CO)_4$ and Bu^tSnCl_2 in 50% yield. Its structure was correctly formulated based on FTIR spectroscopy and molecular weight measurements.[235] We recently found that compound **5**.**1** is also formed in 41% yield by reaction of Bu^t_3SnH with $Fe_2(CO)_9$ in refluxing heptane and its structure as elucidated by single crystal X-ray

diffraction analysis is shown in Figure **5**.1. This structure of **5.1** is virtually identical to the dimethyl tin analog $Fe_2(\mu\text{-}SnMe_2)_2(CO)_8$, **5.2**.[236] The two Fe atoms in compound **5.1** are apart by 4.225(1) Å {4.153(1) Å in the second molecule as there are two molecules in the asymmetric unit} which indicate non-bonding nature. This distance is similar to the Fe-Fe distance in **5.2** which was found to be 4.139(15) Å. Both iron atoms possess an electron count of 18.

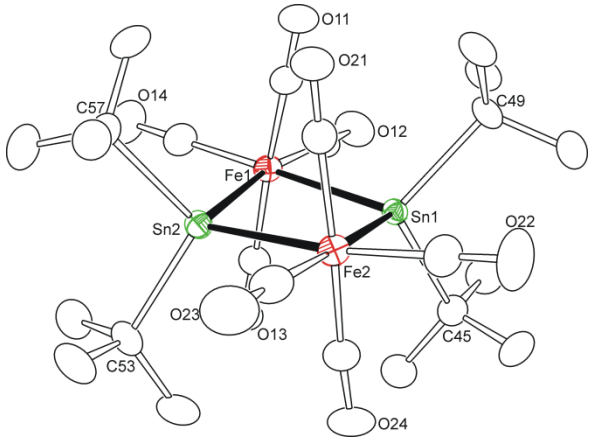

Figure 5.1 The molecular structure for $Fe_2(\mu\text{-}SnBu^t_2)_2(CO)_8$, **5.1**.

When the above reaction of Bu^t_3SnH and $Fe_2(CO)_9$ was carried out in refluxing octane solvent compound **5.1** was obtained in a much lower yield of 8% and the new compound $Fe_4(\mu_4\text{-}Sn)(\mu\text{-}SnBu^t_2)_2(CO)_{16}$, **5.3**, with a "naked" spiro- tin was also isolated in 8 % yield. Compound **5.3** was characterized by FTIR spectroscopy, ^{1}H NMR and single crystal x-ray diffraction, and its molecular structure is shown in Figure 5.2.

Compound **5.3** has a "bow-tie" structure of five metal atoms, that contains two $Fe_2(CO)_8(\mu\text{-}SnBu^t_2)$ groups held together by a central tetrahedral bridging naked tin atom, see Figure 5.2. Formation of compound **5.3** demonstrates the lability of alkyl groups on tin that facilitates the syntheses of mixed metal clusters. Transition metal

complexes containing spiro tin atoms similar to **5.3** have been reported previously.[236, 237] The Fe-Sn distances are similar to those found in the compound $(CH_3)_4Sn_3Fe_4(CO)_{16}$ which also contains a "naked" tin atom.[238] The selected intermolecular distances and bond angles for compounds **5.1** and **5.3** are listed in Table D.1 in Appendix D.

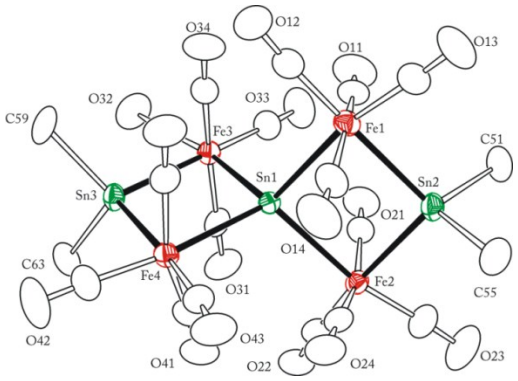

Figure 5.2 The molecular structure for $Fe_4(\mu_4\text{-Sn})(\mu\text{-SnBu}^t_2)_2(CO)_{16}$, **5.3**.

Interestingly, when the reaction of Bu^t_3SnH and $Fe_2(CO)_9$ was carried out in refluxing toluene solvent compound **5.1** was not afforded in any detectable amount, but rather the new compound $Fe_2[\mu\text{-SnBu}^t(CH_2Ph)]_2(CO)_8$, **5.4**, was obtained in 5.5% yield. Compound **5.4** was characterized by a combination of FTIR, NMR and single crystal X-ray diffraction analyses. An ORTEP showing the molecular structure of compound **5.4** is shown in Figure 5.3.

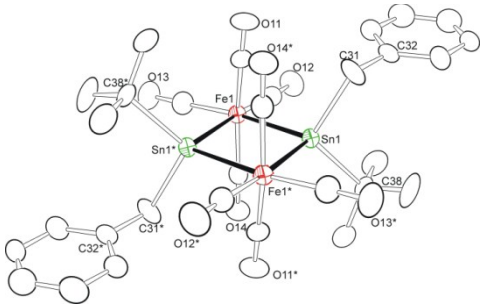

Figure 5.3 The molecular structure for $Fe_2[\mu\text{-SnBu}^t(CH_2Ph)]_2(CO)_8$, **5.4**.

Compound **5.4** is similar to **5.1** except that now a single Bu^t group on each of the Sn atoms in **5.1** has been replaced with a benzyl group from the solvent toluene. When pure compound **5.1** is dissolved in toluene solvent and heated to reflux, compound **5.4** is obtained as the sole metal complex product in 21% yield. As seen in Figure 5.3 the benzyl groups are located *trans* to each other, however ^1H NMR analysis after TLC work-up indicates the another set of resonances which are attributed to the *cis* isomer. The *trans* isomer can be obtained in pure form by fractional crystallizations at -20 °C from a methylene chloride/hexane solvent mixture. Unfortunately, we have been unable to isolate the *cis*-**5.4** in pure form.

Furthermore, when solutions of **5.1** in *m*-xylene solvent was heated to reflux, the compounds, $Fe_2[SnBu^t(m\text{-}CH_2PhMe)]_2(CO)_8$, **5.5**, $Fe_2[SnBu^t(m\text{-}CH_2PhMe)][Sn(m\text{-}CH_2PhMe)_2](CO)_8$, **5.6**, and $Fe_2[Sn(m\text{-}CH_2PhMe)_2]_2(CO)_8$, **5.7**, were obtained in 20%, 19 % and 8% yields respectively. As seen in compound **5.4**, one of the Bu^t groups on each of the two Sn atoms have been replaced with a *m*-xylyl (xylyl=CH_2PhMe) group in compound **5.5**. The *m*-xylyl groups are *trans* with respect to each other (see Figure 5.4).

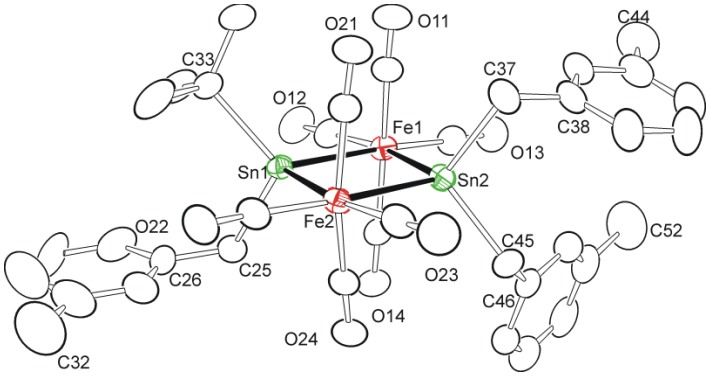

Figure 5.4 The molecular structure of $Fe_2[SnBu^t(m\text{-}CH_2PhMe)]_2(CO)_8$, **5.5**.

For compound **5.6** three of the Bu^t groups have been replaced by *m*-xylyl groups, and in **5.7** all of the Bu^t groups in **5.1** have been replaced with *m*-xylyl groups, see Figure D.1

and D.2 in Appendix D. The reason multiple addition products with *m*-xylene solvent were obtained is probably due to the higher boiling point of *m*-xylene (139 °C) to that of toluene (110 °C).

Appropriately, when a solution of **5.1** in *o*-xylene solvent was heated to reflux, the compounds $Fe_2[SnBu^t(o\text{-}CH_2PhMe)]_2(CO)_8$, **5.8** (18% yield), $Fe_2[SnBu^t(o\text{-}CH_2PhMe)][Sn(o\text{-}CH_2PhMe)_2](CO)_8$, **5.9** (yield 12%), and $Fe_2[Sn(o\text{-}CH_2PhMe)_2]_2(CO)_8$, **5.10** (yield 7.1%) were obtained. Compounds **5.8**, **5.9** and **5.10** were also characterized by a combination of IR, ^{1}H NMR, and single crystal X-ray diffraction analyses. An ORTEP showing the molecular structures of **5.8**, **5.9** and **5.10** are shown in Figures D.3, D.4, and D.5 respectively (see Appendix D). Selected bond angles for compounds **5.8** and **5.9** are listed in Table D.2 in Appendix section D. Compounds **5.9** and **5.10** have similar structures as compounds **5.6** and **5.7** respectively.

As expected, the reaction of complex **5.1** with refluxing in *p*-xylene solvent afforded the compounds $Fe_2[SnBu^t(p\text{-}CH_2PhMe)]_2(CO)_8$, **5.11** (yield 16%), $Fe_2[SnBu^t(p\text{-}CH_2PhMe)][Sn(p\text{-}CH_2PhMe)_2](CO)_8$, **5.12** (yield 14%), and $Fe_2[Sn(p\text{-}CH_2PhMe)_2]_2(CO)_8$, **5.13** (yield 5.4%). Compounds **5.11**, **5.12** and **5.13** were characterized by a combination of FTIR, ^{1}H NMR, and single crystal X-ray diffraction analyses. An ORTEP showing the molecular structures of **5.11**, **5.12** and **5.13** are shown in Figures D.6, D.7, and D.8 respectively (see Appendix D). Again, compounds **5.12** and **5.13** have similar structures as compounds **5.6** and **5.7** respectively, where the Bu^t groups have been replaced by *p*-xylyl groups. Selected bond angles for compounds **5.11** and **5.12** are listed in Table D.3 (see Appendix D).

Proposed reaction mechanism for selective activation of benzylic C-H bond of solevent molecules: The reaction of **5.1** with refluxing solvents toluene, *o*-, *m-,* and *p*-xylene furnished products which were a result of activation of benzylic C-H bonds. We have not seen any evidence for compounds that may have been afforded as a result of aryl C-H activation. A mechanism based on radical processes as shown in Scheme 5.3 is proposed.

The reaction of **5**.**1** in refluxing toluene and in the presence of a radical scavenger TEMPO (2,2,6,6-Tetramethylpiperidine-1-oxyl) altered the course of the reaction (**5.4** was not observed) but the products could not be identified. The first step is the formation of the cluster species **A** formed by the cleavage of the Sn-C bond in **5.1** to expel a Bu^t radical. Light is not required to generate the radical species in solution as we found no significant difference in the rate of formation for **5.4** when the reaction of **5.1** in refluxing toluene was carried out in the dark verses when this reaction was performed under hood light.

The next step is the removal of a hydrogen atom from the solvent methyl group by the Bu^t radical to form isobutane, and the solvent radical. The presence of isobutane was detected by ^{1}H NMR. To this end, compound **5.1** in toluene-d_8 was sealed in an NMR tube under partial vacuum and heated at 150 °C for three hours, to detect the formation of isobutane-d_1 (D-Bu^t).

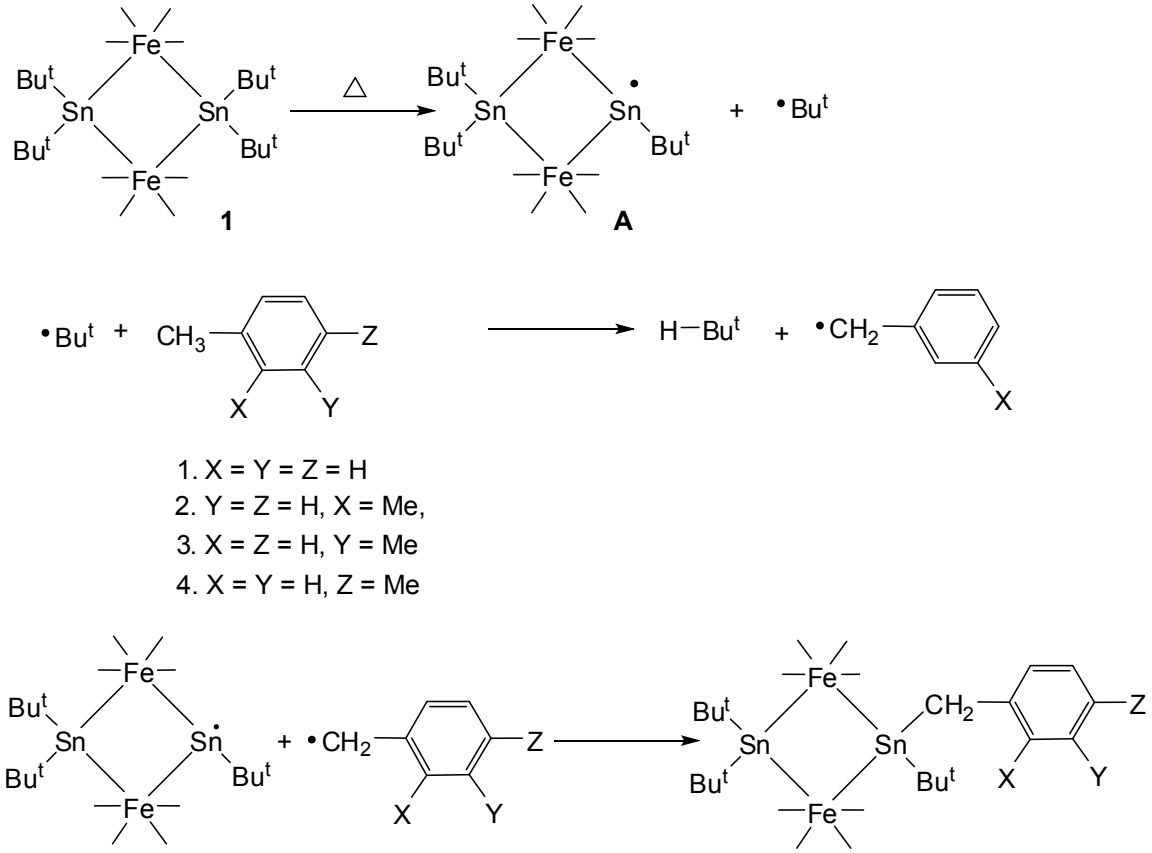

Scheme 5.3

The $^{2}H\{^{1}H\}$ NMR spectrum of the reaction mixture showed a singlet at 1.63 ppm, confirming appropriate formation of isobutane-d_1 (D-Bu^t). However, it should be noted that the ^{1}H NMR spectrum showed large amounts of non-dueterated isobutane, which made it very difficult to detect isobutane-d_1 (D-Bu^t), as well as isobutylene. The observance of non-dueterated isobutane in the reaction mixture can be explained by the fact that two Bu^t radicals can transform to isobutylene and isobutane by losing and gaining one hydrogen atom, respectively (see Eq. 2). Pryor and Tang also observed disproportionation of Bu^t radicals to isobutane and isobutene.[239]

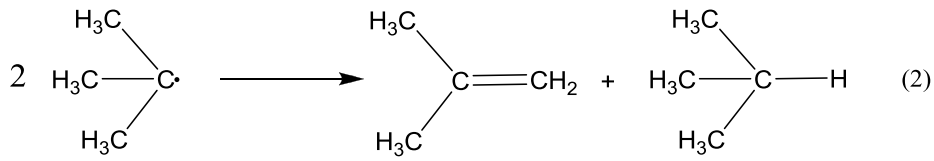

Since the yield of the reaction is only 25% we can account for the mass balance only by the fact that there is a large amount of decomposition products, thus it is not surprising that copious quantities of isobutane and isobutylene were observed. Furthermore, the reaction of **5.1** in toluene-d_8 at 150 °C gave the desired product, in which two of the Bu^t groups in **5.1** had been replaced by two deuterated benzyl groups. The ^1H NMR spectrum shows a mixture of two isomers similar to compound **5.4**, and only the *cis* isomer crystallized from a methylene chloride/hexane solvent mixture at -20 °C, as shown in Figure 5.5. When compound **5.1** was refluxed in toluene-d_8 solvent for three hours only trace amounts of compound **5.4** were obtained. This evidence suggests that there is a large and significant kinetic isotope effect (k_H/k_D = 7.2) and is consistent with the mechanism in which C-H activation plays a prominent role.

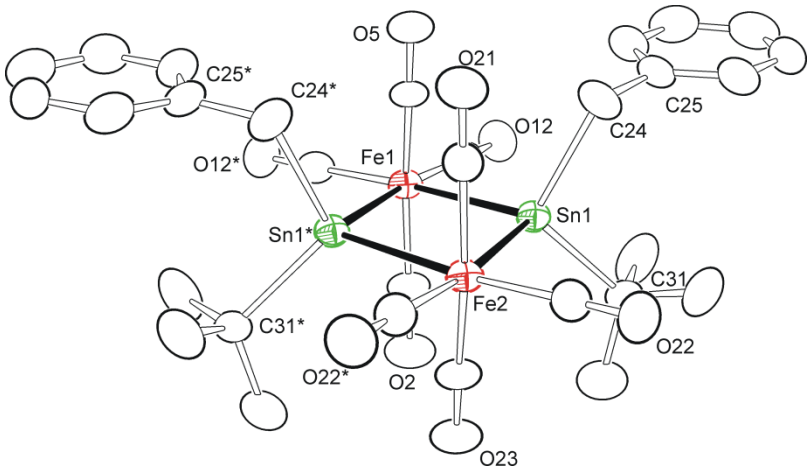

Figure 5.5 The molecular structure of $Fe_2[\mu\text{-}SnBu^t(CD_2(C_6D_5)]_2(CO)_8$, **5.4-d$_{14}$**.

The solvent radical then combined with species **A** to yield the benzylic C-H activated complex. This process was then repeated to replace another Bu^t group with a benzyl or xylene group.

As possible control experiments, there was no reaction of $Fe_2(CO)_9$ in refluxing toluene, of $Bu^t_2SnCl_2$ in refluxing toluene, or of Bu^t_3SnH in toluene at 95 °C. Furthermore, when Bu^t_3SnH in toluene was heated at reflux no reaction was observed after 1.5 hours. However, after a prolonged waiting time (over three hours) the ^1H NMR spectrum of this reaction mixture was full of a number of products which we have not been able to identify. The role of the Fe-cluster framework, we believe, is to provide stability to the Sn radical that is produced in the first step by the homolysis of the Sn-C bond in **5.1**.

We also investigated the reaction of **5.1** with other alkylaromatic compounds. When compound **5.1** reacts with ethylbenzene activation of the α-hydrogen to give the di(α-phenethyl-) derivative, $Fe_2[\mu\text{-}SnBu^t(MeCHPh)]_2(CO)_8$, **5.14**, was found (see Figure 5.6).

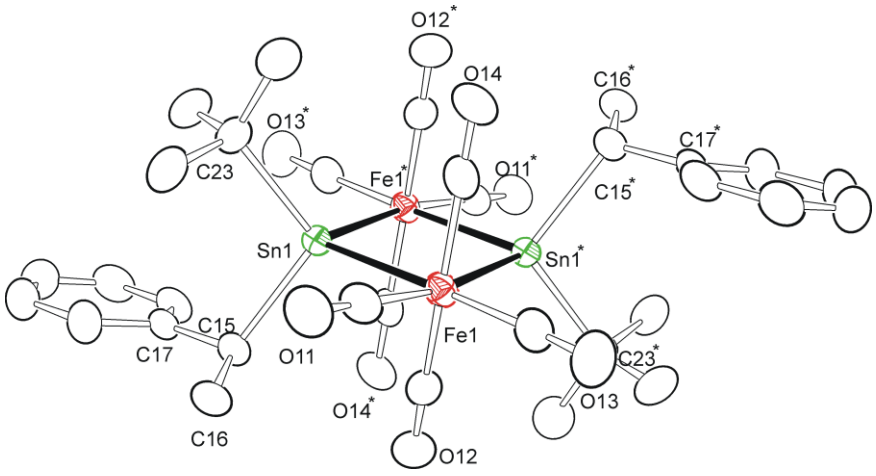

Figure 5.6 The molecular structure of $Fe_2[\mu\text{-}SnBu^t(MeCHPh)]_2(CO)_8$, **5.14**.

This reaction provides an additional supporting evidence for selective activation of the benzylic C-H bond of alkyl aromatic compounds.

5.3. Conclusions

In the previous chapters we have seen the reactivity of Pt-Sn complexes in the activation of small molecules. The results in this chapter clearly demonstrate that TM-Sn bimetallic complexes (TM = transition metal Fe) are also effective in the selective benzylic C-H bond activation of alkyl aromatic compounds.

In summary, we have shown that the bimetallic cluster reacts with the solvents toluene, xylenes, and ethylbenzene to furnish complexes containing benzyl or tolyl groups. The reaction is assisted by the ability of the Bu^t radical that is expelled from **5.1** to attack the benzylic C-H bond in toluene, xylenes, and ethylbenzene. Thus it should also be possible to selectively activate the benzylic C-H bonds in various alkylaromatic compounds. The Fe metal also plays a crucial role in stabilizing the active intermediate Fe-Sn cluster complex, thus providing the proof for the synergetic effect in bimetallic complexes.

The potential of such chemistry in stoichiometric or catalytic organic transformations is an exciting prospect that we are exploring. One interesting area is FCA catalysis (FCA = Friedel-Crafts Alkylation) using the mixture of alkyl aromatic compounds in the presence of **5.1** to isolate cross-coupling products.

5.4. Experimental section

General Data

All the reactions were performed under an argon atmosphere using schlenk techniques. Reagent grade solvents were dried by the standard procedures and were freshly distilled before use. Infrared spectra were recorded on a Nicolet 380 FT-IR spectrophotometer. ^1H NMR were recorded on a Bruker 400 and 300 spectrometer

operating at 399.993 MHz and 300.13 MHz, respectively. $^{2}H\{^{1}H\}$ NMR were recorded on a Varian Mercury/VX 400 operating at 61.395 MHz. Elemental analyses were performed by Columbia Analytical Services (Tucson, AZ). Di-iron nonacarbonyl $Fe_2(CO)_9$, toluene-d_8, magnesium sulfate ($MgSO_4$), sodium hydroxide (NaOH), borane (BH_3 1M in THF), and Xylene solvents were purchased from Alfa Aesar, and ethylbenzene were purchased from Sigma-Aldrich and they were used without further purification. Bu^t_3SnH was prepared by modifying the reported procedures in the literature.[105] Product separations were performed by TLC in air on Analtech preparative silica gel GF 500 μm glass plates.

Synthesis of $Fe_2(\mu\text{-}SnBu^t_2)_2(CO)_8$, 5.1.

A 280 mg amount (0.77 mmol) of $Fe_2(CO)_9$ and 460 mg amount (1.58 mmol) of Bu^t_3SnH were charged into a 100 mL 3-neck flask. 50 mL of heptane was added and heated to reflux for twenty minutes with stirring. The solvent was removed *in vacuo* and the solid residue was dissolved in CH_2Cl_2 and filtered through a silica plug and eluted with CH_2Cl_2 to remove any unreacted $Fe_2(CO)_9$. The solvent was then removed under an argon flow at room temperature to yield a 258 mg amount of light-yellow crystalline solid, **5.1**, in 41% yield. Spectral data for **5.1**: IR ν_{CO} (cm^{-1} in hexane): 2038 (s), 1990 (m), 1970 (s). ^{1}H NMR (C_6D_6, in ppm, 400 MHz): δ = 1.54 (s, 36H, CH_3, $^{3}J_{Sn\text{-}H}$ = 79 Hz). Elemental Anal Calc.: C, 35.95; H, 4.52 % Found: C, 35.65; H, 4.11 %.

Synthesis of $Fe_4(\mu_4\text{-}Sn)(\mu\text{-}SnBu^t_2)_2(CO)_{16}$, 5.3.

A 30 mg amount (0.082 mmol) of $Fe_2(CO)_9$, a 50 mg amount (0.17 mmol) of Bu^t_3SnH, and 10 mL of octane were charged into a 100 mL 3-neck flask. The reaction

was heated to reflux for one hour while stirring. The reaction mixture was cooled and the solvent was removed *in vacuo*. The products were separated by TLC by using hexane solvent to yield, in order of elution, a 5.5 mg (yield 8.3%) of light-yellow $Fe_2(\mu\text{-}SnBu^t_2)_2(CO)_8$ and 3.9 mg (yield 8%) of pink $Fe_4(\mu_4\text{-}Sn)(\mu\text{-}SnBu^t_2)_2(CO)_{16}$. The yield for $Fe_2(\mu\text{-}SnBu^t_2)_2(CO)_8$ was low because it slowly decomposes on TLC, and the chromatography should be performed in a timely manner. Spectral data for **5.3**: IR ν_{CO} (cm^{-1} in CH_2Cl_2): 2051 (s), 2020 (w), 1985 (w), 1974 (m). ^{1}H NMR (toluene-d_8, in ppm): δ = 1.5 (s, 36H, CH_3, $^3J_{^{117}Sn\text{-}H}$ = 77 Hz, $^3J_{^{119}Sn\text{-}H}$ = 80 Hz). Elemental Anal, calc.: C, 30.60; H, 2.88 % Found: C, 30.38; H, 2.39 %.

Synthesis of $Fe_2[\mu\text{-}SnBu^t(CH_2Ph)]_2(CO)_8$, 5.4.

A 30 mg amount (0.082 mmol) of $Fe_2(CO)_9$, a 50 mg amount (0.170 mmol) of Bu^t_3SnH, and 10 mL of toluene were charged into a 50 mL 3-neck flask. The reaction mixture was heated to reflux for three hours, at which time the IR spectrum showed complete consumption of the starting material. The solvent was removed *in vacuo* and the product was separated by preparative TLC with hexane as solvent to yield 3.1 mg (yield 4%) of colorless **5.4** product. The ^{1}H NMR spectrum indicated the presence of another resonance attributed to the *cis* isomer, which we were not able to separate by chromatography. IR ν_{CO} (cm^{-1} in hexane) for the mixture: 2044 (vs), 1998 (m), 1979 (s). By means of fractional crystallization at -20 °C from a methylene chloride/hexane solvent mixture, 5 mg of pure *trans*- $Fe_2[\mu\text{-}SnBu^t(CH_2Ph)]_2(CO)_8$ was separated from 40 mg of the mixture. Spectral data for *trans*- **5.4**: IR ν_{CO} (cm^{-1} in hexane): 2044 (vs), 1997 (m), 1992 (w), 1980 (s). ^{1}H NMR (toluene-d_8, in ppm, 400 MHz): δ = 7.27-6.98 (m, 10H,

Ph), 3.44(s, 4H, CH_2, $^2J_{Sn\text{-}H}$ = 34 Hz), 1.31(s, 18H, CH_3, $^3J_{117Sn\text{-}H}$ = 94 Hz, $^3J_{119Sn\text{-}H}$ = 97 Hz). Elemental Anal. Calc.: C, 41.43; H, 3.71 % Found: C, 41.12; H, 3.97 %.

Conversion of $Fe_2(\mu\text{-}SnBu^t_2)_2(CO)_8$, 5.1, to $Fe_2[\mu\text{-}SnBu^t(CH_2Ph)]_2(CO)_8$, 5.4.

A 20 mg amount (0.025 mmol) of $Fe_2(\mu\text{-}SnBu^t_2)_2(CO)_8$ was dissolved in 10 mL toluene in a 50 mL 3-neck flask and was heated to reflux for fifty minutes. The solvent was removed *in vacuo* and the product was separated by TLC using hexane solvent to yield 4.5 mg (21% yield) of $Fe_2[\mu\text{-}SnBu^t(CH_2Ph)]_2(CO)_8$, **5.4**.

Synthesis of $Fe_2[\mu\text{-}SnBu^t(m\text{-}CH_2PhMe)]_2(CO)_8$, 5.5, $Fe_2[\mu\text{-}SnBu^t(m\text{-}CH_2PhMe)][\mu\text{-}Sn(m\text{-}CH_2PhMe)_2](CO)_8$, 5.6, and $Fe_2[\mu\text{-}Sn(m\text{-}CH_2PhMe)_2]_2(CO)_8$, 5.7.

A 30 mg amount (0.037 mmol) of $Fe_2(\mu\text{-}SnBu^t_2)_2(CO)_8$ was dissolved in 7 mL of *m*-xylene in a 100 mL 3-neck flask. The reaction was heated to reflux for 100 minutes. The solvent was removed *in vacuo* and the product was separated by TLC using hexane solvent to yield, in order of elution, 6.9 mg (yield 20%) of pale yellow $Fe_2[\mu\text{-}SnBu^t(m\text{-}CH_2PhMe)]_2(CO)_8$, **5.5**, 6.7 mg (yield 19%) of pale yellow $Fe_2[\mu\text{-}SnBu^t(m\text{-}CH_2PhMe)][\mu\text{-}Sn(m\text{-}CH_2PhMe)_2](CO)_8$, **5.6**, and 3.1 mg (yield 8.3%) of colorless $Fe_2[\mu\text{-}Sn(m\text{-}CH_2PhMe)_2]_2(CO)_8$, **5.7**. Spectral data for **5.5**: IR ν_{CO} (cm^{-1} in hexane): 2043 (vs), 1996 (m), 1992 (m, sh), 1979 (s), 1955 (w). ^{1}H NMR (C_6D_6, in ppm, 300 MHz): δ = 7.13-6.85 (m, 8H, Ph), 3.51 (s, 4H, CH_2, $^2J_{Sn\text{-}H}$ = 34 Hz), 3.49 (s, 4H, CH_2, $^2J_{Sn\text{-}H}$ = 34 Hz), 2.20 (s, 6H, CH_3), 2.15 (s, 6H, CH_3), 1.33 (s, 18H, CH_3, $^3J_{Sn\text{-}H}$ = 95 Hz), 1.32 (s, 18H, CH_3, $^3J_{Sn\text{-}H}$ = 95 Hz). Note: This is a mixture of *cis*- and *trans*-isomers. Elemental Anal. Calc.: C, 42.81; H, 4.04 % Found: C, 42.99; H, 3.80 %. Spectral data for **5.6**: IR

ν_{CO} (cm^{-1} in hexane): 2065 (w), 2045 (vs), 2006 (m), 1997 (m), 1979 (s), 1955 (w). ^1H NMR (C_6D_6, in ppm, 300 MHz): δ = 7.13-6.84 (m, 12H, Ph), 3.44 (s, 2H, CH_2, $^2J_{Sn-H}$ = 35 Hz), 3.34 (s, 2H, CH_2, $^2J_{Sn-H}$ = 39 Hz), 3.33 (s, 2H, CH_2, $^2J_{Sn-H}$ = 38 Hz), 2.18 (s, 9H, CH_3), 1.30 (s, 9H, CH_3, $^3J_{Sn-H}$ = 96 Hz). Elemental Anal. Calc.: C, 45.71; H, 3.83 % Found: C, 45.67; H, 3.54 %. Spectral data for **5.7**: IR ν_{CO} (cm^{-1} in hexane): 2068 (w), 2049 (vs), 2009 (m), 2003 (m), 1979 (s), 1955 (w). ^1H NMR (C_6D_6, in ppm, 300 MHz): δ = 7.13-6.85 (m, 16H, Ph), 3.28 (s, 8H, CH_2, $^2J_{Sn-H}$ = 38.6 Hz), 2.17 (s, 12H, CH_3). Elemental Anal. Calc.: C, 48.34; H, 3.65 % Found: C, 48.62; H, 3.12 %.

Synthesis of $Fe_2[\mu\text{-}SnBu^t(o\text{-}CH_2PhMe)]_2(CO)_8$, 5.8, $Fe_2[\mu\text{-}SnBu^t(o\text{-}CH_2PhMe)][\mu\text{-}Sn(o\text{-}CH_2PhMe)_2](CO)_8$, 5.9, and $Fe_2[\mu\text{-}Sn(o\text{-}CH_2PhMe)_2]_2(CO)_8$, 5.10.

A 34 mg amount of $Fe_2(\mu\text{-}SnBu^t_2)_2(CO)_8$ (0.033 mmol) was dissolved in 10 mL of *o*-xylene in a 100 mL 3-neck flask. The reaction was heated to reflux for 65 minutes. The solvent was removed *in vacuo* and the product was separated by TLC using hexane solvent to yield, in order of elution, 6.8 mg (yield 18%) of colorless $Fe_2[\mu\text{-}SnBu^t(o\text{-}CH_2PhMe)]_2(CO)_8$, **5.8**, 4.7 mg (yield 12%) of pale yellow $Fe_2[\mu\text{-}SnBu^t(o\text{-}CH_2PhMe)][\mu\text{-}Sn(o\text{-}CH_2PhMe)_2](CO)_8$, **5.9**, and 3.0 mg (yield 7.1%) of pale yellow $Fe_2[\mu\text{-}Sn(o\text{-}CH_2PhMe)_2]_2(CO)_8$, **5.10**. Spectral data for **5.8**: IR ν_{CO} (cm^{-1} in hexane): 2052(w), 2041 (vs), 1995 (m), 1979 (s), and 1955 (w). ^1H NMR ($CDCl_3$, in ppm, 400 MHz): δ = 7.33-7.01 (m, 8H, Ph), 3.52 (s, 4H, CH_2, $^2J_{Sn-H}$ = 36 Hz), 3.51 (s, 4H, CH_2, $^2J_{Sn-H}$ = 36 Hz), 2.41 (s, 6H, CH_3), 2.40 (s, 6H, CH_3), 1.24 (s, 18H, CH_3, $^3J_{^{117}Sn-H}$ = 95 Hz, $^3J_{^{119}Sn-H}$ = 99 Hz), 1.23 (s, 18H, CH_3, $^3J_{^{117}Sn-H}$ = 95 Hz, $^3J_{^{119}Sn-H}$ = 99 Hz). Note: This is a mixture of *cis*- and *trans*-isomers. Elemental Anal. Calc.: C, 42.81; H, 4.04 % Found: C, 42.30; H,

4.19 %. Spectral data for **5**.**9**: IR ν_{CO} (cm^{-1} in hexane): 2065 (w), 2044 (vs), 2007 (w, sh), 1996 (m), 1984(m), 1979 (s), 1957 (w). ^{1}H NMR ($CDCl_3$, in ppm, 400 MHz): δ = 7.09-6.75 (m, 12H, Ph), 3.47 (s, 2H, CH_2, $^2J_{Sn\text{-}H}$ = 36 Hz), 3.31 (s, 2H, CH_2, $^2J_{Sn\text{-}H}$ = 40 Hz), 3.29 (s, 2H, CH_2, $^2J_{Sn\text{-}H}$ = 40 Hz), 2.38 (s, 3H, CH_3), 2.10 (s, 3H, CH_3), 2.09 (s, 3H, CH_3), 1.21 (s, 9H, CH_3, $^3J_{^{117}Sn\text{-}H}$ = 96 Hz, $^3J_{^{119}Sn\text{-}H}$ = 100 Hz). Elemental Anal. Calc.: C, 45.71; H, 3.83 % Found: C, 45.94; H, 3.79 %. Spectral data for **5**.**10**: IR ν_{CO} (cm^{-1} in CH_2Cl_2): 2068 (w), 2047 (vs), 2000 (m, sh), 1982 (s), 1953 (w, sh). ^{1}H NMR ($CDCl_3$, in ppm, 400 MHz): δ = 7.06-6.73 (m, 16H, Ph), 3.25 (s, 8H, CH_2, $^2J_{Sn\text{-}H}$ = 40 Hz), 2.08 (s, 12H, CH_3). Elemental Anal. Calc.: C, 48.32; H, 3.52 % Found: C, 48.62; H, 3.12 %.

Synthesis of Fe_2[μ-$SnBu^t$(*p*-CH_2PhMe)]$_2$$(CO)_8$, 5.11, Fe_2[μ-$SnBu^t$(*p*-CH_2PhMe)][μ-Sn(*p*-$CH_2PhMe)_2$]$(CO)_8$, 5.12, and Fe_2[μ-Sn(*p*-$CH_2PhMe)_2$]$_2$$(CO)_8$, 5.13.

A 30 mg amount (0.037 mmol) of $Fe_2(\mu\text{-}SnBu^t{}_2)_2(CO)_8$ was dissolved in 10 mL of *p*-xylene in a 100 mL 3-neck flask. The reaction was heated to reflux for 70 minutes. The solvent was removed *in vacuo* and the product was separated by TLC using hexane solvent to yield, in order of elution, 5.5 mg (yield 16%) of colorless Fe_2[μ-$SnBu^t$(*p*-CH_2PhMe)]$_2$$(CO)_8$, **5**.**11**, 5.0 mg (yield 14%) of pale yellow Fe_2[μ-$SnBu^t$(*p*-CH_2PhMe)][μ-Sn(*p*-$CH_2PhMe)_2$]$(CO)_8$, **5**.**12**, and 2.0 mg (yield 5.4%) of pale yellow Fe_2[μ-Sn(*p*-$CH_2PhMe)_2$]$_2$$(CO)_8$, **5**.**13**. Spectral data for **5**.**11**: IR ν_{CO} (cm^{-1} in hexane): 2043 (vs), 1997 (m), 1991 (m, sh), 1979 (s), 1952(vw). ^{1}H NMR ($CDCl_3$, in ppm, 400 MHz): δ = 7.22-7.03 (m, 8H, Ph), 3.41 (s, 4H, CH_2, $^2J_{Sn\text{-}H}$ = 33 Hz), 2.28 (s, 6H, CH_3), 1.32 (s, 18H, CH_3, $^3J_{^{117}Sn\text{-}H}$ = 94 Hz, $^3J_{^{119}Sn\text{-}H}$ = 97 Hz). Elemental Anal. Calc.: C, 42.81; H, 4.04 % Found: C, 42.71: H, 3.77 %. Spectral data for **5**.**12**: IR ν_{CO} (cm^{-1} in hexane):

2065 (w), 2046 (vs), 2006 (s), 1997 (s), 1978(vs), 1955 (w). ^{1}H NMR ($CDCl_3$, in ppm, 400 MHz): δ = 7.21-7.02 (m, 12H, Ph), 3.36 (s, 2H, CH_2, $^{2}J_{^{117}Sn\text{-}H}$ = 34 Hz, $^{2}J_{^{119}Sn\text{-}H}$ = 39 Hz), 3.27 (s, 2H, CH_2, $^{2}J_{Sn\text{-}H}$ = 38 Hz), 3.26 (s, 2H, CH_2, $^{2}J_{Sn\text{-}H}$ = 38 Hz), 2.30 (s, 3H, CH_3), 2.29 (s, 3H, CH_3), 2.28 (s, 3H, CH_3), 1.31 (s, 9H, CH_3, $^{3}J_{^{117}Sn\text{-}H}$ = 93 Hz, $^{3}J_{^{119}Sn\text{-}H}$ = 97 Hz). Elemental Anal. Calc.: C, 45.71; H, 3.83 % Found: C, 45.7; H, 3.66 %. Spectral data for **5**.**13**: IR ν_{CO} (cm^{-1} in hexane): 2048 (s), 2008 (m), 1997 (m), 1992 (m, sh), 1979 (s), 1954 (w). ^{1}H NMR ($CDCl_3$, in ppm, 400 MHz): δ = 7.04 (s, 16H, Ph), 3.22(s, 8H, CH_2, $^{2}J_{Sn\text{-}H}$ = 38 Hz), 2.29 (s, 12H, CH_3). Elemental Anal. Calc.: C, 48.32; H, 3.52 % Found: C, 48.47; H, 3.42 %.

Synthesis of $Fe_2[\mu\text{-}SnBu^t(MeCHPh)]_2(CO)_8$, 5.14.

A 40 mg amount (0.050 mmol) of $Fe_2(\mu\text{-}SnBu^t_2)_2(CO)_8$ was dissolved in 10 mL of ethylbenzene in a 100 mL 3-neck flask. The reaction was heated to reflux for 15 minutes. The solvent was removed *in vacuo* and the product was separated by TLC using hexane solvent to yield a 24 mg (yield 44%) of colorless $Fe_2[\mu\text{-}SnBu^t(MeCHPh)]_2(CO)_8$, **5**.**14**. Spectral data for **5**.**14**: IR ν_{CO} (cm^{-1} in hexane): 2042 (vs), 2003 (w), 1997 (m), 1992 (w) 1976 (s). Elemental Anal, calc.: C, 42.67; H, 4.03 % Found: C, 42.67; H, 3.79 %.

Synthesis of $Fe_2(\mu\text{-}SnBu^t(CD_2C_6D_5))_2(CO)_8$, 5.4-$d_{14}$.

A 15 mg amount (0.019 mmol) of $Fe_2(\mu\text{-}SnBu^t_2)_2(CO)_8$ was dissolved in 1.5 mL of anhydrous toluene-d_8 in a *Parr*-reactor and sealed under argon. The reactor was placed in an oil bath and heated to 150 °C for 1.5 hours. The reactor was then cooled to room temperature using an ice bath. The solvent was removed *in vacuo* and the product was

separated by TLC using hexane solvent to yield 2 mg (12% yield) of pale yellow $Fe_2(\mu\text{-}SnBu^t(CD_2C_6D_5))_2(CO)_8$, **5.4-d$_{14}$**. Spectral data for **5.4-d$_{14}$**: IR ν_{CO} (cm^{-1} in hexane): 2044 (vs), 1997 (m), 1979 (s). ^1H NMR (toluene-d_8, in ppm, 400 MHz) 1.31(s, 18H, CH_3, $^3J_{^{117}Sn\text{-}H}$ = 94 Hz, $^3J_{^{119}Sn\text{-}H}$ = 97 Hz). (Note: only *tert*-butyl resonances were observed in the ^1H NMR spectrum as expected).

$^2H\{^1H\}$ NMR experiment for the detection of isobutane-*d$_1$*.

An 85 mg amount (0.11 mmol) of $Fe_2(\mu\text{-}SnBu^t_2)_2(CO)_8$ and 1 mL anhydrous toluene-d_8 were sealed in a NMR tube under vacuum. The sealed NMR tube was placed in an oil bath at 150 °C for two hours. A $^2H\{^1H\}$ NMR spectrum of the reaction mixture showed a singlet at 1.63 ppm for isobutane-d_1 (D-Bu^t). $^2H\{^1H\}$ NMR data was performed at ambient temperature without suppressing the dominant toluene-d_8 resonances. 2.6 second free-induction decays were collected using 45-degree pulses. The data was recorded with a 4k Hz spectral window with 128 transients added for the final dataset.

Determination of the kinetic isotope effect of the C-H activation on toluene

In a typical reaction, a 10 mg of compound **5**.**1**, 1 mL of anhydrous toluene or toluene-d_8, and a magnetic stir bar were sealed in a Parr reactor under an argon atmosphere. The Parr reactor was placed in an oil bath with a stir bar that was pre-heated to 120 º C. The reaction was monitored by IR spectroscopy at different time intervals. At certain time intervals, the intensities of C-O stretching bands in the IR spectrum of the reaction performed in toluene appeared to be identical to that in toluene-d_8. The isotope effect was determined by the ratio of the reaction times, D/H, for the two reactions. For

example, the IR spectrum for the toluene reaction after 25 min was approximately the same as that of toluene-d_8 after three hours, thus $k_H/k_D = 7.2$.

5.5. Crystallographic Analysis

Orange crystals of **5.1** suitable for diffraction analysis were grown by slow evaporation of solvent from pure hexane at -20 °C. Light yellow crystals of **5**.**4** and **5**.**4-*d*$_{14}$** suitable for diffraction analysis were grown by slow evaporation of solvent from solutions in CH_2Cl_2/hexane solvent mixtures at -20 °C. Yellow crystals of **5**.**5**, orange crystals of **5**.**6**, colorless crystals of **5**.**7**, colorless crystals of **5**.**9**, colorless crystals of **5**.**10**, yellow crystals of **5**.**11**, yellow crystals of **5**.**12**, and dark red crystals of **5**.**3** were grown by slow evaporation of solvent from a CH_2Cl_2/hexane solution at -20 °C. Colorless crystals of **5**.**8** and **5**.**13** were grown by slow evaporation of solvent from a hexane/heptane solution at -20 °C. Colorless crystals of **5**.**14** were grown by slow evaporation of solvent from a benzene solution at 5 °C.

Each data crystal was glued onto the end of a thin glass fiber. X-ray intensity data were measured by using a Bruker SMART APEX2 CCD-based diffractometer using Mo Kα radiation (λ = 0.71073 Å).[117] The raw data frames were integrated with the SAINT+ program by using a narrow-frame integration algorithm.[117] Corrections for Lorentz and polarization effects were also applied with SAINT+. An empirical absorption correction based on the multiple measurement of equivalent reflections was applied using the program SADABS. All structures were solved by a combination of direct methods and difference Fourier syntheses and refined by full-matrix least-squares on F^2 by using the SHELXTL software package.[118] All non-hydrogen atoms were refined with anisotropic displacement parameters. Hydrogen atoms were placed in geometrically idealized

positions and included as standard riding atoms during the least-squares refinements. Crystal data, data collection parameters, and results of the analyses are listed in Tables D.4-D.10 in Appendix D.

Compounds **5**.**1**, **5**.**3**, **5**.**4**, **5**.**7**, and **5**.**13** crystallized in the triclinic crystal system. The space group $P\ \bar{1}$ was assumed and confirmed by the successful solution and refinement of the structure. With Z = 4 there are two formula equivalents of the molecule present in the asymmetric unit for compound **5**.**1**. For compounds **5**.**4** and **5**.**13** there are two half molecules present in the asymmetric unit which reside about an inversion center. Compound **5**.**7** contain only half a formula equivalent of the molecule in the asymmetric unit which lies about an inversion center.

Compounds **5.5**, **5**.**8**, **5**.**9**, **5**.**10**, **5.11**, **5.12**, and **5**.**14** crystallized in the monoclinic crystal system. The space group $P2_1/c$ was confirmed on the basis of the systematic absences in the data for compounds **5.5**, **5**.**9**, **5**.**11**, and **5**.**14**. There is only half a formula equivalent of the molecule in the asymmetric unit which lies about an inversion center for compounds **5.5**, **5.11**, and **5**.**14**. One molecule of benzene from the crystallization solvent co-crystallized with complex **5**.**14** and was included in the analysis and refined with isotropic thermal parameters. For compounds **5.8** and **5.10** the systematic absences in the intensity data were consistent with the space group $P2_1/n$. With Z = 2, there is half a formula equivalent of the molecule in the asymmetric unit which lies about an inversion center in compounds **5**.**8** and **5.10**. For compound **5**.**12** the space group was determined to be acentric $P2_1$ from the systematic absences and it contains two equivalents of the molecule in the asymmetric unit.

Compound **5**.**6** crystallized in the orthorhombic crystal system. The space group $P2_12_12_1$ was confirmed on the basis of the systematic absences in the data. One of the xylene groups (C26-C32) is slightly disordered and atoms of this group were refined with isotropic displacement parameters. The disorder was not modeled due to satisfactory low R values (R1 = 2.74 %) during the final stages of the refinement.

Compound **5**.**4**-$\boldsymbol{d_{14}}$ crystallized in the orthorhombic crystal system. The systematic absences in the intensity data were consistent with any of the space groups $Cmc2_1$, *Cmcm*, or *Ama*2. The structure could only be solved in the space group *Ama*2. With half a molecule in the asymmetric unit the complex has crystallographic mirror symmetry. The deuterium atoms were located but refined using geometric restraints (SHELX: DFIX, DANG instructions) and fixed isotropic thermal parameters.

Chapter 6: Synthesis and characterization of bimetallic Fe_4-Ni and Ni-Sn complexes

6.1. Background

In the previous chapters we have discussed synthesis and characterization of bimetallic transition metal complexes with bulky tin ligands. The trimetallic $Pt_2Ru_2Sn_2$ cluster complex supported on mesoporous silica was shown to be an excellent catalyst for the hydrogenation of nitrobenzene to aniline with 100% selectivity.[96] With the aim of synthesizing multimetallic cluster complexes with cheaper metals, we have also synthesized Fe-Ni cluster complexes. We were interested in addition of our bulky organotin ligand Bu_3SnH to this Fe-Ni bimetallic cluster to prepare Fe-Ni-Sn trimetallic cluster complexes and compare their catalytic activity with existing Pt-Ru-Sn cluster complexes. In this chapter we will introduce the synthesis method for preparation of Fe-Ni bimetallic cluster complexes.

The pentairon carbonyl carbide cluster, $Fe_5(\mu_5\text{-}C)(CO)_{15}$, **6.1**, was the first reported carbide cluster in the literature which was characterized crystallographically.[240] Subsequently, carbide clusters of ruthenium,[168, 241, 242] osmium,[241] rhodium[243] were reported and since then there have been pioneering contributions to the chemistry of metal carbide carbonyl clusters.[244-246] The interest in complexes containing an interstitial carbon atom encapsulated in a metal cluster framework came about due to the fact that the carbide ligand can provide stability to the metal cluster when reacted with other substrates allowing the cluster to remain intact and not fragment to lower nuclearity species.[244-246] As in **6.1** the carbide ligand can also be attached to the periphery of a metal cluster framework and is thus exposed.

These 'peripheral carbide clusters' have garnered considerable attraction because the metal framework can rearrange by homolysis of a metal-metal bond when reacted with other substrates. For example, it has been shown that $Ru_5(\mu_5\text{-}C)(CO)_{15}$, **6.2**, reacts with acetonitrile,[247] triethylsilane, (see Eq. 1),[248] and triphenylstannane,[249] to yield products that are comprised of an open $Ru_5(\mu_5\text{-}C)$ metal skeletal where one ruthenium atom bridges a butterfly arrangement of four ruthenium atoms.

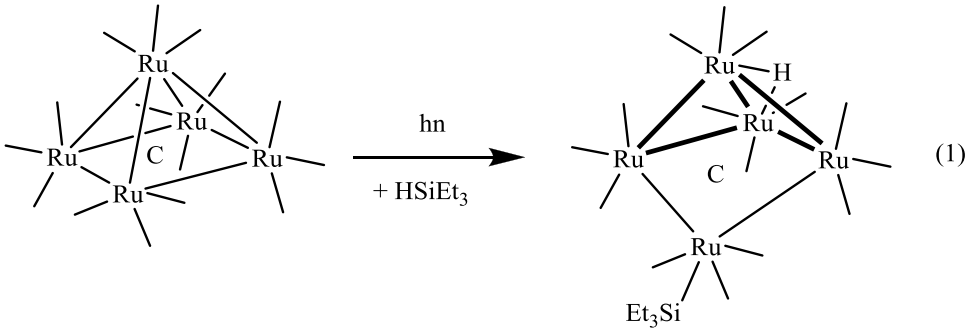

(1)

(6.2) **(6.3)**

There has been much interest in the preparation of bimetallic clusters because of their use as precursors for the preparation of bimetallic nanoparticle heterogeneous catalysts.[56, 58, 61, 62] And these carbide clusters have been subjected to a wide range of synthesis to produce bimetallic carbide clusters. Early work by Muetterties[250, 251] and Shriver[252-254] showed very elegantly how heteronuclear complexes containing the carbido ligand could be prepared, and in later years there was considerable success in the preparation of other heteronuclear carbide containing clusters.[253, 255-262]

It has been shown that **6.1** can also undergo substitution reactions where instead of displacing a ligand on the metal cluster, the metal atom itself can be substituted by another metal atom to result in a metal-metal exchange process and create mixed-metal clusters. An example of this kind of exchange process was seen in the reaction of the

dianion of **6.1** $[Fe_5(C)(CO)_{15}]^{2-}$ with $Pt(PMe_2Ph)_2Cl_2$, as well as in the reaction of **6.1** with $Pt(COD)_2$ (COD = 1,5-cyclooctadiene), where the platinum atom has replaced one of the iron atoms (an $Fe(CO)_3$ unit as shown in Eq. 2) on the base of the square pyramid.[263]

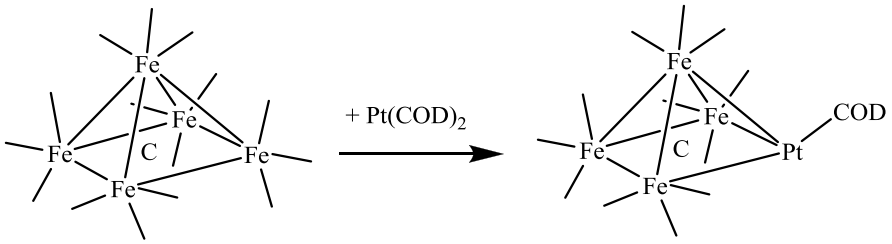

(2)

(6.1)

There are only a handful of mixed-metal carbide clusters containing nickel,[250, 253, 263] and the structures of only a few of these have been determined crystallographically.[264, 265] Herein we report the reaction of **6.1** with nickelocene ($NiCp_2$, Cp = cyclopentadienyl) which proceeds *via* metal atom substitution like in Eq. 2, along with metal skeletal rearrangement like in Eq. 1 to yield the bimetallic carbide cluster $Fe_4Ni(Cp)_2(CO)_{10}(\mu_5\text{-}C)$.

6.2. Results and discussion

The reaction of $Fe_5(\mu_5\text{-}C)(CO)_{15}$, **6.1**, with $NiCp_2$, at 80 °C has afforded the complexes $Fe_4Ni(Cp)_2(CO)_{10}(\mu_5\text{-}C)$, **6.4** (27% yield), $Fe_5(Cp)_2(CO)_{10}(\mu_5\text{-}C)$, **6.5** (16% yield), and $[CpFe(CO)_2]_2$, **6.6** (18% yield). Compound **6.6** has been previously described.[266, 267] The bimetallic Fe_4Ni carbide cluster $Fe_4Ni(Cp)_2(CO)_{10}(\mu_5\text{-}C)$, **6.4**, was characterized by a combination of IR spectroscopy, ^1H NMR, mass spectrometry, elemental, and single crystal X-ray diffraction analyses.

An ORTEP showing the molecular structure of **6.4** is shown in Figure 6.1. Selected bond distances and angles are listed in Table E.1 in Appendix E. This complex is comprised of an open $Fe_4Ni(\mu_5\text{-}C)$ cluster framework with a carbide ligand that is "exposed". The structure is best described as a butterfly arrangement of four metal atoms with a fifth metal atom connected to the 'wing tips' of the butterfly framework.

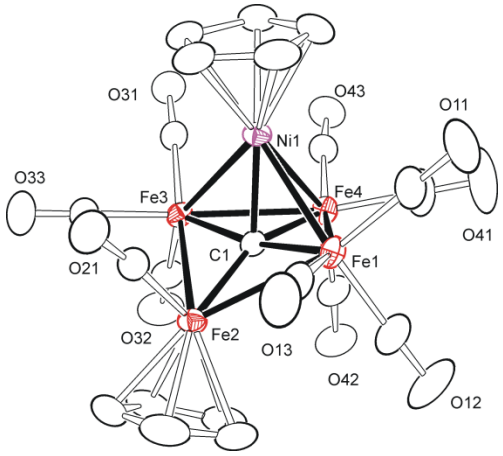

Figure 6.1 The molecular structure of $Fe_4Ni(Cp)_2(CO)_{10}(\mu_5\text{-}C)$, **6.4**.

As seen in Figure 6.1, the butterfly framework consists of atoms Fe1, Fe3, Ni1 and Fe4. The nickel atom occupies a position that is on the hinge bond of the Fe_4Ni butterfly, and atom Fe2 bridges this butterfly arrangement. There is a Cp group that is bonded to nickel in an η^5 fashion as in the starting $NiCp_2$, and another Cp group that is also bonded in an η^5 manner to the bridging iron atom Fe2. The arrangement of the metal atoms in **6.4** can also be viewed as a square pyramid with one metal-metal bond missing. The total cluster valence electron count for **6.4** is 76 electrons which is consistent for a square pyramidal cluster with one less bond (74 + 2 = 76) according to conventional electron counting theories if all five metal atoms formally have an 18-electron configuration.[268, 269] The Fe-Fe bond distances in the butterfly part of the structure, Fe1 - Fe4 = 2.6301(3) and

Fe3 – Fe4 = 2.6574(3) Å, are similar to those found in the parent **6.1**.[240] The Fe-Fe bond distances to the bridging Fe atom Fe2 are slightly longer (Fe1-Fe2 = 2.6923(4) and Fe3-Fe2 = 2.7472(3) Å) as expected due to the distorted square pyramidal structure.

Since there are no examples in the literature for iron carbide bimetallic clusters containing nickel that have been characterized crystallographically we compare the Fe-Ni bonding distances with the Fe_5Ni nitrido cluster that has been recently reported[270] and other Fe-Ni compounds.[271, 272] The average Fe-Ni bonding distances of 2.5082(3) Å in **6.4** are within the range for a Fe-Ni single bond. They are slightly shorter than the Fe-Ni bond distance in the nitride dianion $[HFe_5Ni(CO)_{14}(\mu_6\text{-}N)]^{2-}$ (average 2.638(1) Å)[270] and slightly longer than those found in the tetrahedral Ni_2Fe_2 complex $(\eta^5\text{-}Cp)_2Ni_2Fe_2(CO)_6(\mu_3\text{-}CO)$ (average 2.422 Å)[272] and $[Fe_3Ni(CO)_{12}]^{2-}$ (average 2.481 Å).[271] The two iron atoms Fe4 and Fe2 which are separated by 3.6950(3) Å are non-bonding, and so are atoms Ni1 and Fe2 which are apart at a distance of 3.4348(3) Å.

In the course of this reaction one of the $Fe(CO)_3$ unit in **6.1** has been replaced by a NiCp group from the starting $NiCp_2$ reagent (see Scheme 6.1). The remaining Cp ligand is then transferred to a neighboring iron atom and is able to displace two CO ligands under these reaction condition to form the Fe(Cp)(CO) moiety that bridges the Fe_3Ni butterfly skeleton. It has been reported that $Fe(CO)_3$ serves as a good leaving group that can be readily replaced by units such as NiCp.[273-276] Also it has been shown that thermal decomposition of $NiCp_2$ results in cleavage of a cyclopentadienyl ligand along with generation of NiCp.[275] With 10 CO ligands remaining on the cluster an Fe-Ni bond also cleaves resulting in the $Fe_4Ni(\mu_5\text{-}C)$ metal cluster framework to rearrange as seen in its solid state structure.

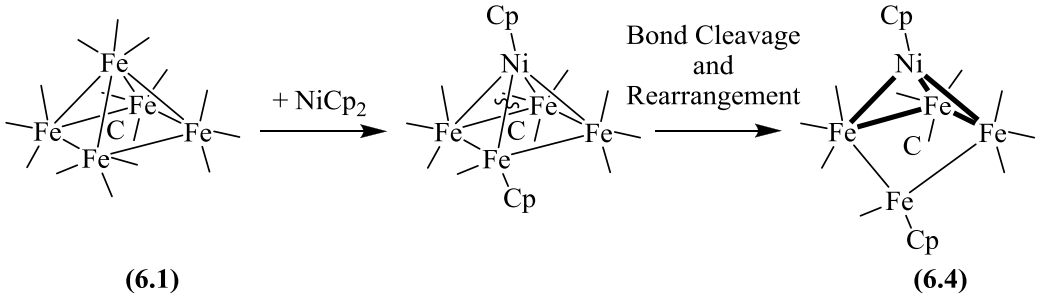

(6.1) **(6.4)**

Scheme 6.1

It has been shown that compound **6.3**, $Ru_5(CO)_{15}(SiEt_3)(\mu_5\text{-}C)(\mu\text{-}H)$, when heated loses one CO ligand with rearrangement of the metal cluster framework to yield $Ru_5(CO)_{14}(SiEt_3)(\mu_5\text{-}C)(\mu\text{-}H)$ which is a square pyramidal cluster of five ruthenium atoms.[248] Thus, compound **6.4** could also lose one CO ligand and yield a compound such as $Fe_4Ni(Cp)_2(CO)_9(\mu_5\text{-}C)$, **6.7**, as shown in Eq. 3.

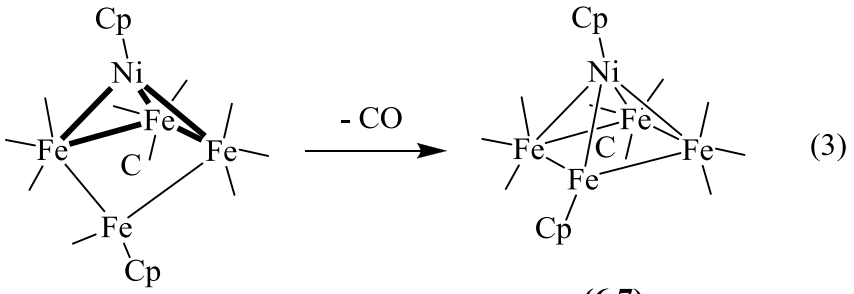

(6.4) **(6.7)** (3)

However, we have not seen any evidence for a product as a result of CO elimination. There was no reaction when compound **6.4** was refluxed in benzene solvent for 2.5 hours. However, at elevated temperatures of 127 °C (octane reflux), compound **6.4** decomposed and yielded only trace amounts of **6.6**. Furthermore it should be noted that the product **6.7** as drawn in Eq. 3 gives the Ni atom an electron configuration of more than 18, hence

to accommodate a molecular formula for **6.7** the Cp ligand on Ni would have to perhaps migrate to an Fe atom with concomitant shift of CO ligands from Fe to Ni.

The new compound, $Fe_5(Cp)_2(CO)_{10}(\mu_5\text{-}C)$, **6.5**, was also obtained from this reaction in 16% yield. The complex contains no nickel and is simply a di-Cp substituted derivative of **6.1**. Compound **6.5** was also characterized by a combination of IR spectroscopy, ^1H NMR, mass spectrometry, elemental, and single crystal X-ray diffraction analyses. An ORTEP showing the molecular structure of **6.5** is shown in Figure 6.2.

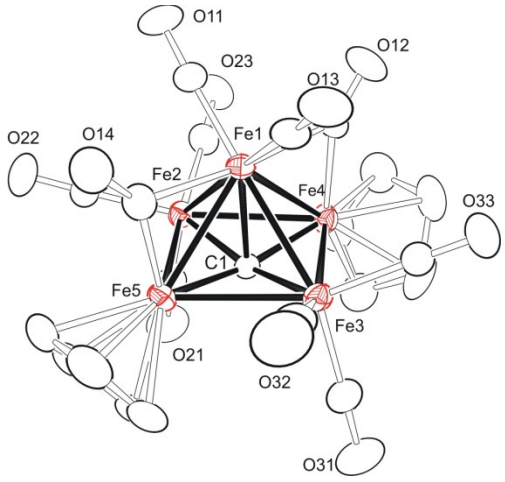

Figure 6.2 The molecular structure of $Fe_5(Cp)_2(CO)_{10}(\mu_5\text{-}C)$, **6.5**.

Selected bond distances and angles are listed in Table E.2. The Fe-Fe bond distances in **6.5** are similar to those in **6.1**,[240] all lie in the range 2.5455(4) - 2.6396(4) Å. The total cluster valence electron count is 74 electrons which is consistent for a square pyramidal cluster containing transition metal atoms if all atoms have an 18 electron configuration.[268, 269] Recently, Sumit from our lab also synthesized similar Fe-Ni bimetallic cluster complexes from the reaction of $Ni(COD)_2$ with **6.1**.[265]

With the aim of synthesizing trimetallic cluster complexes, we have repeated the reaction of **6.1** with $Ni(Cp)_2$ in the presence of two equivalents of Bu^t_3SnH in refluxing toluene solution. After plating the reaction mixture on TLC we have identified a new product: $Ni(CO)_3(SnBu^t_3)_2$, **6.8**, along with the previously observed products **6.4**, **6.5**, and **6.6**. There were no Fe-Sn-Ni cluster complexes isolated in this reaction. We have also investigated the reaction of compound **6.4** with the Bu^t_3SnH in refluxing toluene solution, but the Fe-Ni bimetallic complex **6.4** appears to be inert toward the organotin ligand Bu^t_3SnH. Compound **6.8** was characterized by a combination of IR spectroscopy, ^1H NMR spectroscopy, and single crystal X-ray crystallography. The molecular structure of **6.8** is shown in Figure 6.3.

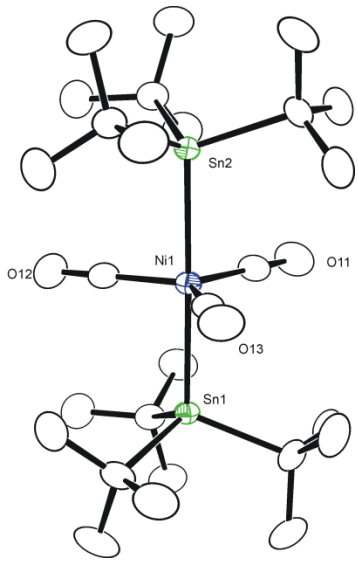

Figure 6.3 The molecular structure of $Ni(CO)_3(SnBu^t_3)_2$, **6.8**.

As seen in Figure 6.3, the molecule has trigonal bipyramidal geometry with the three CO ligands lying in the equatorial plane and two $SnBu^t_3$ groups positioned *trans* to each other in the axial plane. Compound **6.8** is a 18 electron, mononuclear Ni-Sn bimetallic

complex resistant to air and moisture and stable under refluxing conditions, as well. The formation of $Ni(CO)_3(SnBu^t_3)_2$, **6.8** can be explained based on the cleavage of Cp group from $Ni(Cp)_2$ to give an intermediate Ni(Cp) fragment, which abstracts the CO from **6.1** to yield $Ni(CO)_4$. The Bu^t_3SnH adds to the $Ni(CO)_4$ intermediate to yield **6.8**. The compound **6.8** was also obtained in 50% yield as a sole product in the reaction of $Ni(COD)_2$ with two equivalents of Bu^t_3SnH in the presence of CO gas in refluxing heptane solution through the formation of intermediate $Ni(CO)_4$, (see Eq. 4).[277]

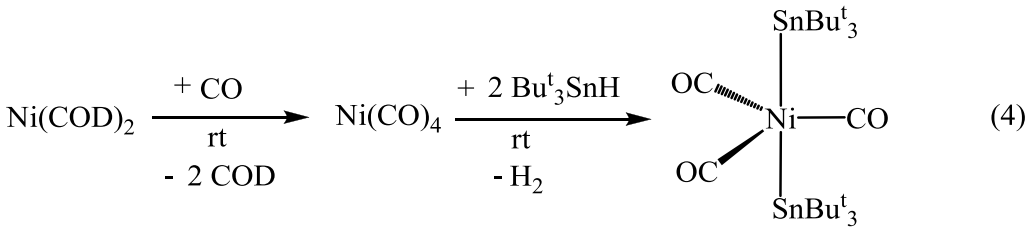

(4)

$Ni(SnBu^t_3)_2(CO)_3$, **(6.8)**

6.3. Conclusions

The new bimetallic Fe-Ni carbide containing cluster complex $Fe_4Ni(Cp)_2(CO)_{10}(\mu_5\text{-}C)$, **6.4**, was synthesized by metal-metal exchange and metal cluster rearrangement processes in the reaction of $Fe_5(\mu_5\text{-}C)(CO)_{15}$, **6.1**, with $NiCp_2$ at 80 °C. A minor product, $Fe_5(Cp)_2(CO)_{10}(\mu_5\text{-}C)$ (**6.5**), was also obtained from this reaction, which contains no nickel and is a di-Cp substituted derivative of **6.1**. Compound **6.4** consists of an open $Fe_4Ni(\mu_5\text{-}C)$ cluster framework with a carbide ligand where one iron atom bridges a butterfly arrangement of one nickel and three iron atoms. Compound **6.4** appears to be stable to the addition of organo tin hydride Bu^t_3SnH, unlike the parent carbide cluster **6.1**.

6.4. Experimental section

General Data.

Infrared spectra were recorded on a Nicolet 380 FT-IR spectrophotometer. ^{1}H NMR were recorded on a Bruker 400 spectrometer operating at 399.993 MHz. Elemental analyses were performed by Columbia Analytical Services (Tucson, AZ). Mass spectrometric measurements performed by direct–exposure probe using electron impact ionization (EI) were made on VG 70S instrument at the University of South Carolina, Columbia, SC. Nickelocene ($NiCp_2$), and $Ni(COD)_2$ were purchased from Strem Chemicals and used without further purification. $Fe_5(\mu_5\text{-}C)(CO)_{15}$, **6.1**,[240] and Bu^t_3SnH[105] were prepared according to the previously published procedure. Product separations were performed by TLC in air on Analtech preparative silica gel GF 500 μm glass plates.

Reaction of 6.1 with $NiCp_2$.

Under an atmosphere of Argon, 70 mg of **6.1** (0.098 mmol) and 28 mg of $NiCp_2$ (0.148 mmol) were dissolved in 25 mL of freshly distilled benzene in a 100 mL three-neck round-bottom flask equipped with a reflux condenser. The reaction mixture was then heated to reflux for 1 h, after which the solvent was removed *in vacuo* and the products were separated by TLC using a 4:1 hexane/methylene chloride solvent mixture to yield in order of elution 1.4 mg (2%) of a green band, $Fe_3(CO)_{12}$; 18.3 mg (27%) of a green band, $Fe_4Ni(Cp)_2(CO)_{10}(\mu_5\text{-}C)$, **6.4**; 10.9 mg (16%) of a brown band, $Fe_5(Cp)_2(CO)_{10}(\mu_5\text{-}C)$, **6.5**; and 16 mg (18%) of a red band, $[CpFe(CO)_2]_2$, **6.6.** Spectral data for **6.4**: IR ν_{CO} (cm^{-1} in hexane): 2054 (m), 2020 (vs), 2004 (s), 1986 (s), 1977 (m), 1956 (w). ^{1}H NMR (C_6D_6 in ppm): δ = 4.44 (s, 5 H, Cp), 4.10 (s, 5 H, Cp). EI/MS: *m/z* 704 (M^+), 676 (M^+- CO), 620 (M^+- 3CO), 592 (M^+- 4CO), 564 (M^+- 5CO), 508 (M^+-

7CO), 480 (M^+- 8CO), 452 (M^+- 9CO), 424 (M^+- 10CO). The isotope pattern is consistent with the presence of four iron atoms and one nickel atom. Elemental Anal. Calc.: C, 35.80; H, 1.43 % Found: C, 35.70; H, 1.39 %. Spectral data for **6.5**: IR ν_{CO} (cm^{-1} in hexane): 2044 (w), 2014 (s), 1999 (m), 1970 (m), 1958 (m), 1844 (w), 1834 (w); ^1H NMR (C_6D_6 in ppm): δ = 4.59 (s, 10 H, Cp). EI/MS: *m/z* 702 (M^+), 674 (M^+-CO), 618 (M^+- 3CO), 590 (M^+- 4CO), 562 (M^+- 5CO), 506 (M^+- 7CO), 478 (M^+- 8CO), 450 (M^+- 9CO), 422 (M^+- 10CO). The isotope pattern is consistent with the presence of five iron atoms. Elemental Anal. Calc.: C, 35.95; H, 1.44 % Found: C, 35.74; H, 1.17 %.

Reaction of 6.1 with $NiCp_2$ and Bu^t_3SnH.

Under an atmosphere of Argon, 70 mg of **6.1** (0.098 mmol) and 28 mg of $NiCp_2$ (0.148 mmol) were dissolved in 25 mL of freshly distilled toluene in a 100 mL three-neck round-bottom flask equipped with a reflux condenser. 30.0 mg of Bu^t_3SnH dissolved in 1mL of toluene was added to above reaction mixture. The reaction mixture was then heated to reflux for one hour, after which the solvent was removed *in vacuo* and the products were separated by TLC using a 4:1 hexane/methylene chloride solvent mixture to yield, in order of elution, 3.4 mg (yield 2%) of a yellow band, $Ni(CO)_3(SnBu^t_3)_2$, **6.8**; 18.3 mg (yield 27%) of a green band, $Fe_4Ni(Cp)_2(CO)_{10}(\mu_5\text{-C})$, **6.4**; 10.9 mg (yield 16%) of a brown band, $Fe_5(Cp)_2(CO)_{10}(\mu_5\text{-C})$, **6.5**; and 16 mg (yield 18%) of a red band, $[CpFe(CO)_2]_2$, **6.6**.

Preparation of $Ni(SnBu^t_3)_2(CO)_3$, 6.8.

A 50 mg (0.18 mmol) amount of $Ni(COD)_2$ was weighed and transferred into a 100 ml three-neck round bottom flask equipped with schlenk adapter, reflux condenser,

rubber septum, and stir bar. A 105 mg (0.36 mmol) amount of Bu^t_3SnH was dissolved in 20 mL of freshly distilled heptane solvent in a 25 mL one-neck schlenk flask and added to the flask containing $Ni(COD)_2$ using a cannula under an argon flow. The yellow-colored reaction mixture was stirred at room temperature for ten minutes to dissolve the $Ni(COD)_2$. The reaction mixture was then heated to reflux at 97 °C while purging CO gas through the solution for thirty minutes. Initially the color of the solution slowly changed to pink, and then gradually turned dark yellow. An IR spectrum of the reaction mixture at this time showed formation of $Ni(SnBu^t_3)_2(CO)_3$, **6.8**. The solvent was removed in *vacuo* and the solid residue was redissolved in CH_2Cl_2 and filtered through a silica plug. A 65 mg amount of light-yellow crystalline solid (yield 50%) was obtained by fast evaporation of solvent under an argon flow at room temperature. Spectral data for **6.8**: IR ν_{CO} (cm^{-1} in hexane): 1991. ^1H NMR ($CDCl_3$, in ppm): δ = 1.41 (s, 54H, CH_3, $^3J_{Sn-H}$ = 62.1 Hz). EI/MS: m/z 722 (M^+), 665 (M^+ -C_4H_9), 609 (M^+ -C_4H_9 -2CO). The isotope pattern is consistent with the presence of one nickel atom.

6.5. Crystallographic analysis

Dark green crystals of **6.4** and brown crystals of **6.5** suitable for diffraction analysis were grown by slow evaporation of solvent from solutions in hexane/methylene chloride solvent mixture at -20 °C. The yellow crystals of **6.8** were grown by slow evaporation of solvent from solutions in hexane solvent mixture at -20 °C. Each data crystal was glued onto the end of a thin glass fiber. X-ray intensity data were measured by using a Bruker SMART APEX2 CCD-based diffractometer using Mo Kα radiation (λ = 0.71073 Å).[117] The raw data frames were integrated with the SAINT+ program by using a narrow-frame integration algorithm.[117] Corrections for Lorentz and polarization effects were also

applied with SAINT+. An empirical absorption correction based on the multiple measurement of equivalent reflections was applied using the program SADABS. All structures were solved by a combination of direct methods and difference Fourier syntheses, and refined by full-matrix least-squares on F^2, by using the SHELXTL software package.[118] All non-hydrogen atoms were refined with anisotropic displacement parameters. Hydrogen atoms were placed in geometrically idealized positions and included as standard riding atoms during the least-squares refinements. Crystal data, data collection parameters, and results of the analyses are listed in Table E.3 in Appendix E.

Compound **6.4** crystallized in the orthorhombic crystal system. The systematic absences in the intensity data identified the unique space group $P2_12_12_1$. Compound **6.5** crystallized in the monoclinic crystal system. The systematic absences in the intensity data were consistent with either of the space groups *Cc* or *C*2/*c*, the latter of which was confirmed by the successful solution and refinement of the structure. Compound **6.8** crystallized in the monoclinic crystal system. The systematic absences in the intensity data were consistent with the unique space groups $P2_1/c$.

Appendix A: Supporting information for chapter 2

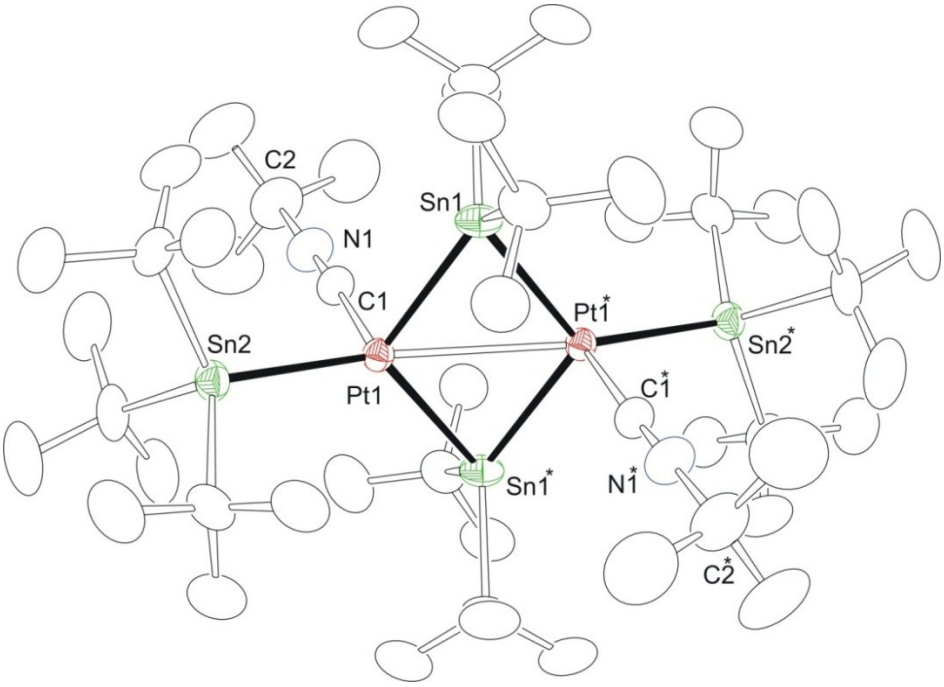

Figure A.1 The molecular structure of $[H_2Pt(SnBu^t_3)(\mu\text{-}SnBu^t_2)(CNBu^t)]_2$, **2.10**.

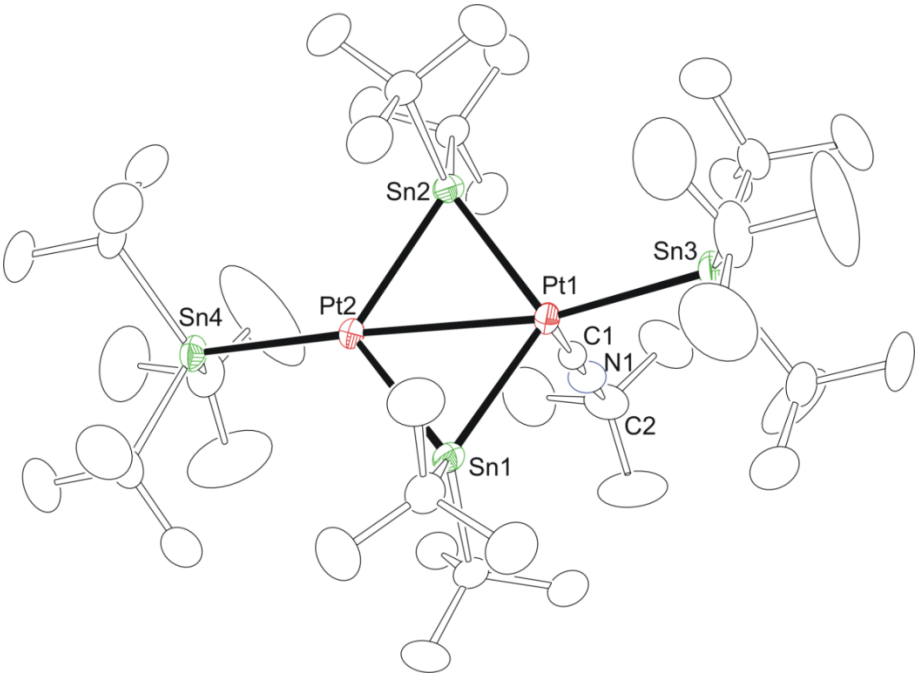

Figure A.2 The molecular structure of $[H_4Pt(SnBu^t_3)_2(\mu\text{-}SnBu^t_2)_2(CNBu^t)]$, **2.11**.

Table 2.1. Crystallographic data for compounds 2.1 and 2.5.

Compound	**2.1**	**2.5**
Empirical formula	$PtSnC_{20}H_{40}$	$PtSn_2C_{26}H_{54}O_2$
Formula weight	594.30	831.16
Crystal system	Monoclinic	Monoclinic
Lattice parameters		
a (Å)	11.1084(4)	15.3248(2)
b (Å)	12.6969(4)	9.19810(10)
c (Å)	15.4779(5)	24.1611(3)
α (deg)	90.00	90.00
β (deg)	102.2130(10)	98.2477(6)
γ (deg)	90.00	90.00
V ($Å^3$)	2133.63(12)	3370.50(7)
Space group	$P2_1/n$ (# 14)	$C2/c$ (# 15)
Z value	4	4
ρ_{calc} (g / cm^3)	1.850	1.638
μ (Mo K_α) (mm^{-1})	7.717	5.627
Temperature (K)	100(2)	296(2)
$2\Theta_{max}$ (°)	63.98	60.00
No. Obs. ($I > 2\sigma(I)$)	212	152
No. Parameters	5996	4301
Goodness of fit GOF*	1.019	1.199
Max. shift in cycle	0.001	0.001
Residuals*: R1; wR2	0.0183; 0.0382	0.0455; 0.1165
Absorption Correction, Max/min	Multi-scan 0.8609/0.3715	Multi-scan 0.7468/0.4928
Largest peak in Final Diff. Map (e^- / $Å^3$)	0.737	1.064

*$R = \Sigma_{hkl}(\,|\,|F_{obs}| - |F_{calc}|\,|)/\Sigma_{hkl}|F_{obs}|$; $R_w = [\Sigma_{hkl}w(|F_{obs}| - |F_{calc}|)^2/\Sigma_{hkl}wF_{obs}^2]^{1/2}$, $w = 1/\sigma^2(F_{obs})$; $GOF = [\Sigma_{hkl}w(|F_{obs}| - |F_{calc}|)^2/(n_{data} - n_{vari})]^{1/2}$.

Table 2.2. Crystallographic data for compounds 2.4 and 2.9.

Compound	**2.4**	**2.9**
Empirical formula	$Pt_2Sn_4C_{40}H_{94}$	$Pt_2Sn_4C_{42}H_{94}O_2$
Formula weight	1440	1496
Crystal system	Monoclinic	Triclinic
Lattice parameters		
a (Å)	9.2175(8)	9.1706(3)
b (Å)	18.2662(15)	11.9962(4)
c (Å)	16.2599(13)	12.7070(5)
α (deg)	90.00	97.1493(5)
β (deg)	104.7720(10)	99.4757(5)
γ (deg)	90.00	102.9447(5)
V ($Å^3$)	2647.2(7)	1324.75(8)
Space group	$P2_1/n$ (# 14)	$P\bar{1}$ (# 2)
Z value	4	1
ρ_{calc} (g / cm^3)	1.802	1.870
μ (Mo K_α) (mm^{-1})	7.144	7.144
Temperature (K)	296(2)	100
$2\Theta_{max}$ (°)	54	60
No. Obs. ($I > 2\sigma(I)$)	223	245
No. Parameters	3979	7055
Goodness of fit GOF*	1.003	1.042
Max. shift in cycle	0.001	0.001
Residuals*: R1; wR2	0.0299; 0.0589	0.0391; 0.0974
Absorption Correction, Max/min	Multi-scan 0.9320/0.7631	Multi-scan 0.7465/0.4005
Largest peak in Final Diff. Map (e^- / $Å^3$)	0.994	0.995

*$R = \Sigma_{hkl}(\,|\,|F_{obs}| - |F_{calc}|\,|\,)/\Sigma_{hkl}|F_{obs}|$; $R_w = [\Sigma_{hkl}w(|F_{obs}| - |F_{calc}|)^2/\Sigma_{hkl}wF_{obs}^2]^{1/2}$, $w = 1/\sigma^2(F_{obs})$; $GOF = [\Sigma_{hkl}w(|F_{obs}| - |F_{calc}|)^2/(n_{data} - n_{vari})]^{1/2}$.

Table 2.3. Crystallographic data for compounds 2.10 and 2.11.

Compound	**2.10**	**2.11**
Empirical formula	$Pt_2Sn_4C_{50}H_{112}N_2$	$Pt_2Sn_4C_{45}H_{113}N$
Formula weight	1606	1523
Crystal system	Triclinic	Monoclinic
Lattice parameters		
a (Å)	12.1734(5)	18.2142(7)
b (Å)	14.5997(6)	17.3843(7)
c (Å)	19.5674(8)	22.6417(9)
α (deg)	75.5330(10)	90.00
β (deg)	89.0380(10)	112.1080(10)
γ (deg)	89.2960(10)	90.00
V (Å^3)	3366.8(2)	6642.2(5)
Space group	$P\bar{1}$ (# 2)	$P2_1/c$ (# 14)
Z value	4	4
ρ_{calc} (g / cm^3)	1.585	1.519
μ (Mo K_α) (mm^{-1})	5.627	5.699
Temperature (K)	296(2)	296(2)
$2\Theta_{max}$ (°)	52	58
No. Obs. (I > 2σ(I))	568	469
No. Parameters	11309	12246
Goodness of fit GOF*	1.044	1.002
Max. shift in cycle	0.001	0.002
Residuals*: R1; wR2	0.0425; 0.1035	0.0381; 0.1150
Absorption Correction, Max/min	Multi-scan 0.2831/0.1652	Multi-scan 0.4819/0.3299
Largest peak in Final Diff. Map (e$^-$ / Å^3)	0.997	1.000

*$R = \Sigma_{hkl}(\,|\,|F_{obs}| - |F_{calc}|\,|\,)/\Sigma_{hkl}|F_{obs}|$; $R_w = [\Sigma_{hkl}w(|F_{obs}| - |F_{calc}|)^2/\Sigma_{hkl}wF_{obs}^2]^{1/2}$, $w = 1/\sigma^2(F_{obs})$; $GOF = [\Sigma_{hkl}w(|F_{obs}| - |F_{calc}|)^2/(n_{data} - n_{vari})]^{1/2}$.

Table 2.4. Crystallographic data for compound 2.12.

Compound	**2.12**
Empirical formula	$Pd_2Sn_4C_{40}H_{94}$
Formula weight	1262
Crystal system	Monoclinic
Lattice parameters	
a (Å)	9.2362(17)
b (Å)	18.265(3)
c (Å)	16.228(3)
α (deg)	90.00
β (deg)	104.634(3)
γ (deg)	90.00
V (Å^3)	2649.0(8)
Space group	$P2_1/n$ (# 14)
Z value	4
ρ_{calc} (g / cm^3)	1.578
μ (Mo K_α) (mm^{-1})	2.543
Temperature (K)	296(2)
$2\Theta_{max}$ (°)	54
No. Obs. (I > 2σ(I))	223
No. Parameters	3512
Goodness of fit GOF*	1.010
Max. shift in cycle	0.001
Residuals*: R1; wR2	0.0419; 0.0827
Absorption Correction, Max/min	Multi-scan 0.9750/0.4295
Largest peak in Final Diff. Map (e$^-$ / Å^3)	0.996

*$R = \Sigma_{hkl}(\,|\,|F_{obs}| - |F_{calc}|\,|)/\Sigma_{hkl}|F_{obs}|$; $R_w = [\Sigma_{hkl}w(|F_{obs}| - |F_{calc}|)^2/\Sigma_{hkl}wF_{obs}^2]^{1/2}$, $w = 1/\sigma^2(F_{obs})$; $GOF = [\Sigma_{hkl}w(|F_{obs}| - |F_{calc}|)^2/(n_{data} - n_{vari})]^{1/2}$.

Appendix B: Supporting information for chapter 3

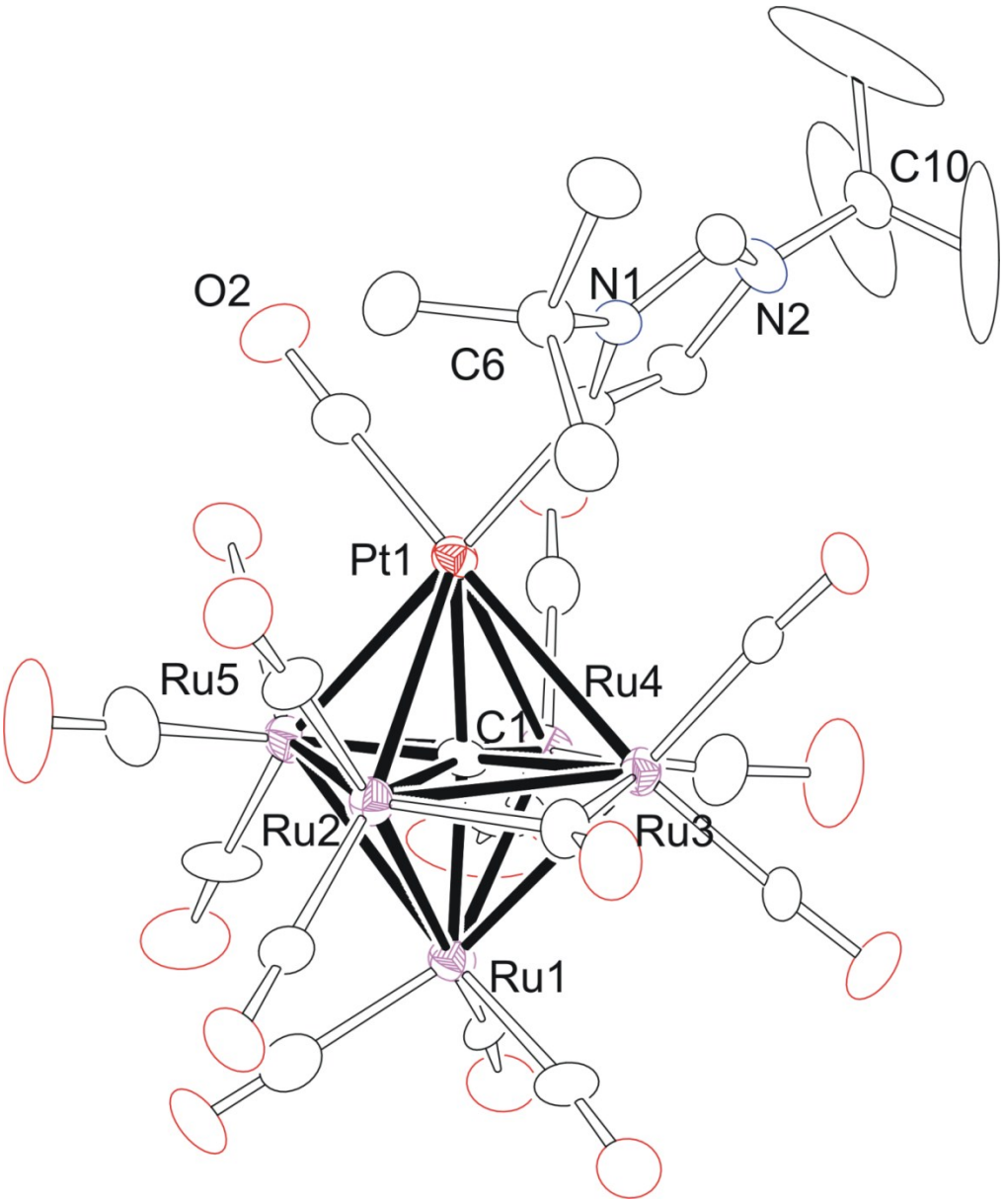

Figure B.1 The molecular structure of $PtRu_5(C)(CO)_{15}(IBu^t)$, **3.8**.

Table B.1. Selected intramolecular distances and angles for compounds 3.3 and 3.7[a]

(a) Distances

Compound **3.3**			Compound **3.7**		
atom	atom	distance (Å)	atom	atom	distance (Å)
Pt(1)	C(1)	1.885(5)	Pt(1)	C(12)	1.855(4)
Pt(1)	C(2)	2.091(3)	Pt(1)	C(1)	2.0549(3)
Pt(1)	Sn(1)	2.611(3)	Pt(1)	Sn(1)	2.7262(3)
C(1)	O(1)	1.133(5)	C(12)	O(12)	1.142(5)

(b) Angles

Compound **3.3**				Compound **3.7**			
atom	atom	atom	angle (deg)	atom	atom	atom	angle (deg)
C(1)	Pt(1)	C(2)	105.06(16	C(12)	Pt(1)	C(1)	173.2(2)
C(1)	Pt(1)	Sn(1)	94.79(13)	C(12)	Pt(1)	Sn(1)	87.70(14)
C(2)	Pt(1)	Sn(1)	160.00(10)	C(1)	Pt(1)	Sn(1)	93.83(10)

[a] Estimated standard deviations in the least significant figure are given in parentheses

Table B.2. Crystallographic data for compounds 3.1 and 3.3.

Compound	**3.1**	**3.3**
Empirical formula	$Pt_2Sn_2C_{46}H_{96}N_4$	$PtSnC_{24}H_{48}N_2O$
Formula weight	1332.83	694
Crystal system	Triclinic	Monoclinic
Lattice parameters		
a (Å)	10.17420(10)	12.6631(3)
b (Å)	11.76800(10)	27.5135(7)
c (Å)	13.5031(2)	17.6146(4)
α (deg)	102.1810(10)	90.00
β (deg)	106.6930(10)	104.69
γ (deg)	113.1550(10)	90.00
V (Å^3)	1324.02(3)	5936.3(2)
Space group	$P\bar{1}$ (# 2)	$P2_1/c$ (# 14)
Z value	1	8
ρ_{calc} (g / cm^3)	1.672	1.553
μ (Mo K_α) (mm^{-1})	6.230	5.564
Temperature (K)	100(2)	296(2)
$2\Theta_{max}$ (°)	58.0	54.0
No. Obs. (I > 2σ(I))	262	557
No. Parameters	6906	9939
Goodness of fit GOF*	1.072	1.018
Max. shift in cycle	0.002	0.005
Residuals*: R1; wR2	0.0145; 0.0366	0.0279; 0.0562
Absorption Correction, Max/min	Multi-Scan 0.7062/0.3163	Multi-scan 0.8969/0.2690
Largest peak in Final Diff. Map (e$^-$ / Å^3)	1.000	1.000

*$R = \Sigma_{hkl}(\,|\,|F_{obs}| - |F_{calc}|\,|)/\Sigma_{hkl}|F_{obs}|$; $R_w = [\Sigma_{hkl}w(|F_{obs}| - |F_{calc}|)^2/\Sigma_{hkl}wF_{obs}^2]^{1/2}$, $w = 1/\sigma^2(F_{obs})$; $GOF = [\Sigma_{hkl}w(|F_{obs}| - |F_{calc}|)^2/(n_{data} - n_{vari})]^{1/2}$.

Table B.3. Crystallographic data for compounds 3.5 and 3.7.

Compound	**3.5**	**3.7**
Empirical formula	$PtSnC_{25}H_{52}N_2$	$PtSnC_{24}H_{74}N_2O$
Formula weight	694.7	977.39
Crystal system	Triclinic	Orthorhombic
Lattice parameters		
a (Å)	9.3026(3)	11.9259(5)
b (Å)	12.3233(5)	13.9050(6)
c (Å)	14.8142(6)	26.0856(10)
α (deg)	96.2210(10)	90.00
β (deg)	93.0120(10)	90.00
γ (deg)	110.3320(10)	90.00
V ($Å^3$)	1575.66(10)	4325.8(3)
Space group	$P\ \bar{1}$ (# 2)	P2(1)2(1)2(1)
Z value	2	4
ρ_{calc} (g / cm^3)	1.464	1.501
μ (Mo K_α) (mm^{-1})	5.238	4.397
Temperature (K)	100(2)	296
$2\Theta_{max}$ (°)	55.0	64.0
No. Obs. ($I > 2\sigma(I)$)	289	402
No. Parameters	6755	11995
Goodness of fit GOF*	1.118	1.005
Max. shift in cycle	0.001	0.002
Residuals*: R1; wR2	Multi-scan 0.0294; 0.0988	Multi-scan 0.0330; 0.0665
Absorption Correction, Max/min	0.7461/0.5448	0.9172/ 0.1778
Largest peak in Final Diff. Map (e^- / $Å^3$)	0.996	1.262

*$R = \Sigma_{hkl}(\ |\ |F_{obs}| - |F_{calc}|\ |\ )/\Sigma_{hkl}|F_{obs}|$; $R_w = [\Sigma_{hkl}w(|F_{obs}| - |F_{calc}|)^2/\Sigma_{hkl}wF_{obs}^2]^{1/2}$, $w = 1/\sigma^2(F_{obs})$; GOF = $[\Sigma_{hkl}w(|F_{obs}| - |F_{calc}|)^2/(n_{data} - n_{vari})]^{1/2}$.

Table B.4. Crystallographic data for compound 3.8

Compound	**3.8**
Empirical formula	$Ru_5PtC_{27}H_{20}N_2O_{15}$
Formula weight	1312.89
Crystal system	Monoclinic
Lattice parameters	
a (Å)	13.451(5)
b (Å)	18.557(7)
c (Å)	15.215(6)
α (deg)	90.00
β (deg)	91.369(7)
γ (deg)	90.00
V (Å^3)	3797(3)
Space group	$P2_1/n$ (# 14)
Z value	4
ρ_{calc} (g / cm^3)	2.297
μ (Mo K_α) (mm^{-1})	5.673
Temperature (K)	293(2)
$2\Theta_{max}$ (°)	52
No. Obs. (I > 2σ(I))	451
No. Parameters	4478
Goodness of fit GOF*	1.026
Max. shift in cycle	0.000
Residuals*: R1; wR2	0.0602; 0.1605
Absorption Correction, Max/min	0.7461/0.4976
Largest peak in Final Diff. Map (e$^-$ / Å^3)	1.000

*$R = \Sigma_{hkl}(\,|\,|F_{obs}| - |F_{calc}|\,|)/\Sigma_{hkl}|F_{obs}|$; $R_w = [\Sigma_{hkl}w(|F_{obs}| - |F_{calc}|)^2/\Sigma_{hkl}wF_{obs}^2]^{1/2}$, $w = 1/\sigma^2(F_{obs})$; $GOF = [\Sigma_{hkl}w(|F_{obs}| - |F_{calc}|)^2/(n_{data} - n_{vari})]^{1/2}$.

Appendix C: Supporting information for chapter 4

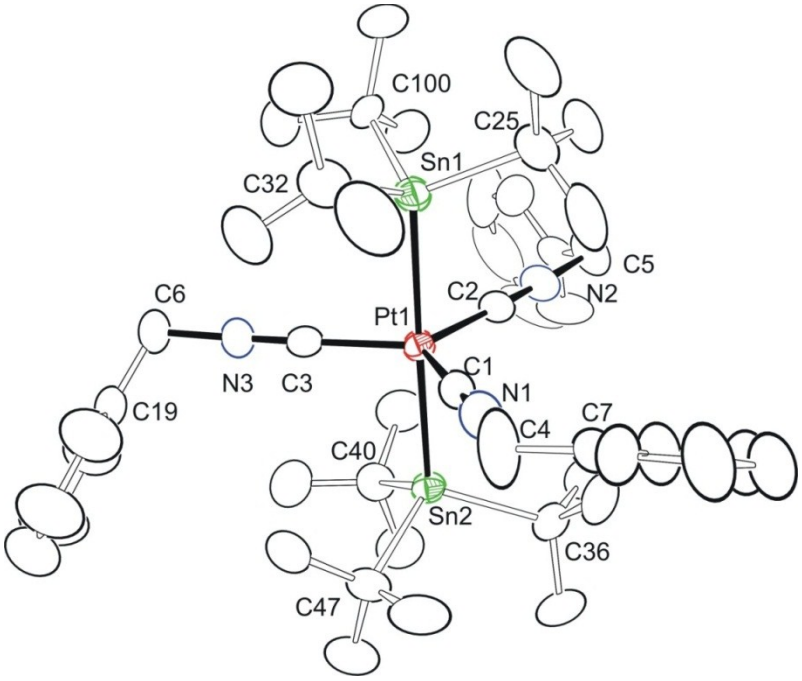

Figure C.1 The molecular structure for $Pt(SnBu^t_{3)2}(CNCH_2Ph)_3$, **4.6**.

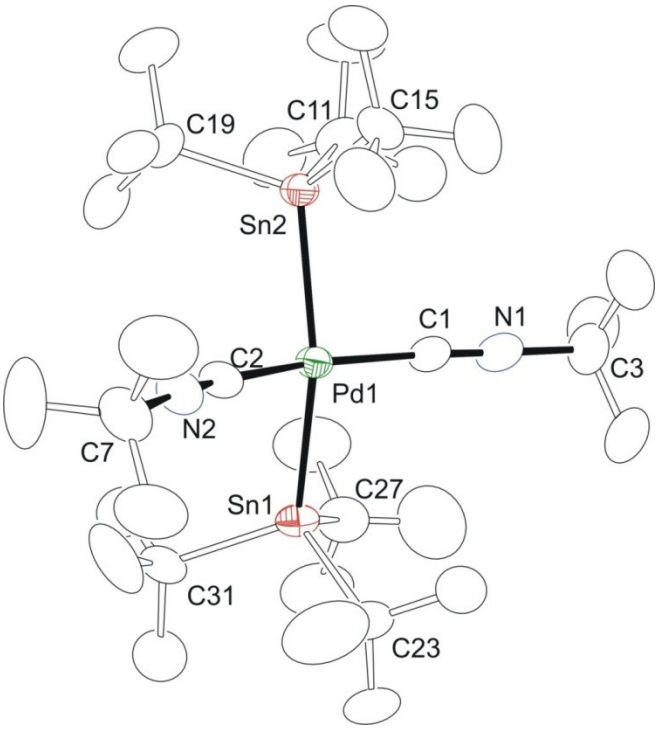

Figure C.2 The molecular structure for $Pd(SnBu^t_3)_2(CNBu^t)_2$, **4.9**.

Table C.1. Crystallographic Data for Compounds 4.1 and 4.2.

Compound	**4.1**	**4.2**
Empirical formula	$PtSn_2N_2C_{34}H_{74}\cdot Et_2O$	$PtSn_2N_2C_{34}H_{72}$
Formula weight	1017.54	941.41
Crystal system	Orthorhombic	Monoclinic
Lattice parameters		
a (Å)	13.1534(7)	13.6893(6)
b (Å)	19.3120(10)	15.7758(7)
c (Å)	9.2366(5)	19.1337(8)
α (deg)	90.00	90.00
β (deg)	90.00	91.0532(7)
γ (deg)	90.00	90.00
V ($Å^3$)	2346.3(2)	4131.4(3)
Space group	*Pmmn* (# 59)	$P2_1/n$ (# 14)
Z value	2	4
ρ_{calc} (g / cm^3)	1.440	1.514
μ (Mo K_α) (mm^{-1})	4.056	4.598
Temperature (K)	100	100
$2\Theta_{max}$ (°)	60.00	60.00
No. Obs. ($I > 2\sigma(I)$)	2959	9231
No. Parameters	120	376
Goodness of fit GOF*	1.080	1.015
Max. shift in cycle	0.001	0.002
Residuals*: R1; wR2	0.0437; 0.1062	0.0293; 0.0552
Absorption Correction, Max/min	Multi-scan 0.9223/0.4690	Multi-scan 0.9136/0.4311
Largest peak in Final Diff. Map ($e^- / Å^3$)	3.100	1.867

*$R = \Sigma_{hkl}(\,|\,|F_{obs}| - |F_{calc}|\,|\,)/\Sigma_{hkl}|F_{obs}|$; $R_w = [\Sigma_{hkl}w(|F_{obs}| - |F_{calc}|)^2/\Sigma_{hkl}wF_{obs}^2]^{1/2}$, $w = 1/\sigma^2(F_{obs})$; $GOF = [\Sigma_{hkl}w(|F_{obs}| - |F_{calc}|)^2/(n_{data} - n_{vari})]^{1/2}$.

Table C.2. Crystallographic Data for Compounds 4.3 and 4.6.

Compound	**4.3**	**4.6**
Empirical formula	$PtSn_2C_{35}H_{72}N_2O$	$PtSn_2C_{48}H_{75}N_3$
Formula weight	969.42	1126.58
Crystal system	Orthorhombic	Monoclinic
Lattice parameters		
a (Å)	13.9304(9)	20.8519(8)
b (Å)	19.0073(13)	21.8255(8)
c (Å)	9.4382(6)	22.7224(9)
α (deg)	90.00	90.00
β (deg)	90.00	91.2990(10)
γ (deg)	90.00	90.00
V (Å^3)	2499.0(3)	10338.4(7)
Space group	*Pmmn* (# 59)	$P2_1/c$ (# 14)
Z value	2	4
ρ_{calc} (g / cm^3)	1.288	1.448
μ (Mo K_α) (mm^{-1})	3.805	3.689
Temperature (K)	296(2)	296(2)
$2\Theta_{max}$ (°)	56.00	54
No. Obs. (I > 2σ(I))	115	1009
No. Parameters	2477	14011
Goodness of fit GOF*	1.133	1.019
Max. shift in cycle	0.001	0.006
Residuals*: R1; wR2	0.0442; 0.1369	0.0445, 0.0910
Absorption Correction, Max/min	Multi-scan 0.7461/0.5194	Multi-scan 0.9467/0.4590
Largest peak in Final Diff. Map (e$^-$ / Å^3)	1.492	1.757

*$R = \Sigma_{hkl}(\,|\,|F_{obs}| - |F_{calc}|\,|)/\Sigma_{hkl}|F_{obs}|$; $R_w = [\Sigma_{hkl}w(|F_{obs}| - |F_{calc}|)^2/\Sigma_{hkl}wF_{obs}^2]^{1/2}$, $w = 1/\sigma^2(F_{obs})$; $GOF = [\Sigma_{hkl}w(|F_{obs}| - |F_{calc}|)^2/(n_{data} - n_{vari})]^{1/2}$.

Table C.3. Crystallographic Data for Compounds 4.9 and 4.10.

Compound	**4.9**	**4.10**
Empirical formula	$PdSn_2H_{72}N_2C_{34}$	$PdSn_2C_{39}H_{81}N_3$
Formula weight	852.72	935.85
Crystal system	Monoclinic	Otrhorhombic
Lattice parameters		
a (Å)	13.776(9)	17.4350(3)
b (Å)	16.267(11)	21.0251(3)
c (Å)	19.377(13)	13.8547(4)
α (deg)	90.00	90.00
β (deg)	90.977(13)	90.00
γ (deg)	90.00	90.00
V ($Å^3$)	4342(5)	5078.8(8)
Space group	P2(1)/n	*Pnnm*
Z value	4	4
ρ_{calc} (g / cm^3)	1.305	1.224
μ (Mo K_α) (mm^{-1})	1.571	1.350
Temperature (K)	296(2)	296(2)
$2\Theta_{max}$ (°)	50	52
No. Obs. ($I > 2\sigma(I)$)	376	223
No. Parameters	3910	3472
Goodness of fit GOF*	0.936	1.084
Max. shift in cycle	0.001	0.008
Residuals*: R1; wR2	0.0820, 0.2131	Multi-scan 0.0444; 0.1719
Absorption Correction, Max/min	Multi-Scan 0.8587/0.6500	0.9735/0.8232
Largest peak in Final Diff. Map (e^- / $Å^3$)	0.975	1.000

*$R = \Sigma_{hkl}(\,|\,|F_{obs}| - |F_{calc}|\,|)/\Sigma_{hkl}|F_{obs}|$; $R_w = [\Sigma_{hkl}w(|F_{obs}| - |F_{calc}|)^2/\Sigma_{hkl}wF_{obs}^2]^{1/2}$, $w = 1/\sigma^2(F_{obs})$; GOF = $[\Sigma_{hkl}w(|F_{obs}| - |F_{calc}|)^2/(n_{data} - n_{vari})]^{1/2}$.

Appendix D: Supporting information for chapter 5

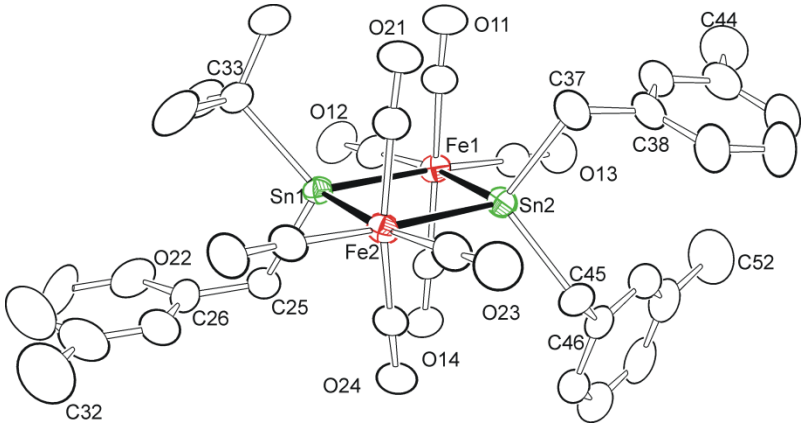

Figure D.1 The molecular structure of $Fe_2[\mu\text{-}SnBu^t(m\text{-}CH_2PhMe)][\mu\text{-}Sn(m\text{-}CH_2PhMe)_2](CO)_8$, **5. 6**.

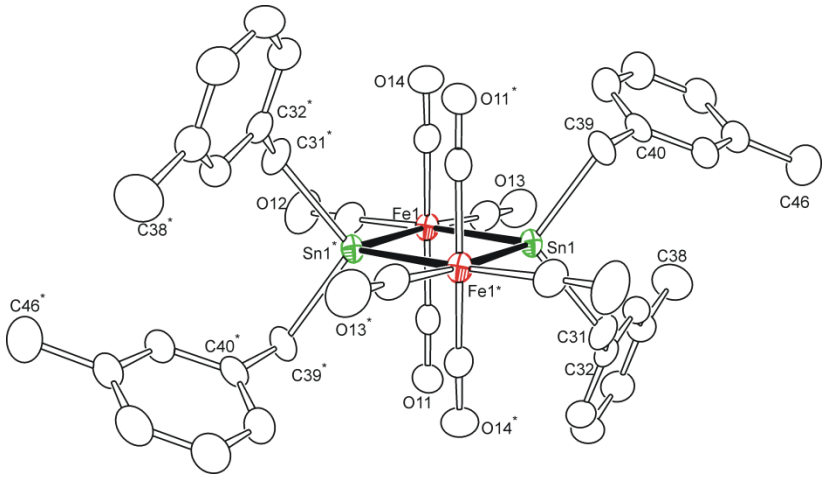

Figure D.2 The molecular structure of $Fe_2[\mu\text{-}Sn(m\text{-}CH_2PhMe)_2]_2(CO)_8$, **5.7**.

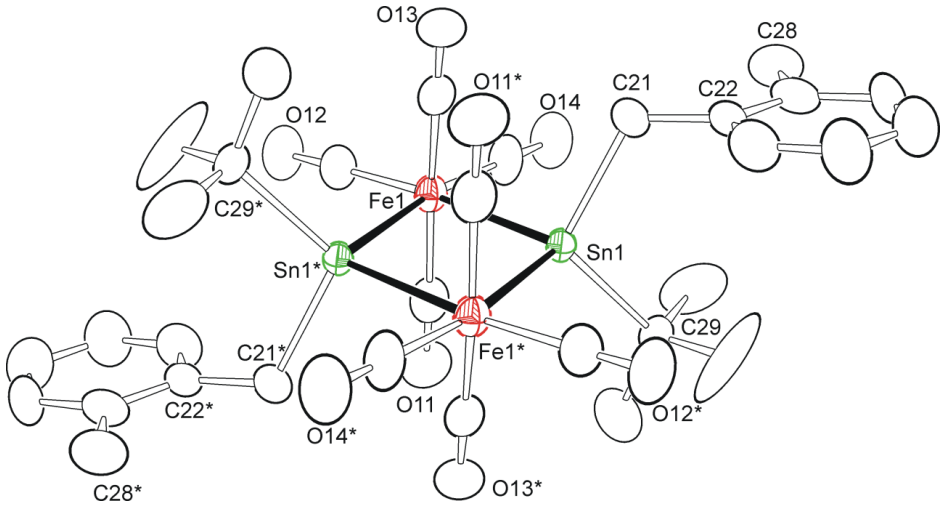

Figure D.3 The molecular structure of $Fe_2[\mu\text{-}SnBu^t(o\text{-}CH_2PhMe)]_2(CO)_8$, **5. 8**.

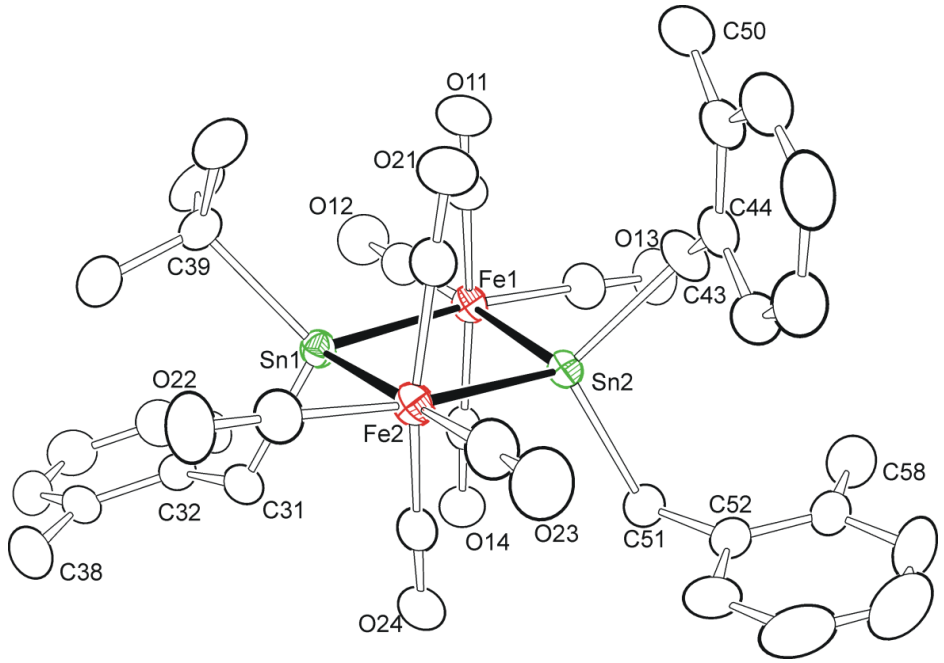

Figure D.4 The molecular structure of $Fe_2[\mu\text{-}SnBu^t(o\text{-}CH_2PhMe)][\mu\text{-}Sn(o\text{-}CH_2PhMe)_2](CO)_8$, **5**. **9**.

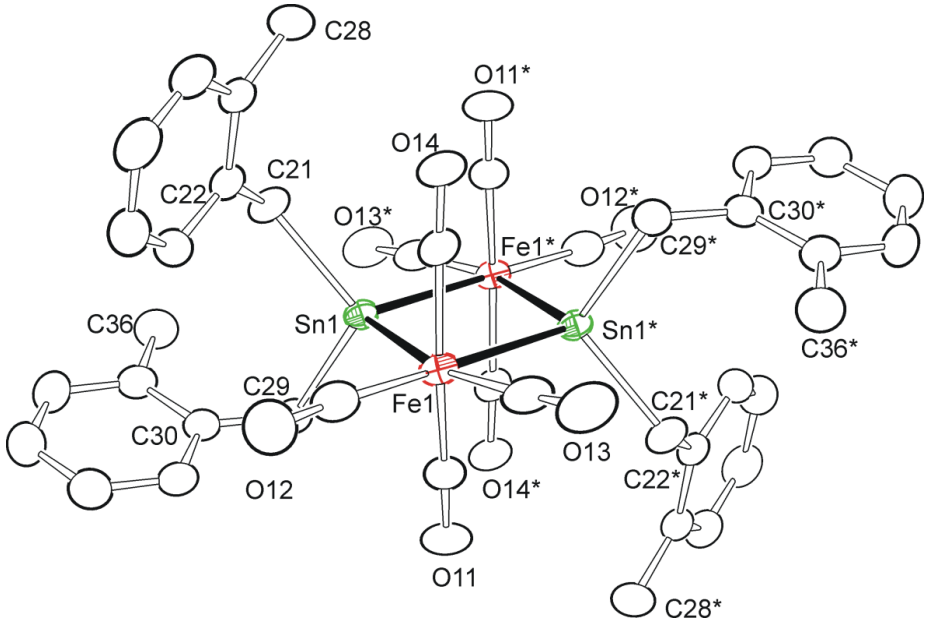

Figure D.5 The molecular structure of $Fe_2[\mu\text{-}Sn(o\text{-}CH_2PhMe)_2]_2(CO)_8$, **5.10**.

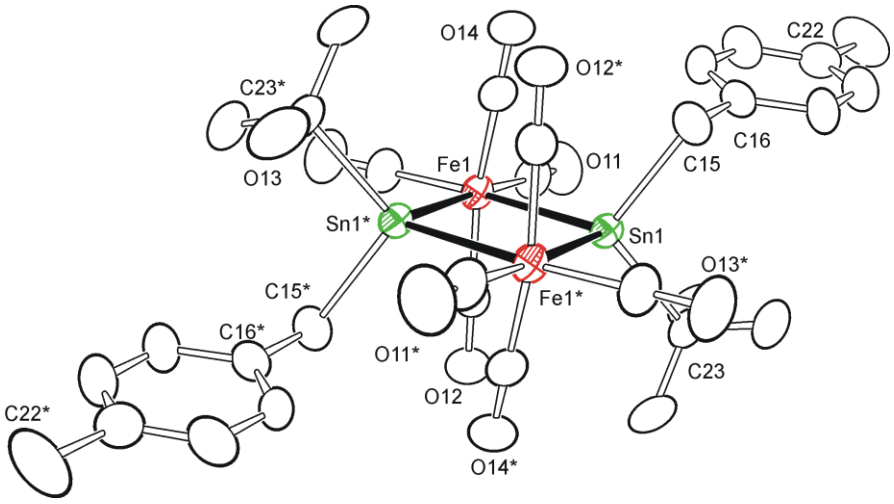

Figure D.6 The molecular structure of $Fe_2[\mu\text{-}SnBu^t(p\text{-}CH_2PhMe)]_2(CO)_8$, **5.11**.

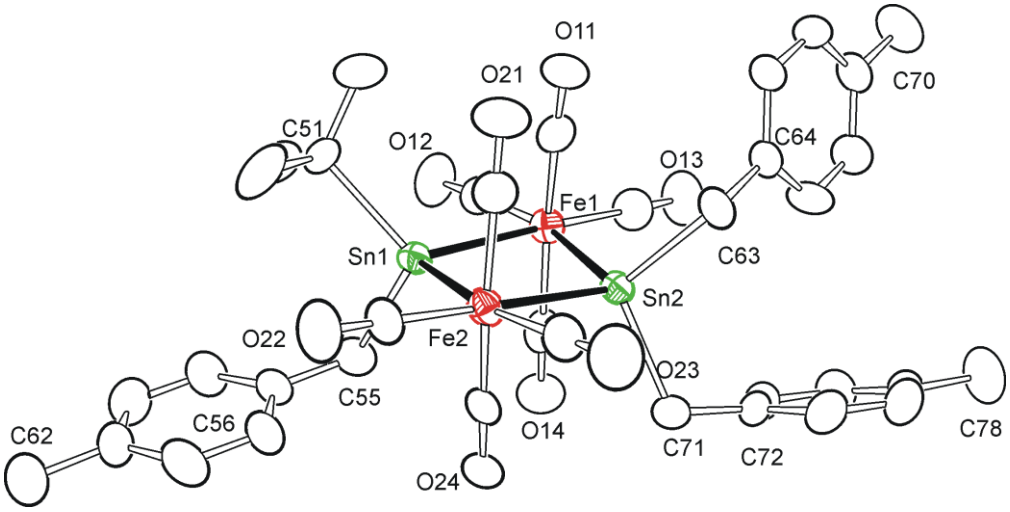

Figure D.7 The molecular structure of Fe_2[μ-SnBu^t(*p*-CH_2PhMe)][μ-Sn(*p*-CH_2PhMe)$_2$]$(CO)_8$, **5.12**.

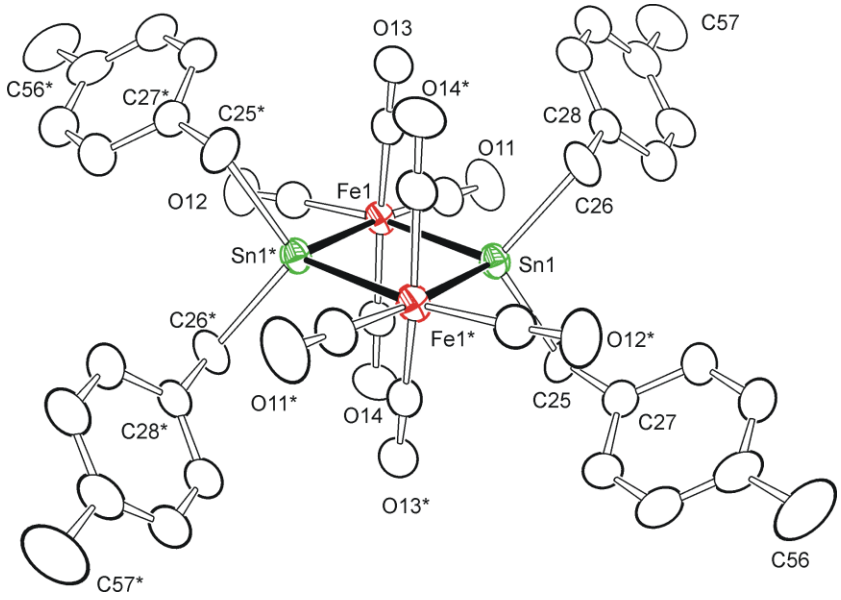

Figure D.8 The molecular structure of Fe_2[μ-Sn(*p*-CH_2PhMe)$_2$]$_2(CO)_8$, **5.13**.

Table D.1. Selected intramolecular distances and angles for compound 5.1 and 5.3[a]

(a) Distances

Compound **5.1**[*]			Compound **5.3**		
atom	atom	distance (Å)	atom	atom	distance (Å)
Fe(1)	Sn(1)	2.7216(9)	Fe(1)	Sn(1)	2.7577(7)
Fe(1)	Sn(2)	2.7156(9)	Fe(1)	Sn(2)	2.7065(7)
Fe(2)	Sn(1)	2.7074(9)	Fe(2)	Sn(1)	2.7736(7)
Fe(2)	Sn(2)	2.7288(9)	Fe(2)	Sn(2)	2.6986(7)
Fe(3)	Sn(3)	2.7248(10)	Fe(3)	Sn(1)	2.7513(6)
Fe(3)	Sn(4)	2.7207(10)	Fe(3)	Sn(3)	2.6951(7)
Fe(4)	Sn(3)	2.7236(10)	Fe(4)	Sn(1)	2.7801(7)
Fe(4)	Sn(4)	2.7106(9)	Fe(4)	Sn(3)	2.6990(7)

(b) Angles

Compound **5.1**				Compound **5.3**			
atom	atom	atom	angle (deg)	atom	atom	atom	angle (deg)
Fe(1)	Sn(2)	Fe(2)	101.79(3)	Fe(1)	Sn(1)	Fe(2)	96.78(2)
Fe(2)	Sn(1)	Fe(1)	102.19(3)	Fe(1)	Sn(1)	Fe(4)	116.53(2)
Sn(2)	Fe(1)	Sn(1)	77.37(2)	Fe(1)	Sn(2)	Fe(4)	116.15(2)
Sn(1)	Fe(2)	Sn(2)	77.38(2)	Fe(2)	Sn(2)	Fe(1)	99.84(2)
Fe(4)	Sn(3)	Fe(3)	99.31(3)	Fe(3)	Sn(1)	Fe(4)	97.00(2)
Fe(4)	Sn(4)	Fe(3)	99.73(3)	Fe(3)	Sn(1)	Fe(1)	116.08(2)
Sn(4)	Fe(3)	Sn(3)	80.21(3)	Fe(3)	Sn(1)	Fe(2)	116.15(2)
Sn(4)	Fe(4)	Sn(3)	80.41(3)	Fe(3)	Sn(3)	Fe(4)	100.35(2)
				Fe(2)	Sn(1)	Fe(4)	115.65 (2)
				Sn(2)	Fe(2)	Sn(1)	81.604(19)
				Sn(3)	Fe(3)	Sn(1)	81.612(18)
				Sn(2)	Fe(1)	Sn(1)	81.754(19)
				Sn(3)	Fe(4)	Sn(1)	81.016(18)

[a] Estimated standard deviations in the least significant figure are given in parentheses

*Compound **5.1** crystallizes as two molecules. Fe1,Fe2 and Sn1 Sn2 correspond to molecule 1. Fe3, Fe4, and Sn3, Sn4 correspond to molecule 2.

Table D.2. Selected intramolecular bond angles for compounds 5.8 and 5.9.[a]

Angles							
Compound **5.8**				Compound **5.9**			
atom	atom	atom	angle (deg)	atom	atom	atom	angle (deg)
C(21)	Sn(1)	C(29)	108.1(2)	C(31)	Sn(1)	C(39)	106.4(2)
C(21)	Sn(1)	Fe(1)	112.8(2)	C(31)	Sn(1)	Fe(1)	113.35(19)
C(29)	Sn(1)	Fe(1)	116.91(17)	C(39)	Sn(1)	Fe(1)	115.04(2)
Fe(1)	Sn(1)	Fe(1)	101.89(2)	Fe(1)	Sn(1)	Fe(2)	101.29(3)
				C(51)	Sn(2)	Fe(2)	114.13(18)

Table D.3. Selected intramolecular bond angles for compounds 5.11 and 5.12.[a]

Angles							
Compound **5.11**				Compound **5.12**			
atom	atom	atom	angle (deg)	atom	atom	atom	angle (deg)
C(15)	Sn(1)	C(23)	103.9(3)	C(55)	Sn(1)	C(51)	105.3(3)
C(15)	Sn(1)	Fe(1)	113.5(3)	C(55)	Sn(1)	Fe(2)	113.46(3)
C(23)	Sn(1)	Fe(1)	116.3(217)	C(71)	Sn(2)	Fe(2)	106.00(18)
Fe(1)	Sn(1)	Fe(1)	100.37(3)	Fe(1)	Sn(1)	Fe(2)	101.29(3)
				C(63)	Sn(2)	C(71)	106.5(3)

[a] Estimated standard deviations in the least significant figure are given in parentheses

Table D.4. Crystallographic Data for Compounds 5.1 and 5.3.

Compound	**5.1**	**5.3**
Empirical formula	$Fe_2Sn_2O_8C_{24}H_{36}$	$Fe_4Sn_3O_{16}C_{32}H_{36}$
Formula weight	801.61	1256.08
Crystal system	Triclinic	Triclinic
Lattice parameters		
a (Å)	11.7046(6)	8.8256(5)
b (Å)	17.3507(9)	14.868(8)
c (Å)	17.5946(9)	17.416(9)
α (deg)	113.439(1)	105.102(8)
β (deg)	100.839(1)	90.980(9)
γ (deg)	101.634(1)	101.626(8)
V (Å^3)	3064.6(3)	2155.3(2)
Space group	$P\ \bar{1}$ (# 2)	$P\ \bar{1}$ (# 2)
Z value	4	2
ρ_{calc} (g / cm^3)	1.737	1.936
μ (Mo K_α) (mm^{-1})	2.579	3.081
Temperature (K)	296	296(2)
$2\Theta_{max}$ (°)	56.0	56.0
No. Obs. (I > 2σ(I))	11237	7403
No. Parameters	673	508
Goodness of fit GOF*	1.081	1.033
Max. shift in cycle	0.001	0.008
Residuals*: R1; wR2	0.0446, 0.1186	0.0394; 0.0885
Absorption Correction, Max/min	Multi-scan 0.7459/0.5945	Multi-scan 0.9409/0.5505
Largest peak in Final Diff. Map (e$^-$ / Å^3)	2.086	0.908

*$R = \Sigma_{hkl}(\ |\ |F_{obs}| - |F_{calc}|\ |)/\Sigma_{hkl}|F_{obs}|$; $R_w = [\Sigma_{hkl}w(|F_{obs}| - |F_{calc}|)^2/\Sigma_{hkl}wF_{obs}^2]^{1/2}$, $w = 1/\sigma^2(F_{obs})$; $GOF = [\Sigma_{hkl}w(|F_{obs}| - |F_{calc}|)^2/(n_{data} - n_{vari})]^{1/2}$.

Table D.5. Crystallographic Data for Compounds 5.4 and 5.4-d_{14}.

Compound	**5.4**	**5.4-d_{14}**
Empirical formula	$Fe_2Sn_2O_8C_{30}H_{32}$	$Fe_2Sn_2O_8C_{30}H_{18}D_{14}$
Formula weight	869.64	883.72
Crystal system	Triclinic	Orthorhombic
Lattice parameters		
a (Å)	9.0660(7)	24.3480(13)
b (Å)	12.7084(9)	15.1801(8)
c (Å)	14.9109(9)	8.9153(5)
α (deg)	89.464(1)	90
β (deg)	86.641(1)	90
γ (deg)	77.270(1)	90
V (Å^3)	1672.8(2)	3295.1(3)
Space group	$P\ \bar{1}$ (# 2)	*Ama*2 (# 40)
Z value	2	4
ρ_{calc} (g / cm^3)	1.726	1.781
μ (Mo K_α) (mm^{-1})	2.370	2.407
Temperature (K)	296	296
$2\Theta_{max}$ (°)	52.0	56.0
No. Obs. ($I > 2\sigma(I)$)	4237	3479
No. Parameters	385	231
Goodness of fit GOF*	1.001	1.124
Max. shift in cycle	0.001	0.002
Residuals*: R1; wR2	0.0409; 0.0749	0.0392; 0.0911
Absorption Correction, Max/min	Multi-scan 0.9767/0.7641	Multi-scan 0.7460/0.5906
Largest peak in Final Diff. Map (e$^-$ / Å^3)	0.839	0.923

*$R = \Sigma_{hkl}(\ |\ |F_{obs}| - |F_{calc}|\ |)/\Sigma_{hkl}|F_{obs}|$; $R_w = [\Sigma_{hkl}w(|F_{obs}| - |F_{calc}|)^2/\Sigma_{hkl}wF_{obs}^2]^{1/2}$, $w = 1/\sigma^2(F_{obs})$; $GOF = [\Sigma_{hkl}w(|F_{obs}| - |F_{calc}|)^2/(n_{data} - n_{vari})]^{1/2}$.

Table D.6. Crystallographic Data for Compounds 5.5 and 5.6

Compound	**5.5**	**5.6**
Empirical formula	$Fe_2Sn_2O_8C_{32}H_{36}$	$Fe_2Sn_2O_8C_{36}H_{36}$
Formula weight	897.69	945.73
Crystal system	Monoclinic	Orthorhombic
Lattice parameters		
a (Å)	13.2927(14)	8.9076(2)
b (Å)	14.4216(15)	14.6422(4)
c (Å)	9.4771(10)	29.4481(8)
α (deg)	90	90
β (deg)	106.210(1)	90
γ (deg)	90	90
V (Å^3)	1744.6(3)	3840.82(17)
Space group	$P2_1/c$ (# 14)	$P2_12_12_1$ (# 19)
Z value	2	4
ρ_{calc} (g / cm^3)	1.709	1.636
μ (Mo K_α) (mm^{-1})	2.276	2.072
Temperature (K)	296	296
$2\Theta_{max}$ (°)	56.0	52.0
No. Obs. (I > 2σ(I))	2636	6978
No. Parameters	203	399
Goodness of fit GOF*	1.048	1.046
Max. shift in cycle	0.000	0.005
Residuals*: R1; wR2	0.0462, 0.1048	0.0274; 0.0678
Absorption Correction, Max/min	Multi-scan 0.9145/0.4208	Multi-scan 0.9404/0.6820
Largest peak in Final Diff. Map (e$^-$ / Å^3)	1.297	0.668

*$R = \Sigma_{hkl}(\,|\,|F_{obs}| - |F_{calc}|\,|)/\Sigma_{hkl}|F_{obs}|$; $R_w = [\Sigma_{hkl}w(|F_{obs}| - |F_{calc}|)^2/\Sigma_{hkl}wF_{obs}^2]^{1/2}$, $w = 1/\sigma^2(F_{obs})$; $GOF = [\Sigma_{hkl}w(|F_{obs}| - |F_{calc}|)^2/(n_{data} - n_{vari})]^{1/2}$.

Table D.7. Crystallographic Data for Compounds 5.7 and 5.8

Compound	**5.7**	**5.8**
Empirical formula	$Fe_2Sn_2O_8C_{40}H_{36}$	$Fe_2Sn_2O_8C_{32}H_{36}$
Formula weight	993.77	897.69
Crystal system	Triclinic	Monoclinic
Lattice parameters		
a (Å)	9.8250(5)	13.7371(12)
b (Å)	10.9039(5)	8.8685(7)
c (Å)	11.3067(6)	14.8126(12)
α (deg)	81.535(1)	90
β (deg)	67.180(1)	102.4530(10)
γ (deg)	63.534(1)	90
V (Å^3)	998.99(9)	1762.1(3)
Space group	$P\ \bar{1}$ (# 2)	$P2_1/n$ (# 14)
Z value	1	2
ρ_{calc} (g / cm^3)	1.652	1.692
μ (Mo K_α) (mm^{-1})	1.996	2.253
Temperature (K)	296	296
$2\Theta_{max}$ (°)	59.0	52.0
No. Obs. (I > 2σ(I))	4651	2413
No. Parameters	237	203
Goodness of fit GOF*	1.018	1.005
Max. shift in cycle	0.003	0.001
Residuals*: R1; wR2	0.0276; 0.0597	0.0403, 0.0957
Absorption Correction, Max/min	Multi-scan 0.9612/0.7539	Multi-scan 0.9778/0.5060
Largest peak in Final Diff. Map (e$^-$ / Å^3)	0.678	0.749

*$R = \Sigma_{hkl}(\ |\ |F_{obs}| - |F_{calc}|\ |)/\Sigma_{hkl}|F_{obs}|$; $R_w = [\Sigma_{hkl}w(|F_{obs}| - |F_{calc}|)^2/\Sigma_{hkl}wF_{obs}^2]^{1/2}$, $w = 1/\sigma^2(F_{obs})$; GOF = $[\Sigma_{hkl}w(|F_{obs}| - |F_{calc}|)^2/(n_{data} - n_{vari})]^{1/2}$.

Table D.8. Crystallographic Data for Compounds 5.9 and 5.10

Compound	**5.9**	**5.10**
Empirical formula	$Fe_2Sn_2O_8C_{36}H_{36}$	$Fe_2Sn_2O_8C_{40}H_{36}$
Formula weight	945.73	993.77
Crystal system	Monoclinic	Monoclinic
Lattice parameters		
a (Å)	24.1047(10)	14.9378(6)
b (Å)	8.9792(4)	9.5752(4)
c (Å)	18.0854(7)	15.3652(6)
α (deg)	90	90
β (deg)	106.3830(6)	116.114(1)
γ (deg)	90	90
V (Å^3)	3755.5(3)	1973.38(14)
Space group	$P2_1/c$ (# 14)	$P2_1/n$ (# 14)
Z value	4	2
ρ_{calc} (g / cm^3)	1.673	1.672
μ (Mo K_α) (mm^{-1})	2.119	2.021
Temperature (K)	296	296
$2\Theta_{max}$ (°)	54.0	56.0
No. Obs. ($I > 2\sigma(I)$)	6663	4073
No. Parameters	439	237
Goodness of fit GOF*	1.024	1.019
Max. shift in cycle	0.003	0.002
Residuals*: R1; wR2	0.0400; 0.1368	0.0234; 0.0547
Absorption Correction, Max/min	Multi-scan 0.8160/0.6766	Multi-scan 0.7457/0.6476
Largest peak in Final Diff. Map (e$^-$ / Å^3)	1.094	0.561

*$R = \Sigma_{hkl}(\,|\,|F_{obs}| - |F_{calc}|\,|)/\Sigma_{hkl}|F_{obs}|$; $R_w = [\Sigma_{hkl}w(|F_{obs}| - |F_{calc}|)^2/\Sigma_{hkl}wF_{obs}^2]^{1/2}$, $w = 1/\sigma^2(F_{obs})$; GOF = $[\Sigma_{hkl}w(|F_{obs}| - |F_{calc}|)^2/(n_{data} - n_{vari})]^{1/2}$.

Table D.9. Crystallographic Data for Compounds 5.11 and 5.12

Compound	**5.11**	**5.12**
Empirical formula	$Fe_2Sn_2O_8C_{32}H_{36}$	$Fe_2Sn_2O_8C_{36}H_{36}$
Formula weight	897.69	945.73
Crystal system	Monoclinic	Monoclinic
Lattice parameters		
a (Å)	13.2652(5)	9.0240(4)
b (Å)	14.7647(5)	15.0591(7)
c (Å)	9.1934(3)	28.3148(13)
α (deg)	90	90
β (deg)	96.8600(10)	90.7650(10)
γ (deg)	90	90
V (Å^3)	1787.70(11)	3847.4(3)
Space group	$P2_1/c$ (# 14)	$P2_1$ (# 4)
Z value	2	4
ρ_{calc} (g / cm^3)	1.668	1.633
μ (Mo K_α) (mm^{-1})	2.221	2.069
Temperature (K)	296	296
$2\Theta_{max}$ (°)	54.0	54.0
No. Obs. (I > 2σ(I))	3559	11057
No. Parameters	203	877
Goodness of fit GOF*	1.029	1.005
Max. shift in cycle	0.008	0.001
Residuals*: R1; wR2	0.0483, 0.2446	0.0417; 0.0643
Absorption Correction, Max/min	Multi-scan 0.8971/0.4703	Multi-scan 0.9598/0.7467
Largest peak in Final Diff. Map (e$^-$ / Å^3)	0.749	0.672

*$R = \Sigma_{hkl}(\,|\,|F_{obs}| - |F_{calc}|\,|)/\Sigma_{hkl}|F_{obs}|$; $R_w = [\Sigma_{hkl}w(|F_{obs}| - |F_{calc}|)^2/\Sigma_{hkl}wF_{obs}^2]^{1/2}$, $w = 1/\sigma^2(F_{obs})$; GOF = $[\Sigma_{hkl}w(|F_{obs}| - |F_{calc}|)^2/(n_{data} - n_{vari})]^{1/2}$.

Table D.10. Crystallographic Data for Compounds 5.13 and 5.14

Compound	**5.13**	**5.14**
Empirical formula	$Fe_2Sn_2O_8C_{40}H_{36}$	$Fe_2Sn_2O_8C_{38}H_{42}$
Formula weight	993.77	975.80
Crystal system	Triclinic	Monoclinic
Lattice parameters		
a (Å)	9.0360(5)	12.1335(9)
b (Å)	12.1270(6)	10.0909(8)
c (Å)	20.1824(11)	16.7340(13)
α (deg)	104.2530(8)	90
β (deg)	96.1440(9)	104.4770(10)
γ (deg)	104.3040(8)	90
V ($Å^3$)	2043.61(19)	1983.8(3)
Space group	$P\bar{1}$ (# 2)	$P2_1/c$ (# 14)
Z value	2	2
ρ_{calc} (g / cm^3)	1.615	1.634
μ (Mo K_α) (mm^{-1})	1.952	2.009
Temperature (K)	296	296
$2\Theta_{max}$ (°)	52	52.0
No. Obs. ($I > 2\sigma(I)$)	6330	2613
No. Parameters	473	215
Goodness of fit GOF*	1.036	1.041
Max. shift in cycle	0.004	0.000
Residuals*: R1; wR2	0.0284; 0.0619	0.0416, 0.0762
Absorption Correction, Max/min	Multi-scan 0.9807/0.5921	Multi-scan 0.9802 / 0.6336
Largest peak in Final Diff. Map (e^- / $Å^3$)	0.476	0.742

*$R = \Sigma_{hkl}(\,|\,|F_{obs}| - |F_{calc}|\,|)/\Sigma_{hkl}|F_{obs}|$; $R_w = [\Sigma_{hkl}w(|F_{obs}| - |F_{calc}|)^2/\Sigma_{hkl}wF_{obs}^2]^{1/2}$, $w = 1/\sigma^2(F_{obs})$; $GOF = [\Sigma_{hkl}w(|F_{obs}| - |F_{calc}|)^2/(n_{data} - n_{vari})]^{1/2}$.

Appendix E: Supporting information for chapter 6

Table E.1. Selected intramolecular distances and angles for compound 6.4[a]

(a) Distances

atom	atom	distance (Å)	atom	atom	distance (Å)
Ni(1)	C(1)	1.9409(16)	Fe(1)	C(1)	1.8524(16)
Ni(1)	Fe(1)	2.5430(3)	Fe(2)	Fe(3)	2.7472 (3)
Ni(1)	Fe(3)	2.5315(3)	Fe(2)	C(1)	1.8921(18)
Ni(1)	Fe(4)	2.4500(3)	Fe(3)	Fe(4)	2.6574 (3)
Fe(1)	Fe(2)	2.6923 (4)	Fe(3)	C(1)	1.8513 (16)
Fe(1)	Fe(4)	2.6301(3)	Fe(4)	C(1)	1.9041 (18)

(b) Angles

atom	atom	atom	angle (deg)	atom	atom	atom	angle (deg)
C(1)	Ni(1)	Fe(4)	49.76(5)	Fe(3)	C(1)	Fe(4)	90.07(7)
C(1)	Ni(1)	Fe(3)	46.63(5)	Fe(1)	C(1)	Fe(4)	88.86 (8)
C(1)	Ni(1)	Fe(1)	46.44(5)	Fe(2)	C(1)	Fe(4)	153.47(9)
Fe(4)	Ni(1)	Fe(1)	63.541(10)	Fe(3)	C(1)	Ni(1)	83.72(6)
Fe(3)	Ni(1)	Fe(1)	93.063(10)	Fe(1)	C(1)	Ni(1)	84.16(7)
Fe(3)	C(1)	Fe(1)	167.82(10)	Fe(2)	C(1)	Ni(1)	127.30(8)
Fe(3)	C(1)	Fe(2)	94.42 (8)	Fe(4)	C(1)	Ni(1)	79.16(7)
Fe(1)	C(1)	Fe(2)	91.94(7)	Fe(1)	Fe(2)	Fe(3)	85.222(10)

[a] Estimated standard deviations in the least significant figure are given in parentheses.

Table E.2. Selected intramolecular distances and angles for compound 6.5.[a]

(a) Distances

atom	atom	distance (Å)	atom	atom	distance (Å)
Fe(1)	Fe(2)	2.5455(4)	Fe(3)	Fe(5)	2.6396(4)
Fe(1)	Fe(3)	2.5504(4)	Fe(1)	C(1)	1.9651(17)
Fe(1)	Fe(4)	2.5542(4)	Fe(2)	C(1)	1.8965(17)
Fe(1)	Fe(5)	2.5560(4)	Fe(3)	C(1)	1.8987(17)
Fe(2)	Fe(4)	2.6171(4)	Fe(4)	C(1)	1.8435(18)
Fe(2)	Fe(5)	2.6162(4)	Fe(5)	C(1)	1.8405(18)
Fe(3)	Fe(4)	2.6362(4)			

(b) Angles

atom	atom	atom	angle (deg)	atom	atom	atom	angle (deg)
Fe(2)	Fe(1)	Fe(3)	95.193(12)	Fe(1)	Fe(5)	Fe(2)	58.951(10)
Fe(2)	Fe(1)	Fe(4)	61.753(11)	Fe(2)	Fe(5)	Fe(3)	91.443(12)
Fe(3)	Fe(1)	Fe(4)	62.187(12)	Fe(5)	C(1)	Fe(4)	168.45(10)
Fe(2)	Fe(1)	Fe(5)	61.705(11)	Fe(5)	C(1)	Fe(2)	88.85(7)
Fe(3)	Fe(1)	Fe(5)	62.250(11)	Fe(4)	C(1)	Fe(2)	88.80(8)
Fe(4)	Fe(1)	Fe(5)	91.659(12)	Fe(5)	C(1)	Fe(3)	89.79(8)
Fe(1)	Fe(2)	Fe(5)	59.344(11)	Fe(4)	C(1)	Fe(3)	89.56(7)
Fe(1)	Fe(2)	Fe(4)	59.285(10)	Fe(2)	C(1)	Fe(3)	165.05(10)
Fe(5)	Fe(2)	Fe(4)	88.915(12)	Fe(5)	C(1)	Fe(1)	84.32(7)
Fe(1)	Fe(3)	Fe(4)	58.976(11)	Fe(4)	C(1)	Fe(1)	84.17(7)
Fe(1)	Fe(3)	Fe(5)	58.978(10)	Fe(2)	C(1)	Fe(1)	82.46(7)
Fe(4)	Fe(3)	Fe(5)	88.016(12)	Fe(3)	C(1)	Fe(1)	82.59(7)
Fe(1)	Fe(4)	Fe(2)	58.962(10)				

[a] Estimated standard deviations in the least significant figure are given in parentheses.

Table E.3. Crystallographic Data for Compounds 6.4 and 6.5.

	6.4	**6.5**
Empirical formula	$NiFe_4O_{10}C_{21}H_{10}$	$Fe_5O_{10}C_{21}H_{10}$
Formula weight	704.40	701.54
Crystal system	Orthorhombic	Monoclinic
Lattice parameters		
a (Å)	9.9929(3)	31.8807(15)
b (Å)	13.8977(5)	9.8885(5)
c (Å)	17.3550(6)	15.3738(7)
β (deg)	90	106.886(1)
V (Å^3)	2410.23(14)	4637.7(4)
Space group	$P2_12_12_1$ (# 19)	$C2/c$ (# 15)
Z value	4	8
ρ_{calc} (g / cm^3)	1.941	2.010
μ (Mo Kα) (mm^{-1})	3.170	3.109
Temperature (K)	294	294
$2\Theta_{max}$ (°)	56.0	62.94
No. Obs. (I > 2σ(I))	5606	5635
No. Parameters	325	325
Goodness of fit	1.093	1.044
Max. shift in cycle	0.002	0.001
Residuals*:R1; wR2	0.0182; 0.0466	0.0333; 0.0782
Absorption Correction, Max/min	Multi-scan 0.3637/0.2521	Multi-scan 0.7463/0.3694
Largest peak in Final Diff. Map (e$^-$ / Å^3)	0.373	0.458

*$R = \Sigma_{hkl}(\,|\,|F_{obs}|-|F_{calc}|\,|)/\Sigma_{hkl}|F_{obs}|$; $R_w = [\Sigma_{hkl}w(|F_{obs}|-|F_{calc}|)^2/\Sigma_{hkl}wF_{obs}^2]^{1/2}$, $w = 1/\sigma^2(F_{obs})$; $GOF = [\Sigma_{hkl}w(|F_{obs}|-|F_{calc}|)^2/(n_{data} - n_{vari})]^{1/2}$.

Table E.4. Crystallographic Data for Compound 6.8.

Compound	**6.8**
Empirical formula	$NiSn_2O_3C_{27}H_{54}$
Formula weight	722.79
Crystal system	Monoclinic
Lattice parameters	
a (Å)	9.0869(4)
b (Å)	14.8041(7)
c (Å)	25.2267(12)
β (°)	93.8980(10)
V (Å^3)	3385.7(3)
Space group	$P2_1/c$ (#14)
Z value	4
ρ_{calc} (g / cm^3)	1.418
μ (Mo Kα) (mm^{-1})	2.036
Temperature (K)	296
$2\Theta_{max}$ (°)	54.14
No. Obs. ($I > 2\sigma(I)$)	6170
No. Parameters	316
Goodness of fit	1.021
Max. shift in cycle	0.002
Residuals*:R1; wR2	0.0232; 0.0518
Absorption Correction, Max/min	Multi-scan 0.7365/0.4965
Largest peak in Final Diff. Map (e$^-$ / Å^3)	0.389

*$R = \Sigma_{hkl}(\,|\,|F_{obs}|-|F_{calc}|\,|\,)/\Sigma_{hkl}|F_{obs}|$; $R_w = [\Sigma_{hkl}w(|F_{obs}|-|F_{calc}|)^2/\Sigma_{hkl}wF_{obs}^2]^{1/2}$, $w = 1/\sigma^2(F_{obs})$; $GOF = [\Sigma_{hkl}w(|F_{obs}|-|F_{calc}|)^2/(n_{data} - n_{vari})]^{1/}$

References

(1) Aki, H.; Taniguchi, Y.; Tamura, I.; Kegasa, A.; Hayakawa, H.; Ishikawa, Y.; Yamamoto, S.; Sugimoto, I. *Int. J. Hydrogen Energy* **2012**, *37*, 1204.

(2) Roman, H. T. *Technology & Engineering Teacher* **2012**, *71*, 30.

(3) Wang, Y.; Chen, K. S.; Mishler, J.; Cho, S. C.; Adroher, X. C. *Applied Energy* **2011**, *88*, 981.

(4) Korol'kov, D. V. *Russ. J. Gen. Chem* **2002**, *72*, 523.

(5) Klooster, W. T.; Koetzle, T. F. *J. Am. Chem. Soc.* **1994**, *116*, 7677.

(6) Koetzle, T.; Schultz, A. *Top. Catal.* **2005**, *32*, 251.

(7) Kubas, G. J. *J. Organomet. Chem.* **2009**, *694*, 2648.

(8) Kubas, G. J. *Science* **2006**, *314*, 1096.

(9) Adams, R. D.; Captain, B. *Angew. Chem. Int. Ed.* **2008**, *47*, 252.

(10) Xiao, J.; Kristof, E.; Vittal, J. J.; Puddephatt, R. J. *J. Organomet. Chem.* **1995**, *490*, 1.

(11) Church, M. J.; Mays, M. J.; Simpson, R. N. F.; Stefanini, F. P. *J. Chem. Soc. (A)* **1970**, 2909.

(12) Lee, J. C.; Peris, E.; Rheingold, A. L.; Crabtree, R. H. *J. Am. Chem. Soc.* **1994**, *116*, 11014.

(13) Weller, A. S.; McIndoe, J. S. *Eur. J. Inorg. Chem.* **2007**, *2007*, 4411.

(14) Otsuka, S.; Yoshida, T.; Matsumoto, M.; Nakatsu, K. *J. Am. Chem. Soc.* **1976**, *98*, 5850.

(15) Gandolfi, C.; Heckenroth, M.; Neels, A.; Laurenczy, G. b.; Albrecht, M. *Organometallics* **2009**, *28*, 5112.

(16) Samantaray, M. K.; Shaikh, M. M.; Ghosh, P. *Organometallics* **2009**, *28*, 2267.

(17) Zenkina, O. V.; Keske, E. C.; Wang, R.; Crudden, C. M. *Organometallics* **2011**, *30*, 6423.

(18) Jia, G.; Meek, D. W. *Inorg. Chem.* **1991**, *30*, 1953.

(19) Arnold, P. L.; Cloke, F. G. N.; Geldbach, T.; Hitchcock, P. B. *Organometallics* **1999**, *18*, 3228.

(20) Turculet, L.; Feldman, J. D.; Tilley, T. D. *Organometallics* **2003**, *22*, 4627.

(21) Butts, M. D.; Bryan, J. C.; Luo, X.-L.; Kubas, G. J. *Inorg. Chem.* **1997**, *36*, 3341.

(22) Rybtchinski, B.; Milstein, D. I. *ACS Symp. Ser*: **2004**; *vol 885*, p 70.

(23) Canepa, G.; Brandt, C. D.; Werner, H. *Organometallics* **2004**, *23*, 1140.

(24) M. Jensen, C. *Chem. Commun.* **1999**, 2443.

(25) Lau, C. P.; Ng, S. M.; Jia, G.; Lin, Z. *Coord. Chem. Rev.* **2007**, *251*, 2223.

(26) King, W. A.; Luo, X.-L.; Scott, B. L.; Kubas, G. J.; Zilm, K. W. *J. Am. Chem. Soc.* **1996**, *118*, 6782.

(27) Evrard, D.; Groison, K.; Mugnier, Y.; Harvey, P. D. *Inorg. Chem.* **2003**, *43*, 790.

(28) Matteoli, U.; Beghetto, V.; Scrivanti, A. *J. Mol. Catal. A: Chem.* **1996**, *109*, 45.

(29) Kubas, G. J.; Unkefer, C. J.; Swanson, B. I.; Fukushima, E. *J. Am. Chem. Soc.* **1986**, *108*, 7000.

(30) Kubas, G. J.; Ryan, R. R.; Swanson, B. I.; Vergamini, P. J.; Wasserman, H. J. *J. Am. Chem. Soc.* **1984**, *106*, 451.

(31) Kubas, G. J. *J. Chem. Soc., Chem. Commun.* **1980**, 61.

(32) Adams, R. D.; Captain, B.; Smith, M. D.; Beddie, C.; Hall, M. B. *J. Am. Chem. Soc.* **2007**, *129*, 5981.

(33) Cai, X.; Majumdar, S.; Fortman, G. C.; Cazin, C. S. J.; Slawin, A. M. Z.; Lhermitte, C.; Prabhakar, R.; Germain, M. E.; Palluccio, T.; Nolan, S. P.; Rybak-Akimova, E. V.; Temprado, M.; Captain, B.; Hoff, C. D. *J. Am. Chem. Soc.* **2011**, *133*, 1290.

(34) Polezhaev, A.; Kuklin, S.; Ivanov, D.; Petrovskii, P.; Dolgushin, F.; Ezernitskaya, M.; Koridze, A. *Russ. Chem. Bull.* **2009**, *58*, 1847.

(35) Suresh, C. H.; Koga, N. *Inorg. Chem.* **2002**, *41*, 1573.

(36) Fernández-Pérez, H. c.; Etayo, P.; Panossian, A.; Vidal-Ferran, A. *Chem. Rev.* **2011**, *111*, 2119.

(37) Gan, W.; Fellay, C.; Dyson, P. J.; Laurenczy, G. *J. Coord. Chem.* **2010**, *63*, 2685.

(38) Dutta, D. K.; Deb, B.; Hua, G.; Woollins, J. D. *J. Mol. Catal. A: Chem.* **2012**, *353-354*, 7.

(39) William, M. A.; Isil, K. H.; Qi, W.; Anatoly, I. F.; Long, L.; Judith, C. Y.; Laurent, D. M.; Ralph, G. N.; Saim, O. z.; Kuang-Hway, Y.; Kimberly, A. J.; Richard, G. F. *Langmuir* **2011**, *27*, 6279.

(40) JuÌˆrgen, K.; Robert, G. B. *Organometallics* **2010**, *29*, 5946.

(41) Adams, R. D.; Trufan, E. *Proc. R. Soc. A* **2010**, *368*, 1473.

(42) Holt, M. S.; Wilson, W. L.; Nelson, J. H. *Chem. Rev.* **1989**, *89*, 11.

(43) Otera, J. *Acc. Chem. Res.* **2004**, *37*, 288.

(44) Steliou, K.; Poupart, M. A. *J. Am. Chem. Soc.* **1983**, *105*, 7130.

(45) Major, R.; Bonarski, J.; Morgiel, J.; Major, B.; Czarnowska, E.; Kustosz, R.; Lackner, J. M.; Waldhauser, W. *Surf. Coat. Technol.* **2006**, *200*, 6340.

(46) Jin-Sang, H.; Myeong-Hwan, K.; Dong-Sung, S.; Jong-Woo, W.; Doo-Kyung, M.; Dong-Pyo, K. *Mol. Cryst. Liq. Cryst. Sci. Technol., Sec. A* **2009**, *514*, 302.

(47) Gaina, C.; Gaina, V.; Cristea, M. *J. Inorg. Organomet. Polym.* **2009**, *19*, 157.

(48) Chernov, O. V.; Smirnov, A. Y.; Portnyagin, I. A.; Khrustalev, V. N.; Nechaev, M. S. *J. Organomet. Chem.* **2009**, *694*, 3184.

(49) Cotton, J. D.; Davidson, P. J.; Lappert, M. F. *J. Chem. Soc., Dalton Trans.* **1976**, 2275.

(50) Esteruelas, M. A.; Lledós, A.; Maresca, O.; Oliván, M.; Oñate, E.; Tajada, M. A. *Organometallics* **2004**, *23*, 1453.

(51) Jetz, W.; Simons, P. B.; Thompson, J. A. J.; Graham, W. A. G. *Inorg. Chem.* **1966**, *5*, 2217.

(52) Creemers, H. M. J. C.; Verbeek, F.; Noltes, J. G. *J. Organomet. Chem.* **1968**, *15*, 125.

(53) Moss, J. R.; Graham, W. A. G. *J. Organomet. Chem.* **1969**, *18*, 24.

(54) Cloke, F. G. N.; Cox, K. P.; Green, M. L. H.; Bashkin, J.; Prout, K. *J. Chem. Soc., Chem. Commun.* **1981**, 117.

(55) Elder, M.; Hall, D. *Inorg. Chem.* **1969**, *8*, 1268.

(56) Johnson, B. F. G.; Raynor, S. A.; Brown, D. B.; Shephard, D. S.; Mashmeyer, T.; Thomas, J. M.; Hermans, S.; Raja, R.; Sankar, G. *J. Mol. Catal. A: Chem.* **2002**, *182–183*, 89.

(57) Alexeev, O. S.; Gates, B. C. *Ind. Eng. Chem. Res.* **2002**, *42*, 1571.

(58) Hungria, A. B.; Raja, R.; Adams, R. D.; Captain, B.; Thomas, J. M.; Midgley, P. A.; Golovko, V.; Johnson, B. F. G. *Angew. Chem. Int. Ed.* **2006**, *45*, 4782.

(59) Lefebvre, F.; Candy, J. P.; Santini, C.; Basset, J. M. *Top. Catal.* **1997**, *4*, 211.

(60) Thomas, J. M.; Raja, R.; Sankar, G.; Johnson, B. F. G.; Lewis, D. W. *Chem. Eur. J.* **2001**, *7*, 2972.

(61) Thomas, J. M.; Johnson, B. F. G.; Raja, R.; Sankar, G.; Midgley, P. A. *Acc. Chem. Res.* **2002**, *36*, 20.

(62) Raja, R.; Khimyak, T.; Thomas, J. M.; Hermans, S.; Johnson, B. F. G. *Angew. Chem. Int. Ed.* **2001**, *40*, 4638.

(63) Oldroyd, R. D.; Sankar, G.; Thomas, J. M.; Özkaya, D. *J. Phys. Chem. B* **1998**, *102*, 1849.

(64) Uffalussy, K. J.; Captain, B. K.; Adams, R. D.; Hungria, A. B.; Monnier, J. R.; Amiridis, M. D. *ACS Catalysis* **2011**, *1*, 1710.

(65) Ayastuy, J. L.; González-Marcos, M. P.; Gutiérrez-Ortiz, M. A. *Catal. Commun.* **2011**, *12*, 895.

(66) Aykaç, H.; Yilmaz, S. *Turk. J. Chem.* **2008**, *32*, 653.

(67) Corro, G.; Fierro, J. L. G.; Montiel, R.; Bañuelos, F. *J. Mol. Catal. A: Chem.* **2005**, *228*, 275.

(68) Håkonsen, S. F.; Walmsley, J. C.; Holmen, A. *Appl. Catal., A* **2010**, *378*, 1.

(69) Vu, B. K.; Song, M. B.; Ahn, I. Y.; Suh, Y.-W.; Suh, D. J.; Kim, W.-I. L.; Koh, H.-L.; Choi, Y. G.; Shin, E. W. *Catal. Today* **2011**, *164*, 214.

(70) Adams, R. W.; Batley, G. E.; Bailar, J. C. *J. Am. Chem. Soc.* **1968**, *90*, 6051.

(71) Frankel, E.; Emken, E.; Itatani, H.; Bailar, J. J. *J. Org. Chem.* **1967**, *32*, 1447.

(72) Llorca, J.; de la Piscina, P. R.; Fierro, J.-L. G.; Sales, J.; Homs, N. *J. Mol. Catal. A: Chem.* **1997**, *118*, 101.

(73) Llorca, J.; de la Piscina, P. R.; Sales, J.; Homs, N. *Chem. Commun.* **1994**, 2555.

(74) Tayal, J.; Rawat, B.; Basu, S. *Int. J. Hydrogen Energy* **2011**, *36*, 14884.

(75) Xizhang, W.; Hua, X.; Lijun, Y.; Huakai, W.; Pengyuan, Z.; Xintai, Q.; Yangnian, W.; Yanwen, M.; Qiang Wu, a.; Zheng, H. *Nanotechnology* **2011**, *22*, 395401.

(76) Shukla, A. K.; Aricò, A. S.; El-Khatib, K. M.; Kim, H.; Antonucci, P. L.; Antonucci, V. *Appl. Surf. Sci.* **1999**, *137*, 20.

(77) Anderson, G. K.; Clark, H. C.; Davies, J. A. *Inorg. Chem.* **1983**, *22*, 427.

(78) Anderson, G. K.; Billard, C.; Clark, H. C.; Davies, J. A.; Wong, C. S. *Inorg. Chem.* **1983**, *22*, 439.

(79) Zabula, A. V.; Pape, T.; Hepp, A.; Hahn, F. E. *Dalton Trans.* **2008**, 5886.

(80) Hu, J. J.; Li, F.; Hor, T. S. A. *Organometallics* **2009**, *28*, 1212.

(81) Forniés, J.; García, A.; Gómez, J.; Lalinde, E.; Moreno, M. T. *Organometallics* **2002**, *21*, 3733.

(82) Krevor, J. V. Z.; Yee, L. *Inorg. Chem.* **1990**, *29*, 4305.

(83) Clark, H. C.; Itoh, K. *Inorg. Chem.* **1971**, *10*, 1707.

(84) Akhtar, M.; Clark, H. C. *J. Organomet. Chem.* **1970**, *22*, 227.

(85) Clemmit, A. F.; Glockling, F. *J. Chem. Soc. (A)* **1971**, 1164.

(86) Eaborn, C.; Pidcock, A.; Steele, B. R. *J. Chem. Soc., Dalton Trans* **1975**, 809.

(87) Al-Allaf, T. A. K. *J. Organomet. Chem.* **1999**, *590*, 25.

(88) White, C. P.; Braddock-Wilking, J.; Corey, J. Y.; Xu, H.; Redekop, E.; Sedinkin, S.; Rath, N. P. *Organometallics* **2007**, *26*, 1996.

(89) Campbell, G. K.; Hitchcock, P. B.; Lappert, M. F.; Misra, M. C. *J. Organomet. Chem.* **1985**, *289*, c1.

(90) Al-Allaf, T. A. K.; Eaborn, C.; Hitchcock, P. B.; Lappert, M. F.; Pidcock, A. *J. Chem. Soc., Chem. Commun.* **1985**, 548.

(91) Ceriotti, A.; Daghetta, M.; El Afefey, S.; Ienco, A.; Longoni, G.; Manca, G.; Mealli, C.; Zacchini, S.; Zarra, S. *Inorg. Chem.* **2011**, *50*, 12553.

(92) Lappert, M. F.; Rowe, R. S. *Coord. Chem. Rev.* **1990**, *100*, 267.

(93) Adams, R. D.; Captain, B.; Zhu, L. *Inorg. Chem.* **2007**, *46*, 4605.

(94) Adams, R. D.; Captain, B.; Hall, M. B.; Trufan, E.; Yang, X. *J. Am. Chem. Soc.* **2007**, *129*, 12328.

(95) Adams, R. D.; Captain, B.; Zhu, L. *Inorg. Chem.* **2005**, *45*, 430.

(96) Manzoli, M.; Shetti, V. N.; Blaine, J. A. L.; Zhu, L.; Isrow, D.; Yempally, V.; Captain, B.; Coluccia, S.; Raja, R.; Gianotti, E. *Dalton Trans.* **2012**, *41*, 982.

(97) Jäkle, F.; Rulkens, R.; Zech, G.; Foucher, D. A.; Lough, A. J.; Manners, I. *Chem. Eur. J.* **1998**, *4*, 2117.

(98) Baratta, W.; Stoccoro, S.; Doppiu, A.; Herdtweck, E.; Zucca, A.; Rigo, P. *Angew. Chem. Int. Ed.* **2003**, *42*, 105.

(99) Hackett, M.; Whitesides, G. M. *J. Am. Chem. Soc.* **1988**, *110*, 1449.

(100) Hackett, M.; Ibers, J. A.; Jernakoff, P.; Whitesides, G. M. *J. Am. Chem. Soc.* **1986**, *108*, 8094.

(101) Adams, R. D.; Trufan, E. *Inorg. Chem.* **2009**, *48*, 6124.

(102) Bertsch, S.; Braunschweig, H.; Forster, M.; Gruss, K.; Radacki, K. *Inorg. Chem.* **2011**, *50*, 1816.

(103) Calabrese, J. C.; Dahl, L. F.; Cavalieri, A.; Chini, P.; Longoni, G.; Martinengo, S. *J. Am. Chem. Soc.* **1974**, *96*, 2616.

(104) Cittadini, V.; Leoni, P.; Marchetti, L.; Pasquali, M.; Albinati, A. *Inorg. Chim. Acta* **2002**, *330*, 25.

(105) Zhu, L.; Yempally, V.; Isrow, D.; Pellechia, P. J.; Captain, B. *J. Organomet. Chem.* **2010**, *695*, 1.

(106) Nakazawa, H. *J. Organomet. Chem.* **2000**, *611*, 349.

(107) Levy, C. J.; Puddephatt, R. J. *Organometallics* **1997**, *16*, 4115.

(108) Bercaw, J. E.; Chen, G. S.; Labinger, J. A.; Lin, B.-L. *J. Am. Chem. Soc.* **2008**, *130*, 17654.

(109) Chen, G. S.; Labinger, J. A.; Bercaw, J. E. *PNAS* **2007**, *104*, 6915.

(110) Adams, R. D.; Blom, D. A.; Captain, B.; Raja, R.; Thomas, J. M.; Trufan, E. *Langmuir* **2008**, *24*, 9223.

(111) Yamada, T.; Tanabe, M.; Osakada, K.; Kim, Y.-J. *Organometallics* **2004**, *23*, 4771.

(112) Grundy, K. R.; Robertson, K. N. *Organometallics* **1983**, *2*, 1736.

(113) Puddephatt, R. J.; Rashidi, M.; Vittal, J. J. *J. Chem. Soc., Dalton Trans.* **1991**, 2835.

(114) Paula, P.; Thomas, K.; Arthur, S. *In Techniques in Inorganic Chemistry*; CRC Press: **2010**, p 53.

(115) Spencer, J. L.; Ittel, S. D.; Cushing, M. A. *Inorg. Synth.*; John Wiley & Sons, Inc.: **2007**, p 213.

(116) Tatsuno, Y.; Yoshida, T.; Seiotsuka; Al-Salem, N.; Shaw, B. L. *Inorg. Synth.*; John Wiley & Sons, Inc.: 2007, p 220.

(117) Apex 2 Version 2.2-0 and SAINT+ Version 7.46 A; Bruker Analytical X-Ray Systems, Inc., Madison, Wisconsin, USA, **2007**.

(118) Sherdick, G. M.; SHELXTL Version 6.1; Bruker Analytical X-Ray Systems, Inc., Madison, Wisconsin, USA, **2000**.

(119) Arduengo, A. J.; Harlow, R. L.; Kline, M. *J. Am. Chem. Soc.* **1991**, *113*, 361.

(120) Herrmann, W. A. *Angew. Chem. Int. Ed.* **2002**, *41*, 1290.

(121) Dorta, R.; Stevens, E. D.; Hoff, C. D.; Nolan, S. P. *J. Am. Chem. Soc.* **2003**, *125*, 10490.

(122) Naziruddin, A. R.; Hepp, A.; Pape, T.; Hahn, F. E. *Organometallics* **2011**, *30*, 5859.

(123) Viciu, M. S.; Germaneau, R. F.; Nolan, S. P. *Org. Lett.* **2002**, *4*, 4053.

(124) Grubbs, R. H. *Org. Process Res. Dev.* **2003**, *8*, 294.

(125) Chatterjee, A. K.; Grubbs, R. H. *Org. Lett.* **1999**, *1*, 1751.

(126) Keitz, B. K.; Bouffard, J.; Bertrand, G.; Grubbs, R. H. *J. Am. Chem. Soc.* **2011**, *133*, 11006.

(127) Clavier, H.; Urbina-Blanco, C. s. A.; Nolan, S. P. *Organometallics* **2009**, *28*, 2848.

(128) Huang, J.; Schanz, H.-J.; Stevens, E. D.; Nolan, S. P. *Organometallics* **1999**, *18*, 5375.

(129) Jafarpour, L.; Nolan, S. P. *Organometallics* **2000**, *19*, 2055.

(130) Rix, D.; Caijo, F. d.; Laurent, I.; Boeda, F.; Clavier, H.; Nolan, S. P.; Mauduit, M. *J. Org. Chem.* **2008**, *73*, 4225.

(131) Hadei, N.; Kantchev, E. A. B.; O'Brie, C. J.; Organ, M. G. *J. Org. Chem.* **2005**, *70*, 8503.

(132) Hadei, N.; Kantchev, E. A. B.; O'Brie, C. J.; Organ, M. G. *Org. Lett.* **2005**, *7*, 3805.

(133) Hadei, N.; Kantchev, E. A. B.; O'Brie, C. J.; Organ, M. G. *Org. Lett.* **2005**, *7*, 1991.

(134) Lee, C. H.; Laitar, D. S.; Mueller, P.; Sadighi, J. P. *J. Am. Chem. Soc.* **2007**, *129*, 13802.

(135) Wu, J.; Faller, J. W.; Hazari, N.; Schmeier, T. J. *Organometallics* **2012**, *31*, 806.

(136) Fantasia, S.; Egbert, J. D.; Jurčík, V.; Cazin, C. S. J.; Jacobsen, H.; Cavallo, L.; Heinekey, D. M.; Nolan, S. P. *Angew. Chem. Int. Ed.* **2009**, *48*, 5182.

(137) Wu, J.; Hazari, N.; Incarvito, C. D. *Organometallics* **2011**, *30*, 3142.

(138) Markó, I. E.; Stérin, S.; Buisine, O.; Mignani, G.; Branlard, P.; Tinant, B.; Declercq, J.-P. *Science* **2002**, *298*, 204.

(139) Praetorius, J. M.; Crudden, C. M. *Dalton Trans.* **2008**, 4079.

(140) Nolan, S. P. *Acc. Chem. Res.* **2010**, *44*, 91.

(141) Marx, T., Wesemann, L., Pantenburg, I. *Z. Naturforsch.* **2003**, *58*, 147.

(142) Berthon-Gelloz, G.; de Bruin, B.; Tinant, B.; Markó, I. E. *Angew. Chem. Int. Ed.* **2009**, *48*, 3161.

(143) Zhao, S.-B.; Wang, R.-Y.; Wang, S. *Organometallics* **2009**, *28*, 2572.

(144) Veige, A. S. *Polyhedron* **2008**, *27*, 3177.

(145) Díez-González, S.; Marion, N.; Nolan, S. P. *Chem. Rev.* **2009**, *109*, 3612.

(146) Gil, W.; Trzeciak, A. M. *Coord. Chem. Rev.* **2011**, *255*, 473.

(147) Albrecht, M. *Chem. Commun.* **2008**, 3601.

(148) Yang, L.; Krüger, A.; Neels, A.; Albrecht, M. *Organometallics* **2008**, *27*, 3161.

(149) Heckenroth, M.; Kluser, E.; Neels, A.; Albrecht, M. *Angew. Chem. Int. Ed.* **2007**, *46*, 6293.

(150) Fortman, G. C.; Scott, N. M.; Linden, A.; Stevens, E. D.; Dorta, R.; Nolan, S. P. *Chem. Commun.* **2010**, *46*, 1050.

(151) Ellul, C. E.; Mahon, M. F.; Saker, O.; Whittlesey, M. K. *Angew. Chem. Int. Ed.* **2007**, *46*, 6343.

(152) Crittall, M. R.; Ellul, C. E.; Mahon, M. F.; Saker, O.; Whittlesey, M. K. *Dalton Trans.* **2008**, 4209.

(153) Bacciu, D.; Cavell, K. J.; Fallis, I. A.; Ooi, L.-l. *Angew. Chem.* **2005**, *117*, 5416.

(154) Auburn, M.; Ciriano, M.; Howard, J. A. K.; Murray, M.; Pugh, N. J.; Spencer, J. L.; Stone, F. G. A.; Woodward, P. *J. Chem. Soc., Dalton Trans.* **1980**, 659.

(155) Hall, M. B.; Fenske, R. F. *Inorg. Chem.* **1972**, *11*, 768.

(156) Hall, M. B. W., C. E.; Dykstra, C. E., Frenking, G., KIm, K.S., Scuseria, G.E., Ed.; Elsevier: Amsterdam, 2005; Vol. Chapter 40, p 1143.

(157) Manson, J., Webster, C.E., Hall, M. B. *JIMP Development version 0.1.v117* (built for Windows PC and Redhat Linux); Department of chemistry,Texas A&M University:College station,TX; http://www.chem.tamu.edu/jimp/,accessed July **2004**.

(158) Furlani, A.; Licoccia, S.; Russo, M. V.; Villa, A. C.; Guastini, C. *J. Chem. Soc., Dalton Trans.* **1982**, 2449.

(159) Darensbourg, D. J., Hyde, C. L. *J. Chem. Phys.* **1973**, *59*, 3869.

(160) Gründemann, S.; Kovacevic, A.; Albrecht, M.; Faller, J. W.; Crabtree, R. H. *J. Am. Chem. Soc.* **2002**, *124*, 10473.

(161) Nuzzo, R. G.; McCarthy, T. J.; Whitesides, G. M. *Inorg. Chem.* **1981**, *20*, 1312.

(162) Sakakura, T.; Choi, J.-C.; Yasuda, H. *Chem. Rev.* **2007**, *107*, 2365.

(163) Cokoja, M.; Bruckmeier, C.; Rieger, B.; Herrmann, W. A.; Kühn, F. E. *Angew. Chem. Int. Ed.* **2011**, *50*, 8510.

(164) Heckenroth, M.; Neels, A.; Garnier, M. G.; Aebi, P.; Ehlers, A. W.; Albrecht, M. *Chem. Eur. J.* **2009**, *15*, 9375.

(165) Chianese, A. R.; Li, X.; Janzen, M. C.; Faller, J. W.; Crabtree, R. H. *Organometallics* **2003**, *22*, 1663.

(166) Kelly Iii, R. A.; Clavier, H.; Giudice, S.; Scott, N. M.; Stevens, E. D.; Bordner, J.; Samardjiev, I.; Hoff, C. D.; Cavallo, L.; Nolan, S. P. *Organometallics* **2007**, *27*, 202.

(167) Yempally, V.; Zhu, L.; Captain, B. *Inorg. Chem.* **2010**, *49*, 7238.

(168) Johnson, B. F. G.; Lewis, J.; Nicholls, J. N.; Puga, J.; Raithby, P. R.; Rosales, M. J.; McPartlin, M.; Clegg, W. *J. Chem. Soc., Dalton Trans.* **1983**, 277.

(169) Singleton, E.; Oosthuizen, H. E.; Stone, F. G. A., Robert, W. *Adv. Organomet. Chem*., Academic Press: **1983**; *vol 22*, p 209.

(170) Keim, W.; Mastrorilli, P.; Nobile, C. F.; Ravasio, N.; Corain, B.; Zecca, M. *J. Mol. Catal.* **1993**, *81*, 167.

(171) Corain, B.; Basato, M.; Zecca, M.; Braca, G.; Galletti, A. M. R.; Lora, S.; Palma, G.; Guglielminotti, E. *J. Mol. Catal.* **1992**, *73*, 23.

(172) Giannandrea, R.; Mastrorilli, P.; Zaccaria, G.; Nobile, C. F. *J. Mol. Catal. A: Chem.* **1996**, *109*, 113.

(173) Sarapu, A. C.; Fenske, R. F. *Inorg. Chem.* **1975**, *14*, 247.

(174) Weber, L. *Angew. Chem. Int. Ed.* **1998**, *37*, 1515.

(175) Yamamoto, Y. *Coord. Chem. Rev.* **1980**, *32*, 193.

(176) Bigorgne, M. *J. Organomet. Chem.* **1963**, *1*, 101.

(177) Cotton, F. A.; Parish, R. V. *J. Chem. Soc.* **1960**, 1440.

(178) Vetter, A. J.; Rieth, R. D.; Brennessel, W. W.; Jones, W. D. *J. Am. Chem. Soc.* **2009**, *131*, 10742.

(179) Labios, L. A.; Millard, M. D.; Rheingold, A. L.; Figueroa, J. S. *J. Am. Chem. Soc.* **2009**, *131*, 11318.

(180) Emerich, B. M.; Moore, C. E.; Fox, B. J.; Rheingold, A. L.; Figueroa, J. S. *Organometallics* **2011**, *30*, 2598.

(181) Treichel, P. M.; Knebel, W. J. *Inorg. Chem.* **1972**, *11*, 1289.

(182) Tanase, T.; Yamamoto, Y.; Puddephatt, R. J. *Organometallics* **1996**, *15*, 1502.

(183) Tanase, T.; Ukaji, H.; Kudo, Y.; Ohno, M.; Kobayashi, K.; Yamamoto, Y. *Organometallics* **1994**, *13*, 1374.

(184) Crociani, B.; Boschi, T.; Belluco, U. *Inorg. Chem.* **1970**, *9*, 2021.

(185) Boehm, J. R.; Doonan, D. J.; Balch, A. L. *J. Am. Chem. Soc.* **1976**, *98*, 4845.

(186) Ros, R.; Michelin, R. A.; Carturan, G.; Belluco, U. *J. Organomet. Chem.* **1977**, *133*, 213.

(187) Marx, T.; Wesemann, L.; Dehnen, S. *Organometallics* **2000**, *19*, 4653.

(188) Marx, T.; Pantenburg, I.; Wesemann, L. *Organometallics* **2001**, *20*, 5241.

(189) Hornung, M.; Wesemann, L. *Eur. J. Inorg. Chem.* **2010**, *2010*, 2949.

(190) Crociani, B.; Boschi, T.; Nicolini, M. *Inorg. Chim. Acta* **1970**, *4*, 577.

(191) Suginome, M.; Oike, H.; Shuff, P. H.; Ito, Y. *J. Organomet. Chem.* **1996**, *521*, 405.

(192) Bonati, F.; Minghetti, G.; Boschi, T.; Crociani, B. *J. Organomet. Chem.* **1970**, *25*, 255.

(193) Schlögl, R. *Angew. Chem. Int. Ed.* **2003**, *42*, 2004.

(194) Parshall, G. W.; Ittel, S. D. *Homogeneous Catalysis: the applications and chemistry of catalysis by soluble transition metal complexes*, 2 nd ed.; Wiley: Newyork, **1992**.

(195) Nishimura, S. *Handbook of Heterogeneous Catalytic Hydrogenation for Organic Synthesis*,Wiley: Newyork, **2001**.

(196) Vaska, L.; DiLuzio, J. W. *J. Am. Chem. Soc.* **1962**, *84*, 679.

(197) Vaska, L. *Acc. Chem. Res.* **1968**, *1*, 335.

(198) Halpern, J.; Eley, P. W. S., Paul, B. W. *Advances in Catalysis*, Academic Press: **1959**, *vol* 11, p 301.

(199) Kubas, G. J. *Chem. Rev.* **2007**, *107*, 4152.

(200) Hlatky, G. G.; Crabtree, R. H. *Coord. Chem. Rev.* **1985**, *65*, 1.

(201) Borowski, A. F.; Sabo-Etienne, S.; Christ, M. L.; Donnadieu, B.; Chaudret, B. *Organometallics* **1996**, *15*, 1427.

(202) Crabtree, R. H.; Lavin, M.; Bonneviot, L. *J. Am. Chem. Soc.* **1986**, *108*, 4032.

(203) Gusev, D. G.; Notheis, J. U.; Rambo, J. R.; Hauger, B. E.; Eisenstein, O.; Caulton, K. G. *J. Am. Chem. Soc.* **1994**, *116*, 7409.

(204) Rubinstein, L. I.; Pignolet, L. H. *Inorg. Chem.* **1996**, *35*, 6755.

(205) Sbraccia, C.; Zipoli, F.; Car, R.; Cohen, M. H.; Dismukes, G. C.; Selloni, A. *J. Phys. Chem. B* **2008**, *112*, 13381.

(206) Albinati, A.; Bakhmutov, V. I.; Caulton, K. G.; Clot, E.; Eckert, J.; Eisenstein, O.; Gusev, D. G.; Grushin, V. V.; Hauger, B. E. *J. Am. Chem. Soc.* **1993**, *115*, 7300.

(207) Huang, Z.; White, P. S.; Brookhart, M. *Nature* **2010**, *465*, 598.

(208) Conroy-Lewis, F. M.; Simpson, S. J. *J. Chem. Soc., Chem. Commun.* **1986**, 506.

(209) Upmacis, R. K.; Poliakoff, M.; Turner, J. J. *J.Am. Chem. Soc.* **1986**, *108*, 3645.

(210) Kubas, G. J.; Unkefer, C. J.; Swanson, B. I.; Fukushima, E. *J. Am. Chem. Soc.* **1986**, *108*, 7000.

(211) Delis, J. G. P.; Aubel, P. G.; Vrieze, K.; van Leeuwen, P. W. N. M.; Veldman, N.; Spek, A. L.; van Neer, F. J. R. *Organometallics* **1997**, *16*, 2948.

(212) Otsuka, S.; Yoshida, T.; Tatsuno, Y. *J. Am. Chem. Soc.* **1971**, *93*, 6462.

(213) Adams, R. D.; Captain, B. *Acc. Chem. Res.* **2009**, *42*, 409.

(214) Adams, R. D.; Boswell, E. M.; Captain, B. *Organometallics* **2008**, *27*, 1169.

(215) Labinger, J. A.; Bercaw, J. E. *Nature* **2002**, *417*, 507.

(216) Crabtree, R. H. *J. Organomet. Chem.* **2004**, *689*, 4083.

(217) Lersch, M.; Tilset, M. *Chem. Rev.* **2005**, *105*, 2471.

(218) Chen, M. S.; White, M. C. *Science* **2007**, *318*, 783.

(219) Adams, C. S.; Legzdins, P.; McNeil, W. S. *Organometallics* **2001**, *20*, 4939.

(220) Burger, P.; Bergman, R. G. *J. Am. Chem. Soc.* **1993**, *115*, 10462.

(221) Del Rossi, K. J.; Wayland, B. B. *J. Am. Chem. Soc.* **1985**, *107*, 7941.

(222) Lail, M.; Bell, C. M.; Conner, D.; Cundari, T. R.; Gunnoe, T. B.; Petersen, J. L. *Organometallics* **2004**, *23*, 5007.

(223) Verat, A. Y.; Pink, M.; Fan, H.; Tomaszewski, J.; Caulton, K. G. *Organometallics* **2007**, *27*, 166.

(224) Zhang, F.; Kirby, C. W.; Hairsine, D. W.; Jennings, M. C.; Puddephatt, R. J. *J. Am. Chem. Soc.* **2005**, *127*, 14196.

(225) Zhao, S.-B.; Song, D.; Jia, W.-L.; Wang, S. *Organometallics* **2005**, *24*, 3290.

(226) Rabinovich, D.; Zelman, R.; Parkin, G. *J. Am. Chem. Soc.* **1992**, *114*, 4611.

(227) Ng, S. H. K.; Adams, C. S.; Hayton, T. W.; Legzdins, P.; Patrick, B. O. *J. Am. Chem. Soc.* **2003**, *125*, 15210.

(228) Wang, D.; Villa, A.; Porta, F.; Prati, L.; Su, D. *J. Phys. Chem. C* **2008**, *112*, 8617.

(229) Choudhury, J.; Roy, S. *J. Mol. Cat. A: Chem* **2008**, *279*, 37.

(230) Choudhury, J.; Podder, S.; Roy, S. *J. Am. Chem. Soc.* **2005**, *127*, 6162.

(231) Evans, W. J.; Davis, B. L.; Champagne, T. M.; Ziller, J. W. *PNAS* **2006**, *103*, 12678.

(232) Grushin, Vladimir V.; Marshall, William J.; Thorn, David L. *Adv. Synth. Catal.* **2001**, *343*, 433.

(233) Ohki, Y.; Hatanaka, T.; Tatsumi, K. *J. Am. Chem. Soc.* **2008**, *130*, 17174.

(234) Jana, A.; Roesky, H. W.; Schulzke, C.; Samuel, P. P. *Organometallics* **2010**, *29*, 4837.

(235) Gilmore, C. J.; Woodward, P. *J. Chem. Soc., Dalton Trans.* **1972**, 1387.

(236) Lindley, P. F.; Woodward, P. *J. Chem. Soc.* **1967**, 382.

(237) Anema, S. G.; Mackay, K. M.; Nicholson, B. K. *J. Organomet. Chem.* **1989**, *372*, 25.

(238) Sweet, R. M.; Fritchie, C. J.; Schunn, R. A. *Inorg. Chem.* **1967**, *6*, 749.

(239) Pryor, W. A.; Tang, F. Y.; Tang, R. H.; Church, D. F. *J. Am. Chem. Soc.* **1982**, *104*, 2885.

(240) Braye, E. H.; Dahl, L. F.; Hubel, W.; Wampler, D. L. *J. Am. Chem. Soc.* **1962**, *84*, 4633.

(241) Eady, C. R.; Johnson, B. F. G.; Lewis, J.; Matheson, T. *J. Organomet. Chem.* **1973**, *57*, c82.

(242) Johnson, B. F. G.; Lewis, J.; Williams, I. G. *J. Chem. Soc.* **1970**, 901.

(243) Albano, V. G.; Sansoni, M.; Chini, P.; Martinengo, S. *J. Chem. Soc., Dalton Trans.* **1973**, 651.

(244) Bradley, J. S.; Stone, F. G. A., Robert, W. *Adv. Organomet. Chem*, Academic Press: **1983**; *vol 22*, p 1.

(245) Dyson, P. J..; Robert, W.; Anthony, F. H. *Adv. Organomet. Chem*, Academic Press: **1998**, *vol 43*, p 43.

(246) Tachikawa, M.; Muetterties, E. L. *In Prog. Inorg. Chem.*; John Wiley & Sons, Inc.: **2007**, p 203.

(247) Johnson, B. F. G.; Lewis, J.; Nicholls, J. N.; Oxton, I. A.; Raithby, P. R.; Rosales, M. J. *J. Chem. Soc., Chem. Commun.* **1982**, 289.

(248) Adams, R. D.; Captain, B.; Fu, W. *Organometallics* **2000**, *19*, 3670.

(249) Adams, R. D.; Captain, B.; Fu, W.; Smith, M. D. *Inorganic Chemistry* **2002**, *41*, 2302.

(250) Tachikawa, M.; Geerts, R. L.; Muetterties, E. L. *J. Organomet. Chem.* **1981**, *213*, 11.

(251) Tachikawa, M.; Sievert, A. C.; Muetterties, E. L.; Thompson, M. R.; Day, C. S.; Day, V. W. *J. Am. Chem. Soc.* **1980**, *102*, 1725.

(252) Hriljac, J. A.; Holt, E. M.; Shriver, D. F. *Inorg. Chem.* **1987**, *26*, 2943.

(253) Hriljac, J. A.; Swepston, P. N.; Shriver, D. F. *Organometallics* **1985**, *4*, 158.

(254) Jensen, M. P.; Henderson, W.; Johnston, D. H.; Sabat, M.; Shriver, D. F. *J. Organomet. Chem.* **1990**, *394*, 121.

(255) Bailey, P. J.; Blake, A. J.; Dyson, P. J.; Johnson, B. F. G.; Lewis, J.; Parisini, E. *J. Organomet. Chem.* **1993**, *452*, 175.

(256) Jeffery, J. C.; Parrott, M. J.; Stone, F. G. A. *J. Organomet. Chem.* **1990**, *382*, 225.

(257) Adams, H.; Gill, L. J.; Morris, M. J. *Organometallics* **1996**, *15*, 464.

(258) Ceriotti, A.; Della Pergola, R.; Longoni, G.; Manassero, M.; Masciocchi, N.; Sansoni, M. *J. Organomet. Chem.* **1987**, *330*, 237.

(259) Albano, V. G.; Braga, D.; Grepioni, F.; Pergola, R. D.; Garlaschelli, L.; Fumagalli, A. *J. Chem. Soc., Dalton Trans.* **1989**, 879.

(260) Bunkhall, S. R.; Holden, H. D.; Johnson, B. F. G.; Lewis, J.; Pain, G. N.; Raithby, P. R.; Taylor, M. J. *J. Chem. Soc., Chem. Commun.* **1984**, 25.

(261) Adams, R. D.; Wu, W. *J. Cluster. Sci.* **1991**, *2*, 271.

(262) Adams, C. J.; Bruce, M. I.; Skelton, B. W.; White, A. H. *Inorg. Chem.* **1992**, *31*, 3336.

(263) Adams, R. D.; Captain, B.; Fu, W. *J. Cluster. Sci.* **2001**, *12*, 303.

(264) Khimyak, T.; Johnson, B. F. G. *J. Cluster. Sci.* **2004**, *15*, 543.

(265) Saha, S.; Zhu, L.; Captain, B. *Inorg. Chem.* **2010**, *49*, 3465.

(266) Mills, O. *Acta Crystallogr.* **1958**, *11*, 620.

(267) Dobos, S.; Nunziante-Cesaro, S.; Lokshin, B. V. *J. Mol. Struct.* **1988**, *174*, 325.

(268) Mingos, D. M. P. *Acc. Chem. Res.* **1984**, *17*, 311.

(269) Mingos, D. M. P. *Introduction to cluster chemistry*, Printice hall, Engelwood Cliffs, NJ, USA: **1990**; chapter 2.

(270) Della Pergola, R.; Fumagalli, A.; Garlaschelli, L.; Manassero, C.; Manassero, M.; Sansoni, M.; Sironi, A. *Inorg. Chim. Acta.* **2008**, *361*, 1763.

(271) Pergola, R. D.; Diana, E.; Garlaschelli, L.; Peli, G.; Manassero, M.; Sansoni, M.; Strumolo, D. *Inorg. Chim. Acta.* **2003**, *350*, 107.

(272) Marinetti, A.; Sappa, E.; Tiripicchio, A.; Tiripicchio Camellini, M. *Inorg. Chim. Acta.* **1980**, *44*, L183.

(273) Sappa, E.; Manotti Lanfredi, A. M.; Tiripicchio, A. *J. Organomet. Chem.* **1981**, *221*, 93.

(274) Bian, Z.-G.; Zhang, W.-Q.; Guan, H.-X.; Yin, Y.-Q.; Li, Q.-S.; Sun, J. *J. Organomet. Chem.* **2002**, *664*, 201.

(275) Mlekuz, M.; Bougeard, P.; McGlinchey, M. J.; Jaouen, G. *J. Organomet. Chem.* **1983**, *253*, 117.

(276) Vahrenkamp, H. *Comments Inorg. Chem.* **1985**, *4*, 253.

(277) Yempally, V.; Zhu, L.; Isrow, D.; Captain, B. *J. Cluster. Sci.* **2010**, *21*, 417.